Functions of Human DNA2 and its Protein Partners in DNA End Resection

DISSERTATION

ZUR

ERLANGUNG DER NATURWISSENSCHAFTLICHEN DOKTORWÜRDE

(Dr. sc. nat.)

VORGELEGT DER

MATHEMATISCH-NATURWISSENSCHAFTLICHEN FAKULTÄT

DER

UNIVERSITÄT ZÜRICH

VON

COSIMO PINTO

VON

HALLAU SH

PROMOTIONSKOMMISSION:

PROF. DR. PETR CEJKA (VORSITZ UND LEITUNG DER DISSERTATION)

PROF. DR. ALESSANDRO A. SARTORI

PROF. DR. RALF SEIDEL

PD DR. PAVEL JANSCAK

ZÜRICH, 2017

TO MY FAMILY

TABLE OF CONTENTS

ZUSAMMENFASSUNG

Alle lebenden Organismen müssen ihre genetische Information, welche in der DNA gespeichert ist, fehlerfrei halten und korrekt an Tochterzellen weitergeben. Diese Aufgaben werden durch die DNA-Replikation und -Reparaturmechanismen erledigt. Falls diese Mechanismen versagen, kann die Integrität des Genoms beeinträchtigt werden und Krankheiten wie zum Beispiel Krebs können entstehen.

Dem DNA2 Enzym werden in der wissenschaftlichen Literatur überlebenswichtige Rollen im DNA-Metabolismus zugeschrieben. In menschlichen Zellen ist DNA2 für die Vervollständigung der DNA-Replikation und die Reparatur von DNA-Doppelstrangbrüchen mittels homologer Rekombination verantwortlich. Des Weiteren ist DNA2 wichtig für die Erhaltung von Telomeren und der mitochondrialer DNA. In Hefezellen ist DNA2 zusätzlich für die Verarbeitung von Okazaki-Fragmenten und die Aktivierung von Zellzyklus-Kontrollpunkten von Bedeutung.

Meine Arbeit begann mit der Herstellung von rekombinanten Proteinen um deren Funktionen biochemisch zu untersuchen. Ich konnte das menschliche DNA2 Protein und seine mutierten Varianten in hohen Konzentrationen und in aktiver Form aufreinigen. Später habe ich weitere Proteine, wie zum Beispiel die Helikasen WRN und BLM und das DNA-Einzelstrang-bindende Protein RPA aufgereinigt.

In meinen Experimenten konnte ich die Nuklease-Aktivität von DNA2 und dessen Regulierung durch RPA bestätigen. Frühere Studien haben vorgeschlagen, dass DNA2 eine Helikase-Aktivität hat, die jedoch umstritten war. Ich konnte zeigen, dass DNA2 tatsächlich eine Helikase-Aktivität besitzt. DNA2 interagiert mit den Helikasen WRN und BLM während der Resektion von DNA-Enden. Ich konnte demonstrieren, dass die Helikase-Aktivität von DNA2 hilft, die Resektionmaschinerie zu beschleunigen. Zusätzlich zeigten unsere Ergebnisse, dass die Motor-Aktivität von DNA2 als sogenannte Translokase auf einzelsträngiger DNA agiert und die Degradation davon dadurch vorantreibt.

Ich war ausserdem an verschiedenen Kollaborationen beteiligt: Mithilfe von *in vitro* und *in vivo* Experimenten konnten wir zeigen, dass DNA2 mit WRN/BLM in der DNA-Endresektion und mit WRN beim Neustart von DNA-Replikationsgabeln verantwortlich ist. In einer weiteren Publikation haben wir gezeigt, dass RPA die Fähigkeit hat doppelsträngige DNA zu öffnen.

SUMMARY

Living organisms must keep their DNA content intact to assure the integrity of their genomic information. DNA replication and DNA damage repair are the main efforts to accomplish this task. Hence, the failure of these mechanisms could lead to genomic instability and subsequently development of diseases such as cancers could occur.

The DNA2 enzyme was shown to have essential roles in DNA metabolism. In human cells DNA2 was implicated in the completion of DNA replication and the repair of DNA double-strand breaks via the homologous recombination pathway. In addition, DNA2 was shown to be important for telomeric and mitochondrial DNA maintenance as well as Okazaki fragment processing and cell cycle checkpoint activation in yeast cells.

My PhD project started with the preparation of recombinant proteins that allowed biochemical investigations of their functions. I could purify human DNA2 and its variants in an active state and in concentrations sufficient for our assays. Further I produced DNA2 partners WRN and BLM helicases and various single-stranded DNA binding proteins such as the replication protein A (RPA). In my experiments, I could recapitulate DNA2's nuclease activity and its regulation by RPA. While in the absence of RPA DNA2 degrades 3' or 5' terminated single-stranded DNA, the nuclease is restricted to degrade 5' terminated DNA in the presence of RPA.I was able to describe the helicase activity of human DNA2 nuclease-deficient mutant that had been a matter of contradiction in the field. We observed that the helicase activity of hDNA2 is cryptic and it is masked by its nuclease activity. Studying DNA end resection processes, we found that DNA2 functionally integrates with BLM and WRN helicases. We showed that the helicase activity of DNA2 acts as a motor speeding up the degradation of ssDNA produced by its helicase partners WRN or BLM. We propose that the DNA2 motor acts as a translocase on single-stranded DNA accelerating the degradation by the nuclease domain of hDNA2.

I also participated in several collaborative projects showing that DNA2 cooperates with WRN/BLM in DNA end resection and the restart of reversed replication forks with WRN but not BLM in vitro and in vivo. Finally, we showed that RPA possesses double-stranded DNA melting capacity and characterized its dynamics at DNA forks.

1. INTRODUCTION

Cancer is a general term for a broad range of diseases that can affect every part of the body. During the development of cancer, cells undergo a transition from normal growth to expansion in an uncontrolled way forming new tissues that eventually become tumours. Some cancer cells acquire the ability to grow beyond their natural boundaries, spread all over the body and invade other tissues or organs, leading in the worst case to death of the whole organism. Ten hallmarks of cancer are described in the literature so far (1), including deregulating cellular energetics, enabling replicative immortality or evading growth suppressors. Of special interest here is a further characteristic defined as genome instability and mutation. The DNA serves as the main carrier of genomic information (2). When the genetic information is changed due to mutations or larger genomic rearrangements, this can lead to the activation of oncogenes or to the loss of tumour suppressors. Therefore, maintaining genomic stability is a fundamental task during the entire lifespan of each organism. Only if the entire information stored in the DNA is constantly and correctly passed from one cell generation to the next one via mitosis or meiosis genomic stability is guaranteed. To fulfil these requirements cells have evolved many mechanisms to replicate, repair and recombine their DNA in a correct way. However, if these mechanisms fail, genomic instability could become a consequence leading to pathological situations.

1.1 DNA repair mechanisms

1.1.1 General overview

The DNA is damaged through the whole life span of a cell. Two main groups of possible causes were defined: environmental influences such as ionizing radiation (IR), UV light and DNA intercalating chemicals or endogenous sources such as reactive oxygen species (ROS), replication errors or aberrant DNA repair (3). These causes can result in a wide range of various DNA lesions, including DNA strand breaks (due to ionizing radiation and collapsed replication forks), dimerization of thymine bases (UV), oxidation of bases (ROS) or

mismatches (incorrect replication). A plethora of DNA repair mechanisms have evolved to maintain genome stability (Figure 1; (4)).

DNA damage that results from methylation, deamination and hydroxylation of bases or similar lesions generated by reactive oxygen species (ROS) and do not alter the structure of the DNA are repaired by the base-excision repair (BER) mechanism. In the BER pathway, the altered bases become flipped out of the DNA double helix and are subsequently removed from their nucleotide backbone due to the action of various glycosylases (5). Additionally, spontaneous hydrolysis of intact bases may also result in an abasic site (6). In the repair pathway named as short-patch BER, the APE1 endonuclease nicks the strand at the abasic site generating a single-strand break (7). DNA polymerase β (Polβ) fills the single nucleotide gap and removes the abasic nucleotide from the strand (8). Then the DNA ligase 1 re-ligates the inserted nucleotide creating an intact DNA strand (9). In long-patch BER, 2-10 bases are replaced by the combined action of Polβ, Polδ/ε and Proliferating-Cell-Nuclear-Antigen (PCNA) that incorporate new nucleotides. The generated DNA flap is then cleaved by the FEN1 nuclease and the DNA ligase 1 finally ligates the DNA strands (reviewed in (10, 11)).

Bulky DNA lesions that affect the structure of DNA, including DNA adducts and pyrimidine dimers, mainly arise from exogenous influences such as oxidative damage or UV light (12). Nucleotide-excision repair (NER) that is sub-divided into global genome NER (GG-NER) and transcription-coupled repair (TCR-NER) is needed to repair such lesions. In TCR, the RNA polymerase II is stopped by a DNA lesion and needs to be removed giving access to the repair pathway proteins to fulfill their function (13). GG-NER does not depend on transcription and thus only differs from TCR-NER the initial step of the repair (14). Components of multi-subunit transcription factor TFIIH unwind ~30 base pairs around the damage leading to the formation of single-stranded DNA (ssDNA; (12)). The ssDNA gets bound by Replication Protein A (RPA) and stabilized in the open conformation. A ~24-32 nucleotides-long gap is created by the action of NER-endonucleases cleaving the damaged strand up- and down-stream from the lesion. The gap is then filled and ligated by the regular DNA replication machinery creating an intact double-stranded DNA (dsDNA) molecule again (reviewed in (12)).

DNA polymerase errors lead to the incorporation of wrong nucleotides during replication, leading to mismatches or short insertion-deletion loops (15). Such lesions are repaired by the mismatch repair (MMR) pathway. The heterodimer hMSH2/hMSH6 (hMutSα) detects

mismatches or single-base loops and the hMSH2/hMSH3 (hMutSβ) heterodimer senses larger insertion/deletions loops (16-18). The second step in DNA mismatch repair involves the recruitment of additional MMR factors, such as hMLH1/hPMS2 (hMutLα) and hMLH1/hPMS1 (hMutLβ) and the nicking of the damaged strand (18). The newly synthesized strand needs to be detected during this process to determine the strand containing the mismatch error. It is possible that this identification is supported by contact with the replication machinery close to the mismatch, strand discontinuities in the lagging strand or by recently misincorporated ribonucleotides (19). Strand degradation and correct synthesis of the lacking DNA property is mediated by many proteins including Polδ/ε, RPA, PCNA, RFC, EXO1 and FEN1 upon the recognition of the strand containing the false nucleotide(s) (reviewed in (18, 20-22)).

The covalent linking of two complementary DNA strands (named as interstrand crosslink, ICL) leads to serious issues in the DNA metabolism since both replication and transcription can be blocked. In brief, the linked strands are separated and the damage is repaired by the coordinated action of proteins of the Fanconi anemia (FA) pathway and the help of several additional factors from the NER, translesion synthesis (TLS) and homologous recombination (HR) pathways (reviewed in (23, 24)). TLS polymerases have the ability to bypass such crosslinks to help the replication fork to progress (25) and the repair of the lesion could occur subsequently.

DNA strand breaks are sub-divided into DNA single-strand breaks and DNA double-strand breaks (DSB). DSBs occur through replication across a single-strand break or damage caused by ionizing radiation, free radicals or chemicals (26). In the case of a DSB the chromosome is separated into two parts losing the covalent bonds in the backbone in both DNA strands, while in a single-strand break the chromosome stays as an entity. It can occur that the DNA ends of a DSB are chemically “clean”, for example after a restriction enzyme cleavage, and ready to be re-ligated immediately. However, for example IR induces DSB ends that are modified and which need processing of the molecules to make them suitable for re-ligation (26, 27). Likewise, DNA breaks caused by aberrant topoisomerase reactions result in DSBs with covalently attached topoisomerase polypeptides (28).

DSBs can lead to point mutations or nucleotide insertions and deletions, changing the reading frameshift, but also to chromosomal rearrangements such as insertions,

translocations or lager deletions. Nature has evolved various pathways to handle the repair of DSBs.

Non-homologous end joining (NHEJ) is a mechanism that repairs broken chromosomes by ligating the DNA breaks. NHEJ can happen during the whole cell cycle but is predominant in the G1 phase and is considered as a fast repair mechanism compared to HR (29). Briefly, the NHEJ mechanism includes the binding of the Ku70/80 heterodimer to the two ends of the broken chromosome most likely acting as a scaffold for further proteins involved in the NHEJ pathway. The enzyme DNA-dependent protein kinase catalytic subunit (DNA-PK_{CS}) is recruited to DNA ends via the Ku70/80-DNA complex and helps to form a synaptic complex brining the two fragments of a broken chromosome together. The DNA ends are then processed by several enzymes including nucleases and polymerases to make the ends suitable for re-ligation. The ligation process is catalyzed by the ligase IV/XRCC4 complex. NHEJ is considered as error-prone due to the processing at the break site potentially leading to mutations such as small deletions, as well as due to the possible ligation of two fragments from different chromosomes leading to translocations (reviewed in (30, 31)).

In the S/G2 phase of the cell cycle, when each chromosome consists of two sister chromatids, homologous recombination can operate as a mechanism for the repair of DSBs. The broken chromatid is processed and resynthesized using the intact chromatid as template to copy the missing information. The mechanisms of HR are explained in detail in the next section. Sister chromatid is preferred over a homologue chromosome as repair template during HR in vegetative cells (32). HR does not only occur to repair DSBs generated upon pathological DNA damage events but also during meiosis, where germ cells use DSB formation and subsequent repair via HR with preferentially the homologous chromosome as a template to increase the genomic diversity of the progeny and to ensure proper segregation of chromosomes (33, 34).

Single-strand annealing (SSA) is an additional pathway to repair DSBs in case the break occurs in a region of a chromosome where tandemly repeated DNA sequences exist. Similarly, as in HR, 3’ overhangs are produced via DNA end resection. However, the resected overhangs do not invade another chromosome but can anneal to their complementary ssDNA sequence. Notably, the interstitial DNA as well as one of the repeated homologous sequences are lost during SSA (35). In SSA the complementary sequence is often more than

100 bp in size, while in microhomology-mediated NHEJ (MMEJ or alternative NHEJ) the complementary DNA is only few base pairs in length (36).

The DSB repair pathway choice is tightly regulated in cells. Depending on the cell cycle phase, cyclin-dependent kinases (CDKs) help to determine which mechanism is used. In G0 and G1 the initial resection of a DSB is suppressed dependent on 53BP1 guiding the repair towards canonical NHEJ. In S/G2 S-phase CDKs promote DNA end resection via phosphorylation of downstream factors (such as Sae2/CtIP) leading to the use of annealing-dependent pathways (HR, alternative NHEJ, SSA). Furthermore, the resection/annealing-dependent pathways compete for the repair of DSBs. In a complex interplay many factors regulate which machinery is used (reviewed in (37)).

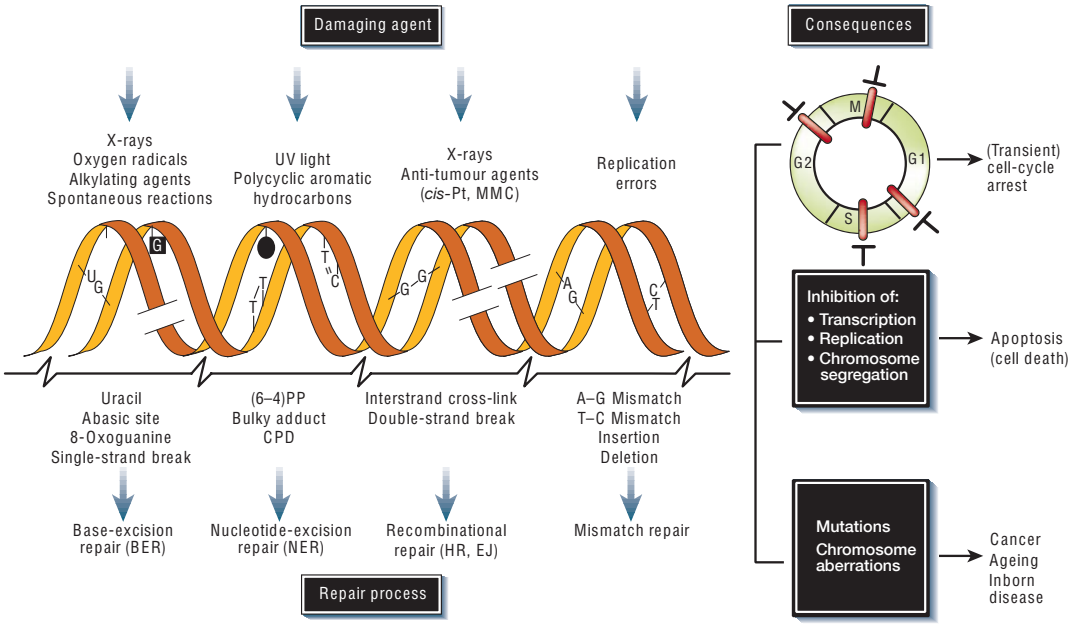

Figure 1: Overview of different types of DNA damages, their sources, corresponding repair mechanisms and consequences. Multiple DNA repair mechanisms cope with various types of DNA damages induced by different DNA damaging causes. DNA damage can lead to cell-cycle arrest providing the cell time to properly repair the damage. Cell death but also the development of diseases such as cancers can be the consequences if the repair fails. Abbreviations: *cis*-Pt, cisplatin; MMC, mitomycin C; (6-4)PP, 6-4 photoproduct; CPD, cyclobutane pyrimidine dimer; BER, base-excision repair; NER, nucleotide-excision repair; HR, homologous recombination; EJ, end joining. Modified from (4).

1.1.2 Repair of DNA double strand breaks by homologous recombination

Homologous recombination is considered as a mostly error-free mechanism of DSB repair. DNA end resection is required as a start point for every HR sub-pathway (38). The 5' to 3' nucleolytic degradation of the broken DNA ends via the action of several enzymes leads to the production of a 3' terminated overhang (reviewed in (39)). This resection procedure is explained in more detail below. The Replication Protein A (RPA), known for its high affinity to ssDNA (40), covers the generated 3' terminated ssDNA overhang. Recombination mediators such as Rad52 and Rad51 paralogues (Rad55, Rad57) in yeast or BRCA2 and RAD51 paralogues in humans catalyze the replacement of RPA with RAD51 or DMC1 (41-43). Rad51 recombinase then searches for homologous sequences in other DNA molecules (44). Rad51 can bind two different DNA strands bringing them into close proximity (reviewed in (45)). Upon a stable interaction, the invasion of the 3' overhang into the double-stranded sister chromatid (or the homologous chromosome) leads to a displacement loop (D-loop, (46, 47)). However, the exact mechanism and the timing of the homology search are still a matter of discussion (45). The invading 3' terminated strand serves as a primer, while the recipient DNA strand acts as a template for the DNA synthesis by DNA polymerases. The 3' overhang is extended until it can be ligated to the 5' end of the other end of the DSB without losing any genomic information (35). In a process termed as second-end capture, the other (resected) end of a DSB can either anneal to the D-loop or invade the intact molecule as well using either one as synthesis template. The resulting structure linking to two different DNA molecules is termed as a double Holliday junction (dHJ, (48)). Rad52 is considered as a key protein in the second-end capture process in yeast. Rad52 can anneal ssDNA bound by RPA to the other end of the DSB forming a double Holliday junction. RAD52, the human homolog of yeast Rad52, shows strand annealing capability in the human system as well but most likely there are other proteins for example BRCA2 having redundant functions (49, 50).

Various mechanisms have been described to resolve dHJs in order to finish HR leading to two intact and separate DNA molecules. In a process called resolution, the cleavage of a dHJ via human MUS81-EME1, SLX1-SLX4 or GEN1 endonucleases results in either crossover or non-crossover products depending on the symmetry of the cleavage (51). A dissolution pathway exists in addition to the resolution pathway. The BLM (Bloom syndrome protein)

helicase in concert with TopoIIIα topoisomerase and RMI1/2 can dissolve dHJ leading to non-crossover products (51). However, the classical HR sub-pathway involving the formation and resolution/dissolution of dHJ is neither considered as the only nor as the most common HR pathway.

During Synthesis-dependent strand annealing (SDSA) the invading strand is elongated after D-loop formation but then released from the intact DNA molecule without subsequent second-end capture. Complementary sequences in the newly synthesized strand help to anneal to the other chromosome part and to re-ligate the two fragments. SDSA leads to a non-crossover product (Figure 2; (35, 41)).

In a third HR sub-pathway termed as break-induced replication (BIR), the 3' terminated ssDNA from a broken fragment end invades an intact template chromosome and copies the whole missing sequence to restore a complete chromosome. Repairing DSB via BIR can result in a phenomenon called loss of heterozygosity (LOH) if the homologous chromosome is used as template since both resulting chromosomes show then the same genetic information in the whole newly synthesized part (compared to only partial overlaps due to SDSA or dHJ pathways; Figure 2; (35, 41)).

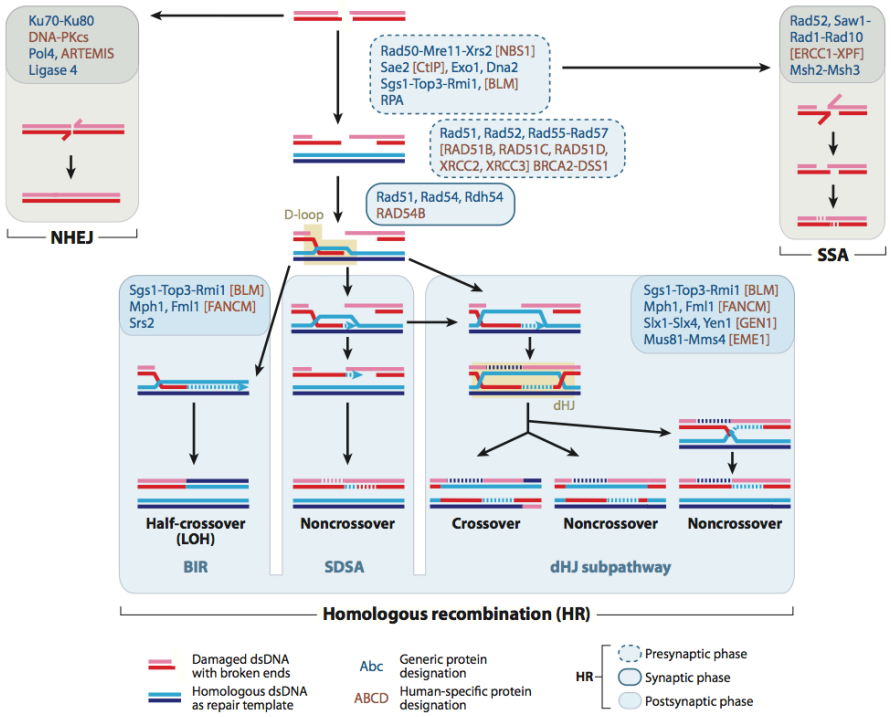

Figure 2: Scheme of DSB repair pathways. DNA double strand breaks are repaired using Non-Homologous End Joining (NHEJ), Single-Strand Annealing (SSA) and Homologous

Recombination (HR). NHEJ is sub-divided into canonical and alternative (also known as microhomology-mediated end joining, MMEJ, not indicated here). HR consist of the double Holliday Junction (dHJ), Synthesis Dependent Strand Annealing (SDSA) and Break-Induced Replication (BIR, leading to loss of heterozygosity (LOH)). Yeast proteins are indicated in blue, human proteins in brown. Modified from (35).

1.1.3 Regulation of HR initiation

Cells have to determine which repair pathway to use upon a DSB has occurred. DNA end resection is an initial and essential process for DSB repair by homologous recombination (38).

In eukaryotic cells, it seems that the phosphorylation of Sae2 in yeast or CtIP in humans by cyclin-dependent kinases (CDKs) is a common mechanism to commit DSB repair to HR. Six different CDKs driving cell-cycle progression were described in mammals compared to one in the yeast system. These six different CDKs vary in their importance from tissue to tissue and cell cycle phase (35). In yeast Sae2 is phosphorylated by Cdc28 at serine 267 mediating DSB end resection (52, 53). Replacing Sae2 S267 to a non-phosphorylatable alanine leads to a mutant phenotype showing unresected DSBs similar like in *sae2Δ* mutants (52). On the other hand, changing S267 to the phosphomimetic aspartic acid gives rise to cells that show extensive DSB resection (52). CtIP, the human homolog of Sae2, fulfills similar function in the initiation of DSB end resection (54). CtIP threonine 847 phosphorylation is essential for DNA end resection. Replacing T847 by alanine abolishes resection while introducing the phosphomimetic mutation results in DSB resection even upon CDK inhibition (55). Both Mre11 and Xrs2 show residues that are potential CDK targets. However, mutating these residues does not change the resection phenotype in mutant cells (53).

While phosphorylation of Sae2/CtIP initiates DSB end resection and will be covered in more detail later, phosphorylation of Exo1 by Rad53 reduces its nuclease activity (56). In human cells EXO1 phosphorylation by ATR (ataxia telangiectasia and Rad3-related protein) kinase targets the enzyme for degradation (57).

1.2 Biochemistry and functions of DNA2

1.2.1 Overview of human and yeast DNA2

Saccharomyces cerevisiae Dna2 (DNA replication ATP-dependent helicase/nuclease, yDna2) is described as a protein with a wide variety of functions in the eukaryotic DNA metabolism. Previously, it was shown that yDna2 participates in Okazaki fragment processing (58-60), telomere maintenance (61), aging (62), long-patch base excision repair (63) and the processing of intermediates at stalled replication forks (64, 65).

The yDna2 polypeptide consists of a RecB family nuclease domain (Figure 3), whose function can be suppressed by a substitution of the glutamic acid at position 675 to alanine (E675A, (66)). yDna2 shows single-strand DNA specific nuclease activity with both 5'-3' as well as 3'-5' polarity, whereas in the presence of yeast RPA (yRPA) 5' tailed DNA substrates were preferred (67, 68). Beside its more prominent nuclease activity, yDna2 contains a superfamily I helicase domain located in the C-terminal region of the protein showing 5'-3' helicase activity (69, 70). The helicase function is dependent on the hydrolysis of ATP (71) and mutating the amino acid residue 1080 from lysine to glutamic acid (K1080E) abrogates the ATPase and the helicase activity (71). In contrast to its nuclease activity, yDna2 helicase activity was believed to be weak and to play only a minor role in its function (59, 69, 72). However, more recently it was shown that yDna2 exhibits a strong helicase activity comparable to the most efficient helicases in eukaryotes (70). The helicase function of yDna2 is regulated by the protein's nuclease function (70). Nuclease-deficient yDna2 preferentially binds to ssDNA structures and its helicase activity is the highest when a 5' overhang is present (70). However, the nuclease of the wild type enzyme degrades these 5' overhangs and therefore lowers the binding to the substrates that is prerequisite for the helicase function (70). Thus, the helicase activity of yDna2 is cryptic and becomes apparent upon inactivation of the nuclease (70). Yeast cells expressing the helicase-deficient yDna2 protein are only viable under certain growth conditions, but highly sensitive to DNA damaging agents, while the nuclease function of yDna2 is essential (71, 73). Dna2 seems to be largely conserved from yeast to human, although significant differences exist and the function of the human DNA2 (hDNA2) in DNA metabolism is not completely clear. Human

DNA2 consists of 1060 amino acids and contains a nuclease- and a helicase-domain like yDna2, while the N-terminal region is missing (Figure 3; (74)). Human cells depleted of hDNA2 show genomic instability (75) and a high expression of hDNA2 negatively correlated with the disease outcome in human cancers (76). Heterozygous $DNA2^{+/-}$ mice showed higher cancer susceptibility than wild type mice and the complete knockout of DNA2 leads to embryonic lethality (77).

Yeast and human DNA2 contain an iron-sulfur cluster consisting of an iron ion coordinated by four cysteine residues located in the nuclease domain. The putative role of the iron-sulfur could be the stabilization of the protein's structure (78, 79). Mutating the cysteine residues in the yeast protein led to decreased nuclease and ATPase activity (78). Due to the iron-sulfur cluster the protein is very prone to oxidation and likely unstable. yDna2 showed highly specific ssDNA nuclease activity and helicase function upon minimizing oxidation during the protein purification and reducing the duration of the procedure (67, 70)

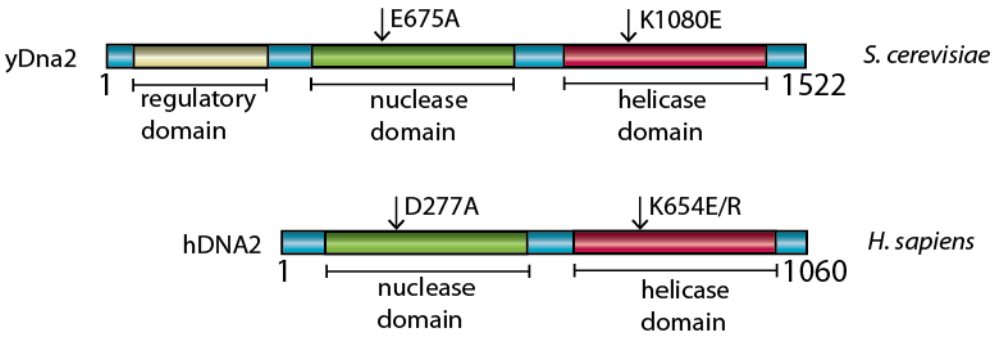

Figure 3: Schematic overview of the yeast enzyme yDna2 and the human homologue hDNA2 (courtesy of P. Cejka). Both enzymes contain a nuclease- and helicase-domain whereas the N-terminal regulatory domain is lacking in hDNA2. Mutations inactivating the respective biochemical activity are indicated.

1.2.2 DNA2 in Okazaki fragment processing

Before each cell division, cells must double their complete genetic information to pass it on to the next generation. The copying of the DNA occurs during the S-phase of the cell cycle. The replication machinery uses both strands of a double-stranded DNA molecule as templates (reviewed in (80)). However, eukaryotic DNA polymerases can only synthesize the

new DNA strand in 5'-3' direction (81). Since the opening of the dsDNA and the synthesis occurs almost at the same time, only one strand can be synthesized in a continuous manner (leading strand), while the other one (lagging strand) is synthesized discontinuously starting at many origins forming the Okazaki fragments (82). The replication machinery opens the dsDNA molecule and Pol α (DNA polymerase alpha catalytic subunit)-primase complex synthesizes RNA-DNA primers needed for the replicative polymerases to start (83). Such a primer usually consists of ~10 RNA followed by ~20 DNA subunits (84). Pol δ (DNA polymerase delta) continues replicating the DNA (85) until after ~150 (in eukaryotes) the replication machinery hits a downstream primer of the lagging strand. While *Escherichia coli's* DNA polymerase I has 5' to 3' exonuclease activity and can remove a primer (86), eukaryotic polymerases do not exhibit this 5' to 3' exonuclease activity (86). In addition, Pol α is lacking a proofreading activity, making the DNA part of every primer prone to errors (87). Therefore, it is essential to remove not only the RNA portion, but also the DNA part of a primer in order to reduce the risk of mutagenesis (88, 89). The current model for Okazaki fragment processing suggests that Pol δ converts the RNA-DNA primer into a 5' flap during the synthesis of the DNA strand in a process termed strand displacement synthesis (58, 90, 91). This is stimulated by the helicase Pif1, which leads to longer 5' flaps (92, 93). These flap structures need to be removed to allow ligation of Okazaki fragments forming a continuous linear duplex DNA molecule again (94, 95).

Short flaps generated during lagging strand replication are degraded by FEN1 (Rad27/Fen1 in yeast), a 5' to 3' flap endonuclease (96). RPA covers the single-stranded 5' flap if it becomes longer than 20-25 nts due to RNA-DNA primer displacement by Polδ. RPA inhibits Fen1 cleavage but stimulates yDna2 cleavage of the flap (58). yDna2 cleaves the long flap generating a shorter one, that does not bind RPA and subsequently can be cleaved by Fen1. RPA plays an important regulatory role in the two-step processing of long flaps (58). Previously, yDna2 was shown to be incapable of the flap processing on its own, and Fen1 was believed to function downstream of Dna2 in all cases (58). Short flaps can be also degraded by other nucleases such as Exo1, which becomes essential when Fen1 is absent (97), and the overexpression of Exo1 suppresses growth defects observed in yDna2 mutants (98). The DNA ligase I ligates the nicked double-stranded DNA after the flap is removed (63, 99).

yDna2 is an essential protein in yeast (71, 100). However, cells lacking yDna2 became viable when the generation of long 5' flaps was suppressed in *pif1-m2* mutants (101). This finding strongly indicates that the essential function of yDna2 is the removal of long 5' flaps (101), and that long flaps that necessitate Dna2 functions only occur when Pif1 is present. Furthermore, growth defects that were observed in cells that were *rad27* (Fen1) deleted were rescued by yDna2 overexpression (102), showing that Dna2 can partially process Fen1's substrates. In addition, overexpression of Fen1 helped to overcome the lethality of *dna2* deleted cells (102). This indicated that yDna2 and Fen1 might work in separate pathways. However, *in vitro* reconstitution assays of Okazaki fragment processing using recombinant yDna2 suggested that yDna2 was not able to cleave the flap on its own since the enzyme left a ~5-8 nt long flap that would require the cleavage by an additional nuclease (58, 60, 69). In contrast to this, new findings could show that yDna2 was able to cleave the flap near its base leading to a product that could be ligated by the DNA Ligase 1 and therefore accomplish Okazaki fragment maturation on its own without the need of Fen1 *in vitro* (103).

hDNA2 is essential in the human DNA metabolism (75). However, in contrast to yeast, where the essential role of yDna2 is strongly linked to replication and Okazaki fragment processing, the function in human cells is less clear. Human FEN1 is essential for Okazaki fragment maturation, while the depletion of hDNA2 did not result in a detectable defect in Okazaki fragment processing (75). No significant differences in the DNA maturation were observed comparing FEN1 single mutants to FEN1-hDNA2 co-depleted mutants (75). These findings indicated that hDNA2 may possess distinct function in DNA replication than the processing of Okazaki fragments (75). Importantly, hDNA2-depleted cells showed more DNA damage than FEN1-depleted cells, while the depletion of hDNA2 did not change the replication fork rate (75). Together these results indicate that hDNA2 contribute to DNA integrity with other yet unknown functions, but not via Okazaki fragment processing (75). Of note, it is also possible that the contribution of hDNA2 in Okazaki fragment processing is very limited in human cells and escaped the limit of detection in the performed assays. Ectopic expression of either nuclease- or helicase-deficient hDNA2 in hDNA2-depleted cells did not rescue the mutant phenotype indicating that both functions are essential for genome integrity (75).

1.2.3 DNA2 in the DNA double strand break end resection

The resection of the broken DNA ends after a DSB is the initial step towards homologous recombination (38). A 3’ overhanged DNA molecule is generated by the specific nucleolytic degradation of the 5’ terminated strand (39). This 3’ terminated moiety will invade a template DNA molecule after successful homology search and will serve to prime DNA synthesis (45). At least three nucleases including MRE11, EXO1 and DNA2 are suggested to be involved in the current models for DNA end resection (39, 104).

Mre11, as part of the MRX (Mre11, Rad50, Xrs2) complex, together with Sae2 are proposed to catalyze the initial steps in DSB processing in the yeast system (39). This short-range end resection removes about 50-100 nucleotides at a DSB (104). Mre11 was initially described to possesses a 3’-5’ exonuclease activity that cannot be responsible for the 5’-3 cleavage that is needed for establishing a long 3’ overhang (105). Later, it was shown that Mre11 exhibits an endonuclease activity that can nick the DNA strand near the DSB from where then DNA degradation could start (106). The current model suggests that MRX nicks the 5’ terminated DNA strand in an Sae2-dependent manner (107). The incised strand is then degraded towards the DSB most likely using the 3’-5’ nuclease of Mre11. It was shown that the nicking activity of the complex is strictly dependent on the ATP hydrolysis function of Rad50 and highly stimulated by phosphorylated Sae2 (107). The Xrs2 subunit is dispensable for the nicking, though needed for the nuclear localization of the MRX complex as well as for its function other than DNA end resection, namely in Tel1 signaling and NHEJ (108). The human MRN (MRE11, RAD50, NBS1) complex endonuclease activity was shown to have very similar roles in DNA end resection as MRX, but its function is completely dependent on NBS1 (the homolog of yeast Xrs2) as well as on phosphorylated CtIP (the homolog of yeast Sae2, (109)).

Two separate pathways are responsible for the extended DNA end resection. The helicase Sgs1 in a synergy with the nuclease activity of yDna2 or the exonuclease Exo1 catalyze the long-range 5’-3’ degradation of broken DNA ends leading to 3’ overhangs of hundreds to thousands of nucleotides in length (110, 111). Biochemical analysis of the Sgs1-yDna2 pathway suggested that the DNA unwinding activity of Sgs1 as well as the nuclease activity of yDna2 were essential for DNA resection while the helicase-deficient version of yDna2 possessed less efficient degradation capacity (67).

Purified yDna2 exhibits ssDNA-dependent 3’-5’ and 5’-3’ nuclease activities (59). Adding yRPA to the reaction mixture modulates the polarity of yDna2 nuclease by abolishing the 3’-5’ and stimulating the 5’-3’ degradation (67, 68). This preference for the 5’ terminated ssDNA strand fits very well to the *in vivo* DNA end resection model where exclusively 3’ overhanged DNA ends are produced by yDna2. Supplementing the reaction with *E. coli* SSB inhibited the yDna2 nuclease completely indicating that the ability of yRPA to regulate yDna2 is specific (67).

Sgs1 functions as a helicase to unwind dsDNA to ssDNA that then serves as substrate for nucleolytic degradation by yDna2. Sgs1 and yDna2 are form a functional cognate complex since neither Pif1 nor Srs2 helicases could show similar synergistic effects in dsDNA degradation in concert with yDna2 (67). *E. coli* RecQ helicase could only support yDna2 in DNA resection at 1000-fold higher concentrations (67). Furthermore, it was shown that Sgs1 physically interacts with yDna2 and that the Top3-Rmi1 complex increases the DNA resection capability of the Sgs1-yDna2 complex (67). The stimulatory effects of Top3-Rmi1 on Sgs1-yDna2 are more likely due to the stimulation of the Sgs1 helicase than via increasing the nuclease of yDna2. In addition, the MRX complex helps to recruit Sgs1 to DNA ends and therefore enhances the degradation capacity of the Sgs1-yDna2 complex (67). Figure 4 summarizes the DNA end resection in the yeast system.

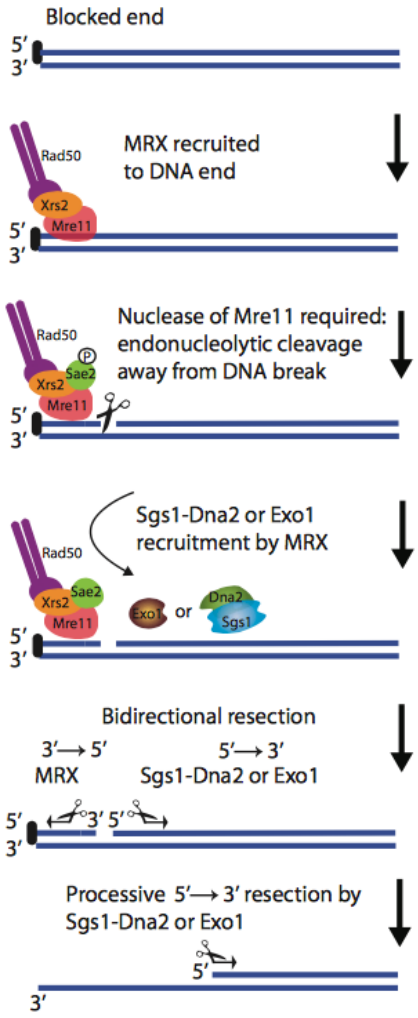

Figure 4: Schematic overview of the DNA end resection in budding yeast. The MRX complex is rapidly recruited to blocked DNA ends followed by Sae2. MRX incises the 5′ terminated DNA strand nucleolytically stimulated by phosphorylated Sae2. The MRX complex helps to recruit Sgs1-Dna2 and Exo1. In a bidirectional resection process MRX might degrade towards the DNA end using its 3′-5′ exonuclease activity while Sgs1-Dna2 and Exo1 perform processive 5′-3 resection leading to a long 3′ overhang. Modified from (39).

Human DNA2 possesses single-stranded DNA-dependent 5'-3' and 3'-5' nuclease activities, similar to its yeast homologue (112, 113). The addition of human RPA to the reaction buffer abolishes the degradation of 3' tailed DNA and enhances the degradation of 5' tail (113). The helicase activity of recombinant hDNA2 was either described as weak (112) or non-existent (114). hDNA2 together with BLM helicase, a human homolog of yeast Sgs1, could degrade dsDNA substrates (113, 115, 116). The resection was dependent on the hDNA2 nuclease and BLM helicase, but not on the helicase of DNA2 (113, 116). Initially when BLM was exchanged with another human helicase dsDNA degradation could not be observed, while yeast Sgs1 could adopt BLM's function as leading helicase in the interplay with hDNA2 to degrade dsDNA (113). Physical interaction between hDNA2 and BLM was detected and this interaction was not dependent on DNA (113). The MRN complex was shown to recruit BLM to dsDNA stimulating its DNA unwinding and boosting the degradation of dsDNA by the hDNA2-BLM complex (113). It is well established that BLM interacts with the Topo IIIα-

RMI1-RMI2 complex (TRR complex) in the dissolution of dHJ (117). Furthermore, it was reported that the TRR complex enhances the ability of BLM-hDNA2 to resect dsDNA (115). Later it was shown that WRN (Werner syndrome ATP-dependent helicase) together with hDNA2 can degrade dsDNA (116). These results coming from biochemical assays using recombinant proteins could be supplemented with *in vivo* data using single-strand DNA annealing reporter assays and RPA foci formations as readouts for efficacy of resection *in vivo* (116). Not only BLM helicase but also WRN helicase seem to interact with hDNA2 in the resection of DSBs (116). Beside the functional interplay of hDNA2 and WRN, a direct physical interaction was demonstrated (116). The helicase function of BLM/WRN and the nuclease but not the helicase activity of hDNA2 were essential for resection (113, 115, 116). Together, these data suggest that hDNA2 can either associate with BLM or WRN helicase to resect dsDNA, but detailed biochemical investigations of the mechanisms were lacking.

Recent work on the architecture of full-length mouse DNA2 showed that the nuclease domain is located in a tunnel-like structure through which the DNA substrate has to thread (Figure 5; (118)). The narrow structure of the tunnel could explain why the DNA2 nuclease activity is ssDNA-dependent since the tunnel is too narrow for dsDNA to reach the active site (59, 118). *In vitro* yDna2 cleaves ssDNA with 5'-3' and 3'-5' polarity, while addition of yRPA to the reaction abolishes the 3'-5' polarity (67, 68). Mouse DNA2 was able to remove RPA from ssDNA only from the 5' but not 3' end leading to "uncovered" ssDNA explaining how RPA could confer the DNA2 nuclease polarity (118). Furthermore, the nucleases domain is located ahead of the helicase domain (118), which may degrade the DNA substrate before it can reach the helicase domain. This would explain why the strong helicase activity of yDna2 was only observed using a nuclease-deficient yDna2 variant, and why the nuclease of Dna2 apparently masks its helicase activity (70).

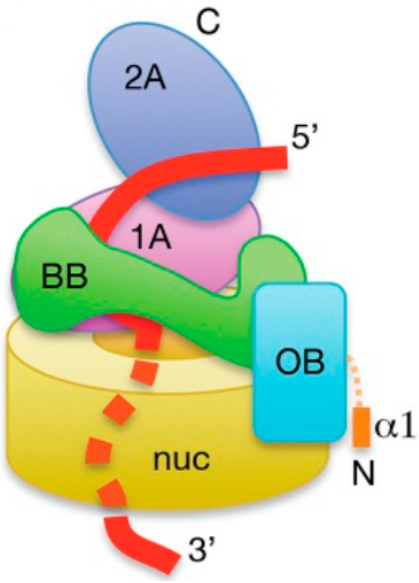

Figure 5: Schematic domain structure of mouse DNA2. The nuclease domain (nuc) forms a narrow tunnel that only ssDNA (depicted in red) can reach and is located ahead of the helicase domain (1A, 2A). Modified from (118).

1.2.4 Replication fork reversal

The reversal of a typical replication fork (three-way junction) to a reversed fork (four-way junction) was initially believed to be a pathological event in eukaryotes (Figure 6). However, more recent studies identified fork reversal as a global response to replication stress protecting from fork collapse (reviewed in (119)). This fork reversal was observed upon treatment of cells with the DNA topoisomerase I inhibitor camptothecin (CPT, (120)), but also after treatments with a wide variety of chemicals such as etoposide, mitomycin C, methyl methanosulfate (MMS) or hydroxyurea (HU, (121)). The fork reversal is dependent on RAD51 (121) and other factors, such as FBH1, SMARCAL1 or ZRANB3, are believed to be important in the fork reversal (122-125). It was shown that the human RECQ1 helicase catalyzes the restart of reversed replication fork using its ATPase-dependent branch migration activity in a PARP1-regulated manner (126). Data from *Schizosaccharomyces pombe* show that DNA2 can prevent stalled replication forks from reversing upon HU treatment (64).

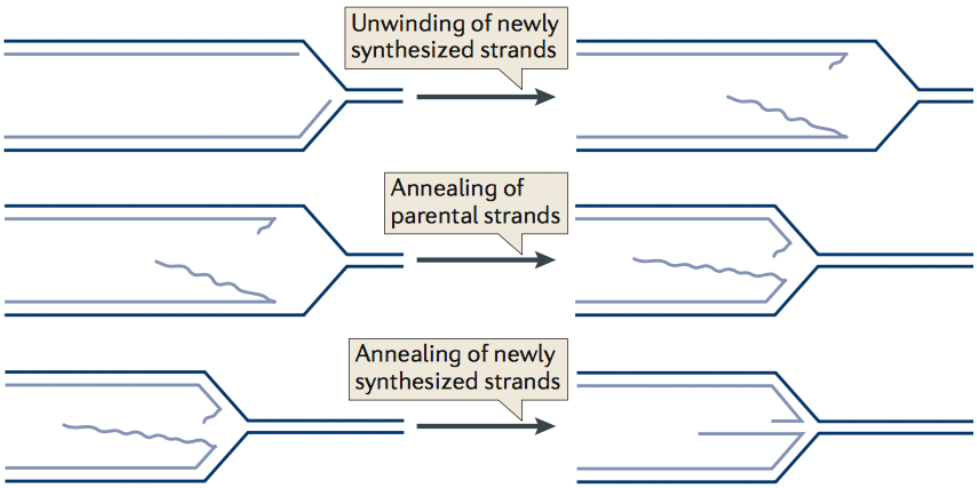

Figure 6: Schematic overview of replication fork reversal. In a first step, the newly synthesized strands (light blue) are separated from the parental strands (dark blue). Then the parental strands as well as the nascent strands reanneal. Modified from (119).

1.2.5 DNA2 in the telomere maintenance

The linear nature of eukaryotic chromosomes causes challenges at its ends, the telomeres. Replication at telomeres faces several difficulties, for example repetitive TTAGGG sequences forming so called G-quadruplex (G4) structures that are difficult to replicate or the replication of the lagging strand at telomeres, where the “last” Okazaki fragment cannot be synthesized (127, 128). This effect could lead to telomere shortening. To avoid the loss of genetic information, the telomeres are elongated by a telomerase (129). The telomeres can then function as template for the priming of new Okazaki fragments. DNA2 localizes to telomeres as shown by immunofluorescence experiments (61, 77). G4 structures are expected to block replication fork progression and stall replication and therefore need to be removed to allow proper replication of telomeres. Various helicases including RTEL1, BLM, WRN and RECQL4 are expected to reduce the formation of such structures (130, 131). hDNA2 was shown to act in a nuclease-dependent way to resolve G4 structures and therefore allow efficient telomeric DNA replication (77). Shelterin complex consisting of several proteins, e.g. TRF1/TRF2, functions in suppressing ATM/ATR-mediated DNA damage response and therefore protects telomere ends from DNA repair activities (132). hDNA2 was shown to interact with TRF1/TRF2, suggesting a role for hDNA2 in telomere maintenance (77).

1.2.6 Human DNA2 in the mitochondrial DNA metabolism

hDNA2 localizes to the nucleus (133) and to the mitochondria (63, 133), where it interacts with Pol γ (DNA polymerase subunit gamma (63)). Pol γ is part of the mitochondrial DNA replication and the base excision repair (BER) machinery (134). It was proposed that hDNA2 helicase supports the mitochondrial replication by unwinding the DNA and providing a template for Pol γ (63). BER is considered to play an important role in the repair of oxidative DNA damage, since plenty of a cell's oxidative metabolism happens in the mitochondria (10). hDNA2 together with FEN1 was needed for the efficient removing of RNA primer flaps created during mitochondrial replication (63). Cells that were depleted of hDNA2 upon siRNA treatment showed higher oxidative damage burden in the mitochondria compared to control cells and the recovery rate of mitochondrial DNA was reduced in hDNA2 knockdown cells (63). Such effects were not observed testing the behavior of nuclear DNA after oxidative treatment. From these results, it is proposed that hDNA2 functions in the long-patch BER dealing with oxidative damage in the mitochondria (63). Most likely hDNA2 is involved together with Pol γ and FEN1 in the replication and repair of mitochondrial DNA (63, 135).

1.2.7 DNA2 in the checkpoint activation

The transition from the one cell cycle phase to the subsequent one is strictly regulated by several checkpoints (136). Yeast Tel1 (human ATM) responding to dsDNA breaks and yeast Mec1 (human ATR) sensing ssDNA coated by RPA are the main kinases to activate checkpoints upon DNA damage (137).

The function of the S-phase checkpoint is to avoid that a cell progresses to the G2/M phase before proper DNA replication and repair is completed (138). Mec1 has a major role in the S-phase checkpoint while Tel1 contribution is minor. Depending on the cell cycle phase, the 9-1-1 complex, Dpb11 and yDna2 were shown to activate Mec1 in yeast cells (reviewed in (139)). yDna2 was reported to stimulate Mec1 upon hydroxyurea (HU) treatment that leads to the stalling of replication forks and accumulation off ssDNA (140). This function of yDna2 seems more likely to be structural than enzymatic since it did not require the nuclease or

helicase activity of yDna2. However, the N-terminal domain (NTD), lacking in the human protein, was essential for this function. Further, mutations in the NTD abolished the checkpoint activation (140).

Dna2 is phosphorylated at serine 220 by $Cds1^{Chk1}$ in *Schizosaccharomyces pombe* becoming an S-phase checkpoint target itself. Upon phosphorylation Dna2 was active in preventing the reversal of stalled replication forks. The nuclease but not helicase activity was required to prevent the generation of "chicken foot" structures, while the exact mechanisms of these processes are still a matter of debate (64).

1.3.1 WRN and BLM

Human cells possess five RecQ like helicases, namely RECQ1, BLM, WRN, RECQ4 and RECQ5 all of which playing important roles in the genome maintenance (141-143). Mutations in WRN can cause a disease named Werner syndrome (WS). WS patients usually grow up normally until puberty and then show premature aging and susceptibility to rare types of cancer (144-147). Mutations in BLM can cause Bloom syndrome (BS). BS patients suffer from pre- and post-natal growth retardation leading to dwarfism and show early development of cancer (148).

Human RECQ helicases belong to the SF2 helicase superfamily per the classification of helicases (149, 150). Although the different RecQ helicases vary in size and domain structure, most of them share the highly conserved domains (151): the core helicase domain, the RecQ C-terminal domain and the helicase and RNase D-like C-terminal (HRDC) domain (143). The HRDC is found in *E. coli* RecQ and yeast Sgs1 as well as in human BLM and WRN but not in the other human RecQ helicases (Figure 7; (143, 152, 153)) pointing towards a specialized role. The HRDC domain is important to localize WRN and BLM to damaged DNA (154-156). Both BLM and WRN are 3'-5' helicases (144, 157). WRN is linked to BER, for example due to its stimulation of NEIL1 glycosylase (158) or inhibition of APE1 glycosylase (159). Further, WRN can stimulate Polβ (160) and WRN's exonuclease activity could act as proofreading mechanism that is intrinsically missing in Polβ (161). WRN interacts with components of the NHEJ machinery such as Ku70/80 (162, 163) or DNA-PK_{CS} (164).

Moreover, WS cells are sensitive to IR-induced DSBs (164). However, the contribution of WRN to NHEJ is not well understood. In the past, BLM was suggested as the main helicase important for HR via its role in DNA end resection. BLM was shown to enhance the affinity of EXO1 to DNA ends (113) and to interact with hDNA2 stimulating DNA end resection (113) in contrast to WRN, where such behaviour was not observed. However, more recent data contradict with these findings and suggest a role for WRN in DNA end resection (65, 116, 165), which will be further extended in my thesis. Physical interactions between BLM and WRN with hDNA2 were reported in addition to functional interactions (113, 116). WRN and BLM show pro-recombinational properties due to their function in DNA end resection. On the other hand, however, BLM was linked with anti-recombinational activity by disrupting RAD51 nucleoprotein filaments (166, 167), while such effects were not observed for WRN (168). In the later steps of HR, Both WRN and BLM were shown to interact with HJ/double HJ and could branch migrate or even dissolve them (BLM with TopoIIIα/RMI1/RMI2, (117, 169-171)). In addition to their contribution to DNA repair human RECQ helicases are proposed to have roles in DNA replication. Replication appears to be slower in cells from WS and BS patients, since these cells show a longer S-phase (172, 173) and DNA fiber analysis of such cells support the notion that defects in WRN or BLM reduces the replication fork progression rate (174, 175). WRN and BLM were suggested to help restart regressed replication forks via branch migration activity (176-178). Furthermore, BLM and WRN are suggested to participate in Okazaki fragment maturation due to their interaction with FEN1 (179-182), but a detailed model is lacking.

Finally, it was shown that RECQ1 could help to restart regressed replication forks (126) that were reversed upon CPT-induced Topoisomerase I inhibition (120). This function of RECQ1 is regulated by PARP1 preventing premature fork restart (126). Since CPT and other topoisomerase inhibitors are used as cancer treatment, interfering with DNA replication restart mechanism could lead to a beneficial effect for the patients. Interestingly, synthetic lethality was observed using topoisomerase inhibitors in WRN-depleted cells (183-185).

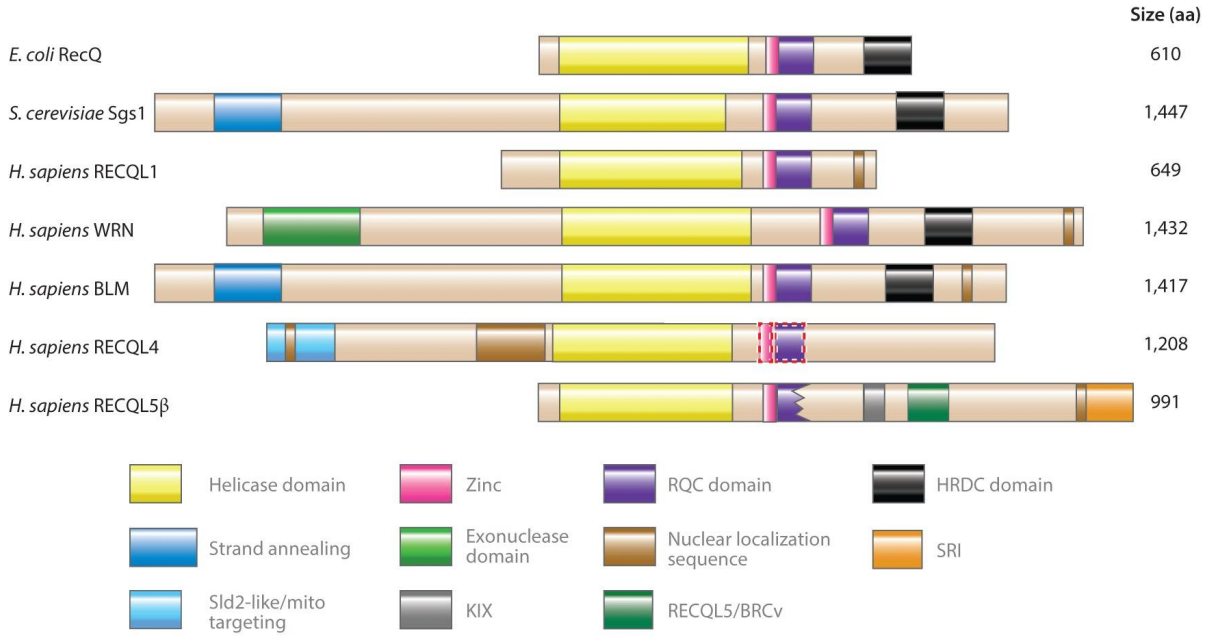

Figure 7: Schematic overview of the domain structure of RecQ helicases from *E. coli, S. cerevisiae* and *H. sapiens*. The RecQ helicases differ in size and structure but partially share several domains such as the helicase domain and the RQC domain. The HRDC domain is found in *E. coli* RecQ, yeast Sgs1 and human WRN and BLM. Modified from (143)

2. RESULTS

2.1 Summary of results

My work started with optimizing the expression and purification of the human DNA2 enzyme. I could purify highly active and pure wild type, nuclease-, helicase- and nuclease-helicase-deficient variants of hDNA2 by applying biochemical strategies that helped to improve the purification. These strategies included codon-optimization of the hDNA2 gene (for the expression in *Sf9* cells), working under reducing conditions to prevent oxidation of hDNA2's iron-sulfur cluster, as well as shortening the purification procedure. Further, I purified WRN and BLM helicases plus their enzymatically-inactive forms and several single-strand DNA binding proteins (RPA, human mitochondrial SSB, SOSS complex). Together, these recombinant proteins gave a solid base for studying the contribution of hDNA2 in DNA metabolism.

I could recapitulate that hDNA2 possesses a nuclease activity that is regulated by SSBs. My work showed that hDNA2 is a strong and processive helicase, although this helicase activity is masked by its nuclease activity. I showed that hDNA2 synergies with WRN/BLM to resect dsDNA, and observed that DNA2 stimulates BLM/WRN activities and vice versa. This indicated that hDNA2-BLM and hDNA2-WRN form a functional integrated complex (see 2.2.1 (186)).

We proposed that the hDNA2 motor activity however functions more likely as a ssDNA translocase than as a DNA unwinding enzyme. The translocase activity accelerates the degradation of ssDNA by wild type hDNA2, which results from dsDNA unwinding by BLM/WRN. Thus, DNA2 does not rely on diffusion to degrade ssDNA, but it is using its motor activity to facilitate ssDNA resection. Such ssDNA degradation capacity was enhanced by the presence of WRN/BLM in the reactions (see 2.2.2, (187)). These data fit very well to the *in vivo* evidence from our collaborators showing that DNA2 cooperate with WRN or BLM helicase in the long-range DNA end resection in human cell lines (see 2.3.3, (116)). Together, our data support a model for DNA end resection in which WRN and BLM can act as lead helicases opening dsDNA leading to ssDNA that is covered by RPA. RPA confers the degradation of the 5' terminated ssDNA strand by hDNA2, which is exploiting the interplay

of motor and nuclease activities to efficiently degrade 5'-terminated DNA. This establishes a 3’ overhanged DNA molecule that is needed for HR.

Additionally, in a collaborative project we showed that DNA2 and WRN function together in the restart of stalled replication forks upon replication stress-induced reversal (see 2.3.2, (65)).Also, we helped define the dsDNA melting activity of human RPA in biochemical assay setups and followed up the behaviour and dynamics of RPA at DNA forks (see 2.3.1, (188)).

2.2 Primary results

2.2.1 Human DNA2 possesses a cryptic DNA unwinding activity that functionally integrates with BLM or WRN helicases

Cosimo Pinto, Kristina Kasaciunaite, Ralf Seidel and Petr Cejka

The article was published in eLIFE 2016; 5: e18574.

I designed the research together with R. S and P. C. and performed most of the experiments. The single molecule experiments in Figure 4 and Figure 4—figure supplement 1 were performed by K. K. All authors analysed the data and I wrote the manuscript together with R. S. and P. C.

eLIFE elifesciences.org

RESEARCH ARTICLE

Human DNA2 possesses a cryptic DNA unwinding activity that functionally integrates with BLM or WRN helicases

Cosimo Pinto[1], Kristina Kasaciunaite[2], Ralf Seidel[2], Petr Cejka[1]*

[1]Institute of Molecular Cancer Research, University of Zurich, Zurich, Switzerland; [2]Institute of Experimental Physics I, University of Leipzig, Leipzig, Germany

Abstract Human DNA2 (hDNA2) contains both a helicase and a nuclease domain within the same polypeptide. The nuclease of hDNA2 is involved in a variety of DNA metabolic processes. Little is known about the role of the hDNA2 helicase. Using bulk and single-molecule approaches, we show that hDNA2 is a processive helicase capable of unwinding kilobases of dsDNA in length. The nuclease activity prevents the engagement of the helicase by competing for the same substrate, hence prominent DNA unwinding by hDNA2 alone can only be observed using the nuclease-deficient variant. We show that the helicase of hDNA2 functionally integrates with BLM or WRN helicases to promote dsDNA degradation by forming a heterodimeric molecular machine. This collectively suggests that the hDNA2 motor promotes the enzyme's capacity to degrade dsDNA in conjunction with BLM or WRN and thus promote the repair of broken DNA.
DOI: 10.7554/eLife.18574.001

***For correspondence:** cejka@imcr.uzh.ch

Competing interests: The authors declare that no competing interests exist.

Funding: See page 21

Received: 07 June 2016
Accepted: 08 September 2016
Published: 09 September 2016

Reviewing editor: Antoine M van Oijen, University of Wollongong, Australia

Introduction

DNA replication, repair and recombination require the function of multiple DNA helicases and nucleases (***Tsutakawa et al., 2014***; ***Wu and Hickson, 2006***). The DNA replication ATP-dependent helicase/nuclease 2 (DNA2) is an enzyme that contains both helicase and nuclease domains within the same polypeptide (***Bae et al., 1998***), and has important functions in a variety of DNA metabolic processes. Dna2 was first described in *Saccharomyces cerevisiae* where it is required for DNA replication under unperturbed conditions (***Budd and Campbell, 1995***; ***Kuo et al., 1983***). Specifically, during Okazaki fragment processing, yeast Dna2 (yDna2) cleaves long 5'-flaps that are coated by the Replication Protein A (RPA) and are therefore refractory to cleavage by Rad27 (FEN1) (***Bae et al., 2001***; ***Levikova and Cejka, 2015***). Moreover, yDna2 is one of the nucleases that resect 5'-terminated strands of DNA double-strand breaks (DSBs) (***Cejka et al., 2010***; ***Niu et al., 2010***; ***Zhu et al., 2008***). This process leads to the formation of 3'-tailed DNA, which becomes a substrate for the strand exchange protein Rad51 to initiate homology search and accurate DSB repair by the recombination machinery (***Cejka, 2015***; ***Heyer et al., 2010***; ***Symington, 2014***). Yeast Dna2 also functions upon replication stress to degrades structures such as reversed replication forks (***Hu et al., 2012***; ***Thangavel et al., 2015***) and has a structural role in DNA damage signaling, where it is a component in one out of three signaling branches that activate the Mec1 kinase in response to ssDNA in S-phase (***Kumar and Burgers, 2013***). Additionally, yDna2 was described to be required for the proper function of telomeres (***Choe et al., 2002***). In contrast to Okazaki fragment processing and DNA end resection, the involvement of yDna2 in these latter DNA metabolic processes is poorly understood. The yeast Dna2 protein contains a large unstructured N-terminal domain, which mediates a physical interaction with yRPA (***Bae et al., 2003***), is required for Dna2's checkpoint function (***Kumar and Burgers, 2013***) and its capacity to melt secondary structures within 5' DNA flaps (***Lee et al., 2013***). The N-terminal domain is followed by a RecB-like nuclease domain

(*Budd et al., 2000*) and a Superfamily I helicase domain in the C-terminal part of the polypeptide (*Budd and Campbell, 1995*). With the exception of checkpoint signaling, all Dna2 functions are exclusively dependent on its nuclease activity (*Sturzenegger et al., 2014*; *Thangavel et al., 2015*; *Wanrooij and Burgers, 2015*; *Zhu et al., 2008*). Dna2 homologs are present in all eukaryotic organisms including human cells (*Budd and Campbell, 1995*; *Eki et al., 1996*; *Gould et al., 1998*). Both helicase and nuclease domains are well conserved in evolution, but the unstructured N-terminal domain is only present in lower eukaryotes (*Bae et al., 1998*; *Kang et al., 2010*; *Wanrooij and Burgers, 2015*).

Human DNA2 (hDNA2) also functions in DNA end resection (*Gravel et al., 2008*; *Nimonkar et al., 2011*; *Sturzenegger et al., 2014*) and in the processing of non-canonical DNA replication structures, such as reversed replication forks upon replication stress (*Duxin et al., 2012*; *Thangavel et al., 2015*). In contrast to yeast, however, hDNA2 appears to be dispensable for the processing of most Okazaki fragments (*Duxin et al., 2012*). Specific inactivation of the nuclease, as well as the depletion or knockout of the protein/gene, result in lethal phenotypes in all organisms tested to date (*Budd et al., 2000*; *Duxin et al., 2012*; *Kang et al., 2000*; *Lin et al., 2013*). In yeast, this has been ascribed to yDna2's role in Okazaki fragment processing (*Kang et al., 2010*). Human DNA2-depleted cells arrest at late S/G2 phase of the cell cycle (*Duxin et al., 2012*). The nature of DNA intermediates that require the processing by hDNA2 is still rather elusive. It is conceivable that the lethality of hDNA2-depleted cells results from the failure to process reversed replication forks or other aberrant structures that arise during replication stress even in the absence of treatment with genotoxic drugs (*Duxin et al., 2012*; *Thangavel et al., 2015*). The role of hDNA2 in DSB end resection in contrast does not appear to be essential for viability as it functions redundantly with another nuclease, Exonuclease 1 (EXO1) (*Gravel et al., 2008*; *Nimonkar et al., 2011*; *Tomimatsu et al., 2012*). EXO1 is not involved in the processing of reversed replication forks, pointing towards an essential function of hDNA2 in the response to intermediates arising during DNA replication (*Thangavel et al., 2015*).

The nuclease of hDNA2 is specific for ssDNA (*Kim et al., 2006*; *Masuda-Sasa et al., 2006*) and therefore requires an associated helicase activity to resect/degrade dsDNA. This was shown to be either BLM or WRN during DSB end resection (*Gravel et al., 2008*; *Nimonkar et al., 2011*; *Sturzenegger et al., 2014*), or primarily WRN to degrade non-canonical DNA structures arising during DNA replication (*Thangavel et al., 2015*). Interestingly, the inherent helicase of hDNA2 was not required for these processes (*Sturzenegger et al., 2014*; *Thangavel et al., 2015*), and the function of the hDNA2 motor activity remains unclear. The helicase function is not essential for viability in yeast (*Bae et al., 2002*), where it was proposed to unwind secondary structures forming on long flaps at the 5' ends of Okazaki fragments (*Lee et al., 2013*). Yeast *dna2* cells lacking the helicase activity are dramatically sensitive to alkylating agents such as methyl methanesulfonate (MMS) (*Budd and Campbell, 1995*), suggesting that the yDna2 helicase might also play a role in the response to replication stress. In contrast to yeast, both helicase and nuclease functions are essential for viability in human cells (*Duxin et al., 2012*). Similarly to hDNA2 nuclease-deficient cells, hDNA2 helicase-deficient cells also exhibit a terminal S/G2 cell cycle arrest, most likely due to the inability to resolve structures arising in S-phase (*Duxin et al., 2012*). Furthermore, hDNA2 nuclease-deficient cells displayed cell cycle defects that were even more severe than upon depletion of hDNA2; interestingly, this phenotype was dependent on the integrity of the Walker A motif within the helicase domain (*Duxin et al., 2012*). This suggested that the hDNA2 helicase performs essential functions during DNA replication, yet it becomes toxic in the absence of the nuclease (*Duxin et al., 2012*), although mechanistic insights into the interplay between both activities have been lacking. Therefore, it remains to be determined how the hDNA2 helicase contributes to the overall function of the polypeptide.

The clear requirement for the helicase of hDNA2 for the viability of human cells (*Duxin et al., 2012*) stands in contrast to the inconclusive reports regarding the capacity of the human recombinant hDNA2 polypeptide to unwind dsDNA. One work concluded that hDNA2 lacks a helicase activity (*Kim et al., 2006*), whereas another study could detect DNA unwinding, albeit very weak and distributive (*Masuda-Sasa et al., 2006*). It has been also proposed that the helicase domain may be more responsible for DNA binding rather than as a motor activity per se (*Zhou et al., 2015*). Here we present that hDNA2 possesses a processive helicase activity capable of unwinding dsDNA of several kilobases in length. Paradoxically, the helicase is cryptic and becomes detectable only upon

inactivation of the nuclease. This explains the more pronounced phenotypes of the hDNA2 nuclease-deficient cells as opposed to double nuclease- and helicase-deficient cells or depletions of the polypeptide (**Duxin et al., 2012**). Finally, we show that the helicase of hDNA2 contributes to dsDNA degradation in complex with Bloom syndrome protein (BLM) or Werner syndrome protein (WRN) helicases, and may play a supporting role in the resection of DSBs or other aberrant structures arising during DNA replication. The motor activities within hDNA2 and BLM/WRN function in a synergistic manner, and the stimulatory effect observed with the hDNA2-WRN and hDNA2-BLM pairs is highly specific. This shows that the hDNA2-BLM and hDNA2-WRN complexes are functionally more integrated molecular machines than previously thought.

Results

Expression and purification of human DNA2

Human DNA2 was prepared using a construct, which contained an N-terminal 6x-histidine and a C-terminal FLAG affinity tags (**Figure 1A**). The sequence of hDNA2 was codon-optimized (**Supplementary file 1A**) for the expression in *Spodoptera frugiperda 9 (Sf9)* cells, which improved the yield ~2–3 fold (data not shown). Considering that hDNA2 contains an iron-sulfur cluster (**Pokharel and Campbell, 2012**; **Yeeles et al., 2009**), all buffers were degassed and contained reducing agents throughout the preparation procedure to prevent oxidation of the cluster, as described previously for *S. cerevisiae* Dna2 (**Levikova et al., 2013**). Wild type hDNA2, nuclease-deficient D277A, helicase-deficient K654R as well as nuclease- and helicase-deficient D277A K654R variants were purified in the same manner to near homogeneity (**Figure 1B** and **Figure 1—figure supplement 1A–C**). The yield of the recombinant proteins was ~330–390 µg from 3 liters of *Sf9* cell culture except for the variant containing the K654R mutation, which yielded only ~27 µg.

hDNA2 preferentially degrades 5′-tailed DNA in the presence of RPA

Human DNA2 is known to possess ssDNA-specific nuclease activity (**Kim et al., 2006**; **Masuda-Sasa et al., 2006**). Considering that hDNA2 performs multiple functions during DNA metabolism, we set out to analyze the preference of its nuclease activity using various oligonucleotide-based DNA structures. Without the human Replication Protein A (hRPA), hDNA2 most efficiently degraded ssDNA, while 5′-overhanged, 3′-overhanged and Y-structured DNA were degraded ~7–20-fold less efficiently, based on the hDNA2 concentration required for the degradation of 50% DNA substrate (**Figure 1C** and **Figure 1—figure supplement 1D**). In contrast, dsDNA was largely refractory to cleavage (**Figure 1C** and **Figure 1—figure supplement 1D**), in agreement with the observations that hDNA2 needs a helicase partner in DNA end resection to initiate homologous recombination (**Cejka et al., 2010**; **Gravel et al., 2008**; **Nimonkar et al., 2011**; **Sturzenegger et al., 2014**; **Zhu et al., 2008**). As reported previously (**Masuda-Sasa et al., 2006**), the helicase-deficient hDNA2 (K654R) variant displayed a nuclease activity indistinguishable from that of the wild type enzyme on a 5′-tailed DNA substrate (**Figure 1—figure supplement 1D–F**). Using a 3′-end labeled ssDNA, we observed that hRPA directs the nuclease of hDNA2 towards the 5′ terminus; while at the same time inhibits the 3′-5′ nuclease activity (**Figure 1D**). This is in agreement with previous observations in various organisms (**Cejka et al., 2010**; **Nimonkar et al., 2011**; **Zhou et al., 2015**) and explains how hRPA enforces the correct polarity of DNA degradation during DNA end resection. Interestingly, in the presence of hRPA, hDNA2 most efficiently cleaved Y-structured and 5′-tailed DNA substrates, which were degraded ~5–10-fold more efficiently than ssDNA (**Figure 1E** and **Figure 1—figure supplement 1G**). In summary, the nuclease activities of yeast Dna2 and human DNA2 are very similar qualitatively, but human DNA2 appears somewhat less active (~2-fold in degradation of 5′-tailed DNA) than its yeast homologue (**Levikova et al., 2013**).

The nuclease-deficient hDNA2 D277A was subsequently used to determine DNA binding preference. hDNA2 D277A strongly bound ssDNA, with K_D ~2 nM for ssDNA of 50 nucleotides in length (**Figure 1F,G**). Similar binding affinity was observed for Y-structured DNA, while the apparent DNA binding to 5′ and 3′-tailed structures was reduced ~8–12-fold, respectively, compared to ssDNA. In contrast, dsDNA was bound very poorly (**Figure 1G** and **Figure 1—figure supplement 2A–D**). Further experiments revealed that the DNA binding affinity was determined by the length of ssDNA rather than the specific structure (**Figure 1H,I** and **Figure 1—figure supplement 2A–F**).

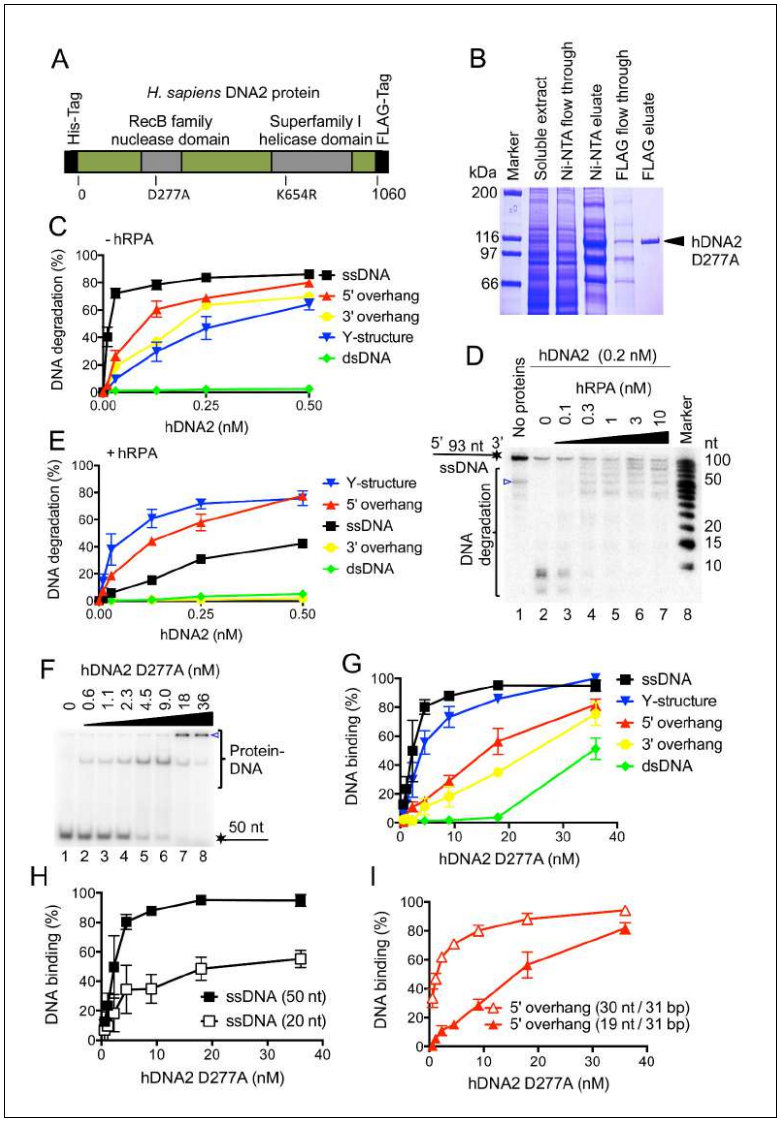

Figure 1. Human DNA2 preferentially binds and degrades 5′ terminated ssDNA. (**A**) A schematic representation of the recombinant hDNA2 protein used in this study. The polypeptide contains an N-terminal 6xHis- and a C-terminal FLAG affinity tag. The positions of the mutations inactivating the nuclease (D277A) activity or the helicase (K654R) activity are indicated. (**B**) A 10% polyacrylamide gel stained with Coomassie blue showing fractions from a representative purification of hDNA2 D277A. (**C**) Quantitation of hDNA2 nuclease activity on various DNA substrates in the absence of hRPA from experiments such as shown in ***Figure 1—figure supplement 1D***. Averages shown, n = 2; error bars, SEM. (**D**) Human DNA2 (0.2 nM) was incubated with ssDNA ^{32}P-labeled at

Figure 1 continued on next page

Figure 1 continued

its 3′ end and various concentrations of hRPA. The panel shows a representative denaturing 20% polyacrylamide gel. The blue triangle indicates a truncation of the substrate. (**E**) Quantitation of hDNA2 nuclease activity on various DNA substrates in the presence of hRPA (15 nM) from experiments such as shown in ***Figure 1—figure supplement 1G***. Averages shown, n = 2; error bars, SEM. (**F**) A representative 6% polyacrylamide gel showing the binding of hDNA2 D277A to ssDNA of 50 nt in length. The blue triangle indicates the position of the wells. (**G**) Quantitation of DNA binding from experiments such as shown in ***Figure 1F*** and ***Figure 1—figure supplement 2A–D***. Averages shown, n = 2–3; error bars, SEM. (**H**) DNA binding and its dependence on the length of ssDNA. Quantitation is based on experiments such as shown in ***Figure 1F*** and ***Figure 1—figure supplement 2E***. Long ssDNA was more efficiently bound by hDNA2. Averages shown, n = 2–3, error bars, SEM. (**I**) DNA binding and its dependence on the length of 5′ single-stranded DNA overhang. Quantitation is based on experiments such as shown in ***Figure 1—figure supplement 2B,F***. Averages shown, n = 3; error bars, SEM.

DOI: 10.7554/eLife.18574.002

The following figure supplements are available for figure 1:

Figure supplement 1. Human RPA guides the hDNA2 nuclease to 5′ terminated ssDNA.

DOI: 10.7554/eLife.18574.003

Figure supplement 2. hDNA2 binds ssDNA.

DOI: 10.7554/eLife.18574.004

Interestingly, the hDNA2-bound DNA species either entered the polyacrylamide gels during electrophoresis, or remained stuck in the wells, indicative of a multiprotein-DNA complex and most likely a non-specific aggregate. Remarkably, the distinct DNA-protein species that entered the polyacrylamide gel were only observed with substrates containing a free 5′ end such as Y-structured, 5′ tailed or ssDNA substrates (***Figure 1F*** and ***Figure 1—figure supplement 2A,B,F***), suggesting that hDNA2 exhibits a preference for this structure even in the absence of hRPA. This likely reflects its role in 5′ DNA end degradation in various metabolic processes (***Kang et al., 2010***; ***Nimonkar et al., 2011***; ***Sturzenegger et al., 2014***; ***Zheng et al., 2008***).

hDNA2 shows DNA structure-dependent ATPase activity

Previous reports concluded that hDNA2 hydrolyses ATP, as expected from a protein containing an SFI helicase domain (***Budd and Campbell, 1995***). We next determined the ATP hydrolysis rate of nuclease-deficient hDNA2 D277A in the presence of various DNA structures. The ATPase activity was strongly enhanced in the presence the DNA cofactors. The greatest stimulation, ~13-fold, was observed with 5′-tailed DNA (***Figure 2A***), in agreement with the 5′-3′ polarity of the hDNA2 helicase (***Balakrishnan et al., 2010a***; ***Balakrishnan et al., 2010b***; ***Masuda-Sasa et al., 2006***). The apparent turnover rate (k_{cat}) of the ATP hydrolysis in the presence of 5′-tailed substrates of different lengths was 6.9 ± 1.1 s^{-1} and 6.2 ± 0.9 s^{-1}. In contrast, dsDNA stimulated the hDNA2 ATPase to the lowest extent, ~four-fold, compared to reactions without DNA. Next we performed the ATPase assays in the presence of various amounts of poly(dT) DNA, which is a ssDNA devoid of any secondary structure. As expected, the ATP hydrolysis rate increased with poly(dT) concentration. The measured reaction rate values were fitted into a Michaelis-Menten curve with V_{max} = 3.1 ± 0.3 μM·min^{-1} and K_M = 115 ± 45 nM (in nucleotides, ***Figure 2B***), which corresponds to k_{cat} = 4.3 ± 0.4 s^{-1}. The nuclease-deficient DNA2 D277A variant was used for the above assays, as the nuclease of wild type DNA2 interferes with its capacity to hydrolyze ATP by degrading DNA that serves as a co-factor of the ATPase activity. As demonstrated in ***Figure 2C***, the rate of ATP hydrolysis by the nuclease-deficient D277A variant incubated with 5′-tailed substrate was constant over time. In contrast the rate of ATP consumption decreased quickly in case of wild type DNA2 (***Figure 2C***). We believe that the nuclease activity of hDNA2 rapidly degrades the 5′ ssDNA overhang, producing a substrate that is less efficient as a cofactor for the ATPase activity. Very similar behavior was previously observed with yeast Dna2 (***Levikova et al., 2013***). Collectively, these experiments establish that the ATPase activity of hDNA2 qualitatively resembles that of the yeast Dna2 homologue in terms of DNA substrate preference and interplay with the nuclease activity, but it is ~10-fold less active in quantitative terms (***Levikova et al., 2013***).

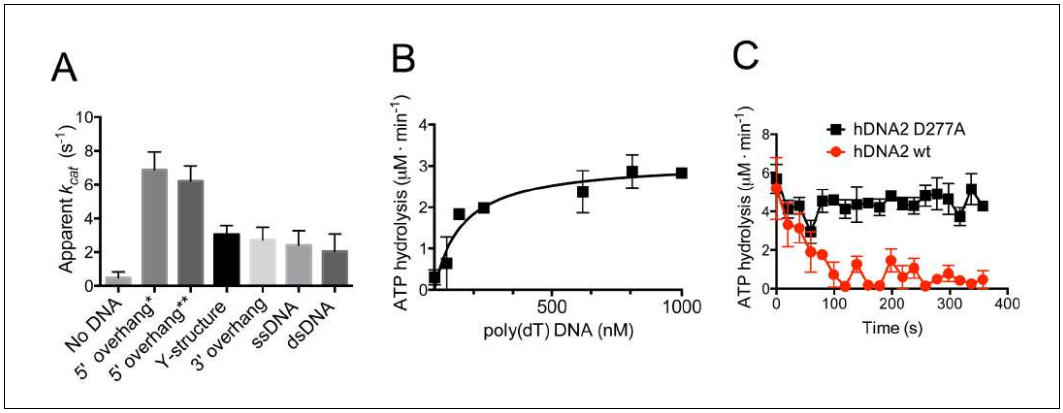

Figure 2. hDNA2 D277A shows DNA structure-dependent ATPase activity. (**A**) Apparent ATP turnover number k_{cat} with various DNA cofactors, including short 5′ overhang* (19 nt/31 bp), long 5′ overhang** (30 nt/31 bp), Y-structure (19 nt/ 31 bp), 3′ overhang (19 nt/ 31 bp), ssDNA (50 nt), dsDNA (31 bp). The reactions contained 12 nM hDNA2 D277A. Averages shown, n = 2–8; error bars, SEM. (**B**) Rate of ATP hydrolysis and its dependence on the DNA substrate concentration. The reactions contained 12 nM hDNA2 D277A and the indicated concentrations of poly(dT) DNA. Averages shown, n = 2; error bars, SEM. (**C**) Wild type hDNA2 or the D277A variant (both 12 nM) was incubated with 5′ overhang DNA substrate and the rate of ATP hydrolysis was determined over time. The ATP hydrolysis rate was constant at ~4–5 μM·min^{-1} for hDNA2 D277A and decreased over time for wild type hDNA2. Averages shown, n = 3; error bars, SEM.

DOI: 10.7554/eLife.18574.005

The helicase of hDNA2 is capable to unwind plasmid-length dsDNA substrates

The capacity to unwind DNA by human DNA2 has been controversial. Previously, hDNA2's helicase activity was either described as undetectable (***Kim et al., 2006***) or very weak (***Balakrishnan et al., 2010a***; ***Masuda-Sasa et al., 2006***), capable to unwind only short duplexes. In our earlier studies, we could show that *S. cerevisiae* Dna2 possesses a vigorous and processive helicase activity that is masked by its nuclease activity (***Levikova et al., 2013***). To this point, we set out to test whether our preparation of hDNA2 is capable to unwind dsDNA. The nuclease-deficient hDNA2 D277A variant was used in these experiments, as the nuclease activity of wild type hDNA2 may mask its helicase activity similarly as for the yeast enzyme (***Levikova et al., 2013***). We incubated various concentrations of the hDNA2 D277A variant with bacteriophage λDNA that had been digested with HindIII, resulting in dsDNA fragments of various lengths. ***Figure 3A and B*** demonstrate that hDNA2 D277A efficiently unwound dsDNA fragments of up to 2.3 kbp in length, whereas unwinding of ≥9.4 kbp-long fragments was barely detectable within the 30 min incubation time. Unwinding of these long DNA molecules was however evident in kinetic experiments upon longer incubation times (***Figure 3C*** and ***Figure 3—figure supplement 1A***). This unexpected dsDNA unwinding capacity of hDNA2 D277A was fully dependent on hRPA and ATP (***Figure 3A***). The nuclease-deficient hDNA2 D277A variant also similarly unwound a 2.7 kbp-long plasmid-based dsDNA substrate in a concentration-dependent manner (***Figure 3D,E***). In contrast, the nuclease- and helicase-deficient DNA2 D277A K654R mutant did not unwind DNA, as expected, showing that the unwinding capacity is inherent to the helicase activity of hDNA2 (***Figure 3—figure supplement 1B***). The above assays require the use of a high hRPA concentration to fully saturate DNA (~200–350 nM range), which can lead to dsDNA melting in the vicinity of the ends (***Georgaki and Hübscher, 1993***; ***Kemmerich et al., 2016***). This might provide hDNA2 with ssDNA overhangs that are required for the unwinding activity. To define substrate preference for the hDNA2 D277A helicase, we next used a variety of oligonucleotide-based DNA structures. The hRPA concentration (7.5 nM) used in these assays did not result in a significant dsDNA melting. We found that the Y-structure was unwound most efficiently (***Figure 3F,G***), followed by the 5′ overhang (***Figure 3G*** and ***Figure 3—figure***

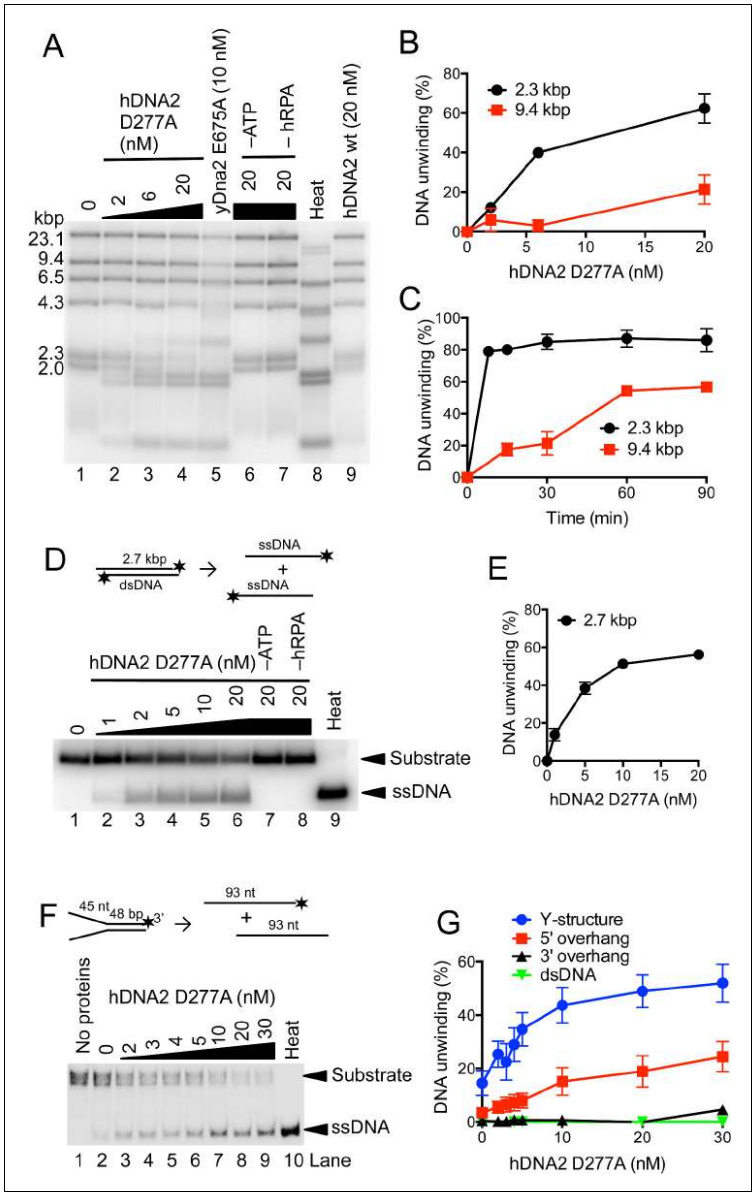

Figure 3. hDNA2 D277A unwinds kilobase-lengths of dsDNA. (**A**) Representative 1% agarose gel showing the helicase activity of hDNA2 D277A on λDNA/HindIII substrate with 346 nM hRPA. DNA unwinding leads to products that co-migrate with heat-denatured substrate (Lane 8). Lane 5, helicase activity of nuclease-deficient yeast Dna2 E675A at 30°C; Lane 6, no ATP; Lane 7, no RPA; Lane 8, heat-denatured DNA substrate; Lane 9, wild

Figure 3 continued on next page

Figure 3 continued

type hDNA2. (**B**) Unwinding of selected λDNA/HindIII fragments by various concentrations of hDNA2 D277A upon 30 min reaction time. Quantitation of experiments such as shown in ***Figure 3A***. Averages shown, n = 2–4; error bars, SEM. (**C**) Unwinding of selected λDNA/HindIII fragments by hDNA2 D277A (20 nM) and its dependence on reaction time. Quantitation of experiments such as shown in ***Figure 3—figure supplement 1A***. Averages shown, n = 2–4; error bars, SEM. (**D**) Representative 1% agarose gel showing the helicase activity of hDNA2 D277A on a 2.7 kbp-long substrate. Reactions contained 215 nM RPA. Heat, heat-denatured DNA substrate. (**E**) Quantitation of experiments such as shown in ***Figure 3D***. Averages shown, n = 4–9; error bars, SEM. (**F**) Representative 10% polyacrylamide gel showing the helicase activity of hDNA2 D277A on an oligonucleotide-based Y-structure (45 nt/ 48 bp). Reactions contained 7.5 nM RPA. Heat, heat-denatured DNA substrate. (**G**) Quantitation of experiments such as shown in ***Figure 3F*** and ***Figure 3—figure supplement 1C–E***. Beside Y-structure (45 nt/48 bp), DNA substrates with 5′ or 3′ overhangs (both 45 nt/ 48 bp) and blunt-ended dsDNA (50 bp) were tested. Reactions contained 7.5 nM RPA. Averages shown, n = 2–4; error bars, SEM. Heat, heat-denatured DNA substrate.

DOI: 10.7554/eLife.18574.006

The following figure supplement is available for figure 3:

Figure supplement 1. hDNA2 D277A unwinds plasmid- and oligonucleotide-based DNA substrates.

DOI: 10.7554/eLife.18574.007

supplement 1C). In contrast, no DNA unwinding was observed with 3′ overhang and dsDNA (***Figure 3G*** and ***Figure 3—figure supplement 1D,E***), in agreement with the 5′-3′ polarity of DNA unwinding by hDNA2 and its homologues (***Bae et al., 1998***).

Importantly, no dsDNA unwinding was observed with wild type hDNA2 (***Figure 3A***, lane 9). The hDNA2 nuclease is efficient in ssDNA degradation at sub-nanomolar concentrations (***Figure 1E***), and thus likely degrades the 5′ ssDNA overhangs that are required for the initiation of DNA unwinding. By degrading 5′-tailed DNA the nuclease of hDNA2 masks the helicase capacity of the wild type polypeptide, similarly as in yeast (***Levikova et al., 2013***). This is in agreement with a recent structural study, which determined that the nuclease of DNA2 is situated ahead of the helicase domain, and therefore has the capacity to degrade 5′-terminated ssDNA tails to prevent DNA loading of the helicase domain (***Zhou et al., 2015***). Our observation that the inactivation of the hDNA2 nuclease unleashes the hDNA2 helicase likely provides explanation for the pronounced toxicity of a nuclease-deficient hDNA2 construct *in vivo*, which was dependent on the integrity of the Walker A motif within hDNA2 (***Duxin et al., 2012***). In summary, we show that nuclease-deficient hDNA2 possesses the capacity to unwind dsDNA of kilobases in length in a reaction dependent on hRPA and ATP. Wild type hDNA2 is devoid of any apparent dsDNA unwinding activity, which likely infers the existence of mechanisms that allow the manifestation of the motor activity in the context of the wild type polypeptide under specific conditions.

DNA unwinding by hDNA2 D277A is slow but highly processive

DNA unwinding experiment with λDNA (***Figure 3A–C*** and ***Figure 3—figure supplement 1A***) showed that hDNA2 D277A can unwind long stretches of dsDNA. We next performed a kinetic experiment with a 2.7 kbp-long DNA substrate, and compared the DNA unwinding of the nuclease-deficient human DNA2 D277A and the yeast Dna2 E675A. As DNA2 cannot unwind DNA from internal sites and can only initiate from a free DNA end (***Balakrishnan et al., 2010a***; ***Zhou et al., 2015***), we used a 20-fold excess of each helicase over the substrate to saturate the DNA ends. We detected ssDNA after only one minute of the reaction with the yeast enzyme, whereas it took eight minutes to detect a similar amount of unwound DNA for the human DNA2 variant (***Figure 3—figure supplement 1F,G***). To better define the unwinding rate and processivity of the hDNA2 D277A helicase, we applied a single molecule unwinding assay based on magnetic tweezers. We used a 5′ tailed dsDNA substrate of 6.1 kbp in length, which was tethered at one end to the surface of a fluidic cell and at the other end to a magnetic bead. An externally applied magnetic field gradient allowed thus to hold the DNA in a stretched configuration. DNA unwinding (***Levikova et al., 2013***) was monitored by a change of the position of the magnetic bead as a result of different lengths of double- and single-stranded DNA (***Figure 4A***). We observed that hDNA2 unwound the dsDNA substrate slowly but consecutively over time (***Figure 4B***). Most of the DNA molecules underwent significant dsDNA unwinding of several kilobases in length, with some molecules showing unwinding of the full-length

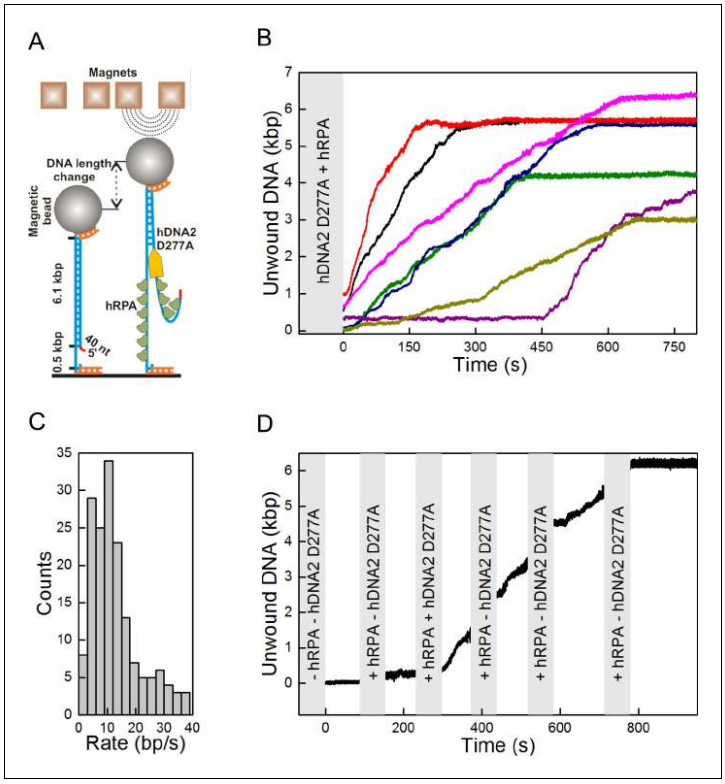

Figure 4. Single molecule experiments reveal highly processive DNA unwinding by hDNA2 D277A. (**A**) A sketch of the magnetic tweezers assay. (**B**) Representative DNA unwinding events (n = 7, colored) catalyzed by hDNA2 D277A at 22 ± 3 pN force. Experiments were conducted at 37°C in a reaction buffer supplemented with 25 nM hDNA2 D277A and 25 nM hRPA. DNA lengthening was observed only after the addition of hDNA2 D277A. (**C**) Histogram of the observed unwinding rates. Unwinding trajectories were divided into segments with approximately constant rate. The unwinding rates of the individual segments were determined from a linear fit of the data. (**D**) DNA unwinding experiment at 21 pN force, initiated by adding hRPA (25 nM) at 100 s and hDNA2 D277A (25 nM) at 220 s. The buffer containing hDNA2 D277A was washed away subsequently as indicated by the gray bars.

DOI: 10.7554/eLife.18574.008

The following figure supplement is available for figure 4:

Figure supplement 1. Single molecule experiments reveal that DNA unwinding by hDNA2 D277A is dependent on ATP and hRPA.

DOI: 10.7554/eLife.18574.009

6.1 kbp substrate. To quantify the unwinding rate, unwinding trajectories (n = 30) were split into successive segments that each had approximately a constant unwinding velocity. Unwinding rates were determined from the slope of a linear fit to each segment (***Figure 4C***). The unwinding rates were broadly distributed between 0 to 40 bp/s. Such a broad distribution is in agreement with measurements for yDna2 (***Levikova et al., 2013***). The distribution had a pronounced maximum at around 10 $bp{\cdot}s^{-1}$ and the mean unwinding rate was 12.8 ± 0.8 $bp{\cdot}s^{-1}$, which is ~3-fold slower than that of the yeast homologue (***Levikova et al., 2013***). Long-range processive dsDNA unwinding was dependent

on ATP and hRPA (***Figure 4—figure supplement 1A–D***), in agreement with the experiments shown above. To confirm that the observed dsDNA unwinding events resulted from the activity of a single hDNA2 D277A molecule, we performed an unwinding experiment similar that that in ***Figure 4B***, but flushed in ATP and hRPA containing buffer at regular intervals (***Figure 4D***) such that any free hDNA2 D277A was removed. DNA unwinding continued despite successive washing steps, indicating that the originally acting unwinding complex remained bound and active during the course of the observation period. This demonstrated that the DNA2 D277A helicase is highly processive (***Figure 4D***). The recently-published structure of DNA2 shows that ssDNA must feed through a narrow tunnel to reach the helicase domain (***Zhou et al., 2015***), which likely prevents dissociation of DNA2 from its substrate and corroborates the high processivity observed in our assays. In agreement with this no direction reversals during unwinding (i.e. rezipping) that could originate from strand–switches were observed (***Dessinges et al., 2004***; ***Klaue et al., 2013***).

Regulation of hDNA2 nuclease and helicase activities by single-stranded DNA binding proteins

The hRPA protein is a critical cofactor of the hDNA2 nuclease (***Figure 1***) as well as the helicase activities (***Figure 3***) (***Nimonkar et al., 2011***; ***Zhou et al., 2015***). We next set out to define the interplay of hDNA2 with other cognate ssDNA binding proteins. Initially, hDNA2 was described as a mitochondrial protein (***Zheng et al., 2008***) before its function in nuclear DNA metabolism was determined (***Duxin et al., 2009***; ***Gravel et al., 2008***). Mitochondria are devoid of hRPA; instead, they contain the mitochondrial single-stranded DNA binding protein (mtSSB), a homotetramer similar to the SSB protein of *Escherichia coli* (***Curth et al., 1994***). Furthermore, the sensor of single-stranded DNA (SOSS) complex was described in the nucleus of human cells (***Huang et al., 2009***; ***Li et al., 2009***). SOSS likely regulates various aspects of DNA metabolism including DNA recombination and DNA end resection by the MRE11-RAD50-NBS1 (MRN) complex and EXO1 (***Richard et al., 2011***; ***Yang et al., 2013***). We purified both mtSSB and SOSS and ascertained that both complexes bind ssDNA with a high affinity (***Figure 5—figure supplement 1A–D***). Next we investigated whether dsDNA unwinding by hDNA2 D277A can be promoted by mtSSB or the SOSS complex similarly as by hRPA. Neither mtSSB (***Figure 5A–C*** and ***Figure 5—figure supplement 1E***) nor SOSS (***Figure 5C*** and ***Figure 5—figure supplement 1E***) were able to substitute hRPA to promote dsDNA unwinding. The hDNA2-hRPA functional interaction was largely species-specific, as yRPA from *S. cerevisiae* promoted DNA unwinding to a much lesser extent than the cognate hRPA (***Figure 5A–C*** and ***Figure 5—figure supplement 1E***). Therefore, hRPA is a unique and an essential co-factor of the hDNA2 helicase, which is required for the unwinding of all DNA duplex substrate lengths tested.

In contrast to dsDNA unwinding, hRPA could be replaced by yRPA in ssDNA degradation, which similarly directed the nuclease activity of hDNA2 towards the 5′ end of ssDNA (***Figure 1D***, ***Figure 5D*** and ***Figure 5—figure supplement 1F***). Similar, albeit much weaker effect was observed in the presence of the SOSS complex (***Figure 5—figure supplement 1F***, lane 28), possibly due to a lower affinity of SOSS towards ssDNA compared to the RPA proteins. Considering the postulated function of the hDNA2 nuclease in mitochondrial DNA metabolism, the mtSSB unexpectedly dramatically inhibited all nuclease activities of hDNA2 (***Figure 5D*** and ***Figure 5—figure supplement 1F***). Therefore it remains to be elucidated how the hDNA2 nuclease/helicase functions in mitochondria.

The helicase of hDNA2 promotes DNA end resection in conjunction with WRN or BLM helicases

It has been established that hDNA2 functions in conjunction with a helicase partner in DNA end resection. Initially, it has been described that the cognate partner is BLM (***Gravel et al., 2008***; ***Nimonkar et al., 2011***). Later, it was demonstrated that also WRN could function in a redundant manner instead of BLM, or even be the sole helicase partner of hDNA2 during resection of reversed replication forks (***Sturzenegger et al., 2014***; ***Thangavel et al., 2015***). Having demonstrated that hDNA2 possesses a helicase activity, we wondered whether either BLM or WRN could stimulate hDNA2 or *vice versa*, i.e., whether the enzyme complex may form an integrated unit. To this point, we expressed wild type WRN and BLM helicases as well as their variants in *Sf9* insect cells and purified all polypeptides to near homogeneity (***Figure 6—figure supplement 1A–D***). We next monitored the resection of a 2.7 kbp-long dsDNA substrate. We selected wild type WRN and BLM

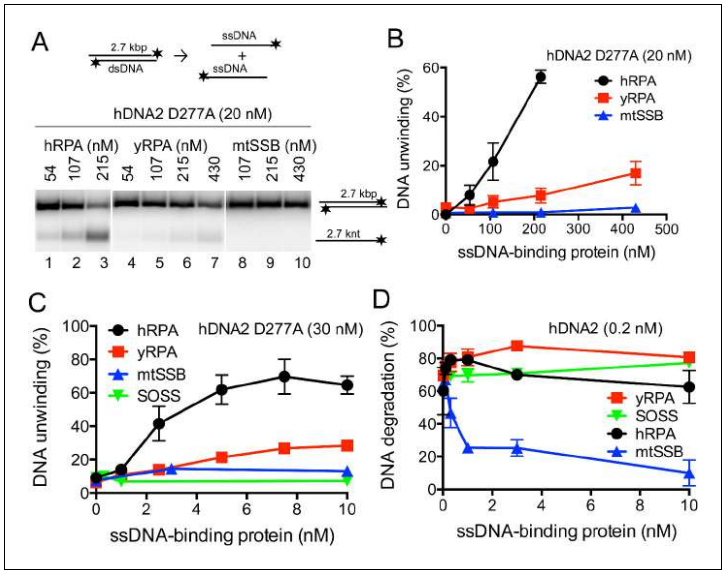

Figure 5. hDNA2 nuclease and helicase activities are regulated by ssDNA-binding proteins. (**A**) Representative 1% agarose gels showing the helicase activity of hDNA2 D277A supplemented with indicated ssDNA-binding proteins on a ^{32}P-labeled 2.7 kbp-long dsDNA substrate. (**B**) Quantitation of experiments such as shown in ***Figure 5A***. Averages shown, n = 3–9; error bars, SEM. (**C**) Quantitation of unwinding experiments with Y-structured oligonucleotide-based DNA such as shown in ***Figure 5—figure supplement 1E***. Averages shown, n = 2; error bars, SEM. (**D**) Quantitation of ssDNA degradation from experiments such as shown in ***Figure 1D*** and ***Figure 5—figure supplement 1F***. Averages shown, n = 2; error bars, SEM.

DOI: 10.7554/eLife.18574.010

The following figure supplement is available for figure 5:

Figure supplement 1. hDNA2 nuclease and helicase activities are regulated by ssDNA-binding proteins.

DOI: 10.7554/eLife.18574.011

concentrations that led to a partial unwinding of the substrate (***Figure 6A*** lane 2, ***Figure 6B***, lane 2). Titrating wild type or helicase-deficient (K654R) hDNA2 into these reactions led to the degradation of the unwound ssDNA, as expected. At the same time, the overall degradation of the dsDNA substrate increased as well (***Figure 6A–C***). Under the same conditions, hDNA2 did not degrade dsDNA without the helicase partner (***Figure 6A***, lane 11). This indicates a synergistic relationship between the two enzyme pairs, i.e. that dsDNA unwinding/degradation by the enzyme pair is up to six-fold higher than the sum of activities of the polypeptides acting individually (***Figure 6C***). Furthermore, wild type hDNA2 was more efficient in DNA degradation than its helicase-deficient variant, in particular together with the WRN helicase (***Figure 6A,C***). As shown above, both wild type and helicase-deficient hDNA2 variants had indistinguishable nuclease activity on 5'-labeled oligonucleotide based substrate (***Figure 1—figure supplement 1E,F***). We could observe a similar stimulatory effect when using a fixed concentration of hDNA2 and titrating either WRN or BLM helicases into the reactions (***Figure 6D,E,J***).

To this point, the experiments demonstrated that DNA degradation by hDNA2 was stimulated by a DNA helicase added in *trans*. To determine whether the stimulatory effect by WRN or BLM is specific for these two helicases, we tested if other human RecQ helicase family members could substitute WRN or BLM in the DNA end resection assays. We did not observe any enhancement of DNA degradation by hDNA2 upon adding either RecQ1 or RecQ5 helicases (***Figure 6—figure***

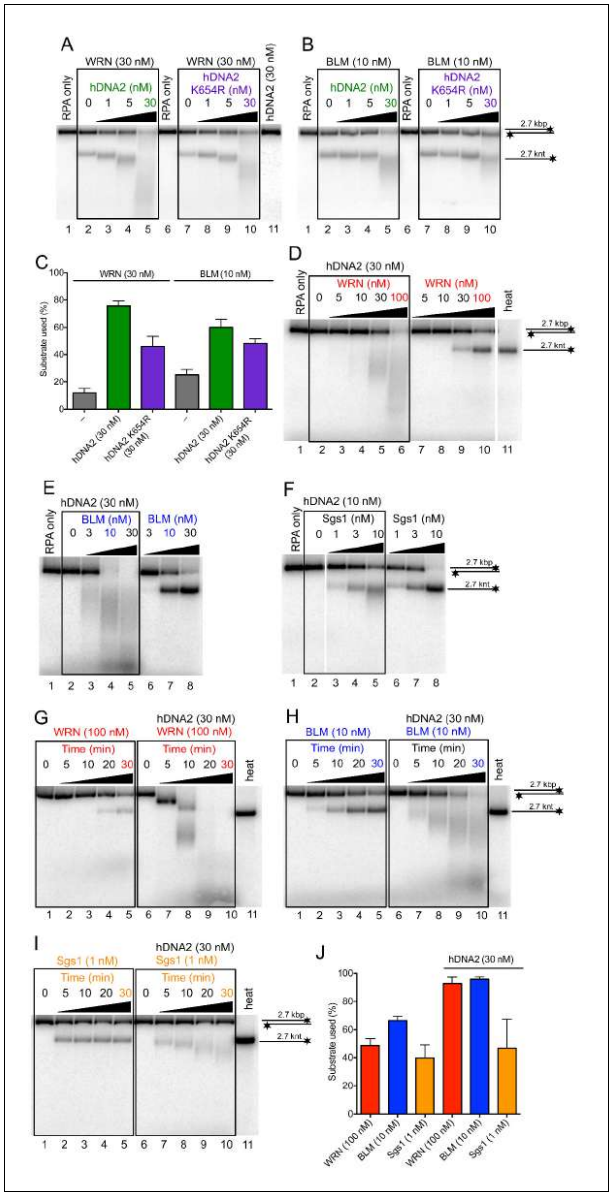

Figure 6. hDNA2 synergizes with WRN and BLM in the degradation of dsDNA. Representative 1% agarose gels showing dsDNA degradation by wild type or helicase-deficient hDNA2 K654R variant with (**A**) WRN or (**B**) BLM. The reactions were supplemented with 50 mM NaCl and 215 nM hRPA. (**C**) Quantitation of experiments such as shown in ***Figure 6A,B***. Averages shown, n = 4–6; error bars, SEM. Representative 1% agarose gels showing dsDNA processing by hDNA2 and (**D**) WRN, (**E**) BLM or (**F**) yeast Sgs1. The reactions were supplemented with 50 mM NaCl and 215 nM hRPA. Representative

Figure 6 continued on next page

Figure 6 continued

1% agarose gels showing the kinetics of dsDNA processing by hDNA2 and (**G**) WRN (**H**) BLM and (**I**) yeast Sgs1. The reactions were supplemented with 50 mM NaCl and 215 nM hRPA. (**J**) Quantitation of experiments such as shown in ***Figure 6D,E,G–I***. Averages shown, n = 3; error bars, SEM.

DOI: 10.7554/eLife.18574.012

The following figure supplement is available for figure 6:

Figure supplement 1. Purification of WRN and BLM proteins.

DOI: 10.7554/eLife.18574.013

supplement 1E). However, RecQ1 and RecQ5 did not show detectable unwinding of the 2.7 kbp-long dsDNA on their own. Therefore, we next used Sgs1, which shows a vigorous DNA helicase activity and functions in conjunction with yDna2 in resection (***Cejka et al., 2010***). Importantly, adding hDNA2 to reactions together with Sgs1 resulted in the degradation of unwound ssDNA, but in contrast to the reactions with BLM or WRN, no additional double-stranded substrate was degraded. Moreover, hDNA2 even appeared to inhibit dsDNA unwinding by Sgs1 (***Figure 6F***). The specific stimulatory effect was also observed in kinetic experiments with BLM and WRN, while no stimulation was observed with hDNA2 and Sgs1 (***Figure 6G–J***). The stimulation of DNA degradation by hDNA2 was particularly pronounced together with WRN, where a gradual degradation of the substrate was observed (***Figure 6G***). As our substrate is labeled on the 3' end, the observed degradation pattern is indicative of a 5'-3' polarity of DNA degradation by hDNA2, and appears unrelated to the 3'-5' exonuclease of WRN on recessed 3' ends (***Figure 6G***). Together, these experiments show that the hDNA2-BLM and hDNA2-WRN functionally integrate and that the helicase of hDNA2 may have a stimulatory role in DNA end resection.

The WRN or BLM helicases functionally integrate with the helicase of hDNA2

Our previous work revealed that nuclease-deficient yDna2 E675A exhibits a very vigorous DNA helicase activity similar to the helicase of Sgs1, one of the most active helicases in eukaryotes (***Cejka and Kowalczykowski, 2010***; ***Levikova et al., 2013***). Interestingly, we found here that under elevated ionic strength conditions, the yDna2 E675A variant was even more active than Sgs1 (***Figure 7A***). In contrast DNA unwinding by hDNA2 D277A was highly sensitive to NaCl, to a much greater extent than dsDNA unwinding by BLM or WRN (***Figure 7B***). Having established that hDNA2 with WRN or BLM synergize in DNA resection (***Figure 6***), we decided to determine the specific interplay of the helicases in more detail. At first, we tested whether helicase-deficient BLM K695A or helicase-deficient WRN K577M can stimulate DNA unwinding by nuclease-deficient hDNA2 D277A. At low salt concentrations (25 mM), the helicase activity of hDNA2 D277A is already strongly reduced (***Figure 7B***). Supplementing the reaction with WRN K577M or BLM K695A stimulated the hDNA2 D277A helicase activity ~7 or ~4-fold, respectively (***Figure 7C,D***). Therefore, both BLM and WRN have structural roles to promote dsDNA unwinding by the nuclease-deficient hDNA2 D277A. This stimulatory effect was specific for WRN and BLM helicases, as none of the other helicase-deficient enzymes tested stimulated DNA unwinding to a comparable extent (***Figure 7—figure supplement 1A–C***). At 50 mM NaCl, the unwinding by the nuclease-deficient hDNA2 D277A alone was completely inhibited (***Figure 7B,E–H***). Under the same conditions, we could observe that adding the hDNA2 D277A variant to dsDNA unwinding reactions containing wild type WRN resulted in an increase in DNA unwinding (~2.4-fold), which was more that upon the addition of the nuclease- and helicase-deficient hDNA2 D277A K654R variant (~1.5-fold stimulation, ***Figure 7E,F***). Therefore, the hDNA2 helicase functionally integrates with WRN even under experimental conditions when no inherent helicase activity was detected. In contrast, we observed that hDNA2 has only a structural role to promote dsDNA unwinding by wild type BLM, as both hDNA2 D277A and DNA2 D277A K654R variants stimulated DNA unwinding by BLM to the same extent (***Figure 7G,H***), as noted by Sung and colleagues previously (***Daley et al., 2014***). Taken together, these data strongly suggest that the helicases of hDNA2 and WRN or BLM, respectively, function in an integrated manner, where one polypeptide stimulates the motor activity of its partner, in a mode reminiscent to that observed in prokaryotic resection machineries (***Dillingham and Kowalczykowski, 2008***). This is in agreement

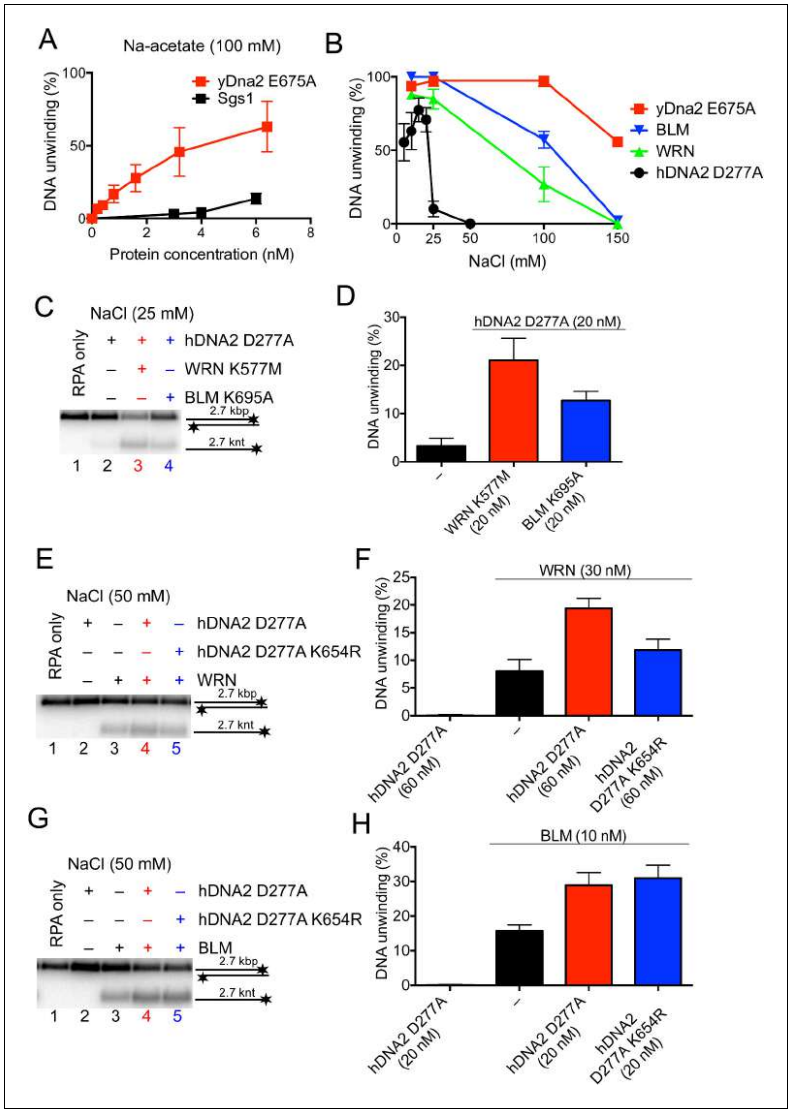

Figure 7. The helicase activity of hDNA2 functionally integrates with BLM or WRN helicases. (**A**) Quantitation of 2.7 kbp-long dsDNA unwinding by yDna2 E675A or Sgs1 with 400 nM of yeast RPA. Reactions were supplemented with 100 mM sodium acetate and 5 mM magnesium acetate and incubated at 30°C. Averages shown, n = 2–3; error bars, SEM (**B**) Quantitation of DNA unwinding by yDna2 E675A (1 nM), BLM (10 nM), WRN (30 nM), hDNA2 D277A (30 nM) and its dependence on NaCl concentration. Reactions were supplemented with indicated NaCl concentrations and 2 mM magnesium acetate and incubated at 37°C. Averages shown, n = 2–3; error bars, SEM. (**C**) Representative 1% agarose gel showing DNA unwinding by hDNA2 D277A (20 nM) and its stimulation by helicase-deficient WRN K577M (20 nM) and BLM K695A (20 nM) variants. The reactions were supplemented with

Figure 7 continued on next page

Figure 7 continued

25 mM NaCl and contained 215 nM hRPA. (**D**) Quantitation of experiments such as shown in ***Figure 7C***. Averages shown, n = 5–7; error bars, SEM. (**E**) Representative 1% agarose gel showing the interplay of wild type WRN (30 nM) and nuclease-deficient hDNA2 D277A (60 nM) or nuclease- and helicase-deficient hDNA2 D277A K654R (60 nM) mutants. The reactions were supplemented with 50 mM NaCl and 215 nM hRPA. (**F**) Quantitation of experiments such as shown in ***Figure 7E***. Averages shown, n = 3–4; error bars, SEM. (**G**) Representative 1% agarose gel showing the interplay of wild type BLM (10 nM) and nuclease-deficient hDNA2 D277A (20 nM) or nuclease- and helicase-deficient hDNA2 D277A K654R (20 nM) mutants. The reactions were supplemented with 50 mM NaCl and 215 nM hRPA. (**H**) Quantitation of experiments such as shown in ***Figure 7G***. Averages shown, n = 2–4; error bars, SEM.

DOI: 10.7554/eLife.18574.014

The following figure supplement is available for figure 7:

Figure supplement 1. The functional integration of the helicase activity of hDNA2 is specific for WRN and BLM.

DOI: 10.7554/eLife.18574.015

with physical interactions between hDNA2 and BLM or WRN, respectively (***Nimonkar et al., 2011***; ***Sturzenegger et al., 2014***).

Discussion

The involvement of DNA2 in cellular metabolism is absolutely dependent on its nuclease activity in all organisms tested to date (***Kang et al., 2010***; ***Wanrooij and Burgers, 2015***). The only exception appears to be *S. cerevisiae* Dna2's function in S-phase checkpoint signaling, where yeast Dna2 has a structural and not an enzymatic role (***Kumar and Burgers, 2013***). In all other cases, DNA2 mutants lacking the nuclease activity are as deficient as knockdowns and/or deletion mutants (***Budd et al., 2000***; ***Duxin et al., 2012***; ***Kang et al., 2000***, ***2010***; ***Lin et al., 2013***; ***Wanrooij and Burgers, 2015***). Indeed, DNA2 nuclease-deficiency brings about cellular lethality in yeast as well as human cells (***Budd et al., 2000***; ***Duxin et al., 2012***; ***Lee et al., 2000***). Much less is known about the function of the DNA2 helicase, despite both nuclease and helicase domains are equally conserved in evolution (***Bae et al., 1998***). Helicase-deficient yeast mutants are viable under most growth conditions (***Budd et al., 1995***; ***Formosa and Nittis, 1999***), while in contrast the helicase appears to be essential in human cells (***Duxin et al., 2012***). Here we present that human DNA2 possesses a marked DNA unwinding activity (***Figure 3***), which can separate DNA duplexes of several kilobases in length in a reaction that is dependent on the presence of the single-strand DNA binding protein hRPA. Single molecule experiments using magnetic tweezers revealed that dsDNA unwinding by hDNA2 is highly processive (***Figure 4***). Together, this indicates that the motor activity of the polypeptide is conserved in evolution. Similarly to yeast (***Levikova et al., 2013***), the unwinding capacity of hDNA2 is cryptic as it is masked by the nuclease within the same polypeptide. Therefore, the dsDNA unwinding can only be observed with the nuclease-deficient hDNA2 D277A variant. We showed that the nuclease of hDNA2 degrades 5'-tailed DNA at subnanomolar concentrations. The hDNA2 D277A helicase requires 5'-terminated ssDNA strands for loading onto the DNA substrate; hence, we believe that the nuclease of wild type hDNA2 cleaves these 5' overhangs, which prevents loading of hDNA2 onto the substrate and the engagement of its motor activity. This observation is in agreement with the recently published structure of mouse DNA2, which demonstrated that the nuclease active site is located along the entrance of a narrow tunnel. In order for the 5' terminated DNA to reach the helicase domain, the DNA molecule must thread half way through the tunnel (***Zhou et al., 2015***). Thus, the position of the nuclease domain ahead of the helicase clearly explains the functional interplay we observed in our experiments. Interestingly, in knockdown-rescue experiments, the expression of the nuclease-deficient hDNA2 variant was much more detrimental than the expression of the double nuclease- and helicase-deficient polypeptide (***Duxin et al., 2012***). Duxin *et al.* proposed that the nuclease-deficient hDNA2 variant is likely toxic; our results that revealed that the inactivation of the nuclease unleashes the helicase of hDNA2, which, when uncontrolled, likely explains the cellular toxicity of the D277A mutant seen *in vivo* (***Duxin et al., 2012***).

The observation that the helicase of hDNA2 is only apparent upon inactivation of the nuclease raises the question about the physiological relevance of such motor activity, despite this interplay is

conserved from yeast to man (**Bae et al., 1998**; **Levikova et al., 2013**). Previously, we speculated that the interplay of the helicase and nuclease activities might be regulated by post-translational modifications, protein partners and/or specific DNA structures (**Levikova et al., 2013**). In such a scenario, e.g. a post-translational modification may selectively lower the nuclease activity, which could allow manifestation of the hDNA2 helicase. This may be also achieved by regulating the redox state of the hDNA2 iron-sulfur cluster, which is embedded in the nuclease domain, and the function of which remains unclear (**Pokharel and Campbell, 2012**; **Wu and Brosh, 2012**). Likewise, it is possible that protein partners such as BLM or WRN may functionally integrate with the enzymatic activities of hDNA2, and modulate the interplay of the helicase-nuclease within the polypeptide. The helicase of hDNA2 might therefore only engage when hDNA2 functions in complex with the BLM or WRN factors. Interestingly, the quantitative comparison of yDna2 and hDNA2 unwinding capacities revealed that the human homologue is approximately 3–10-fold slower than its yeast counterpart. Moreover, also human BLM or WRN appear to be about an order of magnitude less active than yeast Sgs1, the partner of yDna2 and the most active RecQ helicase identified to date (**Cejka and Kowalczykowski, 2010**; **Gray et al., 1997**; **Janscak et al., 2003**; **Karow et al., 1997**). These results may suggest that the two motor activities of yDna2/hDNA2 and Sgs1/BLM/WRN might have co-evolved to match the speed of each other's partner, and that Sgs1-yDna2 and BLM-hDNA2 or WRN-hDNA2 pairs might operate as functional units. Indeed, we observed here that adding hDNA2 to reactions containing BLM or WRN, hDNA2 not only degraded the unwound ssDNA, but the concerted activity of the enzyme pair resulted in an overall stimulation of the dsDNA degradation activity. This effect was specific for the hDNA2-WRN and hDNA2-BLM enzyme pairs, as no such stimulation was observed together with Sgs1. These hDNA2-WRN and hDNA2-BLM resection complexes might be the functional analogs of the DNA-end processing machineries in prokaryotes. In most gram-negative bacteria such as *E. coli*, the RecBCD complex consists of subunits that function autonomously but integrate into a molecular machine that has helicase-nuclease activities exceeding the sum of its parts. The RecB subunit contains a 3'-5' helicase (therefore, opposite to DNA2) followed by a dual polarity nuclease, which integrates with the 5'-3' motor of the RecD subunit (**Dillingham et al., 2003**; **Spies et al., 2007**; **Taylor and Smith, 2003**). In gram-positive bacteria such as *Bacillus subtilis*, the AddAB complex has two nucleases but only one helicase (**Rocha et al., 2005**; **Yeeles and Dillingham, 2007**). Similarly to DNA2, the AddB subunit contains an iron-sulfur cluster (**Yeeles et al., 2009**), and the structure of the nuclease domain shows a high level of similarity with mouse DNA2 (**Krajewski et al., 2014**; **Zhou et al., 2015**). Furthermore, most bacteria also contain the RecQ-RecJ complex (**Morimatsu and Kowalczykowski, 2014**; **Persky and Lovett, 2008**), which likewise provides complementary activities that integrate within a complex capable to resect DNA for the RecF recombination pathway. Having uncovered the cryptic helicase capacity within hDNA2, we sought to determine whether it might function synergistically together with the BLM and/or the WRN helicase. The results presented here clearly show that although both wild type and helicase-deficient hDNA2 variants have the same nuclease activity on 5'-tailed DNA, the wild type enzyme is clearly more proficient in DNA end resection under limiting enzyme concentrations (**Figure 6**). This indicated that the motor activity within nuclease-proficient hDNA2 contributes to DNA degradation in reactions containing WRN or BLM helicases. We believe that BLM and WRN helicases provide the lead motor activity, while the hDNA2 motor has an accessory function, possibly to enhance the processivity of the complex, to help traverse strand discontinuities or to degrade unwound ssDNA. Neither WRN nor BLM could inhibit ssDNA degradation by hDNA2 (data not shown), so we do not believe that WRN/BLM's function to facilitate the engagement of hDNA2 motor activity results from an inhibition of its nuclease. How specifically the motor of hDNA2 overcomes the inhibition by the hDNA2 nuclease thus remains to be established. Our results show that the helicase of hDNA2 may play a non-essential but stimulatory role in conjunction with BLM or WRN. Previously, the helicase of hDNA2 and its yeast homologue was found dispensable for resection *in vivo* (**Thangavel et al., 2015**; **Zhu et al., 2008**), which contrasts with the results obtained in this study. However, the previous experiments were carried out under conditions where the complementing hDNA2 variants, either wild type or helicase-deficient, were expressed ectopically from a plasmid. This might have masked the stimulatory role of the hDNA2 helicase. Overexpression of wild type yDna2 leads to cell cycle arrest (**Parenteau and Wellinger, 1999**), showing that the levels of DNA2 must be balanced. Further experiments presented here provided evidence that both WRN and BLM promote dsDNA unwinding by hDNA2 and *vice versa*, showing that the helicases of

hDNA2 and WRN/BLM functionally integrate (*Figure 7*). Taken together, our results suggest that the helicase of hDNA2 might play a supportive role in DNA end resection of DNA double-strand breaks, reversed replication forks and/or other structures arising in S phase. The failure and/or delay in the repair of these structures then result in the pronounced G2 phase cell cycle arrest and checkpoint signaling that had been observed in the absence of the hDNA2 helicase (*Duxin et al., 2012*).

Finally, hDNA2 was found to be overexpressed in various human cancers, and the hDNA2 expression level negatively correlated with disease outcome (*Peng et al., 2012*; *Strauss et al., 2014*). This suggested that hDNA2 might especially promote viability of rapidly-dividing cancer cells with high levels of replication stress. This identified hDNA2 as a potential target for anti-cancer therapy. We show that inhibition of the nuclease activity unleashes the hDNA2 helicase, which is likely to contribute to the cytotoxic effects of the hDNA2 nuclease inhibitors. Duxin *et al.* observed that human cells expressing the nuclease-deficient variant were rapidly selected against during the course of the experiment, unlike in case of the double mutant lacking both nuclease and helicase activities that was maintained at constant levels (*Duxin et al., 2012*). Therefore, subsequent inactivation of the helicase might lead to resistance to the hDNA2 nuclease inhibitors. The assays developed in this study will be invaluable to assess the specificity and the mechanism of action of the various hDNA2 inhibitors that are currently being developed.

Materials and methods

Preparation of recombinant proteins

The *hDNA2* sequence was codon optimized for the expression in *Sf9* insect cells (*Supplementary file 1A*) and was purchased from GenScript (Piscataway, NJ). The *hDNA2* gene was amplified by PCR using primers 5'-TAGGAAGGATCCATGCATCACCATCACCATCACGGTGGTTC TGGTATGGAGCAATTGAACGAACTCGAAC-3' and 5'-GGTCACAAGCTTTTACTTATCGTCGTCA TCCTTGTAATCTTCACGCTGGAAGTCGCCG-3' to introduce BamHI and HindIII restriction sites as well as 6xHis and FLAG tags (*Figure 1A*). The PCR products were digested with BamHI and HindIII restriction endonucleases (New England Biolabs, Ipswich, MA) and ligated into a pFastBac1 vector (Invitrogen, Carlsbad, CA) generating pFB-His-hDNA2-FLAG. The D277A point mutation inactivating the hDNA2 nuclease was introduced with oligonucleotide pair 5'-GGCCTGAAGGGAAAGATCGCTG TCACAGTTGGAGTGAAG-3' and 5'-CTTCACTCCAACTGTGACAGCGATCTTTCCCTTCAGGCC-3' whereas the K654R point mutation abolishing the hDNA2 helicase was introduced with oligonucleotide pair 5'-GGCATGCCGGGAACTGGCAGGACAACCACTATCTGCACA-3' and 5'-TGTGCAGATAG TGGTTGTCCTGCCAGTTCCCGGCATGCC-3' using the QuikChange XL Site-directed mutagenesis kit (Agilent, Santa Clara, CA) according to manufacturer's recommendations. The construct for the expression of the helicase and nuclease-deficient D277A K654R hDNA2 double mutant was prepared sequentially using the primers described above. All hDNA2 variants were expressed in *Sf9* insect cells in SFX Insect serum-free medium (Hyclone, GE Healtcare, UK) using the Bac-to-Bac expression system (Thermo Fisher Scientific, Waltham, MA), according to manufacturer's recommendations. Frozen *Sf9* pellets from 3 liters culture for each variant were re-suspended in lysis buffer (50 mM Tris-HCl pH 7.5, 2 mM β-mercaptoethanol, 1 mM phenylmethanesulfonylfluoride [PMSF], 1 mM ethylenediaminetetraacetic acid [EDTA], 10 mM imidazole, protease inhibitor cocktail [P8340, Sigma-Aldrich, St. Louis, MO] diluted 1:250, 30 µg/ml leupeptin [Merck Millipore, Billerica, MA]) and incubated at 4˚C for 20 min. Glycerol was added to a final concentration of 15%, NaCl was added to a final concentration of 305 mM and the solution was incubated at 4˚C for 30 min. The mixture was centrifuged at 39'000 g at 4˚C for 30 min. The soluble extract was incubated with Ni-NTA agarose resin (Qiagen, Germany) at 4˚C for 1 hr. Ni-NTA resin was washed with Ni-NTA wash buffer 1 M (50 mM Tris-HCl pH 7.5, 2 mM β-mercaptoethanol, 1 mM PMSF, 1 mM EDTA, 10 mM imidazole, 1:1000 protease inhibitor cocktail, 30 µg/ml leupeptin, 10% glycerol, 1 M NaCl) and subsequently washed with Ni-NTA wash buffer 150 mM (the same buffer as above, but only with 150 mM NaCl). Proteins were eluted using Ni-NTA wash buffer 150 mM supplemented with 300 mM imidazole, and subsequently diluted with 4 volumes of FLAG wash buffer 150 mM (50 mM Tris-HCl pH 7.5, 0.5 mM β-mercaptoethanol, 1 mM PMSF, 10% glycerol, 150 mM NaCl) to lower the imidazole and β-mercaptoethanol concentrations. The mixture was incubated with anti-FLAG M2 Affinity Gel (A2220, Sigma-Aldrich) at 4˚C for 1 hr. Proteins were eluted using FLAG wash buffer 150 mM supplemented with

300 µg/ml FLAG peptide (F4799, Sigma-Aldrich), aliquoted, snap-frozen in liquid nitrogen and stored at −80˚C. Yeast Dna2, Sgs1, human and yeast RPA were purified as described previously (**Cejka and Kowalczykowski, 2010**; **Henricksen et al., 1994**; **Kantake et al., 2003**; **Levikova et al., 2013**). Human RecQ1, RecQ5 and yeast Srs2 and their variants were kind gifts from A. Vindigni (Saint Louis University, USA), P. Janscak (University of Zurich, Switzerland) and L. Krejci (Masaryk University, Czech Republic).

The *BLM* gene was amplified by PCR from pZL4 plasmid (**Kanagaraj et al., 2006**) with primers 5′-TAGGAAGCTAGCGGATCCATGGCTGCTGTTCCTCAAAA-3′ and 5′-TAGGAACTCGAGCCCGGG TGAGAATGCATATGAAGGCTT-3′ to introduce XhoI and NheI restriction sites. The *WRN* gene was amplified by PCR from plasmid pBlueBacHis-WRN (**Gray et al., 1997**) with primers 5′-TAGGAAGC TAGCGGATCCATGAGTGAAAAAAAATTGGAAACAA-3′ and 5′-TAGGAACTCGAGCCCGGGAC TAAAAAGACCTCCCCTTTT-3′ to introduce XhoI and NheI restriction sites. The PCR products were cloned into pFB-MBP-Sgs1-his (**Cejka et al., 2010**) generating pFB-MBP-BLM-his and pFB-MBP-WRN-his, respectively. Mutations for the helicase-deficient variants were introduced as described above using oligonucleotide pairs 5′-ACTGGAGGTGGTGCGAGTTTGTGTTACCAGCTC-3′ and 5′-GAGCTGGTAACACAAACTCGCACCACCTCCAGT-3′ for BLM K695A and 5′-GCAACTGGATA TGGAATGAGTTTGTGCTTCCAGTATCC-3′ and 5′-GGATACTGGAAGCACAAACTCATTCCATA TCCAGTTGC-3′ for WRN K577M. All BLM and WRN variants were expressed in *Sf9* cells. Frozen *Sf9* pellets from 1.2–2 l culture for each variant were resuspended in lysis buffer and soluble extract was prepared as for hDNA2 (see above). The soluble extract was incubated with amylose resin (New England Biolabs) at 4˚C for 1 hr. The resin was washed with amylose wash buffer 1 M (50 mM Tris-HCl pH 7.5, 5 mM β-mercaptoethanol, 1 mM PMSF, 10% glycerol, 1 M NaCl). Proteins were eluted using amylose elution buffer (50 mM Tris-HCl pH 7.5, 5 mM β-mercaptoethanol, 1 mM PMSF, 10% glycerol, 300 mM NaCl, 10 mM maltose). The MBP-tagged variants were incubated with PreScission protease (~25 µg PreScission protease per 100 µg of tagged protein) at 4˚C for 1.5 hr to cleave the MBP tag. Subsequently, imidazole was added to a final concentration of 10 mM and the solution was incubated with pre-equilibrated Ni-NTA agarose resin (Qiagen) at 4˚C for 1 hr, in agitation. The resin was washed with NTA Buffer A1 (50 mM Tris-HCl pH 7.5, 5 mM β-mercaptoethanol, 1 mM PMSF, 10% glycerol, 1 M NaCl, 58 mM imidazole) and subsequently with NTA Buffer A2 (50 mM Tris-HCl pH 7.5, 5 mM β-mercaptoethanol, 1 mM PMSF, 10% glycerol, 150 mM NaCl, 58 mM imidazole). The BLM or WRN variants were eluted with NTA Buffer B (50 mM Tris HCl pH 7.5, 5 mM β-mercaptoethanol, 1 mM PMSF, 10% glycerol, 100 mM NaCl, 300 mM imidazole). Fractions containing high protein concentration were pooled and dialyzed against 1 l of dialysis buffer (50 mM Tris-HCl pH 7.5, 5 mM β-mercaptoethanol, 0.5 mM PMSF, 10% glycerol, 100 mM NaCl) for 1 hr at 4˚C. Proteins were aliquoted, snap-frozen in liquid nitrogen and stored at −80˚C. The typical yield was ~50–280 µg from 1.2–2 liters culture for each variant.

The plasmid pSF1-hsmtSSB coding for human mitochondrial single-stranded DNA binding protein (mtSSB) was received from Ute Curth (Hannover Medical School) (**Curth et al., 1994**). The mtSSB gene was amplified by PCR using primers 5′-GTGACCGAATCATGGACTCCGAAACAACTACCAG TTTGG-3′ and 5′-GTGACCGGATCCCTACTCCTTCTCTTTCGTCTGGTCACTC-3′ and cloned into the pMALT-P expression vector (Taeho Kim, Kowalczykowski laboratory, unpublished) using EcoRI and BamHI restriction sites. This placed mtSSB behind an MBP tag and a PreScission Protease site creating pMALT-P-mtSSB. The MBP-mtSSB fusion was expressed in *E. coli* BL21 cells upon induction with Isopropyl β-D-1-thiogalactopyranoside (IPTG, 400 µM) for 3 hr at 37˚C. Frozen *E. coli* pellets from 2 l *E. coli* culture were re-suspended in buffer B1 (50 mM Tris-HCl pH 7.5, 1 mM EDTA, protease inhibitor cocktail [1:400], 30 µg/ml leupeptin, 1 mM PMSF, 1 mM dithiothreitol [DTT], 10% glycerol, 100 mM NaCl) and lysed by sonication. Whole cell extract was centrifuged at 39'000g at 4˚C for 30 min. The supernatant was collected and incubated with pre-equilibrated 3 ml amylose resin (New England Biolabs) for 1 hr at 4˚C. The resin was washed in buffer B2 (50 mM Tris-HCl pH 7.5, 1 mM DTT, 10% glycerol, 100 mM NaCl). MBP-mtSSB was eluted using buffer B3 (50 mM Tris-HCl pH 7.5, 1 mM DTT, 10% glycerol, 100 mM NaCl, 10 mM maltose). The MBP tag was cleaved with PreScission protease (~15 µg per 100 µg MBP-mtSSB) overnight at 4˚C. The solution was then diluted with 1 volume of water. The sample was loaded onto a HiTrap Blue column (GE Healthcare). The column was washed with buffer B2 sequentially supplemented with 50 mM KCl, 800 mM KCl, 0.5 M sodium thiocyanate and 1.5 M sodium thiocyanate. The mtSSB protein was eluted using buffer B4 (20 mM Tris-HCl pH 7.5, 1 mM EDTA, 1 mM DTT, 10% glycerol, 2 M NaCl, 5 M urea). The eluate was dialyzed

twice against 1 l buffer B5 (50 mM Tris-HCl pH 7.5, 1 mM DTT, 10% glycerol, 50 mM NaCl) for 1.5 hr each time. The final mtSSB preparation was aliquoted, snap-frozen in liquid nitrogen and stored at −80°C.

The three pDONR plasmids (Thermo Fisher Scientific) coding for SOSSA, SOSSB1 and SOSSC, respectively, were gifts from Jun Huang (Life Sciences Institute, Hangzhou, Zhejiang University) (***Huang et al., 2009***). The *SOSSA* gene was cloned into pDEST20 vector using Gateway recombination cloning technology (Thermo Fisher Scientific) creating pDEST20-GST-SOSSA. To add a N-terminal 6xhis tag to SOSSB1, the *SOSSB1* gene was amplified by PCR using primers 5′-GTGACCGGATCCATGCATCACCATCACCATCACATGACGACGGAGACCTTTGTGAAGGATATC-3′ and 5′-GTGACCCCCGGGCTATCTCTTGCTGCTCCTCCGGGTTT-3′. The PCR product was cloned into a pFastBac1 vector using BamHI and XmaI restriction sites, creating pFB-hisSOSSB1. The *SOSSC* gene was amplified by PCR using primers 5′-GTGACCGGATCCATGGCAGCAAACTCTTCAGGACAAGGTTTTC-3′ and 5′-GTGACCC′CCGGGTCATTCTGGGTCAAGGCGAGGTAAAACAG-3′. The gene was cloned into pFastBac1 vector using BamHI and XmaI restriction sites, creating pFB-SOSSC. The heterotrimer was expressed as a complex in *Sf*9 cells for in 2 l of culture. The pellet was re-suspended in buffer B1 (50 mM Tris-HCl pH 8, 1 mM EDTA, protease inhibitor cocktail [1:400], 30 µg/ml leupeptin, 1 mM PMSF, 1 mM DTT) and incubated for 20 min at 4°C in agitation. Glycerol was added to a final concentration of 15% and NaCl was added to a final concentration of 305 mM. The solution was incubated for another 30 min at 4°C in agitation. The solution was centrifuged for 30 min at 39′000 g at 4°C. The soluble extract was then incubated with 2 ml pre-equilibrated Glutathione HiCap matrix (Qiagen) for 1 hr at 4°C in agitation. The resin was washed 3x batch-wise and subsequently on column with wash buffer (50 mM Tris-HCl pH 8, protease inhibitor [1:1000], 1 mM PMSF, 2 mM 2-mercaptoethanol). The proteins were eluted using the wash buffer supplemented with 10 mM glutathione. Imidazole was added to the eluate to a final concentration of 10 mM and incubated with pre-equilibrated Ni-NTA agarose resin (Qiagen) for 1 hr at 4°C in agitation. The resin was washed twice with buffer A2 (50 mM Tris HCl pH 7.5, 2 mM 2-mercaptoethanol, 150 mM NaCl, 10% glycerol, 1 mM PMSF, 58 mM imidazole) and the proteins were eluted with buffer B (50 mM Tris-HCl pH 7.5, 2 mM 2-mercaptoethanol, 100 mM NaCl, 10% glycerol, 1 mM PMSF, 300 mM imidazole). The eluate was dialyzed against 1 l of dialysis buffer (50 mM Tris-HCl pH 7.5, 2 mM 2-mercaptoethanol, 100 mM NaCl, 10% glycerol, 0.5 mM PMSF) for 1.5 hr at 4°C.

DNA substrates

Oligonucleotides were labeled either at the 5′ terminus with [γ-^{32}P]ATP and T4 polynucleotide kinase (New England Biolabs), or at the 3′ terminus with [α-^{32}P] cordycepin-5-triphosphate and terminal transferase (New England Biolabs) according to standard protocols. The sequences of all oligonucleotides are listed in ***Supplementary file 1B***. The substrates were prepared by annealing the ^{32}P-labeled oligonucleotide with a two-fold excess of the unlabeled oligonucleotide in a PNK buffer (New England Biolabs). The substrates and component oligonucleotides are listed in ***Supplementary file 1C***.

λDNA/HindIII fragments (Bacteriophage λ DNA-HindIII Digest, New England Biolabs) were labeled at the 3′ ends with [α-^{32}P]dATP and Klenow fragment of DNA polymerase I (New England Biolabs) in NEBuffer 2. The pUC19 plasmid was digested by HindIII-HF restriction enzyme and purified by phenol-chloroform extraction and ethanol precipitation. The resulting linear dsDNA was labeled at the 3′ ends with [α-^{32}P]dATP and Klenow fragment of DNA polymerase I (New England Biolabs) in NEBuffer 2. Unincorporated radioactive ATP was in all cases removed using Micro Spin G25 columns (GE Healthcare). The positions of the radioactive labels are indicated in the substrate schematics with a star symbol.

Electrophoretic mobility shift assays

The reactions (15 µl volume) were performed in a binding buffer (25 mM Tris-acetate pH 7.5, 2 mM magnesium acetate, 1 mM DTT, 0.1 mg/ml BSA) with the respective DNA substrate (1 nM). The reactions were incubated at 37°C for 30 min. Loading dye (50% glycerol, bromophenol blue) was added and the products were separated by polyacrylamide gel electrophoresis (6%, ratio acrylamide-bisacrylamide 19:1, BioRad) in Tris-Acetate-EDTA (TAE) buffer. The electrophoresis was carried out in a gel tank surrounded by ice. The gels were dried on DE81 chromatography paper (Whatman, UK).

The dried gels were then exposed to Storage Phosphor screens (GE Healthcare) and scanned by Typhoon 9400 (GE Healthcare). The data was quantified using Image Quant TL software (GE Healthcare).

Nuclease assays

Nuclease assays (15 µl volume) were performed in a reaction buffer (25 mM Tris-acetate pH 7.5, 2 mM magnesium acetate, 1 mM ATP, 1 mM DTT, 0.1 mg/ml BSA, 1 mM phosphoenolpyruvate (PEP), 0.02 units/µl pyruvate kinase [Sigma]) containing DNA substrates (1 nM) and recombinant proteins as indicated. Reactions were incubated at 37˚C for 30 min. For analysis on native gels the reactions were stopped by adding 5 µl 2% stop solution (150 mM EDTA, 2% sodium dodecyl sulfate [SDS], 30% glycerol, bromophenol blue) and 1 µl Proteinase K (14-22 mg/ml, Roche, Switzerland) and incubated at 37°C for 10 min. The samples were then analyzed by native polyacrylamide gel electrophoresis (10%, ratio acrylamide-bisacrylamide 19:1, Biorad, Hercules, CA). For analysis on denaturing gels the reactions were stopped by adding an equal amount of formamide dye (95% [v/v] formamide, 20 mM EDTA, bromophenol blue), samples were heated at 95˚C for 4 min and separated on 20% denaturing polyacrylamide gels (ratio acrylamide:bisacrylamide 19:1, Biorad). After fixing in a solution containing 40% methanol, 10% acetic acid and 5% glycerol for 30 min the gels were dried and analyzed as described above.

Helicase and ATPase assays

Helicase assays (15 µl volume) were performed in a reaction buffer (25 mM Tris-acetate pH 7.5, 2 mM magnesium acetate, 1 mM ATP, 1 mM DTT, 0.1 mg/ml BSA, 1 mM PEP, 0.02 units/µl pyruvate kinase) with the respective DNA substrate (1 nM for oligonucleotide- and pUC19/HindIII-based and 0.15 nM for λDNA/HindIII-based substrates). Recombinant proteins were added as indicated. Reactions were incubated at 37˚C for 30 min and stopped as described above in the nuclease assay section. To avoid re-annealing of the oligonucleotide-based substrates, the stop solution was supplemented with a 20-fold excess of the oligonucleotide with the same sequence as the ^{32}P-labeled one. The products were analyzed either by polyacrylamide gel electrophoresis (10%) for oligonucleotide-based DNA substrates or 1% agarose gels for plasmid and λDNA-based DNA substrates. The gels were dried on DE81 chromatography paper (Whatman) and analyzed as described above. The ATPase assays were performed as described previously (***Kowalczykowski and Krupp, 1987***). The reaction buffer contained 25 mM Tris-acetate pH 7.5, 1 mM magnesium acetate, 1 mM DTT, 0.1 mg/ml BSA, 1 mM ATP and 1 mM PEP, 0.025 units/µl pyruvate kinase, 0.025 units/µl L-lactic dehydrogenase (Sigma).

Magnetic tweezers assay

The DNA construct was prepared as described before (***Levikova et al., 2013***). The central part is a 6.1 kbp dsDNA having a ssDNA flap of 40 nt in length placed 1 kbp from its proximal DNA end. A digoxigenin- and a biotin-modified handle of 600 bp length were attached to the 6.1 kbp fragment at its flap-proximal and distal ends, respectively. The magnetic tweezers experiments were carried out as described previously (***Klaue and Seidel, 2009***; ***Levikova et al., 2013***). In brief, the DNA substrate was bound to 2.8 µm streptavidin-coated magnetic beads (M280, Invitrogen) and were flushed into the fluidic cell, whose bottom glass slide was covered with digoxigenin. After a brief incubation to allow the attachment of the digoxigenin-modified DNA end, a pair of magnets above the flow cell was approached to remove unbound beads and to stretch the bead tethered DNA molecules. The DNA length was obtained by videomicroscopy of the beads and GPU-accelerated real-time particle tracking (***Huhle et al., 2015***). The stretching force was adjusted by changing the distance of the magnet to the fluidic cell. Forces were calibrated for each bead using fluctuation analysis (***Daldrop et al., 2015***). The unwinding assays were performed in a reaction buffer (25 mM Tris-acetate pH 7.5, 5 mM magnesium acetate, 1 mM ATP, 1 mM DTT, 0.1 mg/ml BSA) supplemented with 25 nM hRPA and 25 nM hDNA2 D277A at 37°C. For temperature control of the setup an objective heater (Okolab, Pozzuoli, Italy) was employed. With respect to the bulk assays, the magnesium acetate concentration was increased to 5 mM to prevent DNA melting by hRPA (***Kemmerich et al., 2016***). The DNA extension resulting from unwinding was converted from µm into bp applying a

conversion factor that was calculated from the force extension curves for the DNA molecule at the certain force (***Kemmerich et al., 2016***).

Acknowledgements

We would like to thank Pavel Janscak (University of Zurich), Ute Curth (Hannover Medical School), Jun Huang (Zhejiang University), Lumir Krejci (Masaryk University) and Alessandro Vindigni (Saint Louis University) for recombinant proteins and expression constructs. We thank Andrey Krivoy for helping establish the temperature control within the magnetic tweezers. We thank Elda Cannavo, Maryna Levikova, Roopesh Anand and Lucie Mlejnkova for critical reading of the manuscript. This work was supported by the Swiss National Science foundation grant PP00P3 159323 to PC, Swiss Cancer League grant KFS-3089-02-2013 to PC and ERC starting grant (GA 261224) to RS.

Additional information

Funding

Funder	Grant reference number	Author
Schweizerischer Nationalfonds zur Förderung der Wissenschaftlichen Forschung	PP00P3 159323	Petr Cejka
Krebsliga Schweiz	KFS-3089-02-2013	Petr Cejka
European Research Council	GA 261224	Ralf Seidel

The funders had no role in study design, data collection and interpretation, or the decision to submit the work for publication.

Author contributions

CP, Conception and design, Acquisition of data, Analysis and interpretation of data, Drafting or revising the article; KK, Acquisition of data, Analysis and interpretation of data, Drafting or revising the article; RS, PC, Conception and design, Analysis and interpretation of data, Drafting or revising the article

Author ORCIDs

Petr Cejka, http://orcid.org/0000-0002-9087-032X

Additional files

Supplementary files

• Supplementary file 1. DNA sequences used in this study. (A) Codon-optimized nucleotide sequence of hDNA2 gene for the expression in *Sf9* cells. (B) Sequences of oligonucleotides used in this study. (C) Oligonucleotide-based DNA substrates used in this study.

DOI: 10.7554/eLife.18574.016

References

Bae KH, Kim HS, Bae SH, Kang HY, Brill S, Seo YS. 2003. Bimodal interaction between replication-protein A and Dna2 is critical for Dna2 function both in vivo and in vitro. *Nucleic Acids Research* **31**:3006–3015. doi: 10.1093/nar/gkg422

Bae SH, Bae KH, Kim JA, Seo YS. 2001. RPA governs endonuclease switching during processing of Okazaki fragments in eukaryotes. *Nature* **412**:456–461. doi: 10.1038/35086609

Bae SH, Choi E, Lee KH, Park JS, Lee SH, Seo YS. 1998. Dna2 of Saccharomyces cerevisiae possesses a single-stranded DNA-specific endonuclease activity that is able to act on double-stranded DNA in the presence of ATP. *Journal of Biological Chemistry* **273**:26880–26890. doi: 10.1074/jbc.273.41.26880

Bae SH, Kim DW, Kim J, Kim JH, Kim DH, Kim HD, Kang HY, Seo YS. 2002. Coupling of DNA helicase and endonuclease activities of yeast Dna2 facilitates Okazaki fragment processing. *Journal of Biological Chemistry* **277**:26632–26641. doi: 10.1074/jbc.M111026200

Balakrishnan L, Polaczek P, Pokharel S, Campbell JL, Bambara RA. 2010a. Dna2 exhibits a unique strand end-dependent helicase function. *Journal of Biological Chemistry* **285**:38861–38868. doi: 10.1074/jbc.M110.165191

Balakrishnan L, Stewart J, Polaczek P, Campbell JL, Bambara RA. 2010b. Acetylation of Dna2 endonuclease/helicase and flap endonuclease 1 by p300 promotes DNA stability by creating long flap intermediates. *Journal of Biological Chemistry* **285**:4398–4404. doi: 10.1074/jbc.M109.086397

Budd ME, Campbell JL. 1995. A yeast gene required for DNA replication encodes a protein with homology to DNA helicases. *PNAS* **92**:7642–7646. doi: 10.1073/pnas.92.17.7642

Budd ME, Choe W, Campbell JL. 2000. The nuclease activity of the yeast DNA2 protein, which is related to the RecB-like nucleases, is essential in vivo. *Journal of Biological Chemistry* **275**:16518–16529. doi: 10.1074/jbc.M909511199

Budd ME, Choe WC, Campbell JL. 1995. DNA2 encodes a DNA helicase essential for replication of eukaryotic chromosomes. *Journal of Biological Chemistry* **270**:26766–26769. doi: 10.1074/jbc.270.45.26766

Cejka P, Cannavo E, Polaczek P, Masuda-Sasa T, Pokharel S, Campbell JL, Kowalczykowski SC. 2010. DNA end resection by Dna2-Sgs1-RPA and its stimulation by Top3-Rmi1 and Mre11-Rad50-Xrs2. *Nature* **467**:112–116. doi: 10.1038/nature09355

Cejka P, Kowalczykowski SC. 2010. The full-length Saccharomyces cerevisiae Sgs1 protein is a vigorous DNA helicase that preferentially unwinds holliday junctions. *Journal of Biological Chemistry* **285**:8290–8301. doi: 10.1074/jbc.M109.083196

Cejka P. 2015. DNA end resection: Nucleases team up with the right partners to initiate homologous recombination. *Journal of Biological Chemistry* **290**:22931–22938. doi: 10.1074/jbc.R115.675942

Choe W, Budd M, Imamura O, Hoopes L, Campbell JL. 2002. Dynamic localization of an Okazaki fragment processing protein suggests a novel role in telomere replication. *Molecular and Cellular Biology* **22**:4202–4217. doi: 10.1128/MCB.22.12.4202-4217.2002

Curth U, Urbanke C, Greipel J, Gerberding H, Tiranti V, Zeviani M. 1994. Single-stranded-DNA-binding proteins from human mitochondria and Escherichia coli have analogous physicochemical properties. *European Journal of Biochemistry* **221**:435–443. doi: 10.1111/j.1432-1033.1994.tb18756.x

Daldrop P, Brutzer H, Huhle A, Kauert DJ, Seidel R. 2015. Extending the range for force calibration in magnetic tweezers. *Biophysical Journal* **108**:2550–2561. doi: 10.1016/j.bpj.2015.04.011

Daley JM, Chiba T, Xue X, Niu H, Sung P. 2014. Multifaceted role of the Topo IIIα-RMI1-RMI2 complex and DNA2 in the BLM-dependent pathway of DNA break end resection. *Nucleic Acids Research* **42**:11083–11091. doi: 10.1093/nar/gku803

Dessinges MN, Lionnet T, Xi XG, Bensimon D, Croquette V. 2004. Single-molecule assay reveals strand switching and enhanced processivity of UvrD. *PNAS* **101**:6439–6444. doi: 10.1073/pnas.0306713101

Dillingham MS, Kowalczykowski SC. 2008. RecBCD enzyme and the repair of double-stranded DNA breaks. *Microbiology and Molecular Biology Reviews* **72**:642–671. doi: 10.1128/MMBR.00020-08

Dillingham MS, Spies M, Kowalczykowski SC. 2003. RecBCD enzyme is a bipolar DNA helicase. *Nature* **423**:893–897. doi: 10.1038/nature01673

Duxin JP, Dao B, Martinsson P, Rajala N, Guittat L, Campbell JL, Spelbrink JN, Stewart SA. 2009. Human Dna2 is a nuclear and mitochondrial DNA maintenance protein. *Molecular and Cellular Biology* **29**:4274–4282. doi: 10.1128/MCB.01834-08

Duxin JP, Moore HR, Sidorova J, Karanja K, Honaker Y, Dao B, Piwnica-Worms H, Campbell JL, Monnat RJ, Stewart SA. 2012. Okazaki fragment processing-independent role for human Dna2 enzyme during DNA replication. *Journal of Biological Chemistry* **287**:21980–21991. doi: 10.1074/jbc.M112.359018

Eki T, Okumura K, Shiratori A, Abe M, Nogami M, Taguchi H, Shibata T, Murakami Y, Hanaoka F. 1996. Assignment of the closest human homologue (DNA2L:KIAA0083) of the yeast Dna2 helicase gene to chromosome band 10q21.3-q22.1. *Genomics* **37**:408–410. doi: 10.1006/geno.1996.0581

Formosa T, Nittis T. 1999. Dna2 mutants reveal interactions with Dna polymerase alpha and Ctf4, a Pol alpha accessory factor, and show that full Dna2 helicase activity is not essential for growth. *Genetics* **151**:1459–1470.

Georgaki A, Hübscher U. 1993. DNA unwinding by replication protein A is a property of the 70 kDa subunit and is facilitated by phosphorylation of the 32 kDa subunit. *Nucleic Acids Research* **21**:3659–3665. doi: 10.1093/nar/21.16.3659

Gould KL, Burns CG, Feoktistova A, Hu CP, Pasion SG, Forsburg SL. 1998. Fission yeast cdc24(+) encodes a novel replication factor required for chromosome integrity. *Genetics* **149**:1221–1233.

Gravel S, Chapman JR, Magill C, Jackson SP. 2008. DNA helicases Sgs1 and BLM promote DNA double-strand break resection. *Genes & Development* **22**:2767–2772. doi: 10.1101/gad.503108

Gray MD, Shen JC, Kamath-Loeb AS, Blank A, Sopher BL, Martin GM, Oshima J, Loeb LA. 1997. The Werner syndrome protein is a DNA helicase. *Nature Genetics* **17**:100–103. doi: 10.1038/ng0997-100

Henricksen LA, Umbricht CB, Wold MS. 1994. Recombinant replication protein A: expression, complex formation, and functional characterization. *Journal of Biological Chemistry* **269**:11121–11132.

Heyer WD, Ehmsen KT, Liu J. 2010. Regulation of homologous recombination in eukaryotes. *Annual Review of Genetics* **44**:113–139. doi: 10.1146/annurev-genet-051710-150955

Hu J, Sun L, Shen F, Chen Y, Hua Y, Liu Y, Zhang M, Hu Y, Wang Q, Xu W, Sun F, Ji J, Murray JM, Carr AM, Kong D. 2012. The intra-S phase checkpoint targets Dna2 to prevent stalled replication forks from reversing. *Cell* **149**:1221–1232. doi: 10.1016/j.cell.2012.04.030

Huang J, Gong Z, Ghosal G, Chen J. 2009. SOSS complexes participate in the maintenance of genomic stability. *Molecular Cell* **35**:384–393. doi: 10.1016/j.molcel.2009.06.011

Huhle A, Klaue D, Brutzer H, Daldrop P, Joo S, Otto O, Keyser UF, Seidel R. 2015. Camera-based three-dimensional real-time particle tracking at kHz rates and Ångström accuracy. *Nature Communications* **6**:5885. doi: 10.1038/ncomms6885

Janscak P, Garcia PL, Hamburger F, Makuta Y, Shiraishi K, Imai Y, Ikeda H, Bickle TA. 2003. Characterization and mutational analysis of the RecQ core of the bloom syndrome protein. *Journal of Molecular Biology* **330**:29–42. doi: 10.1016/S0022-2836(03)00534-5

Kanagaraj R, Saydam N, Garcia PL, Zheng L, Janscak P. 2006. Human RECQ5beta helicase promotes strand exchange on synthetic DNA structures resembling a stalled replication fork. *Nucleic Acids Research* **34**:5217–5231. doi: 10.1093/nar/gkl677

Kang HY, Choi E, Bae SH, Lee KH, Gim BS, Kim HD, Park C, MacNeill SA, Seo YS. 2000. Genetic analyses of Schizosaccharomyces pombe dna2(+) reveal that dna2 plays an essential role in Okazaki fragment metabolism. *Genetics* **155**:1055–1067.

Kang YH, Lee CH, Seo YS. 2010. Dna2 on the road to Okazaki fragment processing and genome stability in eukaryotes. *Critical Reviews in Biochemistry and Molecular Biology* **45**:71–96. doi: 10.3109/10409230903578593

Kantake N, Sugiyama T, Kolodner RD, Kowalczykowski SC. 2003. The recombination-deficient mutant RPA (rfa1-t11) is displaced slowly from single-stranded DNA by Rad51 protein. *Journal of Biological Chemistry* **278**:23410–23417. doi: 10.1074/jbc.M302995200

Karow JK, Chakraverty RK, Hickson ID. 1997. The Bloom's syndrome gene product is a 3'-5' DNA helicase. *Journal of Biological Chemistry* **272**:30611–30614. doi: 10.1074/jbc.272.49.30611

Kemmerich FE, Daldrop P, Pinto C, Levikova M, Cejka P, Seidel R. 2016. Force regulated dynamics of RPA on a DNA fork. *Nucleic Acids Research* **44**:5837–5848. doi: 10.1093/nar/gkw187

Kim JH, Kim HD, Ryu GH, Kim DH, Hurwitz J, Seo YS. 2006. Isolation of human Dna2 endonuclease and characterization of its enzymatic properties. *Nucleic Acids Research* **34**:1854–1864. doi: 10.1093/nar/gkl102

Klaue D, Kobbe D, Kemmerich F, Kozikowska A, Puchta H, Seidel R. 2013. Fork sensing and strand switching control antagonistic activities of RecQ helicases. *Nature Communications* **4**:2024. doi: 10.1038/ncomms3024

Klaue D, Seidel R. 2009. Torsional stiffness of single superparamagnetic microspheres in an external magnetic field. *Physical Review Letters* **102**:028302. doi: 10.1103/PhysRevLett.102.028302

Kowalczykowski SC, Krupp RA. 1987. Effects of Escherichia coli SSB protein on the single-stranded DNA-dependent ATPase activity of Escherichia coli RecA protein. Evidence that SSB protein facilitates the binding of RecA protein to regions of secondary structure within single-stranded DNA. *Journal of Molecular Biology* **193**:97–113. doi: 10.1016/0022-2836(87)90630-9

Krajewski WW, Fu X, Wilkinson M, Cronin NB, Dillingham MS, Wigley DB. 2014. Structural basis for translocation by AddAB helicase-nuclease and its arrest at χ sites. *Nature* **508**:416–419. doi: 10.1038/nature13037

Kumar S, Burgers PM. 2013. Lagging strand maturation factor Dna2 is a component of the replication checkpoint initiation machinery. *Genes & Development* **27**:313–321. doi: 10.1101/gad.204750.112

Kuo C, Nuang H, Campbell JL. 1983. Isolation of yeast DNA replication mutants in permeabilized cells. *PNAS* **80**:6465–6469. doi: 10.1073/pnas.80.21.6465

Lee CH, Lee M, Kang HJ, Kim DH, Kang YH, Bae SH, Seo YS. 2013. The N-terminal 45-kDa domain of Dna2 endonuclease/helicase targets the enzyme to secondary structure DNA. *Journal of Biological Chemistry* **288**:9468–9481. doi: 10.1074/jbc.M112.418715

Lee KH, Kim DW, Bae SH, Kim JA, Ryu GH, Kwon YN, Kim KA, Koo HS, Seo YS. 2000. The endonuclease activity of the yeast Dna2 enzyme is essential in vivo. *Nucleic Acids Research* **28**:2873–2881. doi: 10.1093/nar/28.15.2873

Levikova M, Cejka P. 2015. The Saccharomyces cerevisiae Dna2 can function as a sole nuclease in the processing of Okazaki fragments in DNA replication. *Nucleic Acids Research* **43**:7888–7897. doi: 10.1093/nar/gkv710

Levikova M, Klaue D, Seidel R, Cejka P. 2013. Nuclease activity of Saccharomyces cerevisiae Dna2 inhibits its potent DNA helicase activity. *PNAS* **110**:E1992–2001. doi: 10.1073/pnas.1300390110

Li Y, Bolderson E, Kumar R, Muniandy PA, Xue Y, Richard DJ, Seidman M, Pandita TK, Khanna KK, Wang W. 2009. HSSB1 and hSSB2 form similar multiprotein complexes that participate in DNA damage response. *Journal of Biological Chemistry* **284**:23525–23531. doi: 10.1074/jbc.C109.039586

Lin W, Sampathi S, Dai H, Liu C, Zhou M, Hu J, Huang Q, Campbell J, Shin-Ya K, Zheng L, Chai W, Shen B. 2013. Mammalian DNA2 helicase/nuclease cleaves G-quadruplex DNA and is required for telomere integrity. *The EMBO Journal* **32**:1425–1439. doi: 10.1038/emboj.2013.88

Masuda-Sasa T, Imamura O, Campbell JL. 2006. Biochemical analysis of human Dna2. *Nucleic Acids Research* **34**:1865–1875. doi: 10.1093/nar/gkl070

Morimatsu K, Kowalczykowski SC. 2014. RecQ helicase and RecJ nuclease provide complementary functions to resect DNA for homologous recombination. *PNAS* **111**:E5133–E5142. doi: 10.1073/pnas.1420009111

NimonkarAV , Genschel J, Kinoshita E, Polaczek P, Campbell JL, Wyman C, Modrich P, Kowalczykowski SC. 2011. BLM-DNA2-RPA-MRN and EXO1-BLM-RPA-MRN constitute two DNA end resection machineries for human DNA break repair. *Genes & Development* **25**:350–362. doi: 10.1101/gad.2003811

Niu H, Chung WH, Zhu Z, Kwon Y, Zhao W, Chi P, Prakash R, Seong C, Liu D, Lu L, Ira G, Sung P. 2010. Mechanism of the ATP-dependent DNA end-resection machinery from Saccharomyces cerevisiae. *Nature* **467**:108–111. doi: 10.1038/nature09318

Parenteau J, Wellinger RJ. 1999. Accumulation of single-stranded DNA and destabilization of telomeric repeats in yeast mutant strains carrying a deletion of RAD27. *Molecular and Cellular Biology* **19**:4143–4152. doi: 10.1128/MCB.19.6.4143

Peng G, Dai H, Zhang W, Hsieh HJ, Pan MR, Park YY, Tsai RY, Bedrosian I, Lee JS, Ira G, Lin SY. 2012. Human nuclease/helicase DNA2 alleviates replication stress by promoting DNA end resection. *Cancer Research* **72**: 2802–2813. doi: 10.1158/0008-5472.CAN-11-3152

Persky NS, Lovett ST. 2008. Mechanisms of recombination: lessons from E. coli. *Critical Reviews in Biochemistry and Molecular Biology* **43**:347–370. doi: 10.1080/10409230802485358

Pokharel S, Campbell JL. 2012. Cross talk between the nuclease and helicase activities of Dna2: role of an essential iron-sulfur cluster domain. *Nucleic Acids Research* **40**:7821–7830. doi: 10.1093/nar/gks534

Richard DJ, Cubeddu L, Urquhart AJ, Bain A, Bolderson E, Menon D, White MF, Khanna KK. 2011. hSSB1 interacts directly with the MRN complex stimulating its recruitment to DNA double-strand breaks and its endonuclease activity. *Nucleic Acids Research* **39**:3643–3651. doi: 10.1093/nar/gkq1340

Rocha EP, Cornet E, Michel B. 2005. Comparative and evolutionary analysis of the bacterial homologous recombination systems. *PLoS Genetics* **1**:e15. doi: 10.1371/journal.pgen.0010015

Spies M, Amitani I, Baskin RJ, Kowalczykowski SC. 2007. RecBCD enzyme switches lead motor subunits in response to chi recognition. *Cell* **131**:694–705. doi: 10.1016/j.cell.2007.09.023

Strauss C, Kornowski M, Benvenisty A, Shahar A, Masury H, Ben-Porath I, Ravid T, Arbel-Eden A, Goldberg M. 2014. The DNA2 nuclease/helicase is an estrogen-dependent gene mutated in breast and ovarian cancers. *Oncotarget* **5**:9396–9409. doi: 10.18632/oncotarget.2414

Sturzenegger A, Burdova K, Kanagaraj R, Levikova M, Pinto C, Cejka P, Janscak P. 2014. DNA2 cooperates with the WRN and BLM RecQ helicases to mediate long-range DNA end resection in human cells. *Journal of Biological Chemistry* **289**:27314–27326. doi: 10.1074/jbc.M114.578823

Symington LS. 2014. End resection at double-strand breaks: mechanism and regulation. *Cold Spring Harbor Perspectives in Biology* **6**:a016436. doi: 10.1101/cshperspect.a016436

Taylor AF, Smith GR. 2003. RecBCD enzyme is a DNA helicase with fast and slow motors of opposite polarity. *Nature* **423**:889–893. doi: 10.1038/nature01674

Thangavel S, Berti M, Levikova M, Pinto C, Gomathinayagam S, Vujanovic M, Zellweger R, Moore H, Lee EH, Hendrickson EA, Cejka P, Stewart S, Lopes M, Vindigni A. 2015. DNA2 drives processing and restart of reversed replication forks in human cells. *The Journal of Cell Biology* **208**:545–562. doi: 10.1083/jcb.201406100

Tomimatsu N, Mukherjee B, Deland K, Kurimasa A, Bolderson E, Khanna KK, Burma S. 2012. Exo1 plays a major role in DNA end resection in humans and influences double-strand break repair and damage signaling decisions. *DNA Repair* **11**:441–448. doi: 10.1016/j.dnarep.2012.01.006

Tsutakawa SE, Lafrance-Vanasse J, Tainer JA. 2014. The cutting edges in DNA repair, licensing, and fidelity: DNA and RNA repair nucleases sculpt DNA to measure twice, cut once. *DNA Repair* **19**:95–107. doi: 10.1016/j.dnarep.2014.03.022

Wanrooij PH, Burgers PM. 2015. Yet another job for Dna2: Checkpoint activation. *DNA Repair* **32**:17–23. doi: 10.1016/j.dnarep.2015.04.009

Wu L, Hickson ID. 2006. DNA helicases required for homologous recombination and repair of damaged replication forks. *Annual Review of Genetics* **40**:279–306. doi: 10.1146/annurev.genet.40.110405.090636

Wu Y, Brosh RM. 2012. DNA helicase and helicase-nuclease enzymes with a conserved iron-sulfur cluster. *Nucleic Acids Research* **40**:4247–4260. doi: 10.1093/nar/gks039

Yang SH, Zhou R, Campbell J, Chen J, Ha T, Paull TT. 2013. The SOSS1 single-stranded DNA binding complex promotes DNA end resection in concert with Exo1. *The EMBO Journal* **32**:126–139. doi: 10.1038/emboj.2012.314

Yeeles JT, Cammack R, Dillingham MS. 2009. An iron-sulfur cluster is essential for the binding of broken DNA by AddAB-type helicase-nucleases. *Journal of Biological Chemistry* **284**:7746–7755. doi: 10.1074/jbc.M808526200

Yeeles JT, Dillingham MS. 2007. A dual-nuclease mechanism for DNA break processing by AddAB-type helicase-nucleases. *Journal of Molecular Biology* **371**:66–78. doi: 10.1016/j.jmb.2007.05.053

Zheng L, Zhou M, Guo Z, Lu H, Qian L, Dai H, Qiu J, Yakubovskaya E, Bogenhagen DF, Demple B, Shen B. 2008. Human DNA2 is a mitochondrial nuclease/helicase for efficient processing of DNA replication and repair intermediates. *Molecular Cell* **32**:325–336. doi: 10.1016/j.molcel.2008.09.024

Zhou C, Pourmal S, Pavletich NP. 2015. Dna2 nuclease-helicase structure, mechanism and regulation by Rpa. *eLife* **4**:e09832. doi: 10.7554/eLife.09832

Zhu Z, Chung WH, Shim EY, Lee SE, Ira G. 2008. Sgs1 helicase and two nucleases Dna2 and Exo1 resect DNA double-strand break ends. *Cell* **134**:981–994. doi: 10.1016/j.cell.2008.08.037

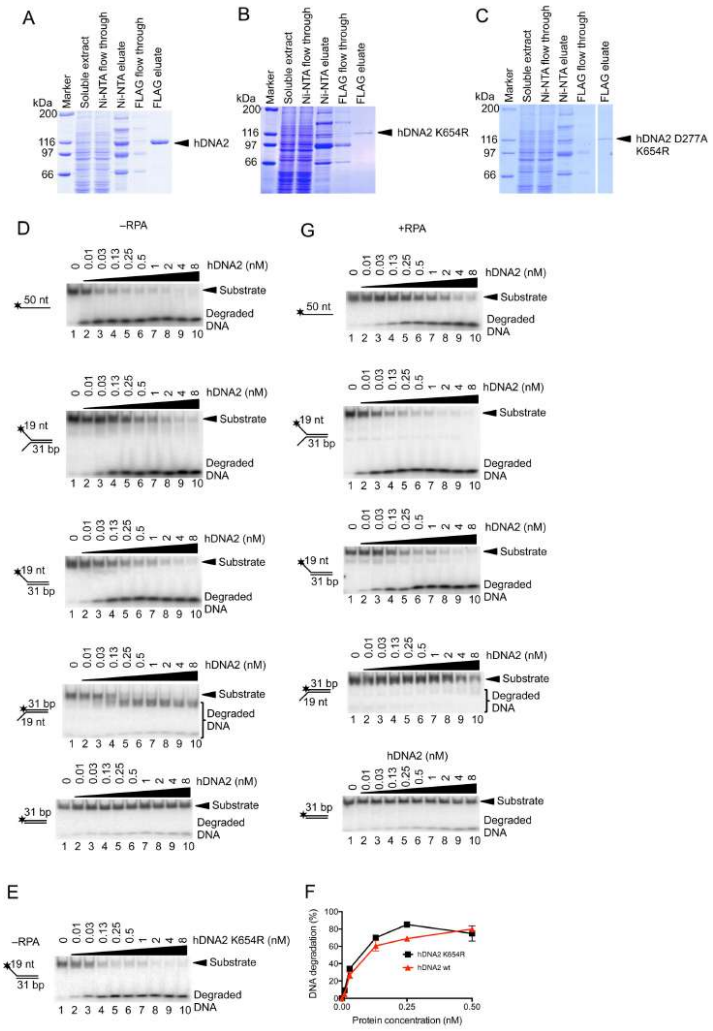

Figure 1—figure supplement 1. Human RPA guides the hDNA2 nuclease to 5' terminated ssDNA. (A–C) Representative 10% polyacrylamide gels stained with Coomassie blue showing samples from (A) wild type hDNA2, (B) helicase-deficient hDNA2 K654R, and (C) nuclease- and helicase-deficient hDNA2 D277A K654R purifications. A mutation within the helicase motif leads to reduced expression levels. (D) Representative 10% polyacrylamide gels showing the nuclease activity of wild type hDNA2 on various ^{32}P-labeled oligonucleotide-based substrates. Reactions were carried out without hRPA. (E) Nuclease activity of the helicase-deficient hDNA2 K654R mutant. Assay as in panel D with 5' overhanged DNA substrate. (F) Quantitation of data from experiments as shown in Figure 1—figure supplement 1D,E. Averages shown, n = 2; error bars, SEM. (G) Reactions as in D but with 15 nM hRPA.

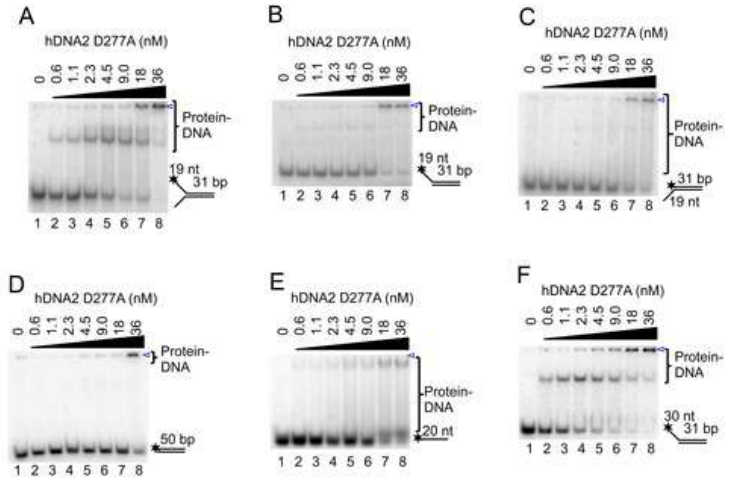

Figure 1—figure supplement 2. hDNA2 binds ssDNA. (A–F) Representative 6% polyacrylamide gels showing the binding of nuclease-deficient hDNA2 D277A to various 32P-labeled oligonucleotide-based substrates. The blue triangle indicates the position of wells.

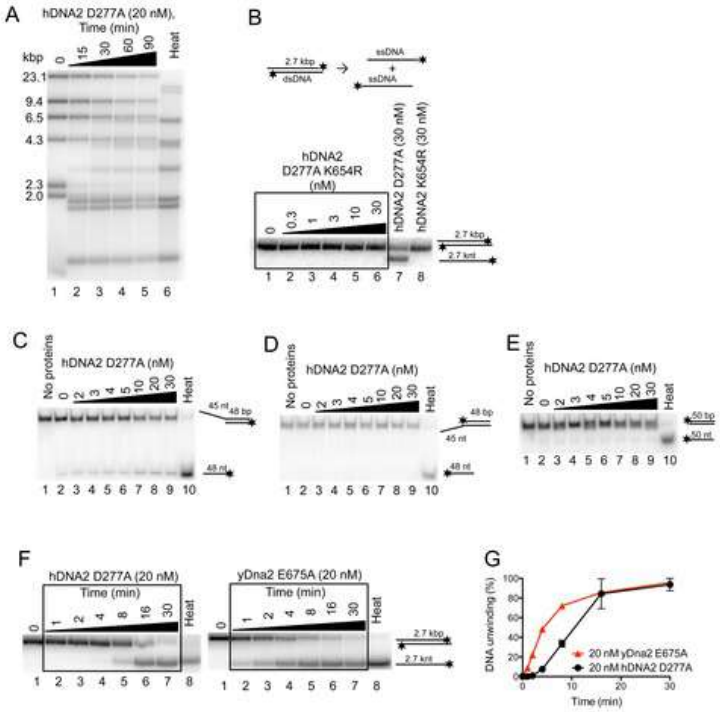

Figure 3—figure supplement 1. hDNA2 D277A unwinds plasmid- and oligonucleotide-based DNA substrates. (A) Representative 1% agarose gel showing hDNA2 D277A helicase activity on a λDNA/HindIII substrate in a time-course experiment with 346 nM hRPA. Heat, heat-denatured DNA substrate. (B) Representative 1% agarose gel showing that nuclease- and helicase-deficient hDNA2 D277A K654R (lanes 2–6) and helicase-deficient hDNA2 K654R (lane 8) do not exhibit helicase activity. Lane 7, DNA unwinding by nuclease-deficient DNA2 D277A. Reactions contained 215 nM hRPA. (C–E) Representative 10% polyacrylamide gels showing the helicase activity of hDNA2 D277A with (C) 5' overhang, (D) 3' overhang and with (E) dsDNA substrates. Reactions contained 7.5 nM RPA. Heat, heat-denatured DNA substrate. (F) Representative 1% agarose gels showing DNA unwinding of a 2.7 kbp-long substrate by either hDNA2 D277A (left part, at 37°C) or yDna2 E675A (right part, at 30°C) in a kinetic experiment with 215 nM human RPA or 267 nM yeast RPA respectively. (G) Quantitation of experiments such as shown in F. Averages shown, n = 2; error bars, SEM.

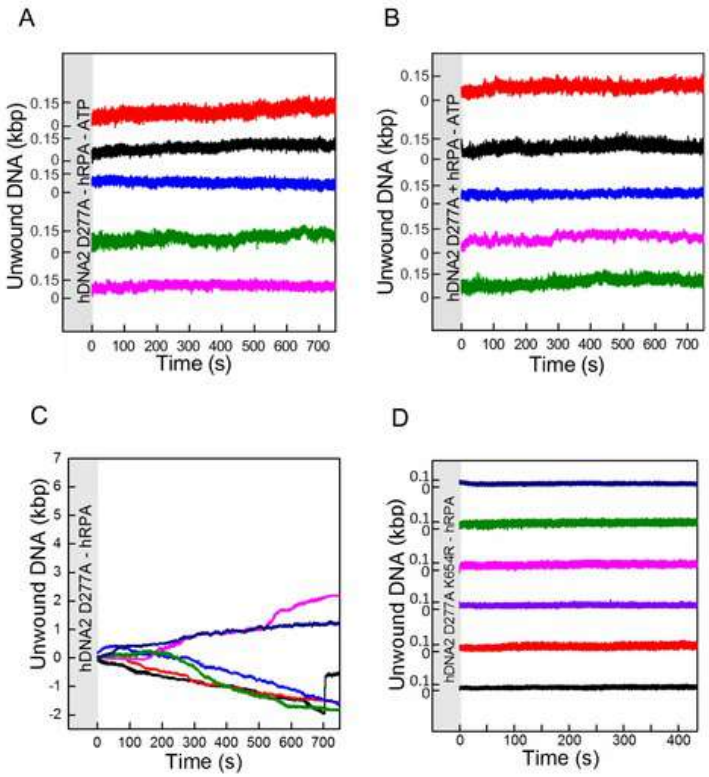

Figure 4—figure supplement 1.Single molecule experiments reveal that DNA unwinding by hDNA2 D277A is dependent on ATP and hRPA.Experiments were carried out as in Figure 4B by adding hDNA2 D277A but omitting (A) both ATP and hRPA, (B) ATP or (C) hRPA only. While no activity was observed at all in the absence of ATP (independently of the presence of hRPA), some slow length changes were observed in presence of ATP but absence of hRPA that indicate a residual unwinding activity of hDNA2 D277A. This activity was dependent on the intact helicase domain of hDNA2 since experiments testing the nuclease- and helicase-deficient hDNA2 D277A K654R variant did not show such length changes as shown in (D). Length shortening may occur due to DNA looping with at least two hDNA2 molecules bound at different positions on the substrate. At this point however we have no evidence that this is physiologically relevant.

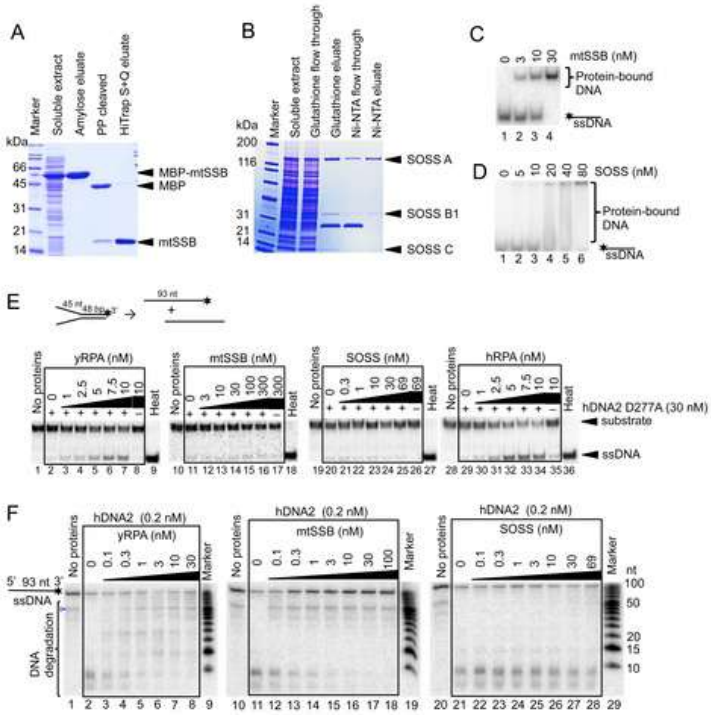

Figure 5—figure supplement 1. hDNA2 nuclease and helicase activities are regulated by ssDNA-binding proteins.10% SDS-PAGE stained with Coomassie blue showing the purification procedures of (A) mtSSB and (B) the SOSS complex. PP, PreScission Protease. The ssDNA-binding properties of (C) mtSSB and (D) SOSS were tested in electrophoretic mobility shift assay. Increasing concentrations of either complex were incubated with 32P-labeled ssDNA. Representative 6% polyacrylamide gels are shown. (E) Representative 10% polyacrylamide gels showing the helicase activity of hDNA2 D277A on a 32P-labeled Y-structured DNA substrate supplemented with increasing concentrations of yRPA, mtSSB, SOSS and hRPA. 10 nM hRPA was able to melt the Y-structure to a minor degree on its own (lane 35). Heat, heat-denatured DNA substrate. Quantitation is shown in Figure 5C. (F) Representative 20% polyacrylamide denaturing urea gels showing the nuclease activity of hDNA2 (0.2 nM) on a 93 nt-long ssDNA 32P-labeled at its 3' end. Reactions were supplemented with increasing concentrations of yRPA, mtSSB and SOSS. The blue triangle indicates a truncation of the substrate. Quantitation is shown in Figure 5D.

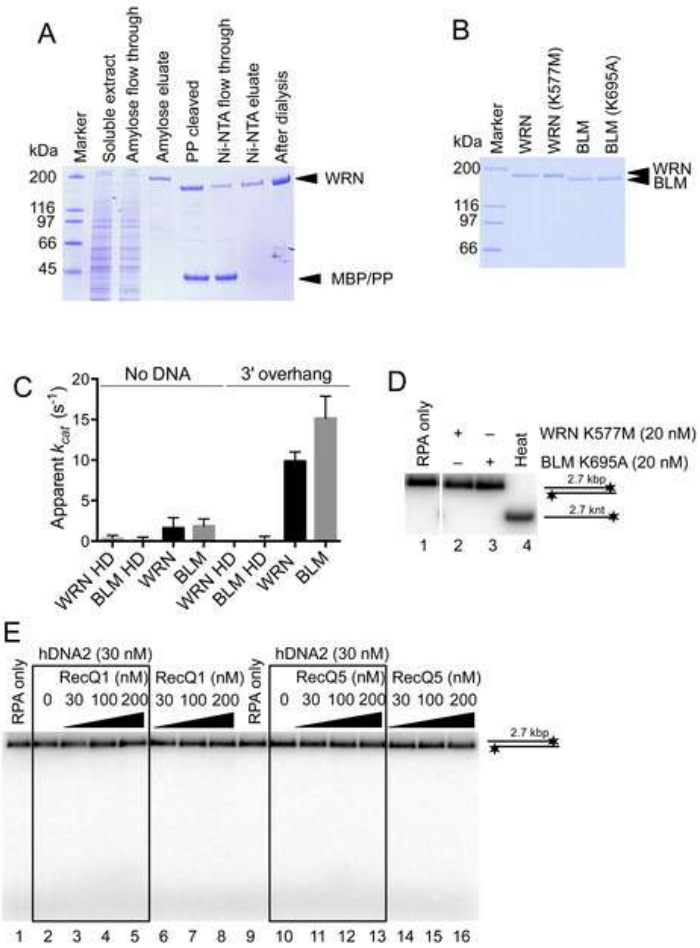

Figure 6—figure supplement 1. Purification of WRN and BLM proteins. (A) 10% SDS-PAGE stained with Coomassie blue showing the purification procedure of wild type WRN. PP, PreScission Protease. (B) 10% SDS-PAGE stained with Coomassie showing wild type WRN, helicase-deficient WRN K577M, wild type BLM and helicase-deficient BLM K695A protein preparations used in this study. (C) Apparent ATP turnover number *kcat* showing the ATPase activity of WRN or BLM incubated with 3' overhang DNA substrate. The reactions contained 12 nM of the respective enzyme. WRN K577M and BLM K695A are devoid of ATPase activity. Averages shown, n = 2; error bars, SEM. (D) Representative 1% agarose gel showing results of unwinding assays with helicase-deficient WRN K577M and BLM K695A variants. The reactions were supplemented with 25 mM NaCl and contained 215 nM hRPA. Heat, heat-denatured DNA substrate. (E) Representative 1% agarose gel showing dsDNA degradation/unwinding reactions containing hDNA2 and RecQ1 or RecQ5 respectively. The reactions were supplemented with 50 mM NaCl and 215 nM RPA.

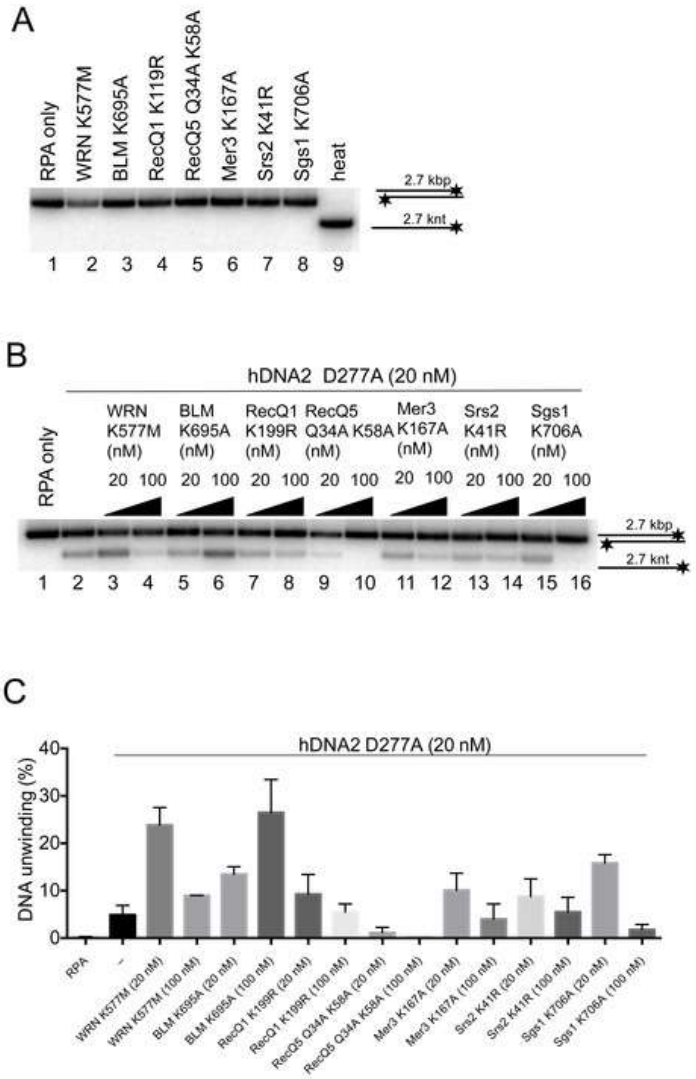

Figure 7—figure supplement 1. The functional integration of the helicase activity of hDNA2 is specific for WRN and BLM. (A) Representative 1% agarose gel showing that the helicase-deficient mutants of various DNA helicases are not able to unwind a 2.7 kbp-long dsDNA substrate. (B) Representative 1% agarose gel showing DNA unwinding by hDNA2 D277A and its stimulation by helicase-deficient variants of various DNA helicases. The reactions were supplemented with 25 mM NaCl and contained 215 nM hRPA. (C) Quantitation of experiments such as shown in Figure 7—figure supplement 1. Averages shown, n = 2–8; error bars, SEM.

Supplementary file 1A: Codon-optimized nucleotide sequence of hDNA2 gene for the expression in *Sf9* cells

ATGGAGCAATTGAACGAACTCGAACTGTTGATGGAAAAGTCATTCTGGGAGGAGGCTG
AACTGCCCGCCGAACTCTTCCAAAAGAAGGTGGTCGCTTCGTTCCCAAGGACTGTCCTG
TCCACAGGAATGGACAACAGATACCTCGTGTTGGCCGTCAACACCGTTCAGAACAAGGA
GGGTAACTGCGAAAAGAGGCTCGTGATCACTGCTTCACAATCGTTGGAGAACAAGGAAT
TGTGCATCCTGAGAAACGACTGGTGTTCAGTTCCCGTGGAGCCTGGCGATATCATCCAC
CTGGAAGGAGACTGCACCTCCGATACTTGGATCATCGACAAGGATTTCGGATACCTGAT
CCTCTACCCTGACATGCTGATCTCTGGTACTAGCATCGCTTCCTCTATCCGTTGTATGCG
TCGCGCCGTCCTCTCCGAGACATTCCGTAGCTCAGACCCCGCCACTCGCCAGATGTTGAT
CGGCACAGTGCTGCACGAAGTCTTCCAAAAGGCTATCAACAACTCTTTCGCCCCTGAGA
AGCTCCAGGAATTGGCTTTCCAGACTATCCAAGAGATCAGGCACCTGAAGGAAATGTAC
AGATTGAACCTGTCCCAGGACGAGATCAAGCAAGAGGTGGAAGATTACCTGCCCTCTTT
CTGCAAGTGGGCTGGAGACTTCATGCACAAGAACACTAGCACAGATTTCCCCCAGATGC
AACTCTCATTGCCTTCGGACAACTCCAAGGATAACTCTACCTGTAACATCGAGGTTGTG
AAGCCCATGGACATCGAGGAATCTATCTGGAGCCCTCGTTTCGGCCTGAAGGGAAAGAT
CGATGTCACAGTTGGAGTGAAGATCCACCGCGGTTACAAGACCAAGTACAAGATCATGC
CACTGGAGCTCAAGACTGGCAAGGAGTCCAACTCTATCGAACACAGGTCTCAGGTCGTT
CTGTACACTCTGCTCAGCCAAGAGAGGAGAGCTGACCCCGAAGCCGGCTTGCTGCTCTA
CCTCAAGACCGGACAGATGTACCCCGTCCCTGCTAACCACCTGGATAAGAGGGAGTTGC
TGAAGCTCAGAAACCAGATGGCCTTCTCTTTGTTCCACCGTATCAGCAAGTCAGCTACC
CGCCAGAAGACTCAACTGGCCAGCCTCCCTCAGATCATCGAGGAAGAGAAGACTTGCAA
GTACTGTTCACAAATCGGCAACTGCGCTCTGTACTCGCGCGCCGTGGAGCAGCAAATGG
ACTGTTCGTCCGTGCCCATCGTCATGCTCCCTAAGATCGAAGAGGAAACACAGCACCTC
AAGCAAACCCACTTGGAGTACTTCTCTCTGTGGTGCTTGATGCTGACCCTCGAATCGCA
GTCCAAGGACAACAAGAAGAACCACCAAAACATCTGGCTGATGCCTGCTTCCGAGATGG
AAAAGTCTGGAAGCTGCATCGGTAACCTCATCCGCATGGAGCACGTTAAGATCGTGTGC
GACGGCCAGTACCTGCACAACTTCCAGTGTAAGCACGGCGCTATCCCAGTGACCAACCT
CATGGCCGGTGACAGGGTCATCGTTTCGGGCGAGGAAAGGTCCTTGTTCGCCCTGTCTA
GAGGTTACGTCAAGGAGATCAACATGACCACTGTTACTTGCCTCTTGGACAGGAACCTC
AGCGTCTTGCCCGAATCAACACTGTTCAGACTCGATCAGGAGGAAAAGAACTGTGACAT
CGATACACCTTTGGGCAACCTGTCCAAGCTCATGGAGAACACCTTCGTGTCTAAGAAGT
TGCGTGACCTGATCATCGATTTCCGCGAACCACAGTTCATCTCCTACTTGTCTAGCGTTC
TGCCGCACGACGCTAAGGATACCGTGGCCTGCATCCTCAAGGGTTTGAACAAGCCACAG
AGGCAAGCCATGAAGAAGGTCCTGCTCAGCAAGGACTACACCCTGATCGTTGGCATGCC
GGGAACTGGCAAGACAACCACTATCTGCACACTCGTGAGAATCTTGTACGCTTGTGGAT
TCTCCGTCTTGCTGACATCCTACACCCACTCTGCTGTTGACAACATCCTCTTGAAGCTGG
CCAAGTTCAAGATCGGCTTCTTGCGTCTGGGACAGATCCAAAAGGTGCACCCCGCTATC
CAGCAATTCACCGAGCAGGAAATCTGCCGCTCAAAGTCGATCAAGTCGCTGGCTCTGCT
CGAGGAACTCTACAACTCCCAGTTGATCGTCGCCACAACCTGTATGGGAATCAACCACC
CTATCTTCTCTCGTAAGATCTTCGACTTCTGCATCGTGGATGAGGCCTCACAGATCTCG
CAACCAATCTGTCTGGGCCCGCTCTTCTTCAGCCGTCGCTTCGTGTTGGTCGGAGACCAC
CAGCAACTGCCCCCTCTCGTCTTGAACCGTGAGGCTCGCGCCCTGGGCATGTCCGAGTCT
CTGTTCAAGAGGCTCGAACAGAACAAGTCTGCTGTGGTCCAGCTGACTGTGCAATACAG
AATGAACAGCAAGATCATGAGCTTGTCAAACAAGCTGACCTACGAGGGCAAGCTCGAAT
GCGGCTCAGACAAGGTTGCTAACGCCGTGATCAACTTGCGCCACTTCAAGGATGTCAAG
CTGGAGCTCGAATTCTACGCCGACTACTCCGATAACCCCTGGTTGATGGGTGTGTTCGA

GCCAAACAACCCGGTCTGCTTCCTGAACACCGACAAGGTCCCAGCTCCGGAGCAGGTTG
AAAAGGGTGGCGTCTCAAACGTTACCGAAGCCAAGCTCATCGTTTTCTTGACTTCGATC
TTCGTGAAGGCTGGATGCTCGCCATCCGACATCGGTATCATCGCCCCGTACCGTCAGCA
ACTGAAGATCATCAACGATTTGCTGGCTCGCTCAATCGGTATGGTTGAGGTGAACACCG
TGGACAAGTACCAGGGCCGTGATAAGTCCATCGTCCTGGTTAGCTTCGTGCGCTCAAAC
AAGGACGGTACAGTCGGCGAGCTCTTGAAGGATTGGAGGAGACTGAACGTCGCTATCAC
CCGTGCCAAGCACAAGCTCATCCTGCTCGGCTGCGTGCCATCCCTGAACTGTTACCCACC
GCTCGAGAAGTTGCTGAACCACCTGAACAGCGAAAAGCTGATCATCGACCTCCCGTCAC
GCGAGCACGAATCCCTCTGCCACATCCTCGGCGACTTCCAGCGTGAATAA

Supplementary file 1A: 5'-3' nucleotide sequence of human DNA2 gene codon-optimized for the expression in Sf9 insect cells.

Supplementary file 1B: Sequences of oligonucleotides used in this study.	
Name	**Sequence (5' to 3')**
Primer 308	GCTGGTTTAGGACGCACTTG
X12-3	GACGTCATAGACGATTACATTGCTAGGACATGCTGTCTAGAGACTATCGC
X12-3 SC	TTGCTAGGACATGCTGTCTAGAGACTATCGC
#292	GGATTACATTGCTAGGACATGCTGTCTAGAGACTATCGC
X12-4C	GCGATAGTCTCTAGACAGCATGTCCTAGCAATGTAATCGTCTATGACGTC
X12-4SC	GCGATAGTCTCTAGACAGCATGTCCTAGCAA
X12-3 HJ1S	AAAAAAAAAAAAAAAAAAAATAACCTAGCGATGGAACGTAAGTCGCGAT
X12-3 TOPL	GACGTCATAGACGATTACATTGCTAGGACATGCTGTCTAGAGACTATCGCGACTTACGTTCCATCGCTAGGTTATTTTTTTTTTTTTTTTTTTT
X12-4NC	GCGATAGTCTCTAGACAGCATGTCCTAGCAAGCCAGAATTCGGCAGGCTA
X12-3 HJ2Sb	ATTACGATTCGTTACCCATTCACTGTCAGAAGGCACCAGATAGATCTC
X12-3 HJ3	GAGATCTATCTGGTGCCTTCTGACAGTGAATGGGTAACGAATCGTAATAGTCTCTAGACAGCATGTCCTAGCAATGTAATCGTCTATGACGTC
Supplementary file 1B: Nucleotide sequences of oligonucleotides used in this study.	

Supplementary file 1C: Oligonucleotide-based DNA substrates used in this study.		
DNA substrate:	**5' labeled oligonucleotide:**	**Unlabeled oligonucleotide:**
ssDNA (20 nt)	Primer 308	-
ssDNA (50 nt)	X12-3	-
dsDNA (31 bp)	X-12-3SC	X12-4SC
dsDNA (50 bp)	X12-3	X12-4C
5’ overhang (19 nt / 31 bp)	X12-3	X12-4SC
5’ overhang (30 nt / 31 bp)	#292	X12-4SC
5’ overhang (45 nt / 48 bp)	X12-3 HJ1S	X12-3 TOPL
3’ overhang (19 nt / 31 bp)	X12-3SC	X12-4NC
3’ overhang (45 nt / 48 bp)	X12-3 HJ2Sb	X12-3 HJ3
Y-structure (19 nt /31 bp)	X12-3	X12-4NC
DNA substrate:	**3' labeled oligonucleotide:**	**Unlabeled oligonucleotide:**
ssDNA (93 nt)	X12-3HJ3	**-**
Y-structure (45 nt / 48 bp)	X12-3HJ3	X12-3TOPL
Supplementary file 1C: Oligonucleotide-based DNA substrates used in this study and their components. The following substrates were used for the assays: ssDNA (50 nt), dsDNA (50 bp), 5' overhang (19 nt / 31 bp), 3' overhang (19 nt / 31 bp), Y-structure (19 nt /31 bp), unless indicated differently in the figure legends.		

2.2.2 The motor activity of DNA2 functions as an ssDNA translocase to promote DNA end resection

Maryna Levikova[#], **Cosimo Pinto[#]** and Petr Cejka

#: These authors contributed equally to this work.

The article was published in Genes & Dev. 2017. 31: 493-502.

I designed the research together with M.L. and P. C. and performed experiments together with M.L. All authors analyzed the data and I wrote the manuscript together with M. L. and P. C.

The motor activity of DNA2 functions as an ssDNA translocase to promote DNA end resection

Maryna Levikova,[1,3] Cosimo Pinto,[1,3] and Petr Cejka[1,2]

[1]Institute of Molecular Cancer Research, University of Zurich, 8057 Zurich, Switzerland; [2]Institute for Research in Biomedicine, Università della Svizzera italiana, 6500 Bellinzona, Switzerland

DNA2 nuclease–helicase functions in DNA replication and recombination. This requires the nuclease of DNA2, while, in contrast, the role of the helicase activity has been unclear. We now show that the motor activity of both recombinant yeast and human DNA2 promotes efficient degradation of long stretches of ssDNA, particularly in the presence of the replication protein A. This degradation is further stimulated by a direct interaction with a cognate RecQ family helicase, which functions with DNA2 in DNA end resection to initiate homologous recombination. Consequently, helicase-deficient yeast *dna2 K1080E* cells display reduced resection speed of HO-induced DNA double-strand breaks. These results support a model of DNA2 and the RecQ family helicase partner forming a bidirectional motor machine, where the RecQ family helicase is the lead helicase, and the motor of DNA2 functions as a ssDNA translocase to promote degradation of 5′-terminated DNA.

[*Keywords*: DNA helicase; DNA nuclease; yDna2; hDNA2; ssDNA translocase; DNA end resection]

Supplemental material is available for this article.

Received December 16, 2016; revised version accepted February 13, 2017.

ssDNA translocases are motor proteins that couple ATP hydrolysis to translocation on ssDNA with either 3′ → 5′ or 5′ → 3′ polarity (Lohman et al. 2008). Some but not all ssDNA translocases are DNA helicases capable of unwinding dsDNA (Lohman et al. 2008). The DNA replication-dependent helicase/nuclease 2 (yDna2 from *Saccharomyces cerevisiae*, hDNA2 from humans) possesses a RecB family nuclease domain and a superfamily I helicase domain (Budd et al. 1995, 2000; Bae et al. 1998). The nuclease of both yeast and human DNA2 is specific for ssDNA and can degrade both 3′- and 5′-terminated ssDNA strands (Bae et al. 1998; Masuda-Sasa et al. 2006). The cognate ssDNA-binding replication protein A (RPA) specifically inhibits 3′ → 5′ DNA degradation by DNA2 (Cejka et al. 2010; Niu et al. 2010; Nimonkar et al. 2011), suggesting that the DNA2 nuclease degrades ssDNA exclusively with a 5′ → 3′ directionality under physiological conditions.

The helicase activity of both yeast and human DNA2 is paradoxically cryptic, as it unwinds dsDNA only when the nuclease activity is inactivated (Levikova et al. 2013; Pinto et al. 2016). The structure of mouse DNA2 revealed that the nuclease active site is located inside a narrow tunnel that accommodates only ssDNA (Zhou et al. 2015). Importantly, the nuclease tunnel is positioned ahead of the superfamily I helicase domain. This supported a model in which the DNA2 nuclease cleaves ssDNA overhangs that are required for loading of the DNA2 helicase domain on the DNA substrate (Levikova et al. 2013; Pinto et al. 2016). Overhang cleavage by the DNA2 nuclease thus prevents DNA unwinding by the DNA2 helicase, but the reason why the helicase domain appears to compete with the nuclease domain for DNA substrate in a physiological context has remained unclear. Genetic and cell biological experiments offer few insights into the function of the DNA2 helicase. These experiments are limited by the fact that DNA2 and its nuclease activity are required for viability in yeast cells, while both helicase and nuclease activities are essential in human cells, making phenotypic analysis associated with DNA2 defects challenging (Formosa and Nittis 1999; Budd et al. 2000; Duxin et al. 2012; Wanrooij and Burgers 2015; Olmezer et al. 2016).

To repair a DNA double-strand break (DSB) by homologous recombination, the 5′-terminated strand of the DSB must be first nucleolytically resected to reveal a 3′-terminated ssDNA overhang (Cejka 2015). This serves as a substrate for the strand exchange protein RAD51 and primes DNA synthesis in later steps of the recombination

[3]**These authors contributed equally to this work.**
Corresponding author: petr.cejka@irb.usi.ch
Article published online ahead of print. Article and publication date are online at http://www.genesdev.org/cgi/doi/10.1101/gad.295196.116.

pathway. There are two main pathways capable of resecting long lengths of dsDNA, catalyzed by either the EXO1 or DNA2 nuclease (Gravel et al. 2008; Mimitou and Symington 2008; Zhu et al. 2008). While EXO1 is able to resect a 5′-terminated DNA strand of a DNA duplex (Tran et al. 2002; Cannavo et al. 2013), research from several laboratories established that DNA2 functions in complex with a cognate RecQ family helicase. This includes Sgs1 in *S. cerevisiae* and the Werner syndrome protein (WRN) or Bloom syndrome protein (BLM) in human cells (Zhu et al. 2008; Nimonkar et al. 2011; Sturzenegger et al. 2014). The helicase activity of the respective RecQ family member and the nuclease of DNA2 are essential in DNA end resection (Zhu et al. 2008; Nimonkar et al. 2011; Sturzenegger et al. 2014). All studies to date failed to explain the function of the DNA2 helicase. Here we report that the motor activity of both yeast and human DNA2 proteins greatly stimulates degradation of long ssDNA molecules by acting as a ssDNA translocase with a 5′ → 3′ polarity. The motor activity within wild-type DNA2 is incapable of unwinding and degrading dsDNA (Levikova et al. 2013; Pinto et al. 2016) but, in contrast, is required to efficiently degrade long ssDNA. These results infer a model in which the cognate RecQ helicase partner is the lead helicase that provides DNA2 with ssDNA, and DNA2 is using its motor coupled with nuclease activity to efficiently degrade the unwound 5′-terminated ssDNA strand. Yeast cells expressing physiological levels of the helicase-deficient Dna2 K1080E variant from its natural locus in genomic DNA display an impaired DNA end resection phenotype, suggesting that the helicase activity of DNA2 functions to promote DNA end resection in vivo.

Results

The motor of yeast and human DNA2 promotes degradation of long ssDNA

Both yeast and human DNA2 possess the capacity to unwind dsDNA, yet this is paradoxically revealed only when the nuclease of DNA2 is inactivated (Levikova et al. 2013; Pinto et al. 2016). In accord with these observations, we show here that nuclease-deficient yDna2 E675A efficiently unwound Y-structured DNA, producing ssDNA. In contrast, the processing of this substrate by wild-type and helicase-deficient yDna2 K1080E variants was indistinguishable and resulted only in DNA degradation (Fig. 1A–C; Supplemental Fig. S1A). The helicase activity of yDna2 thus had no apparent effect on the degradation of the oligonucleotide-based DNA by wild-type yDna2 (Fig. 1A–C; Supplemental Fig. S1A). The nuclease of yDna2 masks its unwinding activity, in agreement with previous data in both yeast and human systems (Levikova et al. 2013; Pinto et al. 2016). To elucidate the function of the DNA2 motor, we investigated the helicase-proficient and helicase-deficient yeast Dna2 variants in the degradation of long ssDNA. As DNA2 proteins in all eukaryotic organisms function in conjunction with a DNA helicase, ssDNA may better mimic the structure on which DNA2 acts in vivo. To this point, we digested λDNA with HindIII, ^{32}P-labeled the restricted fragments at the 3′ end, and heat-denatured the dsDNA to prepare ssDNA fragments of ~100 to ~23,000 nucleotides (nt) in length. Strikingly, wild-type yDna2 was dramatically faster in ssDNA degradation than the helicase-deficient K1080E variant (Fig. 1D) despite equivalent levels of nuclease activity in both preparations when assayed on oligonucleotide-based DNA (Fig. 1A–C; Supplemental Fig. S1A). We detected no endonuclease activity of yDna2 under our experimental conditions when yRPA was present (Supplemental Fig. S1B), which suggested that the ssDNA degradation occurs from an open end. The gradual DNA degradation and the presence of smear below the 3′-labeled substrate bands in Figure 1D clearly indicate that the ssDNA degradation by yDna2 occurred with a 5′ → 3′ polarity, as expected for yDna2 in the presence of yRPA (Cejka et al. 2010; Niu et al. 2010). The motor activity of yDna2 also promoted ssDNA degradation when using a yDna2 mutant lacking the N-terminal regulatory domain (yDna2 ΔN), showing that the first 405 residues of yDna2 are dispensable for the motor-assisted ssDNA degradation (Supplemental Fig. S1C,D). These results could be recapitulated with recombinant human DNA2, which lacks the N-terminal regulatory domain found in yeast (Fig. 1E). In accord with the slower rate of DNA unwinding by hDNA2 compared with yDna2 (Levikova et al. 2013; Pinto et al. 2016), the overall rate of ssDNA degradation was slower by the human protein than by the yeast homolog. Importantly, however, the helicase-deficient hDNA2 K654R was clearly less efficient in ssDNA degradation than wild-type hDNA2, showing that the involvement of the DNA2 motor in accelerating ssDNA degradation is conserved in evolution (Fig. 1E). In summary, we show that, unlike in the processing of duplex DNA, where the helicase of yeast and human DNA2 is entirely masked by its nuclease, the motor activity of DNA2 promotes degradation of long ssDNA.

To gain further insights into the role of the yDna2 motor in DNA degradation, we prepared a 2200-nt-long ssDNA randomly labeled with [α-^{32}P] dATP. We analyzed the degradation of this substrate by wild-type yDna2 and the helicase-deficient yDna2 K1080E variant in a kinetic setup and separated the reaction products on agarose gels (Fig. 2A). Wild-type yDna2 degraded ssDNA rapidly and unexpectedly produced DNA degradation products of two different lengths (indicated by the open and closed arrows in Fig. 2A). In contrast, DNA degradation by helicase-dead yDna2 K1080E was slower and more gradual and resulted in only the shorter ssDNA degradation products (Fig. 2A). We next analyzed the reaction products on denaturing gels to determine the length of the ssDNA products (Fig. 2B). Wild-type yDna2 gave rise to fragments ranging from ~5 to ~100 nt in length (Fig. 2B [lanes 2–4], C), while helicase-deficient yDna2 K1080E yielded only products between ~5 and ~12 nt in length (Fig. 2B [lanes 6–8], C). Kinetic experiments revealed that wild-type yDna2 first produced the longer fragments, which were further degraded at later time points (Fig. 2D,G). In contrast, the majority of the products generated by helicase-deficient yDna2 K1080E were <20 nt at any time point tested (Fig. 2E,G). In the absence of ATP, the rates of

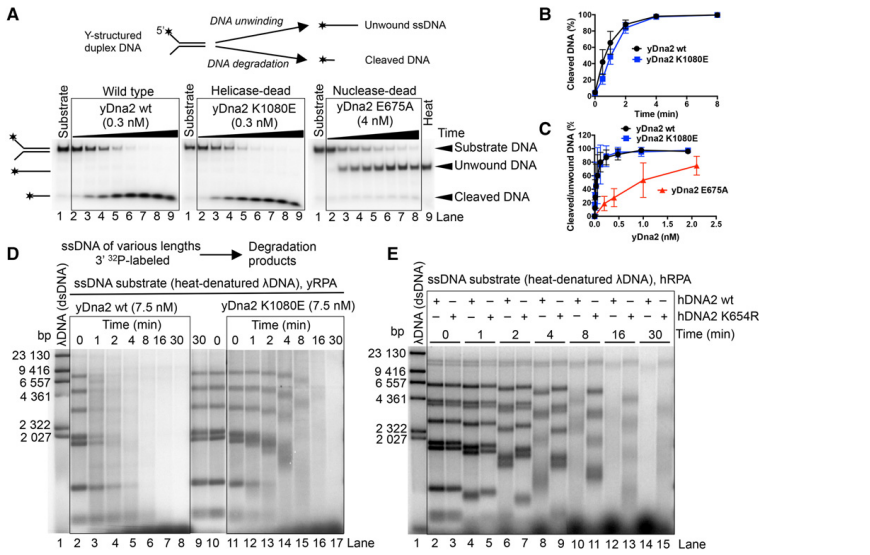

Figure 1. The helicase activity of yeast and human DNA2 promotes ssDNA degradation. (*A*) Processing of 5′ ^{32}P-labeled Y-structured DNA substrate by wild-type, helicase-deficient K1080E, and nuclease-deficient E675A yDna2 variants. The reactions contained 22.5 nM yeast RPA. (Heat) Heat-denatured substrate. The panel shows representative native 10% polyacrylamide gels. (*B*) Quantitation of the assays shown in *A*. Averages are shown for $n = 2$. Error bars indicate range. (*C*) Quantitation of experiments that are shown in Supplemental Figure S1A. Various concentrations of the yDna2 variants were used with the Y-structured DNA substrate. (*D*) Representative 1% agarose gel showing degradation kinetics of 3′ ^{32}P-labeled ssDNA fragments (derived from λDNA) of various lengths by wild-type or helicase-deficient K1080E yDna2 in the presence of 1.08 µM yRPA. The sizes of the corresponding dsDNA fragments are indicated at the *left*. (*E*) Similar experiment as in *D*, showing the degradation kinetics of ssDNA by 20 nM human wild-type and helicase-deficient K654R hDNA2 in the presence of 576 nM hRPA.

DNA degradation by wild-type and helicase-deficient yDna2 variants were indistinguishable, and both enzymes gave rise to only the short DNA degradation products (Fig. 2F; Supplemental Fig. S2A), confirming the involvement of the ATP-dependent motor activity in ssDNA degradation by yDna2. Changing the ATP:Mg^{2+} ratio influenced the product size distribution produced by wild-type but not by helicase-deficient yDna2 K1080E (Fig. 2H; Supplemental Fig. S2B). Specifically, higher ATP to Mg^{2+} ratios are known to favor the yDna2 helicase (Bae and Seo 2000; Budd et al. 2000; Masuda-Sasa et al. 2006; Fortini et al. 2011), which consequently stimulated the production of longer ssDNA fragments (Fig. 2H; Supplemental Fig. S2B). Elevated Mg^{2+} ions instead promote the yDna2 nuclease; hence, we observed a reduction of the long yDna2 translocase-dependent degradation fragments (Supplemental Fig. S2C). The yDna2 ΔN variant lacking the first 405 amino acids behaved similarly to the full-length protein and produced the long ssDNA degradation fragments in an ATP-dependent manner (Supplemental Fig. S2D). As the yDNA2/hDNA2 motor promotes the degradation of ssDNA but not dsDNA, these results collectively imply that the motor of DNA2 functions as a ssDNA translocase rather than a helicase to promote efficient degradation of ssDNA.

RPA is required for the DNA2 motor-dependent degradation of ssDNA

Cognate RPA is a critical regulator of nuclease and helicase activities of DNA2 in both yeast and human cells (Bae et al. 2001, 2003; Cejka et al. 2010; Niu et al. 2010; Nimonkar et al. 2011; Levikova et al. 2013). In accord with previous data, ssDNA degradation by yDna2 without yRPA was slow (cf. Figs. 3A and 2B). Surprisingly, in the absence of yRPA, wild-type yDna2 produced only the short DNA degradation fragments in a manner similar to the helicase-deficient yDna2 K1080E variant even in the presence of ATP (Fig. 3A,B). Thus, the motor activity of yDna2 facilitates ssDNA degradation only when both yRPA and ATP are present. Likewise, the long DNA degradation products can be observed only with wild-type yDna2 in the presence of both ATP and yRPA, implying that the long DNA degradation products result from fast ssDNA degradation (Figs. 2B, 3B). We failed to detect a similar variation of DNA degradation fragment lengths

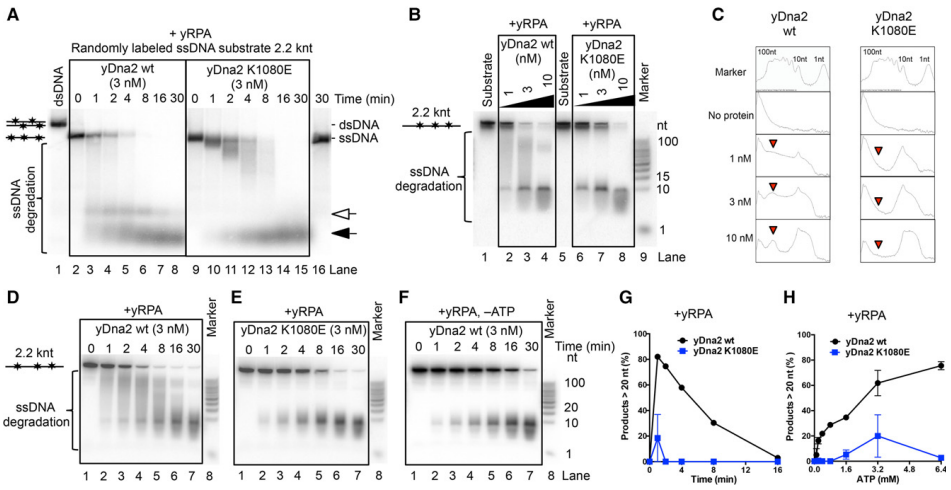

Figure 2. Cleavage of ssDNA by yDna2 results in two groups of DNA degradation products. (*A*) Degradation kinetics of ssDNA randomly labeled with ^{32}P by wild-type and helicase-dead K1080E yDna2 in the presence of 315 nM yRPA as analyzed by 1% agarose gel electrophoresis. The two main groups of DNA degradation products are indicated by the open and closed arrows. (*B*) Representative 20% polyacrylamide denaturing gels showing the degradation of ssDNA randomly labeled with ^{32}P by wild-type and K1080E yDna2. The DNA substrate was incubated with various concentrations of yDna2 for 10 min in the presence of 315 nM yRPA. (*C*) Image analysis of the experiment shown in *B* showing optical density analysis of gel lanes *1–9*. Red arrows indicate the position of ~80-nt-long DNA fragments. (*D*, *E*) Same reactions as in *A*, but the products were separated on 20% polyacrylamide denaturing gels. (*F*) Degradation kinetics of randomly labeled ssDNA by wild-type yDna2 in the absence of ATP with 315 nM yRPA. (*G*) Quantitation of experiments shown in *D* and *E*. The relative proportion of DNA degradation products >20 nt in length was determined. Averages are shown for $n = 2$. Error bars indicate range. (*H*) The effect of ATP concentration on the ssDNA degradation product length by 0.5 nM wild-type and helicase-deficient K1080E yDna2 in the presence of 315 nM yRPA in standard Mg^{2+} concentration (2 mM). Quantitation of experiments that are shown in Supplemental Figure S2B. Averages are shown for $n = 2$. Error bars indicate range.

in reactions with human DNA2 (Supplemental Fig. S3). However, the motor of hDNA2, similar to that in the yeast system, accelerated the speed of ssDNA degradation only in the presence of hRPA (Fig. 3C,D; Supplemental Fig. S3). The results presented here suggest that DNA2 is using its motor activity to facilitate the degradation of RPA-coated ssDNA, which results from DNA unwinding by a cognate RecQ family helicase partner.

WRN or BLM stimulate the ssDNA nuclease activity of DNA2

Recently, we demonstrated that the helicase activity of nuclease-deficient hDNA2 was enhanced by physical interactions with BLM or WRN and vice versa: hDNA2 stimulated DNA unwinding by WRN/BLM in the presence of hRPA (Pinto et al. 2016). This suggested that hDNA2–BLM and hRPA as well as hDNA2–WRN and hRPA form functional complexes, with their subunits stimulating each other. Here we set out to test whether BLM or WRN could promote the degradation of long ssDNA by hDNA2 and hRPA. As above, wild-type hDNA2 was much more efficient in ssDNA degradation than the helicase-deficient enzyme (Fig. 4A [cf. lanes 3 and 4], B,D). Strikingly, helicase-deficient WRN or BLM proteins strongly stimulated ssDNA degradation by both wild-type and helicase-deficient hDNA2 (Fig. 4A–D). Helicase-deficient WRN or BLM preparations alone did not show any nuclease activity, confirming that the ssDNA degradation capacity was inherent to hDNA2 (Fig. 4A, lanes 9,10). Interestingly, wild-type WRN and BLM proteins promoted the degradative capacity of hDNA2 to a lesser extent than helicase-deficient polypeptides (Supplemental Fig. S4A, cf. lanes 4 and 5 and lanes 6 and 7), possibly due to being active translocases, with a fraction of molecules moving on the same DNA strand in the opposite direction from hDNA2 and thus blocking DNA degradation. The structural role of WRN/BLM in promoting DNA degradation by hDNA2 was apparent only on long ssDNA but not when hDNA2 was assayed with WRN on oligonucleotide-based 5′ overhang DNA (Supplemental Fig. S4B). As both wild-type and helicase-deficient hDNA2 variants were stimulated by WRN and BLM (Fig. 4), the acceleration of DNA degradation is a result of WRN/BLM stimulating the hDNA2 nuclease directly and not indirectly through promoting the hDNA2 motor activity. Together, these results indicate that BLM and WRN not only stimulate the hDNA2 motor

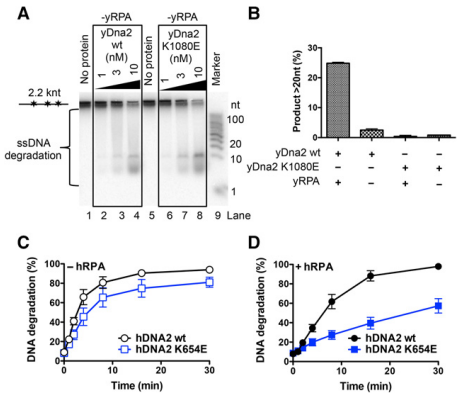

Figure 3. The motor of human and yeast DNA2 promotes degradation of RPA-coated ssDNA. (*A*) Degradation of ssDNA by wild-type and K1080E yDna2 as in Figure 2B but in the absence of yRPA, analyzed by 20% polyacrylamide denaturing gel electrophoresis. (*B*) Quantitation of DNA degradation product lengths by 1 nM wild-type and K1080E yDna2 variants from the experiments shown in *A* and Figure 2B. Averages are shown for $n = 3$. Error bars indicate SEM. (*C*,*D*) Degradation of randomly labeled ssDNA by 20 nM wild-type or helicase-deficient K654E hDNA2 variants. Quantitation of experiments that are shown in Supplemental Figure S3 without (*C*) or with (*D*) 176 nM hRPA. Averages are shown for $n = 4$. Error bars indicate SEM.

as established previously (Pinto et al. 2016) but also have a structural role to promote the ssDNA-specific nuclease activity of hDNA2. This underpins the integrated nature of the hDNA2–WRN and hDNA2–BLM complexes.

DNA end resection by Sgs1 and yDna2 is stimulated by yDna2 helicase in vitro and in vivo

Initial reports suggested that the nuclease but not the helicase activity of DNA2 was required for DNA end resection in yeast and humans (Zhu et al. 2008; Cejka et al. 2010; Nimonkar et al. 2011). These studies suggested that the DNA2 motor function may be dispensable in resection. Using limiting concentrations of recombinant proteins, we instead later observed that the helicase activity of hDNA2 promoted DNA end resection in conjunction with WRN or BLM helicases (Pinto et al. 2016). We could recapitulate this observation with yeast recombinant proteins: Helicase-deficient yDna2 K1080E was approximately twofold less efficient in DNA end resection than wild-type yDna2 in conjunction with Sgs1 (Supplemental Fig. S5A,B). Notably, the stimulatory effect of the yDna2 helicase was also apparent only at limiting yDna2 concentrations, suggesting that higher than physiological yDna2 levels might mask the involvement of the yDna2 helicase in DNA end resection in vivo (Zhu et al. 2008). Therefore, we set out to test for the effect of the yDna2 helicase in yeast cells where each yDna2 variant was expressed from its endogenous promoter on chromosomal DNA and thus was present at physiological levels. To this end, we monitored the resection of a single HO endonuclease-induced DSB by Southern blotting (White and Haber 1990). DNA end resection renders DNA single-stranded, which prevents cleavage by a restriction endonuclease and leads to the disappearance of the Southern blot signal. By using probes complementary to DNA at various distances from the break, the progression of DNA end resection can be monitored at various time points upon DSB induction, as used previously (Fig. 5A; Zhu et al. 2008). We constructed strains containing either wild-type *DNA2* or helicase-deficient *dna2 K1080E* in an *exo1*Δ *rad51*Δ *pif1-m2* background. The *exo1*Δ mutation eliminates long-range resection by the separate Exo1 pathway, making the relative contribution of the yDna2–Sgs1 pathway more apparent. The *rad51*Δ mutation renders the DSB unrepairable, which allows monitoring of resection of long DNA lengths over extended periods of time. The *pif1-m2* mutation is a suppressor of yDna2 function in Okazaki fragment processing (Budd et al. 2006; Zhu et al. 2008). As the *dna2*Δ *exo1*Δ *rad51*Δ *pif1-m2* mutant is not viable, we used *sgs1*Δ *exo1*Δ *rad51*Δ *pif1-m2* cells as a reference strain for deficient long-range DNA end resection. We monitored resection 0, 3, 10, and 28 kb away from the HO-induced DSB at the indicated time points (Fig. 5A,B). The *dna2 K1080E* strain was slower than *DNA2* at every distance measured but faster than the corresponding *sgs1*Δ strain in the *exo1*Δ *rad51*Δ *pif1-m2* background (Fig. 5B,C). Collectively, these observations demonstrate that the yDna2 motor is required for efficient DNA end resection in conjunction with Sgs1 in vivo. This is apparent only when yDna2 is present at physiological levels, and our data thus also provide an explanation for why this effect was not detected when the yDna2 variants were expressed from a plasmid (Zhu et al. 2008).

Finally, we analyzed the length of the DNA degradation products as a footprint for the yDna2 motor activity in DNA end resection. To this end, we reconstituted an in vitro kinetic resection experiment of plasmid-length dsDNA with Sgs1, yDna2 (or its helicase-deficient yDna2 K1080E variant), and yRPA as well as Top3–Rmi1 and Mre11–Rad50–Xrs2 complexes, which stimulate Sgs1–yDna2 (Cejka et al. 2010; Cejka and Kowalczykowski 2010; Niu et al. 2010). As demonstrated in Supplemental Figure S5C,D, reactions with wild-type but not helicase-deficient yDna2 K1080E produced the extended ssDNA degradation products. This is consistent with the model that DNA2 motor activity functions in DNA end resection and further demonstrates that the motor of DNA2 engages even in the presence of other DNA end resection factors.

Discussion

Our results collectively demonstrate that the motors of both yeast and human DNA2 promote the degradation of long ssDNA. DNA2 is known to function together with a cognate RecQ family helicase in DNA end

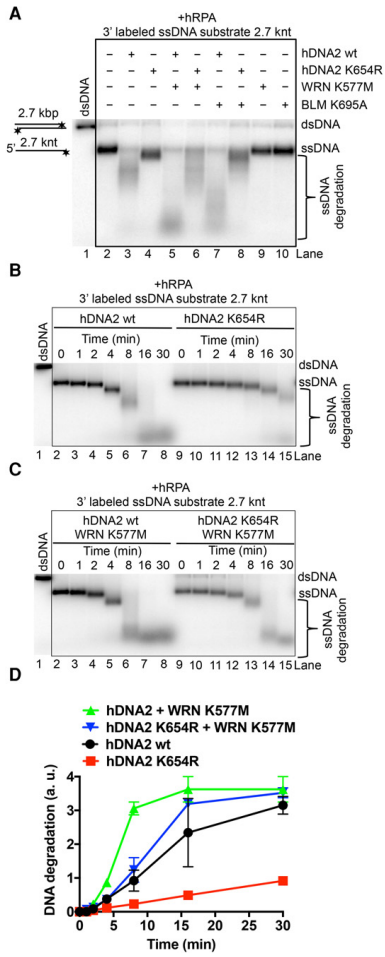

Figure 4. WRN or BLM enhances the ssDNA degradative capacity of hDNA2. (*A*). Representative 1% agarose gel showing degradation of 3′ ^{32}P-labeled ssDNA (heat-denatured pUC19/HindIII) by 30 nM wild-type or helicase-deficient hDNA2 K654R variant with or without 30 nM helicase-deficient WRN K577M or 30 nM BLM K695A. The reactions were supplemented with 50 mM NaCl and 215 nM hRPA. (*B*). Representative 1% agarose gel showing the kinetics of ssDNA degradation (as in *A*) by 30 nM wild-type or helicase-deficient hDNA2 K654R. (*C*). Representative 1% agarose gel showing the kinetics of ssDNA degradation (as in *A*) by 30 nM wild-type or helicase-deficient hDNA2 K654R together with 30 nM helicase-deficient WRN K577M. (*D*). Quantitation of the experiments shown in *B* and *C*. The *Y*-axis shows the distance of the band midpoint from the position of intact ssDNA, relative to the distance between dsDNA and ssDNA. Averages are shown for $n = 2$. Error bars indicate range.

resection (Zhu et al. 2008). Our results support a model in which the RecQ family helicase—either Sgs1 or WRN/BLM—uses its motor activity to translocate in a 3′ → 5′ direction and unwinds duplex DNA. Helicase-deficient Sgs1/WRN/BLM variants in conjunction with the respective yDna2 or hDNA2 are completely inactive in DNA end resection in vitro and in vivo (Zhu et al. 2008; Cejka et al. 2010; Niu et al. 2010; Nimonkar et al. 2011), supporting the notion that the RecQ helicase provides the lead helicase activity (Fig. 6A). The motor of DNA2 then powers its translocation on the unwound 5′-terminated ssDNA strand in a 5′ → 3′ direction. As the motor exclusively accelerates the degradation of ssDNA, the most likely explanation is that the DNA2 motor functions as an ssDNA translocase rather than a helicase to facilitate movement along the unwound ssDNA behind Sgs1/BLM/WRN (Fig. 6A). DNA2 thus likely uses an active translocation mode on ssDNA to accelerate its degradation rather than relying on passive diffusion. RPA promotes DNA unwinding by Sgs1/BLM/WRN and additionally directs the nuclease activity of yDna2/hDNA2 to the 5′-terminated DNA strand in a species-specific manner (Cejka et al. 2010; Niu et al. 2010; Nimonkar et al. 2011; Pinto et al. 2016). Here we show that the motor of DNA2 facilitates DNA degradation in the presence of RPA. This further supports a model in which RPA is an integral component of the Sgs1–yDna2, WRN–hDNA2, and BLM–hDNA2 resection machineries (Fig. 6A).

Previously, we observed that the nucleases of yeast and human DNA2 cleaved short 5′-terminated ssDNA overhangs of DNA duplexes, which prevented loading of DNA2 onto ssDNA and therefore duplex DNA unwinding (Levikova et al. 2013; Pinto et al. 2016). Paradoxically, the nuclease activity of DNA2 thus masks its helicase function in yeast and humans (Levikova et al. 2013; Pinto et al. 2016). The mouse DNA2 structure revealed that the DNA2 nuclease forms a narrow tunnel that accommodates only ssDNA (Zhou et al. 2015). Therefore, upon binding to a DNA end, wild-type DNA2 likely first moves along ssDNA in a passive diffusion-limited manner. DNA2 likely pauses once it encounters a junction between ssDNA and dsDNA, which represents an energy barrier. This provides time to the DNA2 nuclease active site within the tunnel to efficiently cleave the ssDNA overhang before it can reach the helicase domain located behind the tunnel. This prevents the engagement of the DNA2 motor activity and thus DNA unwinding of overhanging substrates by wild-type DNA2. The nuclease-deficient DNA2 instead does not cleave the ssDNA overhang within the tunnel. This allows time for the DNA2 variant to melt into the DNA duplex, possibly exploiting spontaneous "breathing" at the ssDNA and dsDNA junction or through a potential inherent dsDNA destabilization capacity of DNA2. This DNA melting then allows the nuclease-dead DNA2 variant to thread further onto the 5′-terminated DNA strand, which can reach the helicase domain to start the active ATP hydrolysis-dependent translocation and processive dsDNA unwinding observed previously (Levikova et al. 2013; Pinto et al. 2016).

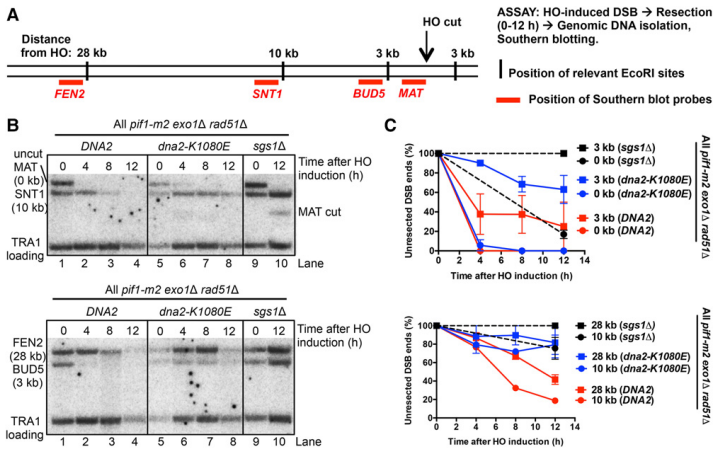

Figure 5. The helicase activity of wild-type yDna2 promotes resection of DSBs in vivo. (*A*) A scheme of the resection assay. DSB is induced by HO endonuclease. Resection past the indicated EcoRI sites (in black) leads to the disappearance of the signal obtained with site-specific probes (in red) by Southern blotting. Only those restriction sites that govern the appearance of the respective DNA fragments are shown. (*B*) Southern blot analysis of 5′ DNA end resection kinetics of HO-induced DSBs in *DNA2*, helicase-deficient *dna2 K1080E*, or *sgs1*Δ cells. All strains are *exo1*Δ *rad51*Δ *pif1-m2*. (*C*) Quantitation of *B*. Plots show the fraction of unresected 5′ strand (percentages) at each distance from the DSB. Averages are shown for $n \geq 2$. Error bars indicate range.

The results presented here show that the nuclease of DNA2 instead does not prevent translocation on extended ssDNA. Translocation along ssDNA represents a lower-energy barrier than the unwinding of duplex DNA, which might allow the ssDNA strand to pass uncleaved with a higher frequency through the nuclease tunnel into the helicase domain, which would power the ssDNA translocation (Fig. 6B). This model is in accord with previous observations that DNA2 nuclease must load onto a free ssDNA end but then cleaves ssDNA endonucleolytically (Balakrishnan et al. 2010). This also implies that DNA2 may cleave ssDNA with a certain frequency, which might depend on the rate of ssDNA translocation. To this point, using yeast Dna2, we observed dramatic variations between the degradation fragment lengths: A passive mode of ssDNA translocation resulted in DNA degradation fragments of ~5 to ~10 nt in length, whereas active mode produced much longer fragments of ~80 to ~100 nt in length. The structure of mouse DNA2 revealed that 7 nt of ssDNA are bound to the helicase domain followed by a 2-nt-long linker and 6-nt-long fragment bound to the nuclease domain; therefore, the distance between the two active sites is larger than the "short" DNA fragments observed in our experiments. The presence of the "long" DNA degradation fragments is thus a clear indicator that the ssDNA passes intact through the nuclease tunnel of yDna2 to the helicase domain. Similar product fragment length variation was not observed with hDNA2, and thus it remains to be determined whether this was due to technical issues or whether the mode of translocation along ssDNA and its degradation by human DNA2 are different. Nevertheless, the ATP-dependent motor activity promoted ssDNA degradation by human DNA2 as well. It is possible that any "long" ssDNA fragments produced by hDNA2 were rapidly converted into shorter ones by other hDNA2 molecules present in solution, which prevented detection. The difference between the yeast and human enzymes could be explained by distinct DNA association versus degradation and translocation rates. Interestingly, ssDNA fragments produced during DNA end resection have been proposed to regulate checkpoint response (Jazayeri et al. 2008; Eapen et al. 2012); however, any function of the DNA2 motor activity in this process has yet to be demonstrated.

The Sgs1–yDna2 and WRN/BLM–hDNA2 complexes have been compared with AddAB, RecBCD, or other bacterial DNA end resection machines (Dillingham et al. 2003; Yeeles and Dillingham 2007; Dillingham and Kowalczykowski 2008; Yeeles et al. 2009; Cejka et al. 2010). Unlike in *Escherichia coli*'s RecBCD, where both RecB and RecD are per se DNA helicases capable of unwinding dsDNA, we propose that the motor of DNA2 is engaged only downstream from the RecQ family helicase partner. Despite this difference, Sgs1–yDna2, WRN/BLM–hDNA2, and RecBCD appear quite similar, as both complexes likely use a bidirectional DNA translocation mode and form a complex that is more than the sum of its parts (Dillingham and Kowalczykowski 2008). This bidirectional mode of DNA translocation is likely not used by *Bacillus subtilis*'s AddAB, which contains only one motor activity within the AddA subunit despite the nuclease of AddB being similar to the nuclease of

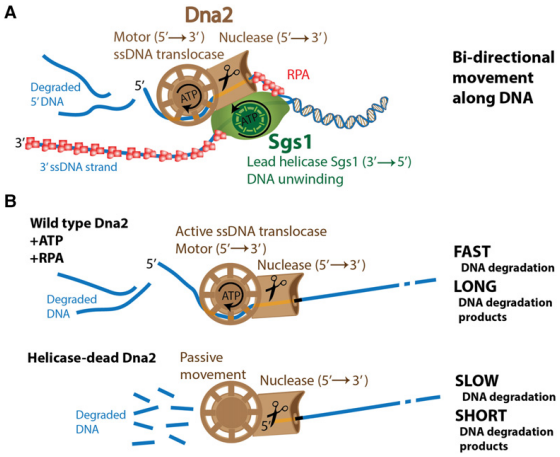

Figure 6. Model for the involvement of yDna2 helicase activity in DNA end resection. (*A*) Sgs1 translocates on the 3′-terminated DNA strand and functions as the lead helicase. Yeast Dna2 is using its motor activity to translocate on the unwound 5′-terminated DNA strand, which is degraded by its nuclease activity. (*B*, *top*) The motor of yDna2 accelerates degradation of ssDNA, which requires ATP hydrolysis and the presence of yRPA. This fast mode of DNA degradation results in long DNA degradation fragments. (*Bottom*) Without active translocation, the ssDNA degradation by yDna2 is slow, resulting in short DNA degradation fragments.

DNA2 due to the presence of the iron–sulfur cluster (Yeeles et al. 2009). However, the DNA2 domain organization in which the nuclease of DNA2 precedes its motor is unique and not found in other prokaryotic resection enzymes characterized to date.

Many DNA helicases unwind dsDNA as a result of their ssDNA translocase activity, although not all ssDNA translocases are DNA helicases (Lohman et al. 2008). In fact, it has been demonstrated that several superfamily I DNA helicases, including *E. coli* UvrD, are ssDNA translocases as monomers and become capable of processive dsDNA unwinding only upon dimerization or interaction with a protein partner (Maluf et al. 2003; Fischer et al. 2004). Although direct DNA binding between DNA2 and the respective cognate RecQ family helicase has been demonstrated (Cejka et al. 2010; Nimonkar et al. 2011; Sturzenegger et al. 2014), there are no data on oligomerization of DNA2. DNA2 might thus be an unusual example of an enzyme in which the motor functions as a ssDNA translocase, and the nuclease domain prevents duplex DNA unwinding. The results presented here identify a conserved function for the DNA2 helicase to promote DNA end resection in conjunction with a cognate RecQ family helicase both in vitro and in vivo. The mechanism might be also relevant for the degradation of reversed replication forks that form upon replication stress, which might explain reduced viability and/or pronounced sensitivity of helicase-deficient yeast cells to alkylating agents and ionizing radiation, treatments that also lead to DSBs (Formosa and Nittis 1999; Budd and Campbell 2000; Thangavel et al. 2015).

Materials and methods

Recombinant proteins

Wild-type yDna2 as well yDna2 E675A and yDna2 K1080E variants were expressed and purified as described previously (Levikova et al. 2013). The construct for the expression of the yDna2 ΔN variant was prepared by cloning the y*DNA2* sequence lacking the first 1215 residues (corresponding to 405 amino acids) between the 5′-terminal Flag tag and the 3′-terminal 6His tag into BamHI and EcoRI sites in a pYes2 vector (Invitrogen). The truncated protein was expressed and purified as the full-length protein. Wild-type hDNA2, hDNA2 K654E, and hDNA2 K654R were prepared as described previously (Pinto et al. 2016). No difference was observed between the hDNA2 K654E and hDNA2 K654R variants in the experiments presented in this report (data not shown). Wild-type BLM, WRN, BLM K695A, and WRN K577M were expressed and purified as described (Pinto et al. 2016). Sgs1, Top3–Rmi1, and Mre11–Rad50–Xrs2 were expressed and purified as described previously (Cejka and Kowalczykowski 2010; Cejka et al. 2010; Cannavo and Cejka 2014). The yRPA and hRPA proteins were expressed and purified as described (Henricksen et al. 1994; Kantake et al. 2003).

DNA substrates

The oligonucleotides X12-3 and X12-4NC were used for the preparation of the Y-structured DNA substrate, and oligonucleotides X12-3 and X12-4SC were used for the preparation of the 5′ tailed DNA, as described previously (Cejka and Kowalczykowski 2010; Levikova et al. 2013). Bacteriophage λ dsDNA (New England Biolabs) was digested by HindIII (New England Biolabs). The linearized dsDNA fragments were then labeled with [α-^{32}P] dATP and a Klenow fragment of DNA polymerase I (New England Biolabs) at the 3′ end. Unincorporated nucleotides were removed using MicroSpin G25 columns (GE Healthcare). The substrate was denatured by heating for 5 min at 95°C prior to each experiment. The 6.4-kb-long ssDNA (M13mp18) was purchased from New England Biolabs. The 2686-base-pair-long pUC19 dsDNA was linearized with HindIII, purified by phenol-chloroform extraction and ethanol precipitation, and denatured as described above where necessary.

The randomly labeled 2200-nt-long substrate was prepared by amplification of the *S. cerevisiae LIG1* gene by PCR from yeast genomic DNA (yWH436 strain) (see Supplemental Table S2) using Phusion high-fidelity DNA polymerase (New England

Biolabs) and the following primers: forward, 5′-ACGCATTAGC TAGCGGATCCCTGGAAGTTCTGTTCCAGGGGCCCATGC GCAGATTACTGACCGGTTG-3′; and reverse, 5′-ACGCATT ACTCGAGATTTTGCATGTGGGATTGGT-3′. In addition to the standard dNTP concentration in the PCR reaction (200 µM each), 66 nM [α-^{32}P] dATP was added. The PCR reaction product was purified using Chroma Spin TE-400 columns (Clontech). The substrate was denatured by heating for 5 min at 95°C before the experiment to obtain ssDNA where necessary. The 10- to 100-nt low-molecular-weight marker (Affymetrix) was ^{32}P-labeled at the 5′ terminus with [γ-^{32}P] ATP and T4 polynucleotide kinase (New England Biolabs). An asterisk indicates the position of the radioactive label where indicated.

Nuclease and helicase assays

Unless indicated otherwise, the experiments were performed in a 15-µL volume in 25 mM Tris-acetate (pH 7.5), 2 mM magnesium acetate, 1 mM ATP, 1 mM dithiothreitol, 0.1 mg/mL bovine serum albumin (New England Biolabs), 1 mM phosphoenolpyruvate, 16 U/mL pyruvate kinase (Sigma), and 1 nM (in molecules) ^{32}P-labeled oligonucleotide-based, pUC19-based, or PCR-based DNA substrate or 0.15 nM λ DNA-based substrate (corresponding to 2.4 nM 5′-terminated ssDNA ends upon denaturation). For reactions with unlabeled substrates, 100 ng of DNA was used. Where indicated, human and yeast RPA was included to saturate all ssDNA. Recombinant proteins were added on ice to the assembled reaction mixtures. The reactions were incubated for 30 min at 30°C for yeast and 37°C for human proteins unless indicated otherwise. Reactions were stopped by adding either 5 µL of 2% stop solution for native gels as described previously (Cejka and Kowalczykowski 2010) or 15 µL of formamide dye for denaturing gels (Cannavo and Cejka 2014). All gels with radioactive substrates were dried on DE81 chromatography paper (Whatman) and exposed to storage phosphor screens (GE Healthcare). The screens were scanned by a Typhoon 9400 phosphorimager (GE Healthcare). Where unlabeled DNA substrates were used, DNA was visualized by staining with ethidium bromide (Sigma) or GelRed (Biotium) as indicated.

Southern blot

Yeast cell growth, HO-break induction, and DNA isolation were performed as described previously (Zhu et al. 2008). The 0-h time point was collected immediately after adding galactose, before the HO cut occurred. DNA samples were separated on 1% agarose gel, and DNA was transferred onto a nylon membrane (GE Healthcare) and hybridized with DNA probes radioactively labeled by random primed DNA labeling kit (Roche) according to manufacturer's instructions. Primers used to prepare the ^{32}P-labeled probes were used as described previously (Zhu et al. 2008) and are listed in Supplemental Table S1. Membranes were exposed to storage phosphor screens (GE Healthcare) that were scanned by a Typhoon 9400 phosphorimager (GE Healthcare).

Yeast strains used in this study are listed in Supplemental Table S2. Briefly, the *dna2 K1080E* mutation was introduced using the allele replacement strategy (Widlund and Davis 2005) by transforming the parental yWH436 strain with the pRS306 plasmid (Sikorski and Hieter 1989) containing the SacII/BamHI fragment of the point-mutagenized y*DNA2* gene that was excised previously from the pGAL18 Dna2 K1080E plasmid (gift from J. Campbell). Gene deletions were performed by PCR-based substitution cassettes, as described previously (Janke et al. 2004; Hegemann et al. 2006). The *EXO1* gene was deleted by using the PCR cassette amplified from pFA6a plasmid using the following primers: forward, 5′-ACCACATTAAAATAAAAGGAGCTCG AAAAAACTGAAAGGCGTAGAAAGGACAGCTGAAGCTTC GTACGCTGC-3′; and reverse, 5′-TTTTCATTTGAAAAATATA CCTCCGATATGAAACGTGCAGTACTTAACTTCATAGGCC ACTAGTGGATCTG-3′.

The *SGS1* gene was deleted by using the PCR cassette amplified from pUG72 with the following primers: forward, 5′-ATTATTGTTGTATATATTTAAAAAATCATACACGTACAC ACAAGGCGGTA-3′; and reverse, 5′-TTGGCGAATGGTGTC GTAGTTATAAGTAACACTATTTATTTTTCTACTCTGCAT AGGCCACTAGTGGATCTG-3′. The *RAD51* gene was deleted by using the PCR cassette amplified from pUG6 using the following primers: forward, 5′-AAGAGCAGACGTAGTTATTT GTTAAAGGCCTACTAATTTGTTATCGTCATCAGCTGAA GCTTCGTACGCTGC-3′; and reverse, 5′-AGAATTGAAAG TAAACCTGTGTAAATAAATAGAGACAAGAGACCAAATACC ATAGGCCACTAGTGGATCTG-3′.

Acknowledgments

We thank Grzegorz Ira and Alma Papusha (Baylor College of Medicine) for the yWH436 strain and help in establishing the in vivo resection assays. We thank members of the Cejka laboratory—including Elda Cannavo, Roopesh Anand, Lepakshi Ranjha, Vera Kissling, and Sean Howard—for comments on the manuscript, and Jim Haber (Brandeis University) for discussions. We thank Patrick Sung (Yale University) and colleagues for communicating their results before publication. This work has been supported by Swiss National Science Foundation professorship PP00P3 133636 and Swiss Cancer League grant KFS-3089-02-2013 to P.C.

References

Bae SH, Seo YS. 2000. Characterization of the enzymatic properties of the yeast dna2 Helicase/endonuclease suggests a new model for Okazaki fragment processing. *J Biol Chem* **275:** 38022–38031.

Bae SH, Choi E, Lee KH, Park JS, Lee SH, Seo YS. 1998. Dna2 of *Saccharomyces cerevisiae* possesses a single-stranded DNA-specific endonuclease activity that is able to act on double-stranded DNA in the presence of ATP. *J Biol Chem* **273:** 26880–26890.

Bae SH, Bae KH, Kim JA, Seo YS. 2001. RPA governs endonuclease switching during processing of Okazaki fragments in eukaryotes. *Nature* **412:** 456–461.

Bae KH, Kim HS, Bae SH, Kang HY, Brill S, Seo YS. 2003. Bimodal interaction between replication-protein A and Dna2 is critical for Dna2 function both in vivo and in vitro. *Nucleic Acids Res* **31:** 3006–3015.

Balakrishnan L, Polaczek P, Pokharel S, Campbell JL, Bambara RA. 2010. Dna2 exhibits a unique strand end-dependent helicase function. *J Biol Chem* **285:** 38861–38868.

Budd ME, Campbell JL. 2000. The pattern of sensitivity of yeast dna2 mutants to DNA damaging agents suggests a role in DSB and postreplication repair pathways. *Mutat Res* **459:** 173–186.

Budd ME, Choe WC, Campbell JL. 1995. DNA2 encodes a DNA helicase essential for replication of eukaryotic chromosomes. *J Biol Chem* **270:** 26766–26769.

Budd ME, Choe W, Campbell JL. 2000. The nuclease activity of the yeast DNA2 protein, which is related to the RecB-like nucleases, is essential in vivo. *J Biol Chem* **275:** 16518–16529.

Budd ME, Reis CC, Smith S, Myung K, Campbell JL. 2006. Evidence suggesting that Pif1 helicase functions in DNA

replication with the Dna2 helicase/nuclease and DNA polymerase δ. *Mol Cell Biol* **26:** 2490–2500.
Cannavo E, Cejka P. 2014. Sae2 promotes dsDNA endonuclease activity within Mre11–Rad50–Xrs2 to resect DNA breaks. *Nature* **514:** 122–125.
Cannavo E, Cejka P, Kowalczykowski SC. 2013. Relationship of DNA degradation by *Saccharomyces cerevisiae* exonuclease 1 and its stimulation by RPA and Mre11–Rad50–Xrs2 to DNA end resection. *Proc Natl Acad Sci* **110:** E1661–E1668.
Cejka P. 2015. DNA end resection: nucleases team up with the right partners to initiate homologous recombination. *J Biol Chem* **290:** 22931–22938.
Cejka P, Kowalczykowski SC. 2010. The full-length *Saccharomyces cerevisiae* Sgs1 protein is a vigorous DNA helicase that preferentially unwinds holliday junctions. *J Biol Chem* **285:** 8290–8301.
Cejka P, Cannavo E, Polaczek P, Masuda-Sasa T, Pokharel S, Campbell JL, Kowalczykowski SC. 2010. DNA end resection by Dna2-Sgs1-RPA and its stimulation by Top3–Rmi1 and Mre11–Rad50–Xrs2. *Nature* **467:** 112–116.
Dillingham MS, Kowalczykowski SC. 2008. RecBCD enzyme and the repair of double-stranded DNA breaks. *Microbiol Mol Biol Rev* **72:** 642–671.
Dillingham MS, Spies M, Kowalczykowski SC. 2003. RecBCD enzyme is a bipolar DNA helicase. *Nature* **423:** 893–897.
Duxin JP, Moore HR, Sidorova J, Karanja K, Honaker Y, Dao B, Piwnica-Worms H, Campbell JL, Monnat RJ Jr, Stewart SA. 2012. Okazaki fragment processing-independent role for human Dna2 enzyme during DNA replication. *J Biol Chem* **287:** 21980–21991.
Eapen VV, Sugawara N, Tsabar M, Wu WH, Haber JE. 2012. The *Saccharomyces cerevisiae* chromatin remodeler Fun30 regulates DNA end resection and checkpoint deactivation. *Mol Cell Biol* **32:** 4727–4740.
Fischer CJ, Maluf NK, Lohman TM. 2004. Mechanism of ATP-dependent translocation of *E. coli* UvrD monomers along single-stranded DNA. *J Mol Biol* **344:** 1287–1309.
Formosa T, Nittis T. 1999. Dna2 mutants reveal interactions with Dna polymerase α and Ctf4, a Pol α accessory factor, and show that full Dna2 helicase activity is not essential for growth. *Genetics* **151:** 1459–1470.
Fortini BK, Pokharel S, Polaczek P, Balakrishnan L, Bambara RA, Campbell JL. 2011. Characterization of the endonuclease and ATP-dependent flap endo/exonuclease of Dna2. *J Biol Chem* **286:** 23763–23770.
Gravel S, Chapman JR, Magill C, Jackson SP. 2008. DNA helicases Sgs1 and BLM promote DNA double-strand break resection. *Genes Dev* **22:** 2767–2772.
Hegemann JH, Guldener U, Kohler GJ. 2006. Gene disruption in the budding yeast *Saccharomyces cerevisiae*. *Methods Mol Biol* **313:** 129–144.
Henricksen LA, Umbricht CB, Wold MS. 1994. Recombinant replication protein A: expression, complex formation, and functional characterization. *J Biol Chem* **269:** 11121–11132.
Janke C, Magiera MM, Rathfelder N, Taxis C, Reber S, Maekawa H, Moreno-Borchart A, Doenges G, Schwob E, Schiebel E, et al. 2004. A versatile toolbox for PCR-based tagging of yeast genes: new fluorescent proteins, more markers and promoter substitution cassettes. *Yeast* **21:** 947–962.
Jazayeri A, Balestrini A, Garner E, Haber JE, Costanzo V. 2008. Mre11–Rad50–Nbs1-dependent processing of DNA breaks generates oligonucleotides that stimulate ATM activity. *EMBO J* **27:** 1953–1962.
Kantake N, Sugiyama T, Kolodner RD, Kowalczykowski SC. 2003. The recombination-deficient mutant RPA (rfa1-t11) is displaced slowly from single-stranded DNA by Rad51 protein. *J Biol Chem* **278:** 23410–23417.
Levikova M, Klaue D, Seidel R, Cejka P. 2013. Nuclease activity of *Saccharomyces cerevisiae* Dna2 inhibits its potent DNA helicase activity. *Proc Natl Acad Sci* **110:** E1992–E2001.
Lohman TM, Tomko EJ, Wu CG. 2008. Non-hexameric DNA helicases and translocases: mechanisms and regulation. *Nat Rev Mol Cell Biol* **9:** 391–401.
Maluf NK, Fischer CJ, Lohman TM. 2003. A Dimer of *Escherichia coli* UvrD is the active form of the helicase in vitro. *J Mol Biol* **325:** 913–935.
Masuda-Sasa T, Imamura O, Campbell JL. 2006. Biochemical analysis of human Dna2. *Nucleic Acids Res* **34:** 1865–1875.
Mimitou EP, Symington LS. 2008. Sae2, Exo1 and Sgs1 collaborate in DNA double-strand break processing. *Nature* **455:** 770–774.
Nimonkar AV, Genschel J, Kinoshita E, Polaczek P, Campbell JL, Wyman C, Modrich P, Kowalczykowski SC. 2011. BLM–DNA2–RPA–MRN and EXO1–BLM–RPA–MRN constitute two DNA end resection machineries for human DNA break repair. *Genes Dev* **25:** 350–362.
Niu H, Chung WH, Zhu Z, Kwon Y, Zhao W, Chi P, Prakash R, Seong C, Liu D, Lu L, et al. 2010. Mechanism of the ATP-dependent DNA end-resection machinery from *Saccharomyces cerevisiae*. *Nature* **467:** 108–111.
Olmezer G, Levikova M, Klein D, Falquet B, Fontana GA, Cejka P, Rass U. 2016. Replication intermediates that escape Dna2 activity are processed by Holliday junction resolvase Yen1. *Nat Commun* **7:** 13157.
Pinto C, Kasaciunaite K, Seidel R, Cejka P. 2016. Human DNA2 possesses a cryptic DNA unwinding activity that functionally integrates with BLM or WRN helicases. *Elife* **5:** e18574.
Sikorski RS, Hieter P. 1989. A system of shuttle vectors and yeast host strains designed for efficient manipulation of DNA in *Saccharomyces cerevisiae*. *Genetics* **122:** 19–27.
Sturzenegger A, Burdova K, Kanagaraj R, Levikova M, Pinto C, Cejka P, Janscak P. 2014. DNA2 cooperates with the WRN and BLM RecQ helicases to mediate long-range DNA end resection in human cells. *J Biol Chem* **289:** 27314–27326.
Thangavel S, Berti M, Levikova M, Pinto C, Gomathinayagam S, Vujanovic M, Zellweger R, Moore H, Lee EH, Hendrickson EA, et al. 2015. DNA2 drives processing and restart of reversed replication forks in human cells. *J Cell Biol* **208:** 545–562.
Tran PT, Erdeniz N, Dudley S, Liskay RM. 2002. Characterization of nuclease-dependent functions of Exo1p in *Saccharomyces cerevisiae*. *DNA Repair (Amst)* **1:** 895–912.
Wanrooij PH, Burgers PM. 2015. Yet another job for Dna2: checkpoint activation. *DNA Repair (Amst)* **32:** 17–23.
White CI, Haber JE. 1990. Intermediates of recombination during mating type switching in *Saccharomyces cerevisiae*. *EMBO J* **9:** 663–673.
Widlund PO, Davis TN. 2005. A high-efficiency method to replace essential genes with mutant alleles in yeast. *Yeast* **22:** 769–774.
Yeeles JT, Dillingham MS. 2007. A dual-nuclease mechanism for DNA break processing by AddAB-type helicase-nucleases. *J Mol Biol* **371:** 66–78.
Yeeles JT, Cammack R, Dillingham MS. 2009. An iron-sulfur cluster is essential for the binding of broken DNA by AddAB-type helicase-nucleases. *J Biol Chem* **284:** 7746–7755.
Zhou C, Pourmal S, Pavletich NP. 2015. Dna2 nuclease–helicase structure, mechanism and regulation by Rpa. *Elife* **4:** e09832.
Zhu Z, Chung WH, Shim EY, Lee SE, Ira G. 2008. Sgs1 helicase and two nucleases Dna2 and Exo1 resect DNA double-strand break ends. *Cell* **134:** 981–994.

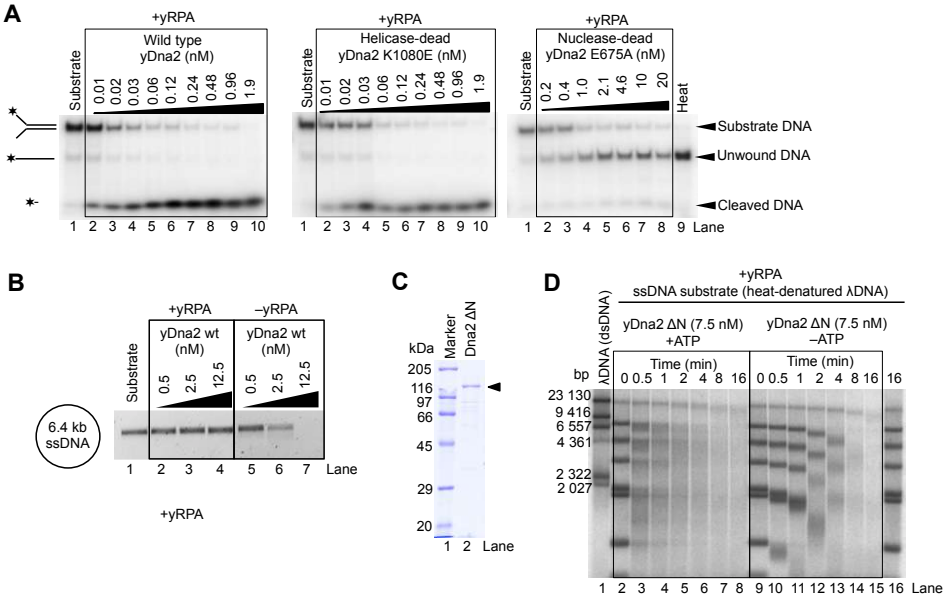

Figure S1.
The role of the Dna2 motor activity in DNA degradation by Dna2. (A) Processing of Y-structured DNA substrate by wild type, helicase-deficient K1080E and nuclease-deficient E675A yDna2 variants. Heat, heat-denatured substrate. The panel shows representative native 10% polyacrylamide gels. Helicase activity of yDna2 does not promote degradation of duplex DNA. (B) A representative agarose gel showing the lack of endonuclease activity of wild type yDna2 on circular 6.4 knt-long ssDNA substrate (1.6 nM) in the presence of yRPA (770 nM). DNA was visualized by post-staining with GelRed. (C) Yeast Dna2 ΔN, lacking 405 amino acids from the N-terminus, used in this study. Panel shows a representative Coomassie blue-stained polyacrylamide gel. (D) Assay as in Fig. 1D, but with yDna2 ΔN.

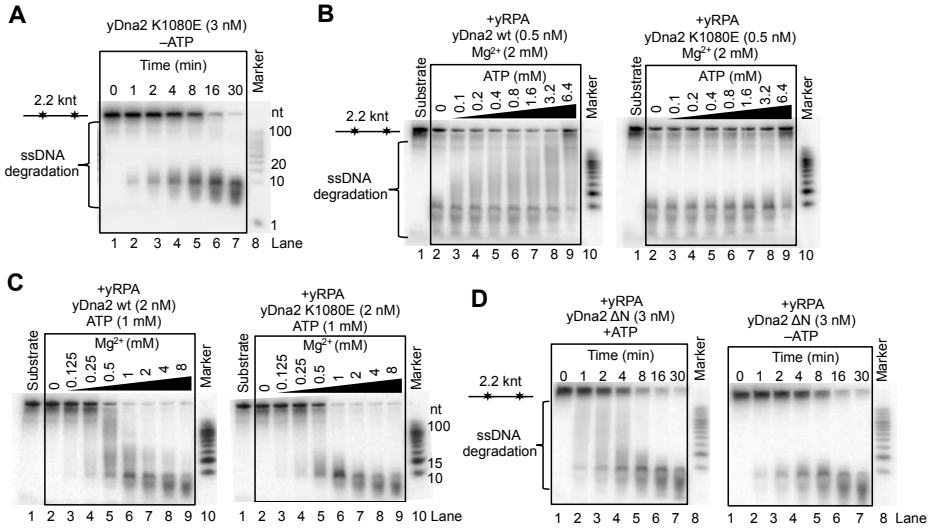

Figure S2.
Influence of ATP and magnesium on the Dna2 motor activity in ssDNA degradation. (A) Degradation kinetics of randomly ^{32}P-labeled ssDNA by yDna2 K1080E in the absence of ATP. Shown is a representative denaturing 20% polyacrylamide gel. (B) The effect of ATP concentration on ssDNA degradation by wt and helicase-deficient K1080E yDna2. (C) The effect of magnesium concentration on ssDNA degradation by wt and helicase-deficient K1080E yDna2. (D) The effect of ATP on ssDNA degradation by yDna2 ΔN.

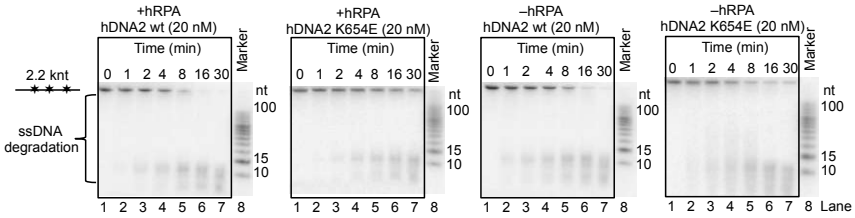

Figure S3.
Helicase activity of hDNA2 accelerates its ssDNA degradation capacity in the presence of hRPA. Representative denaturing 20% polyacrylamide gels showing the ssDNA degradation capacity of wild type or helicase-deficient hDNA2 K654E with (176 nM) or without hRPA. The substrate was ssDNA randomly labeled with ^{32}P.

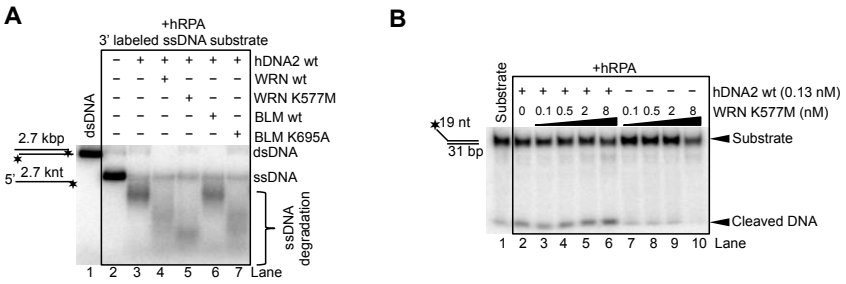

Figure S4.
WRN or BLM promote ssDNA degradation capacity of hDNA2. (A) Representative agarose gel showing 3' ^{32}P-labeled ssDNA degradation by hDNA2 (30 nM) and its stimulation by wild type or helicase-deficient WRN K577M (30 nM) or wild type or helicase-deficient BLM K695A (30 nM). The reactions were supplemented with 50 mM NaCl and 215 nM hRPA. Helicase-deficient BLM or WRN variants promoted ssDNA degradation by hDNA2 to a greater extent than wt polypeptides. (B) The effect of helicase-deficient WRN K577M on the oligonucleotide based 5'-tailed DNA degradation by hDNA2 in the presence of hRPA (9 nM). No stimulation of DNA degradation by hDNA2 was observed on the overhanged substrate.

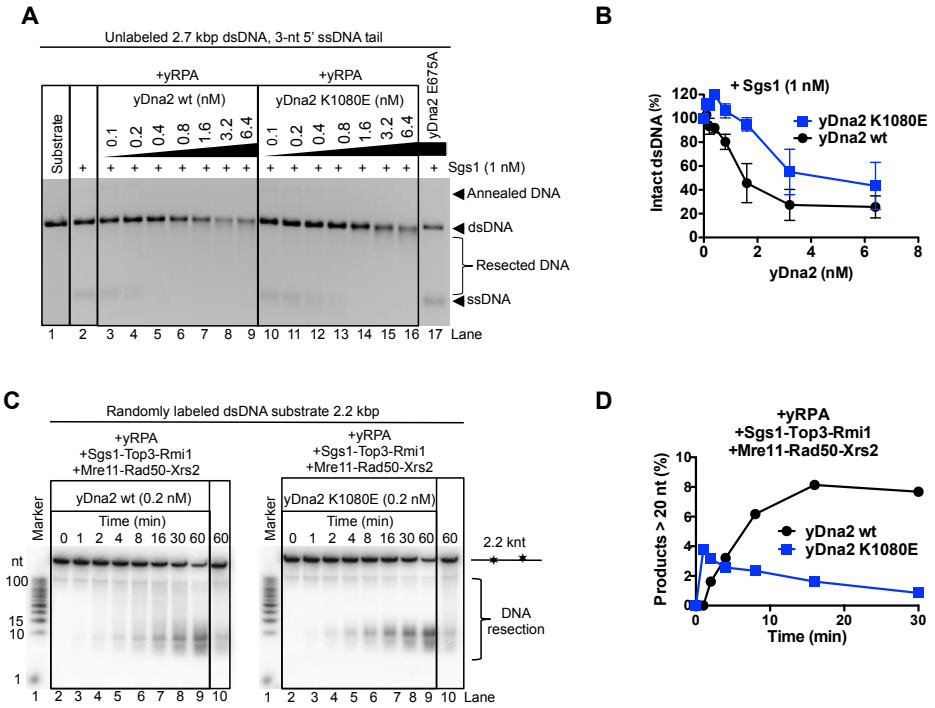

Figure S5.
The motor activity of yDna2 promotes DNA end resection. (A) DNA end resection by wild type yDna2 or helicase-deficient yDna2 K1080E variant in conjunction with 1 nM Sgs1 on 5' tailed 2.7 kbp-long dsDNA substrate. DNA was visualized by staining with ethidium bromide. (B) Quantitation of (A). Averages shown, n=2; error bars, range. (C) Analysis of DNA degradation products lengths of DNA end resection assays with Sgs1 (0.3 nM), Top3-Rmi1 (10 nM), Mre11-Rad50-Xrs2 (40 nM) and either wt yDna2 or yDna2 K1080E with randomly ^{32}P-labeled dsDNA substrate. Reaction buffer contained 100 mM sodium acetate. The reaction products were analyzed by 20% polyacrylamide denaturing electrophoresis, representative gels are shown. Reactions with wt yDna2 gave rise to longer DNA degradation products. This is a footprint of the yDna2 helicase activity in DNA end resection.(D) Quantitation of (C). Relative proportion of DNA degradation products larger than 20 nt in length was determined. Averages shown, n=2; error bars, range.

Table S1.

Primer sequences used to prepare DNA probes for hybridization.

1	MAT_0kb_1	5' CTTGATTGTTTGCTTGAGTCTG
	MAT_0kb_2	5' ACTAACAATACTTCAGTTTA
2	BUD5_3kb_1	5' CCAGTTATCGTCCTACGTTC
	BUD5_3kb_2	5' GGTAAGCCTTGGAACCTTAG
3	SNT1_10kb_1	5' CTATCGATGGCTCTATAAGAC
	SNT1_10kb_2	5' CACGACTTATTGGACTAGTG
4	FEN2_28kb_1	5' CACCAATGCATATATATCCG
	FEN2_28kb_2	5' GAATAGTCGACCAGTCTAAC
5	Ctrl_TRA1_1	5'- GTC CTA ATA CGA CTT TTC AAA TTG TCC TTT ATG TCC GTC A
	Ctrl_TRA1_2	5'- ATA CTT GTA AGC ACT CTT CCT GTA GTG AAT ATC ACT TTT G

Supplementary Table 2 Yeast strains used in this study.

Strain name	Parental strain	Genotype	Source
yWH436	jkm139	*pif1-m2*	Zhu et al. 2008
ML30	yWH436	*exo1:: hphNT1 rad51::KanMX*	This study
ML31	yWH436	*dna2^{K1080E} exo1:: hphNT1 rad51::KanMX*	This study
ML32	yWH436	*sgs1::URA3 exo1:: hphNT1 rad51::KanMX*	This study

2.3 Results from collaborations

2.3.1 Force regulated dynamics of RPA on a DNA fork

Felix E. Kemmerich, Peter Daldrop, **Cosimo Pinto**, Maryna Levikova, Petr Cejka, Ralf Seidel

The article was published in Nucleic Acids Res (2016) 44 (12): 5837-5848.

My contributions to this publication was producing recombinant human RPA and performing the biochemical assays shown in Figure 4 and Supplementary Figures S3, S4 and S7.

Published online 25 March 2016 *Nucleic Acids Research, 2016, Vol. 44, No. 12* ***5837–5848***
doi: 10.1093/nar/gkw187

Force regulated dynamics of RPA on a DNA fork

Felix E. Kemmerich[1,2,†], Peter Daldrop[2,†], Cosimo Pinto[3], Maryna Levikova[3], Petr Cejka[3] and Ralf Seidel[1,2,*]

[1]Institute of Experimental Physics I, Universität Leipzig, Linnéstr. 5, 04103 Leipzig, Germany, [2]Institute for Molecular Cell Biology, University of Münster, Schlossplatz 5, D-48149 Münster, Germany and [3]Institute of Molecular Cancer Research, University of Zurich, Winterthurerstrasse 190, CH-8057 Zürich, Switzerland

Received January 07, 2016; Revised February 26, 2016; Accepted March 04, 2016

ABSTRACT

Replication protein A (RPA) is a single-stranded DNA binding protein, involved in most aspects of eukaryotic DNA metabolism. Here, we study the behavior of RPA on a DNA substrate that mimics a replication fork. Using magnetic tweezers we show that both yeast and human RPA can open forked DNA when sufficient external tension is applied. In contrast, at low force, RPA becomes rapidly displaced by the rehybridization of the DNA fork. This process appears to be governed by the binding or the release of an RPA microdomain (toehold) of only few base-pairs length. This gives rise to an extremely rapid exchange dynamics of RPA at the fork. Fork rezipping rates reach up to hundreds of base-pairs per second, being orders of magnitude faster than RPA dissociation from ssDNA alone. Additionally, we show that RPA undergoes diffusive motion on ssDNA, such that it can be pushed over long distances by a rezipping fork. Generally the behavior of both human and yeast RPA homologs is very similar. However, in contrast to yeast RPA, the dissociation of human RPA from ssDNA is greatly reduced at low Mg^{2+} concentrations, such that human RPA can melt DNA in absence of force.

INTRODUCTION

Replication protein A (RPA) is a highly ubiquitous (1), heterotrimeric (2), protein essential in virtually all aspects of eukaryotic DNA processing involving single-stranded DNA (ssDNA) intermediates (3). Due to the strong binding of RPA to ssDNA (2,4–6). RPA was originally thought to solely prevent the formation of secondary structures and confer protection from nucleolytic degradation. However, strong evidence for direct interactions with specific protein partners has been reported (7–10), and a new paradigm emerged. RPA is now thought to act additionally as a scaffold for the recruitment of other DNA processing enzymes on ssDNA intermediates, in order to channel the processing along specific pathways (11,12). RPA coated ssDNA for example signals the presence of DNA damage to the checkpoint machinery through direct binding of ATR-interacting protein (ATRIP) (8,13,14). From this viewpoint, the boundaries between ssDNA and double-stranded DNA (dsDNA), i.e. the interface upon which a multitude of DNA processing factors are acting, are of particular interest. Here, the binding and release of RPA must be highly dynamic, and organized in such a way that the DNA can be rapidly made accessible to subsequent processing machinery.

The importance of ssDNA–dsDNA boundaries is also highlighted by the fact that despite the low affinity toward dsDNA (15), RPA binds appreciably to ssDNA stretches exposed upon dsDNA damage (16,17), is able to disrupt partially dsDNA structures such as triplexes (18), tetraplexes (19,20) and suppresses formation of secondary structures such as hairpins (11). Under certain circumstances, the ATP-independent melting of dsDNA by RPA has also been shown (21–23), where it was proposed that the observed duplex destabilization proceeds by trapping fluctuations of the helix (23).

Several recent studies have advanced our understanding of the molecular mechanisms that may control the coordination of RPA by employing single-molecule analysis techniques: (i) Using single-molecule DNA supercoiling experiments in magnetic tweezers it was shown that RPA can bind to transiently forming bubbles in the DNA duplex in a torque-dependent manner (24). (ii) Single-molecule imaging of fluorescent RPA has shown that RPA bound ssDNA may undergo more rapid exchange in presence of free RPA in solution (25). (iii) Using a combination of single-molecule fluorescence techniques it was found that under high salt conditions RPA may diffuse/slide along ssDNA (26), suggesting the intriguing possibility that in this way access to the DNA is provided to other enzymes. Recently, Chen and Wold (12) pointed out that central to all of these single-molecule studies is the emerging view that RPA binding is highly dynamic and that microscopic rearrangements

*To whom correspondence should be addressed. Tel: +49 341 97 32501; Fax: +49 341 97 32599; Email: ralf.seidel@physik.uni-leipzig.de
†These authors contributed equally to this work as first authors.

of the RPA DNA binding domains (DBDs) are underlying the observed dynamics. However, it was also emphasized that more work is required to fully understand the rich dynamics of RPA in complex with various DNA structures.

Here, we investigate in detail the dynamics of RPA at the boundary of ssDNA and dsDNA such as present at a replication fork. We utilize magnetic tweezers that allow precise manipulation and length determination of immobilized DNA substrates via an attached magnetic microsphere (27). At the single-molecule level they support the study of fast dynamic processes, and allow dissecting inherent molecular variation with spatial resolution on the scale of one base-pair (bp) (27).

We have characterized the force-dependent binding dynamics of RPA from human and budding yeast (*Saccharomyces cerevisiae*), henceforth referred to as hRPA and yRPA (see Materials and Methods for details) on a DNA fork down to single protein association events. The interplay between RPA, the forked DNA substrate and force tightly regulates the balance of RPA binding and the opening and closing of the fork. Our results indicate that RPA uses a 'toehold'-like mechanism to trap small transient openings of the DNA helix with a microdomain, which are then expanded as the full protein wedges in to bind. Similarly, RPA displacement by the rezipping fork first occurs through an initial rate-limiting displacement of a toehold. This gives rise to a very rapid helix rezipping upon which RPA dissociates much faster than on ssDNA. Facilitated by our observation of both RPA homologs, we can confirm that the described behavior is a general trait of RPA across different organisms. Thus, while RPA protects ssDNA rather firmly and statically, it is extremely dynamic at DNA processing sites. This is additionally supported by the observation that a DNA fork can slide/push RPA upon rezipping.

MATERIALS AND METHODS

DNA substrates

A DNA substrate containing a 488 bp long hairpin was prepared as described previously (28). The 5′-end of the hairpin carried a single biotin modification, while the 3′-end was linked through a 60 nt ssDNA spacer to a 1 kb dsDNA spacer, followed by a 600 bp digoxigenin-modified attachment handle.

Preparation of the flapped DNA duplex substrate has been described previously (29,30). Central part is a 6.1 kb unmodified dsDNA with a flap located 1 kb from its proximal DNA end. Approximately 600 bp attachment handles carrying multiple digoxigenins and biotins were attached to the 6.1 kb fragment at its flap-proximal and distal ends, respectively.

Recombinant proteins

yRPA and hRPA were recombinantly expressed and purified as described previously (31,32). In brief, yRPA was expressed in the yeast strain BJ5464 containing three plasmids, coding for subunits Rfa1, Rfa2 and Rfa3, respectively. Cells were lysed and yeast RPA was purified by affinity on a ssDNA cellulose column (USB corporation, Cleveland, USA) and by ion exchange chromatography using a HiTrap Q column (GE Healthcare, Little Chalfont, UK). Human RPA was expressed from the p11d-tRPA vector (32) in BL21 *E. coli* cells and purified by chromatography using HiTrap Blue and HiTrap Q columns (GE Healthcare, Little Chalfont, UK).

Magnetic tweezers experiments

For the single molecule experiments a custom magnetic tweezers setup was utilized (27,33). Magnetic tweezers experiments were conducted at room temperature using flow cells assembled from two coverslips (Menzel, Braunschweig, Germany) that were separated by a layer of Parafilm (Bemis, Oshkosh, USA) into which a sample chamber was cut out. The bottom coverslip was coated with polystyrene (Sigma-Aldrich, St. Louis, USA). Three micrometers carboxyl-modified latex beads (Life Technologies, Darmstadt, Germany) that served as reference, were attached to the bottom slide of the mounted flow cell by incubation in 1 M NaCl for 1 h. Subsequently, anti-digoxigenin antibodies (Roche, Penzberg, Germany) were allowed to unspecifically bind to the coated surface of the flow cell, by incubation at a concentration of 50 μg/ml for 1 h at room temperature. Subsequently, the flow cell was passivated by overnight incubation with 10 mg/ml bovine serum albumin (BSA, New England Biolabs, Ipswich, USA). DNA constructs were bound to streptavidin-coated M280 magnetic beads (Life Technologies, Darmstadt, Germany) and then flushed into the flow cell. After allowing them to bind for ∼5 min, excess beads were washed out with phosphate buffered saline (PBS) solution rendering the sample chamber ready for experiments. The positions of reference and DNA-attached beads were tracked in all three dimensions at 300 Hz using videomicroscopy and real-time GPU-accelerated image analysis (27). Typically 15-20 beads were evaluated in parallel. Forces were calibrated using a recent methodology that supports the usage of short molecules and high forces (34). Experiments were conducted in 50 mM Tris acetate pH 7.5 supplemented with magnesium acetate in concentrations as described in the results. Data were analyzed in Labview (National Instruments, Austin, USA), Origin 9.1 (OriginLab, Northampton, USA) and Matlab (MathWorks, Natick, USA). Length changes measured in nm for opening of the hairpin or melting of the nicked DNA construct were converted into the number of opened bp (Supplementary Data).

Gel-based DNA melting experiments

As substrate for dsDNA melting experiments by gel electrophoresis, double-stranded Lambda DNA was digested with HindIII (New England Biolabs, Ipswich, United States) and 3′-labeled with [α^{32}P]dATP using the Large Klenow fragment of DNA polymerase I (New England Biolabs, Ipswich, USA). Unincorporated nucleotides were removed using MicroSpin G25 columns (GE Healthcare, Little Chalfont, UK). The resulting labelled DNA fragments had short 3 nt long 5′ ssDNA tails. Experiments were performed in a 15 μl volume in 25 mM Tris-acetate pH 7.5, 1 mM dithiotreitol, 0.1 mg/ml BSA, 1 mM phosphoenolpyruvate, 0.02 U/ml pyruvate kinase (Sigma-Aldrich,

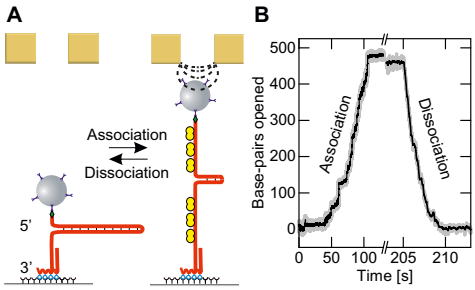

Figure 1. Force controlled association and dissociation of RPA on a DNA fork substrate. (**A**) Schematic of the experiment: a 488 bp long DNA hairpin substrate (red) is immobilized onto a glass surface and tethered to a magnetic bead. When sufficient force is applied to the bead, RPA (yellow) can bind to the ssDNA/dsDNA interface at the fork. As a result, the hairpin is opened to accommodate the entire RPA heterotrimer. Further association proceeds by the contiguous binding of RPA to the fork until the hairpin is fully opened. Upon lowering the magnetic force the DNA helix refolds reversibly and RPA dissociates from the ssDNA. (**B**) Example time trace of force controlled yRPA association and dissociation (in presence of 20 nM yRPA and 3 mM Mg^{2+}). At a force of 13.2 pN, sequential binding of RPA opens the hairpin with a rate of 4.7 bp/s, until it is fully opened and completely covered with RPA. Lowering the force to 4.5 pN causes dissociation of RPA evident in rapid refolding of the hairpin with a rate of 107 bp/s.

St. Louis, USA), 0.15 nM DNA substrate and magnesium acetate and recombinant proteins as indicated. RPA was present in the reactions at saturating concentrations corresponding to an excess over DNA as indicated, assuming all DNA was single-stranded and a DNA-binding site size of 25 nt for human RPA and of 20 nt for yeast RPA. A complete 100% DNA saturation thus corresponds to 576 nM hRPA or 720 nM yRPA. Reactions were incubated at 37°C or 30°C as indicated for 30 min, and then terminated by adding 5 μl stop buffer (150 mM EDTA, 2% SDS, 30% glycerol and 0.01% bromophenol blue), and analyzed on 1% agarose gels in 1X TAE buffer. Gels were dried, exposed to a storage phosphor screen and analyzed on a Typhoon phosphor imager (GE Healthcare, Little Chalfont, UK).

RESULTS

RPA association and dissociation at a DNA fork

We measured the association and dissociation of RPA on a 488 bp long DNA hairpin substrate using magnetic tweezers. One end of the hairpin was immobilized via a dsDNA spacer at the bottom surface of a fluidic cell. The other end was tethered to a 2.8 μm magnetic bead (Figure 1A). A set of permanent magnets was mounted on a movable stage above the fluidic-cell, such that the magnetic force acting on the bead could be controlled by lowering or raising the magnets (see Materials and Methods for details).

The DNA hairpin substrate can be opened mechanically by applying sufficient force to the bead. At forces above a critical force, which will be referred to as unzipping force, a series of sudden, well-defined transitions in DNA extension occurs, amounting to about 475 nm from the fully-closed to the fully-open state over the course of about 1 s (see Supplementary Figure S1). In contrast, after adding yRPA a gradual opening of the hairpin at forces well below the unzipping force was observed. In this case, the opening process lasted for much longer time-scales and continued until the hairpin was extended to the fully-opened state (Figure 1B). Upon reduction of the applied force, a gradual reversion to the closed state took place. We interpret these gradual transitions as the result of RPA binding to the fork of the hairpin. The sequential association of more RPA opened the hairpin and generated RPA-covered ssDNA. Upon lowering the force, RPA is displaced by the rezipping of the DNA (Figure 1A). The slopes of both association and dissociation were approximately constant throughout the complete hairpin opening or closing process, irrespective of length of dsDNA remaining. This suggests that RPA binding occurs only at the fork, and in a contiguous manner with respect to the previously bound RPA. We emphasize that the process is fully reversible and the same substrate molecule can be opened and closed multiple times without systematic alteration of the resulting curves.

Force dependence of RPA binding at the fork

Next we investigated the influence of the applied force on the association and dissociation rates of RPA on the DNA hairpin substrate. These rates showed a strong dependence on the applied force. Above 11 pN we observed a gradual opening of the hairpin and the rate of opening increased with stronger force (Figure 2A). When the force acting on such an RPA covered, open hairpin, was reduced below 11 pN, we observed a gradual closing of the hairpin. The observed closing rates were the faster the lower the applied force (Figure 2B).

Plotting the rates of hairpin opening and closing against the applied force, it became apparent that both the association and dissociation rates varied exponentially with force as shown in Figure 2C. We devised a model in which the net rate of RPA binding to the DNA is the difference between the rates of force-dependent RPA association and RPA dissociation from the fork. Each rate is expressed as an exponential Arrhenius term as obtained from transition-state theory in which the applied force F scales with height of the energetic barrier to the transition state:

$$v_{\mathrm{net}} = k_{\mathrm{on}} \exp\left(\frac{(c_F \cdot F - c_{\mathrm{unz}} \cdot F_{\mathrm{unz}})\,\Delta z_{\mathrm{on}}}{k_B T}\right) - k_{\mathrm{off}} \exp\left(-\frac{c_F \cdot F \cdot \Delta z_{\mathrm{off}}}{k_B T}\right) \quad (1)$$

Pre-exponential factors k_{on} and k_{off} describe the expected rates for association and dissociation at the unzipping force F_{unz} or at zero force, respectively. The second pair of fit parameters (Δz_{on} and Δz_{off}) corresponds to the distance of the initial state (before association/dissociation of a new RPA) to the transition state along the relevant reaction coordinate, in this case the number of bp along the DNA hairpin. For association, Δz_{on} thus corresponds to the number of bp that need to open spontaneously to accommodate a sufficiently long part of an RPA complex, such that the full complex can subsequently bind. For dissociation Δz_{off} is

5840 Nucleic Acids Research, 2016, Vol. 44, No. 12

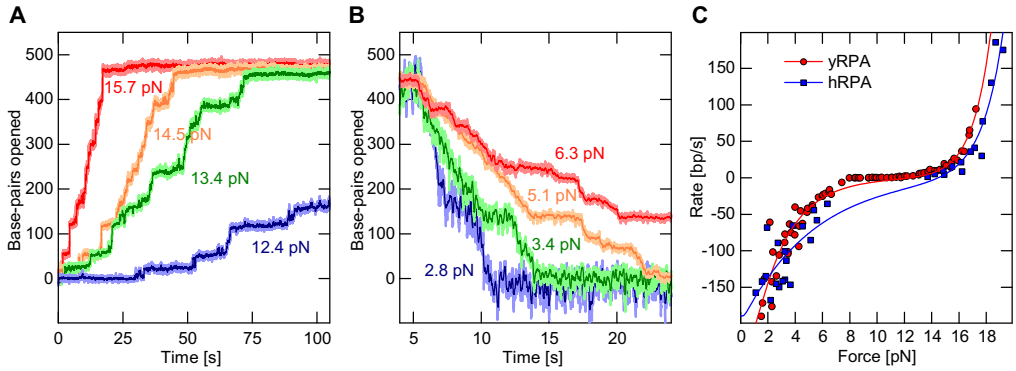

Figure 2. Force dependence of the RPA association/dissociation kinetics at the fork. (**A**) Example time traces of yRPA (20 nM in presence of 3 mM Mg^{2+}) association on the DNA hairpin at different forces. The DNA hairpin sequentially opened due to successive association events of RPA. With increasing forces the overall association rate becomes faster, ranging from 2.8 bp/s at 12.4 pN (blue) to 36.6 bp/s at 15.7 pN (red). (**B**) yRPA (20 nM in presence of 3 mM Mg^{2+}) dissociation time traces for varying force. Following a complete coverage of RPA on the DNA hairpin substrate, the force was lowered to the indicated values causing the hairpin to close and RPA to dissociate. The rate of dissociation is much faster than association and ranges from 107 bp/s at 2.8 pN (blue) to 16.2 bp/s at 6.3 pN (red). (**C**) Association and dissociation rates as a function of force, obtained by tracking multiple DNA tethered magnetic beads in parallel for yRPA (red circles, 20 nM in presence of 3 mM Mg^{2+}) or by tracking a single bead with hRPA (blue squares, 50 nM in presence of 10 mM Mg^{2+}). The data were fit using Equation 1 (red and blue lines for yRPA and hRPA, respectively) with fit parameters listed in Table 1.

the number of bp that need to rezip and displace part of the RPA complex, to allow full complex dissociation. The factor c converts the number of bp into a DNA extension change, i.e. a length. This conversion is a function of force (see Supplementary Figure S2) and was determined as described in the Supplementary Information. The model describes the force-dependent rates well, as evident from the fits to the data (Figure 2C). At concentrations of 20 nM yRPA and 3 mM Mg^{2+} the fit yields a fast hairpin closure rate of at zero force of $k_{off} = 239 \pm 14$ bp/s. Furthermore, values of $\Delta z_{on} = 3.3 \pm 0.6$ bp and $\Delta z_{off} = 1.6 \pm 0.1$ bp were obtained, indicating that spontaneous helix opening or partial RPA displacement amounting to only a few bp is required to overcome the transition state for RPA association or dissociation, respectively. This is analogous to the toehold mechanism in DNA nanotechnology (35), where the association of a small protein microdomain (toehold) is the rate-limiting step for full protein binding and further helix opening. Conversely, the disengagement of a terminal microdomain is rate-limiting for helix rezipping.

The fit also provided the hairpin opening rate $k_{on} = 180 \pm 42$ bp/s at the unzipping force of $F_{unz} = 18.2$ pN. At the unzipping force the hairpin no longer imposes an energetic hurdle for RPA association, such that the extrapolated rate should approximate the RPA association to free ssDNA. Hairpin opening rates at a given force increased linearly with the RPA concentration (between 5 and 50 nM, see Supplementary Figure S5), allowing us to calculate standardized (per nM) rates (see Table 1 for the full set of fit parameters).

Taken together, the data so far show that in the absence of force, dissociation dominates such that the closed hairpin state is favored. Increasing the forces ultimately tips the scales and hairpin opening becomes favored. From our model parameters one can also calculate the force F_{equi} (see Table 1), at which hairpin opening and closing rates are at equilibrium, which is 12.4 pN for 20 nM yRPA in 3 mM Mg^{2+}.

To test whether hairpin opening/closing driven by the association/dissociation of microdomains is a general property of RPA, we repeated our experiments with hRPA. Similarly to yRPA, a force-dependent opening and closing of the DNA hairpin due to the association and dissociation of hRPA at the fork was observed (Figure 2C). Our model (Equation 1) also described the hRPA data well, and a fit to the data yielded parameters that were comparable to yRPA (Table 1). Most importantly the transition state distances again amounted to only few bp also for hRPA, which suggests that both RPA homologs use a toehold mechanism for binding/dissociation at a DNA junction.

RPA binding on a DNA duplex substrate

Next, we probed whether the observed RPA binding behavior is unique to the DNA hairpin geometry, where both ssDNA strands at the junction are subjected to force, or whether it could also be observed on a DNA duplex with an internal 63 nt gap and an adjacent 38 nt 5′-flap. For this substrate only one of the two DNA strands is under force at the junction, while the other strand, bearing the 5′-flap, is free from tension. In this geometry RPA molecules from the two strands at the junction are allowed to interact with each other, which may provide a different behavior. The DNA substrate utilized in this case consisted of a 6.1 kb stretch of dsDNA where the gap was 1 kb away from the 5′-end, followed by a ssDNA flap (see Materials and Methods, Figure 3A). This DNA construct underwent a rapid disruption of the base-pairing in the dsDNA when the applied force exceeds 65 pN, as indicated by a marked increase in the DNA

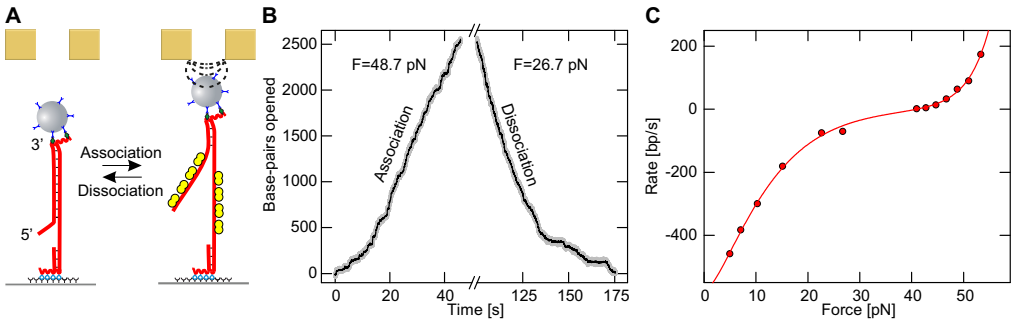

Figure 3. Association and dissociation of yRPA on a flap bearing DNA duplex substrate (at 20 nM yRPA in presence of 3 mM Mg^{2+}). (**A**) RPA also associates reversibly onto a 6.1 kb long DNA duplex with a 38 nt long 5′-end flap subject to force. (**B**) Example time trace of RPA association and dissociation. The duplex is seen to open continuously over several thousand bp, caused by the association of RPA. In this geometry, association proceeds at a rate of 63.8 bp/s, when a magnetic force of 48.7 pN is exerted. Complete opening is avoided, to prevent detachment of the magnetic bead, by lowering the force. At a force of 26.7 pN force, the helix refolds rapidly with a rate of 70 bp/s as RPA dissociates. (**C**) Association and dissociation rates are plotted against the applied force (red circles). Again both the association and dissociation rates vary exponentially with the applied force. A double exponential (see main text) fits the data well (red line), fit Parameters are given in Table 1.

length. This corresponds to the well established DNA overstretching transition (36,37).

In the presence of yRPA, a gradual increase in DNA length was observed at forces well below the overstretching transition. This extension corresponds to the opening of the duplex, which proceeded for several thousand bp (Figure 3B) in agreement with the association of RPA at the junction between ssDNA and dsDNA (Figure 3A and B). As observed for the DNA hairpin geometry, the process was fully reversible such that upon force reduction the DNA extension gradually decreased until full restoration of duplex DNA. Measured hairpin opening and closing rates also varied exponentially with the applied force (Figure 3C). We fit these data with Equation 1, accounting for the altered DNA stretching geometry by means of a different conversion factor c (Supplementary Information). The fit parameters obtained compare well with those obtained for the hairpin geometry, $\Delta z_{on} = 2.9 \pm 0.2$ bp and $\Delta z_{off} = 1.6 \pm 0.1$ bp, suggesting a geometry independent behavior of RPA binding and dissociation. Again microdomain association/dissociation appeared to govern the observed opening or closing of the duplex. The closure rate of $k_{off} = 564 \pm 11$ bp/s suggests extremely rapid exchange. An elevated force of 43 pN was required to bring both competing processes to equilibrium, which can be fully explained by considering the stretching energetics of this geometry (see Discussion).

Magnesium dependence of RPA binding

The ionic strength and in particular the magnesium level are of vital importance for DNA-protein interactions due to both a general screening of charges and also the specific mediation of important contacts (38,39). Earlier work reported that hRPA is capable of melting dsDNA under conditions of low magnesium concentration even in the absence of force (21–23). Here, we investigated this observation in more detail for both hRPA and yRPA.

We first probed DNA melting in bulk solution by gel electrophoresis using Lambda DNA digested with HindIII that produced dsDNA fragments of various lengths. Melting of dsDNA by hRPA occured at Mg^{2+} concentrations below 3 mM (Figure 4B). The extent of melting increased with decreasing Mg^{2+} levels (Supplementary Figure S4), increasing hRPA concentration (Supplementary Figure S3) and de-

Table 1. Fit parameters for yRPA and hRPA association and dissociation kinetics

	yRPA			hRPA		
	1 mM Mg^{2+}	*3 mM Mg^{2+}*	*10 mM Mg^{2+}*	*3 mM Mg^{2+}*	*5 mM Mg^{2+}*	*10 mM Mg^{2+}*
k_{on} [bp s^{-1} nM^{-1}]	34.2 ± 16.9	9.0 ± 2.1	18.2 ± 8.9	2.1 ± 0.3	3.2 ± 0.4	6.2 ± 1.1
k_{off} [bp s^{-1}]	233 ± 19	239 ± 14	336 ± 51	37 ± 7	109 ± 28	189 ± 23
Δz_{on}[bp]	5.0 ± 1.0	3.3 ± 0.6	2.4 ± 0.7	1.6 ± 0.6	2.1 ± 0.4	2.5 ± 0.5
Δz_{off} [bp]	1.8 ± 0.2	1.6 ± 0.1	1.8 ± 0.2	0.6 ± 0.5	1.1 ± 0.5	0.9 ± 0.2
F_{unz} [pN]	17.8	18.2	19.9	18.2	18.8	19.9
F_{equi}[pN]	12.4	12.4	11.1	11.8	12.2	14.5

k_{on} and k_{off} are the rates of association and dissociation at the unzipping force F_{unz} or zero force, respectively. Δz_{on} and Δz_{off} are the transition state distances for binding or dissociation of an RPA heterotrimer in bp. The parameters were obtained by fitting the force-dependent association and dissociation rates of yRPA and hRPA on the 488 bp DNA hairpin, to a model comprised of two Arrhenius terms (see Equation 1).

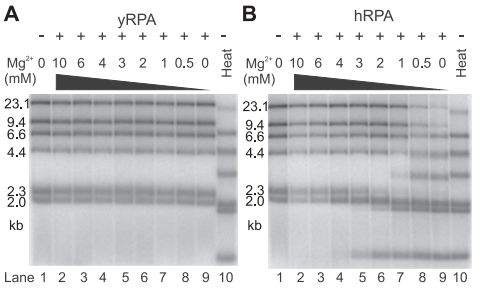

Figure 4. DNA melting capacity of human RPA depends on Mg^{2+} concentration. (**A**) yRPA does not melt dsDNA. Lambda/HindIII DNA (lane 1) was incubated with 2.2 μM yRPA (corresponding to 300% saturation) with various magnesium acetate concentrations (lanes 2–9, 0–10 mM as indicated) for 30 min at 30°C and subsequently analyzed on a 1% agarose gel. Throughout the range of magnesium concentrations tested, no melting occurred (*cf.* heat denatured substrate in lane 10). (**B**) Experiment as in panel a but with 2.2 μM hRPA (corresponds to 375% DNA saturation) incubated for 30 min at 37°C. In contrast to yRPA, hRPA melts dsDNA at Mg^{2+} concentrations below 3 mM (lanes 5–9).

creasing dsDNA fragment length (Figure 4A, Supplementary Figure S4). Surprisingly and in a remarkable contrast, no sign of dsDNA melting was observed with yRPA (Figure 4A, Supplementary Figure S3). We also tested the effect of monovalent salt on the melting activity, which was retained in 50 mM KCl and 0–1 mM Mg^{2+} (Supplementary Figure S7A) but not longer observed at 100 mM or higher concentrations of KCl (Supplementary Figure S7B).

To gain a more detailed insight into this distinct behavior of hRPA versus yRPA, we probed RPA-mediated opening and closing of dsDNA with our single-molecule assay for varying magnesium concentrations, but in the absence of monovalent salt to make the effect easier to characterize. In agreement with the gel electrophoresis experiments, the force-dependent DNA opening and closing remained constant within margins of error for yRPA in Mg^{2+} concentrations between 1 and 10 mM (Figure 5A, Table 1). In the absence of Mg^{2+}, the curve is plainly shifted by 3.5 pN to lower forces, comparable to the reduction of F_{unz} between 1 and 0 mM Mg^{2+} (see Supplementary Figure S5). The absence of melting by yRPA is not simply due to the lower concentration of yRPA (20 nM) as compared to hRPA (50 nM). This is evidenced by the fact that hRPA melts dsDNA across a range of concentrations in bulk whereas this does not occur with yRPA (see Supplementary Figure S3).

For hRPA however, a pronounced effect of the magnesium level on the dissociation rates was observed. Hairpin closure rates at zero force dropped from 189 bp/s at 10 mM Mg^{2+} down to 109 bp/s at 5 mM Mg^{2+} and 32 bp/s at 3 mM Mg^{2+}. Below 3 mM Mg^{2+} hairpin closure did not occur at all, as illustrated by exemplary time trajectories recorded at 2 pN (Figure 5B).

Even in the absence of force the DNA hairpin was already completely opened after introducing hRPA in buffer containing <3 mM Mg^{2+}. Overall the observed DNA melting at low Mg^{2+} concentration in bulk and single-molecule experiments is governed by an inhibited RPA dissociation, since the hairpin opening due to RPA association was much less affected (Figure 5A, Table 1). Linear extrapolation of the hairpin closing rates for hRPA as a function of the Mg^{2+} concentration allows to estimate a value of 2.5 mM Mg^{2+} at which no more dissociation would occur. This is in good agreement with the onset of melting activity observed in bulk.

Stepwise fork opening upon RPA binding

Close examination of the progressive dsDNA opening due to RPA binding revealed that it did not occur uniformly with constant velocity, but rather in a stepwise manner (Figure 3A). To assess whether the observed stepping is introduced by the stepwise association of single RPA molecules, we carried out additional hairpin opening experiments at moderate force and low RPA concentration. These conditions favor slow RPA association such that individual steps became well resolved and discernible (Figure 6A). To evaluate the size distribution of these steps we employed a step finding algorithm (40). Step sizes for hairpin opening follow a Gaussian distribution (Figure 6B), the mean step sizes for dsDNA opening were 21.8 ± 5.5 bp for yRPA and 23.8 ± 2.1 bp for hRPA. These values are in agreement with binding site sizes of RPA on ssDNA reported in literature (26,41) in both their magnitudes (~23 nt for yRPA and ~26 nt for hRPA) and relative extent (with hRPA slightly larger). Thus, the observed steps appear to be single RPA binding events. Most likely, one RPA is binding to one strand and binding to the other strand then rapidly follows suit. We note that under our measurement conditions also a minor fraction of dsDNA closing steps with similar size as the opening steps were observed (Figure 6B). These backward steps stem from the dynamic competition between RPA binding and dissociation at the DNA fork.

Sliding of hRPA along ssDNA induced by a rezipping fork

As shown above, at low force a rezipping hairpin rapidly displaces RPA from ssDNA. Recently, it was however reported that RPA is able to undergo diffusive motion along ssDNA (26). We therefore sought to test whether a rezipping DNA fork is able to push a single RPA heterotrimer along ssDNA in front of it. If this occurred, ssDNA secondary structure might impose pressure onto RPA filaments to keep them in a dense state. To test this hypothesis a hairpin was repetitively opened and closed by alternating between forces above and below the characteristic unzipping force (22.5 and 15.5 pN, respectively). The lower force bound allowed rapid hairpin closure in the absence of RPA in a single abrupt transition, while being sufficiently high to inhibit RPA dissociation from ssDNA. When adding small amounts of hRPA (150 pM in buffer containing 1 mM Mg^{2+}) the hairpin closing transition was blocked in some instances and instead a slower rezipping with approximately constant velocity took place (Figure 7A). Such continuous closing events occurred only about once in 10 force cycles. Given that the applied lower force bound strongly disfavors RPA dissociation, we attribute these RPA induced events to the sliding of a single RPA molecule in front of the rezipping fork. RPA gets pushed along the ssDNA by the fork

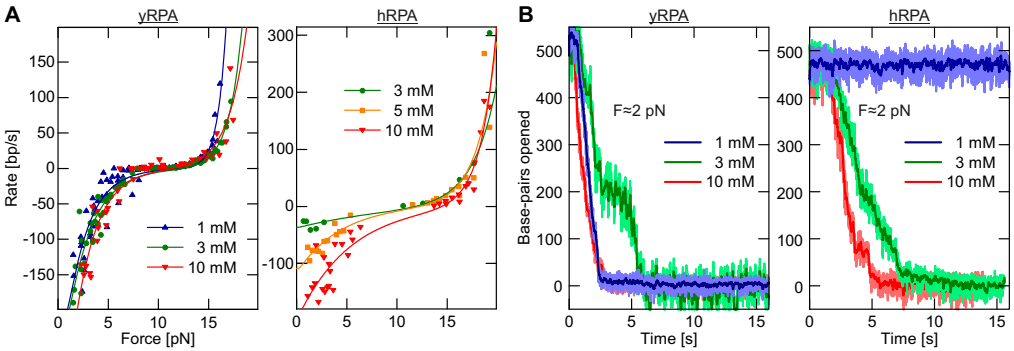

Figure 5. Magnesium dependence of DNA fork opening due to RPA binding. (**A**) Hairpin opening and closing rates of 20 nM yRPA (left panel) and 50 nM hRPA (right panel) as a function of force measured for different Mg^{2+} concentrations. While the behavior of yRPA is rather independent of the Mg^{2+} concentration between 1 to 10 mM, the dissociation of hRPA becomes impeded at low Mg^{2+} levels. Fit parameters are tabulated in Table 1. (**B**) Example trajectories for the dissociation of yRPA and hRPA at ∼2 pN for different magnesium concentrations. For hRPA, closure of an opened hairpin is completely impeded below 3 mM Mg^{2+}.

but slows down the rapid rezipping by the friction it experiences during sliding on ssDNA (see Figure 7B). The fact that the sliding can be interrupted by unzipping the hairpin and reinitiated by closing the hairpin again (see Figure 7A, second highlighted portion) substantiates this explanation.

To determine a friction coefficient and thus a diffusion coefficient for RPA sliding on ssDNA, we carried out RPA pushing experiments for various lower force bounds (13.5 to 16.0 pN). The effective pushing force that moves RPA along the ssDNA is the difference between the characteristic hairpin unzipping force (17.8 pN for the applied conditions) and the applied force. In agreement with friction being responsible for the slowed down dsDNA rezipping, the average hairpin closing rate was inversely proportional to the pushing force (Figure 7C). A linear fit to the data is used to obtain the friction coefficient ζ for RPA sliding along ssDNA according to $F_{\mathrm{push}} = F_{\mathrm{unz}} - F = \zeta \cdot v$. Using the Einstein relation $D = k_B T/\zeta$, the friction coefficient is converted into the diffusion coefficient D, for which we obtain $960 \pm 350 \mathrm{nt}^2/\mathrm{s}$.

DISCUSSION

RPA tightly binds ssDNA. The results presented here demonstrate that RPA binding to a DNA substrate that mimics a replication fork is, however, highly dynamic. In this case, the finely balanced competition between continuous association and dissociation of RPA at the fork determines the degree of bound RPA. The details of the dynamic model that emerges from our findings (illustrated in Figure 8) is discussed below.

RPA supports rapid transactions at DNA forks

RPA binds to ssDNA with a dissociation constant in the low nM to high pM range (3) and dissociates with a rate as low as $0.006\ \mathrm{s}^{-1}$ (hRPA in 5 mM Mg^{2+}) in the absence of free RPA in solution (25,42). The coating of ssDNA by RPA is therefore a rapid process, while an established RPA filament features an extremely slow turnover. In contrast, as shown in this study, RPA can be very rapidly displaced at a DNA replication fork with speeds of several hundred bp per second corresponding to a removal of up to >10 RPA heterotrimers per second. Thus, RPA acts as a versatile platform: it binds and protects ssDNA generated in a number of DNA processing steps, such as DNA repair, stalled replication and homologous recombination. During replication it supposedly also prevents rehybridization of parental DNA strands as long as a replicative helicase acts on the fork. In contrast, RPA rapidly dissociates upon rezipping of DNA at a forked substrate. Despite the stable protection of ssDNA conferred by RPA, the observed speeds (up to 300 bp/s on the fork and 500 bp/s on the flap substrate) exceed the ssDNA translocation and dsDNA unwinding rates of most helicases and translocases. Thus, RPA cannot maintain such a stretch of DNA as single-stranded and will be rapidly expelled once a helicase ceases its activity. This also implies that DNA helicases which orient themselves away from a DNA replication fork with respect to their translocation direction (28,43,44) are not required to strip off RPA but rather remove other proteins that also tightly bind ssDNA such as Rad51. An exception may be enzymes that revert stalled replication forks and that have been shown to actively anneal RPA coated ssDNA in particular in case of negative supercoiling (45). In general, helix refolding appears to be sufficient to return dsDNA to its native RPA-unbound state, once DNA processing has been completed and the processing machinery has dissociated from the DNA.

Microdomain dynamics govern the behavior of RPA

The association and dissociation of RPA at a forked substrate was found to be strongly force dependent. Increasing forces promoted RPA association while slowing down RPA dissociation. The competition between both processes de-

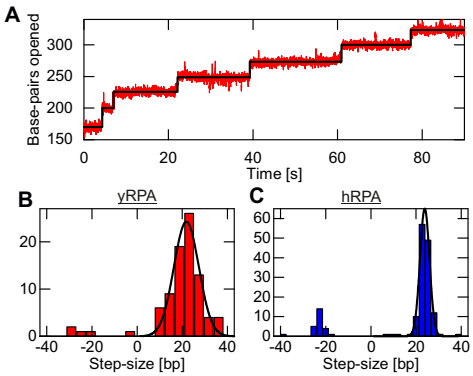

Figure 6. Binding site size of RPA. (**A**) Exemplary time trace yRPA association (2 nM yRPA, 10 mM Mg^{2+}) on the hairpin substrate showing clearly resolved steps at a force of 12.0 pN. (**B**) Step size distribution for yRPA (from multiple traces collected under the same conditions), calculated using a step finding algorithm. The step size of 21.8 bp occurs most frequently in the data). (**C**) The step size distribution for hRPA association data (collected at (5 nM hRPA, 10 mM Mg^{2+}, 12.0 pN) is similar, with the most common size being 23.8 bp.

termined whether fork opening and closing was observed. The force-dependent kinetics of these processes could be described by a simple model using transition-state theory. This provided the distances from the transition states Δz_{on} and Δz_{off} for association and dissociation, respectively, that were on the order of only a few bp throughout the investigated experimental conditions (Table 1). Compared to the binding-site size of RPA these values are quite small. This indicates that only a small terminal portion of RPA has to wedge in at the fork in order to allow the binding of the full RPA heterotrimer, which results in hairpin opening over the entire heterotrimer length. Similarly, for dissociation only a small terminal portion of RPA has to be lifted from the ssDNA due to helix refolding over one to two bp in order to destabilize the binding of RPA sufficiently and to shear it off. Note the transition state distances are consistently slightly lower for dissociation than for association. The mode of RPA engagement and lift off at the DNA fork is analogous to the widely used strand displacement reactions in DNA nanotechnology, where a few nucleotide long toehold provides a sufficient nucleation point for hybridization to a complementary target and displacement of an initially bound strand (35). Structural information of RPA shows that the heterotrimer comprises multiple DBDs that are flexibly linked together (46,47) and interact with the DNA in a defined orientation (48). The toehold estimates we obtain here for RPA binding compare well with the length of ssDNA that interacts with a single DBD, crystallographically determined to be 3 nt for DBDs A and B of hRPA (49). This suggests that association of a single DBD is sufficient for the observed DNA opening by RPA. Previously, such a microdomain association has already been proposed, in order to explain some of the binding properties of RPA (12,24,25). For example, the dissociation of RPA bound to ssDNA was found to be accelerated in the presence of unbound RPA in solution and it was proposed that competing RPA from solution can shear off bound molecules by initial association through a microdomain (25). Here, we directly demonstrated that RPA can melt apart and wedge into dsDNA, or once bound can be sheared off by a rezipping fork and that these processes use microdomain engagement over a length of ∼1 DBD. Given that the loss (23) or inhibition (50) of DBD-F located in the N-terminal region of the large subunit of RPA results in specific inhibition of helix-destabilization, we hypthesize that DBD-F is the likely candidate domain for toehold binding.

DNA melting by RPA occurs without active dsDNA destabilization

When applying sufficient force, RPA is capable of opening a DNA fork. Similar to the unwinding reaction of a helicase, this could be either passive or active (51). For passive opening RPA would only interact with ssDNA and trap spontaneous helix openings (fraying of DNA duplex ends) to accomplish microdomain association. For an active unwinding RPA would also interact with the dsDNA at the fork and cause helix destabilization. The unwinding rate of a DNA hairpin under tension by a passive helicase with step size n has been previously derived in a simplified form as (52):

$$v = v_{max} \exp\left(\frac{\Delta G_F^n - \Delta G_{bp}^n}{k_B T}\right), \quad (2)$$

where v_{max} is the maximum stepping rate of the helicase, ΔG_{bp}^n is the average base-pairing energy over n bp in absence of force and ΔG_F the free energy change due to the work that is done when opening n bp in presence of force. When neglecting the entropic contribution for ssDNA stretching (52), $\Delta G_F = c_F \cdot F \cdot z_n$ and $\Delta G_{bp} = c_{unz} \cdot F_{unz} \cdot z_n$. The latter equation uses the fact that at the hairpin unzipping force the applied work exactly compensates the base-pairing energy. Inserting these two equations into Equation 2, provides an expression that is mathematically similar to the rate of force-dependent DNA opening due to RPA association (left term in Eqn. 1). For a passive helicase, the velocity approaches v_{max} only close to the hairpin unzipping force at which the applied tension keeps the fraying bp at the fork practically fully open, such that the forward stepping is no longer hindered by duplex formation. For an active helicase v_{max} is already reached at considerably lower forces (52). Given the similarities between Equations 1 and 2, we would thus expect a similar distinction to be valid also for active versus passive DNA opening by RPA. As shown above the RPA induced DNA opening velocity is monotonically increasing even when approaching F_{unz}. Furthermore, the velocity for hRPA amounts to only 2–6 bp s^{-1} nM^{-1} at F_{unz} which is comparable to previously determined association rates of RPA with ssDNA of 2 s^{-1} nM^{-1} (53). Thus, the characteristics of the force-dependent DNA opening by RPA support a passive model rather than an active helix destabilization in agreement with previous reports (23). A passive model for DNA duplex opening by RPA is

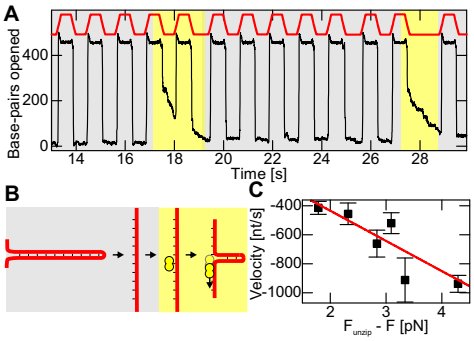

Figure 7. Sliding of RPA along ssDNA upon dsDNA rezipping. (**A**) Repetitive opening and closing the hairpin by alternating the applied force between 22.5 and 15.5 pN (as indicated in red) at a low hRPA concentration of 150 pM (in 1 mM Mg^{2+} buffer). For the majority of the unzipping cycles (gray background) the closing of the hairpin is unperturbed. Approximately once in 10 cycles, a continuous slower closing is however observed (pale yellow background) that is attributed to RPA sliding. (**B**) Cartoon illustrating the observed behavior according to the background colors used in A. In case of sliding events, a single hRPA heterotrimer is thought to bind to the exposed ssDNA after hairpin opening. When the force is reduced, the closing hairpin pushes the hRPA along the ssDNA. (**C**) Mean sliding velocity (black squares, error bars indicate standard errors) as a function of the pushing force applied by the hairpin (difference between characteristic unzipping force and the applied force). A linear fit describes the observed trend well ($R^2 = 0.86$), with the intersection of the velocity axis at −18.23 nt/s for zero force. Furthermore, the slope of this fit can be used to calculate a friction coefficient, as the velocity is expected to vary with the force as given by $F = \zeta \cdot v$, for which we find a value of $\zeta = 0.005 \pm 0.0009$ pN·nt^{-1}·s.

also supported by the observed salt dependence of this reaction for yRPA. In presence of 1 to 10 mM Mg^{2+} no considerable changes to the kinetics were found (Figure 5A). This correlates with the determined unzipping forces of the DNA hairpin that varied only slightly between 1 and 10 mM Mg^{2+} (Table 1). However, when carrying out experiments in absence of Mg^{2+} the DNA opening kinetics shifted by ∼3 pN toward lower forces, though the overall shape of the curve remained similar (Supplementary Figure S6). Again the magnitude of the shift correlates with the measured unzipping force of the hairpin, which was found to be 3.5 pN lower at these ionic conditions. A reduced base-pairing energy thus effects mechanical unzipping and RPA mediated dsDNA opening kinetics to the same measure, lending further support for the passive model.

Fine-tuned RPA binding energetics

The above discussion established a passive mechanism for dsDNA opening by RPA. Since this process already occurs at forces below F_{unz}, it follows that it is driven exclusively by the free energy gain of the RPA–ssDNA association to both strands at the fork. At equilibrium, when the rates of RPA association and dissociation balance out (yielding a net rate of zero), the base-pairing energy (over a single step of DNA opening of ∼23 bp) equals the work done when opening the hairpin under the external force plus the free energy change associated with RPA binding:

$$\Delta G_{bp}^{23\,bp} = \Delta G_{F_{equi}}^{23\,bp} + 2 \cdot \Delta G_{bind}$$

Using the above expressions for ΔG_{bp} and ΔG_F one obtains:

$$\Delta G_{bind} = (c_{unz} F_{unz} - c_{equi} F_{equi})(23\,bp)/2$$

From the values in Table 1, one arrives at an average value of ΔG_{bind} ∼40 ± 9 kJ/mol for both yRPA and hRPA across all Mg^{2+} conditions. Using the equilibrium constant of 10^{10} M^{-1} (3), one arrives at a value of ∼57 kJ/mol which compares well to the value we obtain from our measurements. In a simplified view RPA binding contributes with about one-third of the base-pairing energy to the duplex opening, since the equilibrium force is about one third lower than the unzipping force. Remarkably this is similar for yRPA and hRPA across the range of ionic conditions investigated. In that respect RPA binding appears to be fine-tuned. The binding free energy is strong enough for stable binding but sufficiently weak to avoid DNA melting. This tunable balance is retained in 50 mM KCl between 0–1 mM Mg^{2+} but not observed at higher KCl concentrations (Supplementary Figure S7). We think that melting is meaningful within the intracellular context but probably happens on a much smaller scale. Moreover, crowding effects can shift the salt requirements for RPA-induced melting.

The obtained energetic contribution of RPA binding to DNA opening appears to be geometry independent, since also for the experiments on the DNA duplex substrate (Figure 3) the equilibrium force of 43 pN is one-third lower than the overstretching force during which DNA melts. Most likely the same contribution would be obtained when evaluating RPA induced melting of supercoiled DNA (24). However, in this case interpretation of the data may be complicated by the fact that trapping of transient denaturation bubbles may occur on multiple sites all over the DNA, as suggested by dsDNA overstretching experiments (54,55). Overall the observed force/twist-dependent DNA melting by RPA may be an important regulator in particular circumstances where DNA experiences high tension and torque. This is the case for instance during the formation of anaphase bridges in the S-phase of replication, where the affinity of the Plk1-interacting checkpoint helicase (PICH) for dsDNA greatly increases under tension causing a stabilization of the dsDNA (56).

Regulation of RPA binding by Mg^{2+} ions

The magnesium concentration dependence of the dissociation rate we observed is specific to hRPA, yRPA did not exhibit this behavior. The ionic strength in general and magnesium in particular are of vital importance for DNA–protein interactions. While the DNA duplex is stabilized by charge screening, hindering the association of RPA, the mutual approach of negatively charged RPA and the DNA is assisted. This may account for minute variations in the apparent association rates. However, the much more significant influence on the hRPA dissociation rates seems to involve a highly specific effect of magnesium on the binding of hRPA to DNA. It is conceivable that yRPA may feature an evolutionarily conserved salt independence, in order to allow for

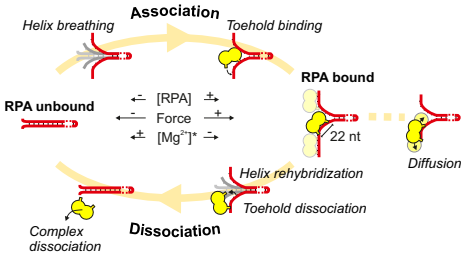

Figure 8. Dynamics of RPA on DNA fork. Initially, **Association** commences from a **RPA unbound** DNA fork. *Helix breathing* exposes small stretches of ssDNA to which RPA attaches via *Toehold binding*. Further binding occurs in the same manner rendering the ssDNA arms of the fork **RPA bound**. Individual bound RPA heterotrimers can slide along the ssDNA by *Diffusion*. **Dissociation** of RPA is triggered when DNA *Helix rehybridization* causes *Toehold dissociation* ultimately leading to *Complex dissociation*. Further dissociation ultimately reverts the DNA fork to the **RPA unbound** state. Both competing processes take place continuously, with the balance being controlled by the concentration of RPA, the applied force and (*in the case of hRPA) the Mg^{2+} concentration. Higher force or RPA concentration favors association, while (for hRPA) more Mg^{2+} shifts the balance toward dissociation.

variable magnesium concentrations in the cell. Yeast cells are expected to have greater variability of their intracellular ion composition due to the diversity of environments in which they grow. Indeed intracellular magnesium concentrations strongly depend on the magnesium concentration outside of the cell (57). Alternatively, hRPA binding could be regulated in a cell cycle dependent manner by controlling the intra-nuclear magnesium levels. Moderate magnesium concentrations are essential for the activity of a whole range of DNA repair proteins (58) and the distribution of intracellular magnesium is both variable (57,59,60) and tightly regulated throughout the cell cycle progression (58).

Pushing of RPA along ssDNA

Despite the strong binding reported for each of the DBD subdomains, with K_d values in the μM range (61), diffusion of hRPA on ssDNA as been recently reported (26). We further substantiated this observation by testing whether single hRPA heterotrimers can slide along ssDNA when pushed by a closing hairpin. Sliding was readily observed and the obtained friction coefficient allowed to calculate a diffusion coefficient of $D = 960 \pm 350$ nt^2/s on ssDNA. This matches the previously reported value of $D = 2800 \pm 200$ nt^2/s (26), considering the high salt concentration of 0.5 M NaCl used in that study. Diffusion of RPA along ssDNA allows bound RPA molecules to rearrange themselves on the ssDNA, e.g. to ensure a dense coverage but also in order to free up access to other ssDNA binding proteins. It may, for example, facilitate the exchange between bound and free RPA molecules (25) and allow the recruitment of other DNA repair proteins. Rad52 for instance binds RPA–ssDNA and stimulates the extension of Rad51 filaments on the ssDNA (62–64) which is an important precursor to later stages of homologous recombination. Additionally, RPA bound to ssDNA directly interacts with ATRIP, which contributes to the activation of the ATR checkpoint kinase as a response to ssDNA arising from processing of DNA double-strand breaks and replication interference (13). *In vitro* reconstitution experiments revealed that the ATR activation is strongly dependent on the length of ssDNA, suggesting a possible cooperative mechanism of RPA–ssDNA in ATRIP mediated ATR activation (14). Therefore, the sliding of RPA along ssDNA might allow the formation of RPA nucleoprotein filaments that is optimally capable of interaction with ATRIP or proteins that might be recruited through a similar mechanism. It was recently also shown that ATR activation further depends on the binding of MutSβ to DNA hairpin loops that persist in RPA-covered ssDNA (65). In order for the formation and persistence of these hairpin regions the ability of rezipping DNA hairpins to cause RPA to slide may also be a functional requirement. Additionally, the sliding capability of RPA on ssDNA suggests that molecular motors such as helicases may also be able to push along RPA bound to the ssDNA along which they track.

CONCLUSION

Our results contribute to the emerging view that RPA filaments are highly 'vivid' cellular structures. The binding affinity of RPA to ssDNA appears to be carefully adjusted, such that ssDNA intermediates arising during DNA processing are stably protected, yet dsDNA is left unchanged. When necessary, RPA can nevertheless be readily dislodged or pushed along permitting access to other enzymes. Once these molecular machines complete their task, rapid removal of RPA at a fork is facilitated by the rehybridization of the DNA helix, recovering the fully processed dsDNA.

SUPPLEMENTARY DATA

Supplementary Data are available at NAR online.

ACKNOWLEDGEMENTS

We thank Dominik Kauert, Jasmina Dikic, Christophe Rouillon and Marius Rutkauskas for discussion and advice. Furthermore, we thank Ina Kowsky and Gerda Scheidtgen-Kleyboldt for general laboratory support.

FUNDING

ERC starting grant [GA 261224 to R.S.]; Swiss National Science Foundation professorship [PP00P3 133636]; Krebsforschung Schweiz grant [KFS 3089-02-2013 to P.C]. Funding for open access charge: European Research Council.
Conflict of interest statement. None declared.

REFERENCES

1. Seroussi,E. and Lavi,S. (1993) Replication protein A is the major single-stranded DNA binding protein detected in mammalian cell extracts by gel retardation assays and UV cross-linking of long and short single-stranded DNA molecules. *J. Biol. Chem.*, **268**, 7147–7154.
2. Wold,M.S. and Kelly,T. (1988) Purification and characterization of replication protein A, a cellular protein required for in vitro replication of simian virus 40 DNA. *Proc. Natl. Acad. Sci. U.S.A.*, **85**, 2523–2527.

3. Wold,M.S. (1997) REPLICATION PROTEIN A:A heterotrimeric, single-stranded DNA-binding protein required for eukaryotic DNA metabolism. *Annu. Rev. Biochem.*, **66**, 61–92.
4. Wobbe,C.R., Weissbach,L., Borowiec,J.A., Dean,F.B., Murakami,Y., Bullock,P. and Hurwitz,J. (1987) Replication of simian virus 40 origin-containing DNA in vitro with purified proteins. *Proc. Natl. Acad. Sci. U.S.A.*, **84**, 1834–1838.
5. Kim,C., Paulus,B.F. and Wold,M.S. (1994) Interactions of human replication protein A with oligonucleotides. *Biochemistry*, **33**, 14197–14206.
6. Brill,S.J. and Stillman,B. (1989) Yeast replication factor-A functions in the unwinding of the SV40 origin of DNA replication. *Nature*, **342**, 92–95.
7. Cejka,P., Cannavo,E., Polaczek,P., Masuda-Sasa,T., Pokharel,S., Campbell,J.L. and Kowalczykowski,S.C. (2010) DNA end resection by Dna2-Sgs1-RPA and its stimulation by Top3-Rmi1 and Mre11-Rad50-Xrs2. *Nature*, **467**, 112–116.
8. Namiki,Y. and Zou,L. (2006) ATRIP associates with replication protein A-coated ssDNA through multiple interactions. *Proc. Natl. Acad. Sci. U.S.A.*, **103**, 580–585.
9. Oakley,G.G., Tillison,K., Opiyo,S.A., Glanzer,J.G., Horn,J.M. and Patrick,S.M. (2009) Physical interaction between replication protein A (RPA) and MRN: involvement of RPA2 phosphorylation and the N-Terminus of RPA1. *Biochemistry*, **48**, 7473–7481.
10. Feldkamp,M.D., Mason,A.C., Eichman,B.F. and Chazin,W.J. (2014) Structural analysis of replication protein A recruitment of the DNA damage response protein SMARCAL1. *Biochemistry*, **53**, 3052–3061.
11. Chen,H., Lisby,M. and Symington,L. (2013) RPA coordinates DNA end resection and prevents formation of DNA hairpins. *Mol. Cell*, **50**, 589–600.
12. Chen,R. and Wold,M.S. (2014) Replication protein A: Single-stranded DNA's first responder. *Bioessays*, **36**, 1156–1161.
13. Zou,L. and Elledge,S.J. (2003) Sensing DNA damage through ATRIP recognition of RPA-ssDNA complexes. *Science*, **300**, 1542–1548.
14. Choi,J.-H., Lindsey-Boltz,L.A., Kemp,M., Mason,A.C., Wold,M.S. and Sancar,A. (2010) Reconstitution of RPA-covered single-stranded DNA-activated ATR-Chk1 signaling. *Proc. Natl. Acad. Sci. U.S.A.*, **107**, 13660–13665.
15. Kim,C., Snyder,R.O. and Wold,M.S. (1992) Binding properties of replication protein A from human and yeast cells. *Mol. Cell. Biol.*, **12**, 3050–3059.
16. Patrick,S.M. and Turchi,J.J. (1999) Replication protein A (RPA) binding to duplex cisplatin-damaged DNA is mediated through the generation of single-stranded DNA. *J. Biol. Chem.*, **274**, 14972–14978.
17. Lao,Y., Gomes,X.V., Ren,Y., Taylor,J.-S. and Wold,M.S. (2000) Replication protein A interactions with DNA. III. Molecular basis of recognition of damaged DNA. *Biochemistry*, **39**, 850–859.
18. Wu,Y., Rawtani,N., Thazhathveetil,A.K., Kenny,M.K., Seidman,M.M. and Brosh,R.M. (2008) Human replication protein A melts a DNA triple helix structure in a potent and specific manner. *Biochemistry*, **47**, 5068–5077.
19. Salas,T.R., Petruseva,I., Lavrik,O., Bourdoncle,A., Mergny,J.-L., Favre,A. and Saintomé,C. (2006) Human replication protein A unfolds telomeric G-quadruplexes. *Nucleic Acids Res.*, **34**, 4857–4865.
20. Prakash,A., Natarajan,A., Marky,L.A., Ouellette,M.M. and Borgstahl,G.E.O. (2011) Identification of the DNA-binding domains of human replication protein A that recognize G-quadruplex DNA. *J. Nucleic Acids*, **2011**, 896947.
21. Georgaki,A., Strack,B., Podust,V. and Hübscher,U. (1992) DNA unwinding activity of replication protein A. *FEBS Lett.*, **308**, 240–244.
22. Treuner,K., Ramsperger,U. and Knippers,R. (1996) Replication protein A induces the unwinding of long double-stranded DNA regions. *J. Mol. Biol.*, **259**, 104–112.
23. Lao,Y., Lee,C.G. and Wold,M.S. (1999) Replication protein A interactions with DNA. 2. Characterization of double-stranded DNA-binding/Helix-destabilization activities and the role of the zinc-finger domain in DNA interactions. *Biochemistry*, **38**, 3974–3984.
24. De Vlaminck,I., Vidic,I., van Loenhout,M.T.J., Kanaar,R., Lebbink,J. H.G. and Dekker,C. (2010) Torsional regulation of hRPA-induced unwinding of double-stranded DNA. *Nucleic Acids Res.*, **38**, 4133–4142.
25. Gibb,B., Ye,L.F., Gergoudis,S.C., Kwon,Y., Niu,H., Sung,P. and Greene,E.C. (2014) Concentration-dependent exchange of replication protein A on single-stranded DNA revealed by single-molecule imaging. *PLoS One*, **9**, e87922.
26. Nguyen,B., Sokoloski,J., Galletto,R., Elson,E.L., Wold,M.S. and Lohman,T.M. (2014) Diffusion of human replication protein A along single-stranded DNA. *J. Mol. Biol.*, **426**, 3246–3261.
27. Huhle,A., Klaue,D., Brutzer,H., Daldrop,P., Joo,S., Otto,O., Keyser,U. and Seidel,R. (2014) Camera-based real-time 3D particle tracking at kHz rates and Ångström accuracy. *Nat. Commun.*, **6**, 5885.
28. Klaue,D., Kobbe,D., Kemmerich,F., Kozikowska,A., Puchta,H. and Seidel,R. (2013) Fork sensing and strand switching control antagonistic activities of RecQ helicases. *Nat. Commun.*, **4**, 2024.
29. Luzzietti,N., Knappe,S., Richter,I. and Seidel,R. (2012) Nicking enzyme-based internal labeling of DNA at multiple loci. *Nat. Protoc.*, **7**, 643–653.
30. Levikova,M., Klaue,D., Seidel,R. and Cejka,P. (2013) Nuclease activity of Saccharomyces cerevisiae Dna2 inhibits its potent DNA helicase activity. *Proc. Natl. Acad. Sci. U.S.A.*, **110**, E1992–E2001.
31. Kantake,N., Sugiyama,T., Kolodner,R.D. and Kowalczykowski,S.C. (2003) The recombination-deficient mutant RPA (rfa1-t11) is displaced slowly from single-stranded DNA by Rad51 protein. *J. Biol. Chem.*, **278**, 23410–23417.
32. Henricksen,L.A., Umbricht,C.B. and Wold,M.S. (1994) Recombinant replication protein A: expression, complex formation, and functional characterization. *J. Biol. Chem.*, **269**, 11121–11132.
33. Klaue,D. and Seidel,R. (2009) Torsional stiffness of single superparamagnetic microspheres in an external magnetic field. *Phys. Rev. Lett.*, **102**, 028302.
34. Daldrop,P., Brutzer,H., Huhle,A., Kauert,D.J. and Seidel,R. (2015) Extending the range for force calibration in magnetic tweezers. *Biophys. J.*, **108**, 2550–2561.
35. Zhang,D.Y. and Winfree,E. (2009) Control of DNA strand displacement kinetics using toehold exchange. *J. Am. Chem. Soc.*, **131**, 17303–17314.
36. Smith,S.B., Cui,Y. and Bustamante,C. (1996) Overstretching B-DNA: the elastic response of individual double-stranded and single-stranded DNA molecules. *Science*, **271**, 795–799.
37. Cluzel,P., Lebrun,A., Heller,C., Lavery,R., Viovy,J.-L., Chatenay,D. and Caron,F. (1996) DNA: an extensible molecule. *Science*, **271**, 792–794.
38. Anderson,C.F. and Record,M. Jr (1995) Salt-nucleic acid interactions. *Annu. Rev. Phys. Chem.*, **46**, 657–700.
39. Guéroult,M., Boittin,O., Mauffret,O., Etchebest,C. and Hartmann,B. (2012) Mg2+ in the major groove modulates B-DNA structure and dynamics. *PLoS One*, **7**, e41704.
40. Kerssemakers,J. W.J., Laura Munteanu,E., Laan,L., Noetzel,T.L., Janson,M.E. and Dogterom,M. (2006) Assembly dynamics of microtubules at molecular resolution. *Nature*, **442**, 709–712.
41. Kumaran,S., Kozlov,A.G. and Lohman,T.M. (2006) Saccharomyces cerevisiae replication protein A binds to single-stranded DNA in multiple salt-dependent modes. *Biochemistry*, **45**, 11958–11973.
42. Deng,S.K., Gibb,B., de Almeida,M.J., Greene,E.C. and Symington,L.S. (2014) RPA antagonizes microhomology-mediated repair of DNA double-strand breaks. *Nat. Struct. Mol. Biol.*, **21**, 405–412.
43. Park,J., Myong,S., Niedziela-Majka,A., Lee,K.S., Yu,J., Lohman,T.M. and Ha,T. (2010) PcrA helicase dismantles RecA filaments by reeling in DNA in uniform steps. *Cell*, **142**, 544–555.
44. Kanagaraj,R., Saydam,N., Garcia,P.L., Zheng,L. and Janscak,P. (2006) Human RECQ5 helicase promotes strand exchange on synthetic DNA structures resembling a stalled replication fork. *Nucleic Acids Res.*, **34**, 5217–5231.
45. Yusufzai,T. and Kadonaga,J.T. (2008) HARP is an ATP-driven annealing helicase. *Science*, **322**, 748–750.
46. Bochkareva,E., Korolev,S., Lees-Miller,S.P. and Bochkarev,A. (2002) Structure of the RPA trimerization core and its role in the multistep DNA-binding mechanism of RPA. *EMBO J.*, **21**, 1855–1863.
47. Brosey,C.A., Yan,C., Tsutakawa,S.E., Heller,W.T., Rambo,R.P., Tainer,J.A., Ivanov,I. and Chazin,W.J. (2013) A new structural framework for integrating replication protein A into DNA processing machinery. *Nucleic Acids Res.*, **41**, 2313–2327.

48. Kolpashchikov,D.M., Khodyreva,S.N., Khlimankov,D.Y., Wold,M.S., Favre,A. and Lavrik,O.I. (2001) Polarity of human replication protein A binding to DNA. *Nucleic Acids Res.*, **29**, 373–379.
49. Bochkarev,A., Pfuetzner,R.A., Edwards,A.M. and Frappier,L. (1997) Structure of the single-stranded-DNA-binding domain of replication protein A bound to DNA. *Nature*, **385**, 176–181.
50. Glanzer,J.G., Carnes,K.A., Soto,P., Liu,S., Parkhurst,L.J. and Oakley,G.G. (2013) A small molecule directly inhibits the p53 transactivation domain from binding to replication protein A. *Nucleic Acids Res.*, **41**, 2047–2059.
51. von Hippel,P.H. and Delagoutte,E. (2001) A general model for nucleic acid helicases and their "Coupling" within macromolecular machines. *Cell*, **104**, 177–190.
52. Lionnet,T., Spiering,M.M., Benkovic,S.J., Bensimon,D. and Croquette,V. (2007) Real-time observation of bacteriophage T4 gp41 helicase reveals an unwinding mechanism. *Proc. Natl. Acad. Sci. U.S.A.*, **104**, 19790–19795.
53. Patrick,S.M. and Turchi,J.J. (2001) Stopped-flow kinetic analysis of replication protein A-binding DNA: damage recognition and affinity for single-stranded DNA reveal differential contributions of k_{on} and k_{off} rate constants. *J. Biol. Chem.*, **276**, 22630–22637.
54. van Mameren,J., Gross,P., Farge,G., Hooijman,P., Modesti,M., Falkenberg,M., Wuite,G.J.L. and Peterman,E.J.G. (2009) Unraveling the structure of DNA during overstretching by using multicolor, single-molecule fluorescence imaging. *Proc. Natl. Acad. Sci. U.S.A.*, **106**, 18231–18236.
55. King,G.A., Gross,P., Bockelmann,U., Modesti,M., Wuite,G.J.L. and Peterman,E.J.G. (2013) Revealing the competition between peeled ssDNA, melting bubbles, and S-DNA during DNA overstretching using fluorescence microscopy. *Proc. Natl. Acad. Sci. U.S.A.*, **110**, 3859–3864.
56. Biebricher,A., Hirano,S., Enzlin,J., Wiechens,N., Streicher,W., Huttner,D., Wang,L.-C., Nigg,E., Owen-Hughes,T., Liu,Y. *et al.* (2013) PICH: a DNA translocase specially adapted for processing anaphase bridge DNA. *Mol. Cell*, **51**, 691–701.
57. Kroeger,H. and Trösch,W. (1974) Influence of the explantation milieu on intranuclear [Na], [K] and [Mg] of Chironomus thummi salivary gland cells. *J. Cell. Physiol.*, **83**, 19–25.
58. Hartwig,A. (2001) Role of magnesium in genomic stability. *Mutat. Res.*, **475**, 113-121.
59. Cohen,S.M. and Burt,C.T. (1977) 31P nuclear magnetic relaxation studies of phosphocreatine in intact muscle: determination of intracellular free magnesium. *Proc. Natl. Acad. Sci. U.S.A.*, **74**, 4271–4275.
60. Adhikari,S., Karmahapatra,S., Karve,T., Bandyopadhyay,S., Woodrick,J., Manthena,P., Glasgow,E., Byers,S., Saha,T. and Uren,A. (2012) Characterization of magnesium requirement of human 5′-tyrosyl DNA phosphodiesterase mediated reaction. *BMC Res. Notes*, **5**, 134–000.
61. Wyka,I.M., Dhar,K., Binz,S.K. and Wold,M.S. (2003) Replication protein A interactions with DNA: differential binding of the core domains and analysis of the DNA interaction surface. *Biochemistry*, **42**, 12909–12918.
62. Sugiyama,T. and Kowalczykowski,S.C. (2002) Rad52 protein associates with replication protein A (RPA)-single-stranded DNA to accelerate Rad51-mediated displacement of RPA and presynaptic complex formation. *J. Biol. Chem.*, **277**, 31663–31672.
63. Sugiyama,T. and Kantake,N. (2009) Dynamic regulatory interactions of Rad51, Rad52, and replication protein-A in recombination intermediates. *J. Mol. Biol.*, **390**, 45–55.
64. Gibb,B., Ye,L.F., Kwon,Y., Niu,H., Sung,P. and Greene,E.C. (2014) Protein dynamics during presynaptic-complex assembly on individual single-stranded DNA molecules. *Nat. Struct. Mol. Biol.*, **21**, 893–900.
65. Burdova,K., Mihaljevic,B., Sturzenegger,A., Chappidi,N. and Janscak,P. (2015) The mismatch-binding factor MutS can mediate ATR activation in response to DNA double-strand breaks. *Mol. Cell*, **59**, 603–614.

Unzipping curve of the DNA hairpin substrate

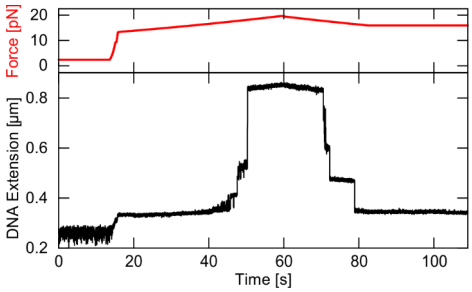

Figure S1: The DNA hairpin substrate can be mechanically unzipped

When the force applied to the DNA hairpin substrate is monotonically increased by lowering the magnets, the DNA extends in a series of sharp transitions amounting to 475 nm over the course of several seconds. The force at the final transition emanating from the intermediate state in which the hairpin is almost half open is defined is as the unzipping force, which is 18.2 pN in this case.

Conversion from DNA extension to 'basepairs-opened'

To convert DNA extensions at a given force into the corresponding number of opened base-pairs, a conversion factor was calculated for yRPA and hRPA on each construct. Force extension curves were measured for bare and RPA covered constructs. In the latter case the rehybridization was prevented conveniently by using buffer containing < 3 mM Mg^{2+} (see Main Text) for hRPA, or by annealing a short oligonucleotide. The conversion factor was then calculated by taking the difference of Freely-Jointed-Chain (FJC) fits to the force extension curves and normalization to one base-pair.

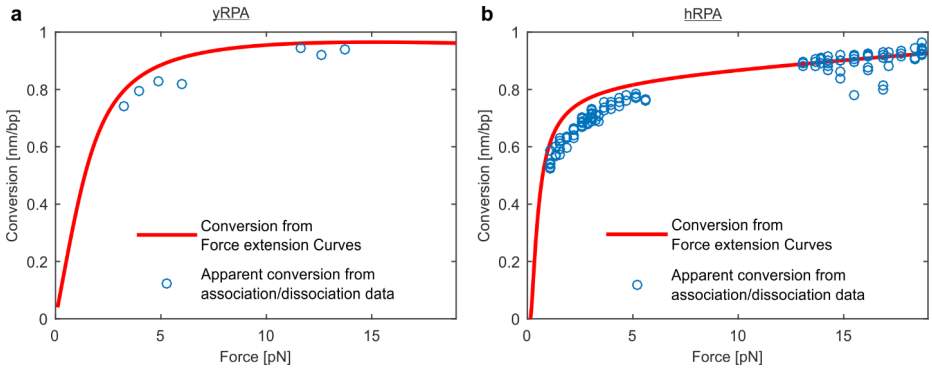

Figure S2: nm-to-bp conversion for the DNA hairpin obtained from force extension curves
The conversion estimates obtained from fitting force extension curves with FJC model for **(a)** yRPA and **(b)** hRPA are shown (red lines) together with individual apparent conversions observed in the association/dissociation data. The latter were obtained from the length difference between bare dsDNA and fully RPA coated ssDNA (or vice versa) for a given force.

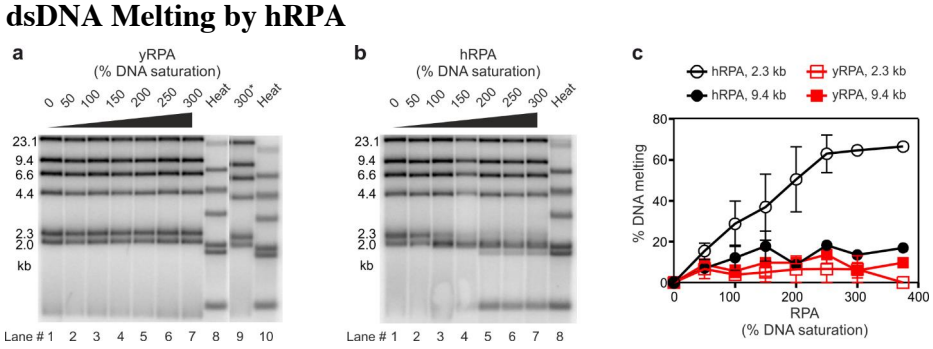

Figure S3: DNA melting capacity of human and yeast RPA
(a) yRPA does not melt dsDNA. Lambda/HindIII DNA substrate (lane 1) was incubated with various concentrations of yRPA (lanes 2-7, 50-300 % of saturation as indicated) in buffer containing 2 mM magnesium acetate for 30 minutes at 30 °C and subsequently analyzed on a 1 % agarose gel. Throughout the range of yRPA concentrations tested, no melting occurred (*cf*. heat denatured substrate in lane 8). The lack of dsDNA melting by yRPA was not due to the lower reaction temperature of experiments with yRPA (30 °C). When yeast RPA was incubated at 37 °C at 300% saturation (lane 9, *) again no DNA melting was observed. **(b)** Experiment as in panel **a,** but with various concentrations of hRPA (as indicated) incubated for 30 minutes at 37 °C. In contrast to yRPA, hRPA melts dsDNA once its concentration reaches a level sufficient for dsDNA saturation (lanes 3-7). **(c)** Quantitation for the RPA concentration dependent dsDNA melting shown in panels **b** and **c**. The 2.3 kb long dsDNA (open symbols) becomes melted to increasing extent by higher concentrations of hRPA (black), but not by yRPA (red). However, the 9.4 kb long dsDNA (filled symbols), is not melted significantly. Error bars, SEM, n=2.

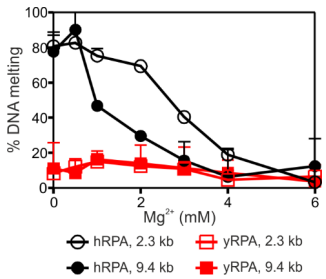

Figure S4: Quantitation of magnesium dependent dsDNA melting by RPA
Quantitation of dsDNA melting by yeast or human RPA and its dependence on the magnesium concentration (see Figure 4 of the Main Text). hRPA (black) melts both the 2.3 kb and 9.4 kb dsDNA (open and filled symbols, respectively) for magnesium concentrations below 3 mM, whereas yRPA (red) does not melt dsDNA throughout the observed range of conditions. Error bars, SEM, n=2.

Concentration dependent association of yRPA on the DNA hairpin

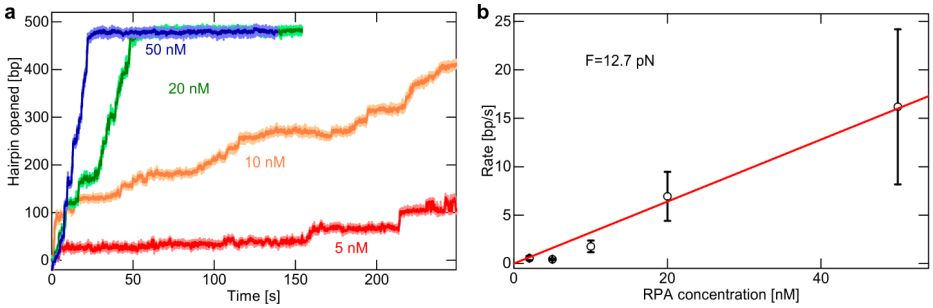

Figure S5: Concentration dependent association of yRPA on the DNA hairpin substrate
(a) Example time-traces of association at a force of 12.7 pN are shown. The rate of association is increased from 0.4 bp/s at 5 nM RPA (red curve), to 16.2 bp/s at 50 nM (blue curve). **(b)** Observed association rates (open circles) vary linearly with the concentration of RPA as indicated by the linear fit (red line). Points shown correspond to mean values of triplicate measurements with error bars representing one standard deviation.

yRPA association/dissociation kinetics in absence of Mg^{2+}

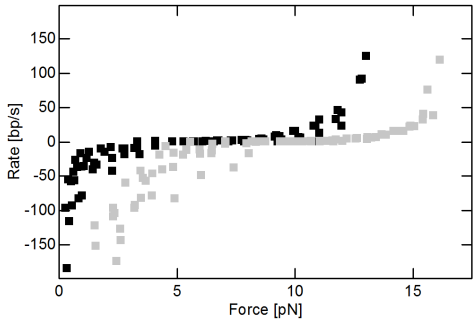

Figure S6: Salt-free association/dissociation kinetics of yRPA/
The measurement of yRPA binding kinetics were repeated in the absence of salt (black), for which we found that the entire curve is shifted towards lower forces (*cf*. the 1 mM Mg^{2+} curve in grey) while its shape is preserved. The shift is roughly consistent with the difference of 3.5 pN which we observe between the unzipping forces under these buffer conditions.

Influence of monovalent salt on dsDNA melting by hRPA

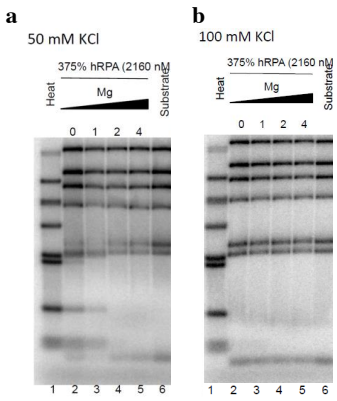

Figure S7: Effect of KCl on the DNA melting capacity of human RPA
(a) In presence of 50 mM KCl, hRPA melts dsDNA at low magnesium concentrations. Lambda/HindIII DNA substrate (lane 6) was incubated in 50 mM KCl buffer supplemented with of 0-4 mM $MgCl_2$ (lanes 2-5) for 30 minutes at 37 °C and subsequently analyzed on a 1 % agarose gel. Compared to conditions in which no monovalent salt is added, the range in which melting is observed is shifted down to 0-1 mM (lane 1 & 2, *cf*. heat denatured substrate in lane 1). **(b)** At higher concentrations of KCl the melting of hRPA is inhibited. The substrate (lane 6) was incubated in 100 mM KCl, in this case no melting was observed across the range of magnesium concentrations tested (0-4 mM $MgCl_2$, lanes 2-5, *cf*. heat denatured substrate in lane 1).

2.3.2 DNA2 drives processing and restart of reversed replication forks in human cells

Saravanabhavan Thangavel, Matteo Berti, Maryna Levikova, **Cosimo Pinto**, Shivasankari Gomathinayagham, Marko Vujanovic, Ralph Zellweger, Hayley Moore, Eu Han Lee, Eric A. Hendrickson, Petr Cejka, Sheila Stewart, Massimo Lopes and Alessandro Vindigni

The article was published in the J Cell Biol. ***2015 Mar 2;208(5):545-62.***

My contributions to this publication was producing recombinant hDNA2 and performing the biochemical assays shown in Figure 8 E and I; Supplementary Figure S4 D, E, H.

THE JOURNAL OF CELL BIOLOGY

Published March 2, 2015

JCB: Article

DNA2 drives processing and restart of reversed replication forks in human cells

Saravanabhavan Thangavel,[1]* Matteo Berti,[1]* Maryna Levikova,[2] Cosimo Pinto,[2] Shivasankari Gomathinayagam,[1] Marko Vujanovic,[2] Ralph Zellweger,[2] Hayley Moore,[3] Eu Han Lee,[4] Eric A. Hendrickson,[4] Petr Cejka,[2] Sheila Stewart,[3] Massimo Lopes,[2] and Alessandro Vindigni[1]

[1]Department of Biochemistry and Molecular Biology, Saint Louis University School of Medicine, St. Louis, MO 63104
[2]Institute of Molecular Cancer Research, University of Zurich, CH-8057 Zurich, Switzerland
[3]Department of Cell Biology and Physiology, Washington University School of Medicine, St. Louis, MO 63110
[4]Department of Biochemistry, Molecular Biology, and Biophysics, University of Minnesota, Minneapolis, MN 55455

Accurate processing of stalled or damaged DNA replication forks is paramount to genomic integrity and recent work points to replication fork reversal and restart as a central mechanism to ensuring high-fidelity DNA replication. Here, we identify a novel DNA2- and WRN-dependent mechanism of reversed replication fork processing and restart after prolonged genotoxic stress. The human DNA2 nuclease and WRN ATPase activities functionally interact to degrade reversed replication forks with a 5′-to-3′ polarity and promote replication restart, thus preventing aberrant processing of unresolved replication intermediates. Unexpectedly, EXO1, MRE11, and CtIP are not involved in the same mechanism of reversed fork processing, whereas human RECQ1 limits DNA2 activity by preventing extensive nascent strand degradation. RAD51 depletion antagonizes this mechanism, presumably by preventing reversed fork formation. These studies define a new mechanism for maintaining genome integrity tightly controlled by specific nucleolytic activities and central homologous recombination factors.

Introduction

The accurate replication of our genome is an essential requirement for the high-fidelity transmission of genetic information to daughter cells. DNA replication forks are constantly challenged and arrested by DNA lesions, induced by endogenous and exogenous agents, and by a diverse range of intrinsic replication fork obstacles, such as transcribing RNA polymerases, unusual DNA structures or tightly bound protein–DNA complexes (Carr and Lambert, 2013). An emerging model of how stalled or damaged forks are processed is that replication forks can reverse to aid repair of the damage (Atkinson and McGlynn, 2009; Ray Chaudhuri et al., 2012; Berti et al., 2013). This model implies significant remodeling of replication fork structures into four-way junctions and the molecular determinants required for reversed fork processing and restart are just beginning to be elucidated. The first evidence that supports the physiological relevance of this DNA transaction during replication stress in human cells arose from studies with DNA topoisomerase I (TOP1) inhibitors (Ray Chaudhuri et al., 2012). Additional studies established that the human RECQ1 helicase promotes the restart of replication forks that have reversed upon TOP1 inhibition by virtue of its ATPase and branch migration activities (Berti et al., 2013). These observations were recently extended to show that the RECQ1 mechanism of reversed fork restart is a more general response to a wide variety of replication challenges (Zellweger et al., 2015). Nonetheless, new lines of evidence point to alternative mechanisms and factors that might mediate either formation or processing of reversed replication forks (Bétous et al., 2012; Gari et al., 2008). These putative mechanisms likely include nucleases that are capable of processing stalled replication intermediates upon genotoxic stress (Cotta-Ramusino et al., 2005; Schlacher et al., 2011; Hu et al., 2012; Ying et al., 2012).

Here, we investigate the contribution of the human DNA2 nuclease/helicase in reversed fork processing. DNA2 is a highly conserved nuclease/helicase initially identified in *Saccharomyces cerevisiae* screening for mutants deficient in DNA replication (Kuo et al., 1983; Budd and Campbell, 1995). Yeast Dna2 plays

*S. Thangavel and M. Berti contributed equally to this paper.

Correspondence to Alessandro Vindigni: avindign@slu.edu

Abbreviations used in this paper: CPT, camptothecin; DSB, double-strand DNA break; EXO1, human exonuclease I; HDR, Homology directed repair; HR, homologous recombination; HU, hydroxyurea; MMC, mitomycin C; MRN, MRE11-RAD50-NBS1; TOP1, DNA topoisomerase I.

Supplemental Material can be found at:
/content/suppl/2015/02/26/jcb.201406100.DC1.html

The Rockefeller University Press $30.00
J. Cell Biol. Vol. 208 No. 5 545–562
www.jcb.org/cgi/doi/10.1083/jcb.201406100

Published March 2, 2015

an essential role in Okazaki fragment maturation during lagging strand DNA replication (Budd and Campbell, 1997; Bae et al., 2001; Ayyagari et al., 2003). However, increasing evidence suggests that DNA2 has important—albeit yet undefined—roles in DNA replication stress response and DNA repair, which go beyond its postulated role in Okazaki fragment processing (Duxin et al., 2012; Karanja et al., 2012; Peng et al., 2012). The notion that DNA2 is important for DNA replication is strengthened by the observation that DNA2 forms a complex with various replication core components, including the replisome protein And-1 (Wawrousek et al., 2010; Duxin et al., 2012). Moreover, human DNA2 seems to play a partially redundant role with human exonuclease I (EXO1) in replication-coupled repair (Karanja et al., 2012), whereas a recent study in *S. pombe* suggested that the nuclease activity of DNA2 is required to prevent stalled forks from reversing upon HU treatment (Hu et al., 2012).

DNA2 also has an independent function in dsDNA break repair. Two distinct pathways act redundantly to mediate processive DSB resection downstream from the MRE11-RAD50-NBS1 (MRN) and CtIP factors in eukaryotic cells: one requires DNA2 and the other EXO1 (Gravel et al., 2008; Mimitou and Symington, 2008; Zhu et al., 2008; Nicolette et al., 2010). Specifically, DNA2 and EXO1 resect the 5′ ends of double-strand DNA breaks (DSBs) to generate 3′ single-stranded overhangs, which are essential to initiate homologous recombination. In yeast, DNA2-dependent dsDNA-end resection reaction requires the Sgs1 helicase to unwind the DNA from the break (Zhu et al., 2008; Cejka et al., 2010; Niu et al., 2010). This mechanism appears to be largely conserved in mammalian cells where DNA2 cooperates with the human BLM helicase to resect dsDNA ends in vitro (Nimonkar et al., 2011). However, mammalian cells possess five human RecQ homologues (RECQ1, RECQ4, RECQ5, BLM, and WRN) and WRN can also assist DNA2-dependent end resection, suggesting that BLM might not be the sole RecQ homologue required for this process (Liao et al., 2008; Sturzenegger et al., 2014). The ability of DNA2 and EXO1 to process dsDNA ends might also be relevant in the context of DNA replication to prevent the accumulation of replication-associated DSBs by promoting homologous recombination (HR) repair (Peng et al., 2012). Alternatively, these nucleases might be involved in the recovery of replication fork blockage by processing specific stalled replication fork structures.

This work uncovers a new DNA2- and WRN-dependent mechanism that mammalian cells use to process replication forks that have reversed as a result of replication inhibition. Importantly, it also shows that this mechanism is tightly regulated by human RECQ1 and the HR factor RAD51. Our observations shed light on a novel pathway for the suppression of chromosomal instability in mammalian cells and provide important new insight into the mechanisms of replication stress response associated with chemotherapeutic drug damage.

Results

DNA2 is required for stalled fork processing and restart

To begin elucidating the role of human DNA2 during replication stress, we monitored replication perturbation by genome-wide single-molecule DNA fiber replication assays. We pulse-labeled human osteosarcoma (U-2 OS) cells with the thymidine analogue CldU for 20 min, followed by a 60-min exposure to a selected genotoxic agent during the CldU labeling period, and by labeling with the second thymidine analogue, IdU, for an additional 40 min after removal of the genotoxic drug. We found that DNA2 plays an important role in restarting replication forks after treatment with the ribonucleotide reductase inhibitor hydroxyurea (HU), the topoisomerase I inhibitor camptothecin (CPT), and the interstrand cross-linking agent mitomycin C (MMC) (Fig. 1 A). In addition, DNA2 depletion increased the percentage of origin firing, but not of fork termination events (Fig. S1 A). Genetic knockdown–rescue experiments confirmed that complementation in DNA2-depleted U-2 OS cells with siRNA-resistant WT DNA2 abrogated the effect of DNA2 depletion on replication fork restart upon HU treatment. Moreover, expression of the nuclease-deficient DNA2 mutant D294A in DNA2-depleted cells revealed that the nuclease activity of DNA2 was essential for its role in replication fork restart (Fig. 1 B and Fig. S1 B).

We next measured whether DNA2 uses its nuclease activity to process stalled replication intermediates by monitoring the integrity of the newly synthesized DNA after HU treatment. To this purpose, we changed the DNA labeling scheme. We first pulsed U-2 OS cells with IdU for 45 min, and then varied the exposure time to HU from 0 to 8 h. The mean length of the IdU tracts progressively decreased during HU treatment from 18.2 µm (0 h) to 12.0 µm (8 h; Fig. 1 C). However, shRNA-mediated DNA2 depletion largely prevented IdU tract shortening, confirming that DNA2 is responsible for the observed nascent strand degradation (Fig. 1 D). Double-labeling experiments confirmed that the observed nascent tract shortening is indeed caused by the DNA2-dependent processing of ongoing replication forks and that this degradation is important to mediate efficient replication fork restart upon prolonged HU treatment (Fig. 1 E). Clonogenic analysis of U-2 OS cells treated with the same HU concentration used for the DNA fiber experiments showed a significantly reduced cell survival upon DNA2 depletion, indicating that the DNA2-dependent processing of stalled replication intermediates is critical for recovery from replication fork blockage (Fig. 2 A). The results obtained with the shRNA DNA2-depleted U-2 OS cells were validated using a new conditional knockout human colorectal carcinoma cell line (HCT116) where addition of tamoxifen to the culture medium led to DNA2-null cells. Analysis of the mean tract lengths confirmed that DNA2 knockout in HCT116 cells abrogates the prominent degradation observed upon HU treatment (Fig. 2 B). Collectively, these results indicate that human DNA2 degrades nascent strands at stalled replication forks to facilitate fork restart and promote viability after genotoxic stress induction.

RECQ1 regulates the fork processing activity of DNA2

On the basis of the recent discovery that RECQ1 is required to restart replication forks that have reversed upon genotoxic stress induction (Berti et al., 2013), we investigated whether RECQ1 regulates the fork processing activity of DNA2. Nascent IdU

Published March 2, 2015

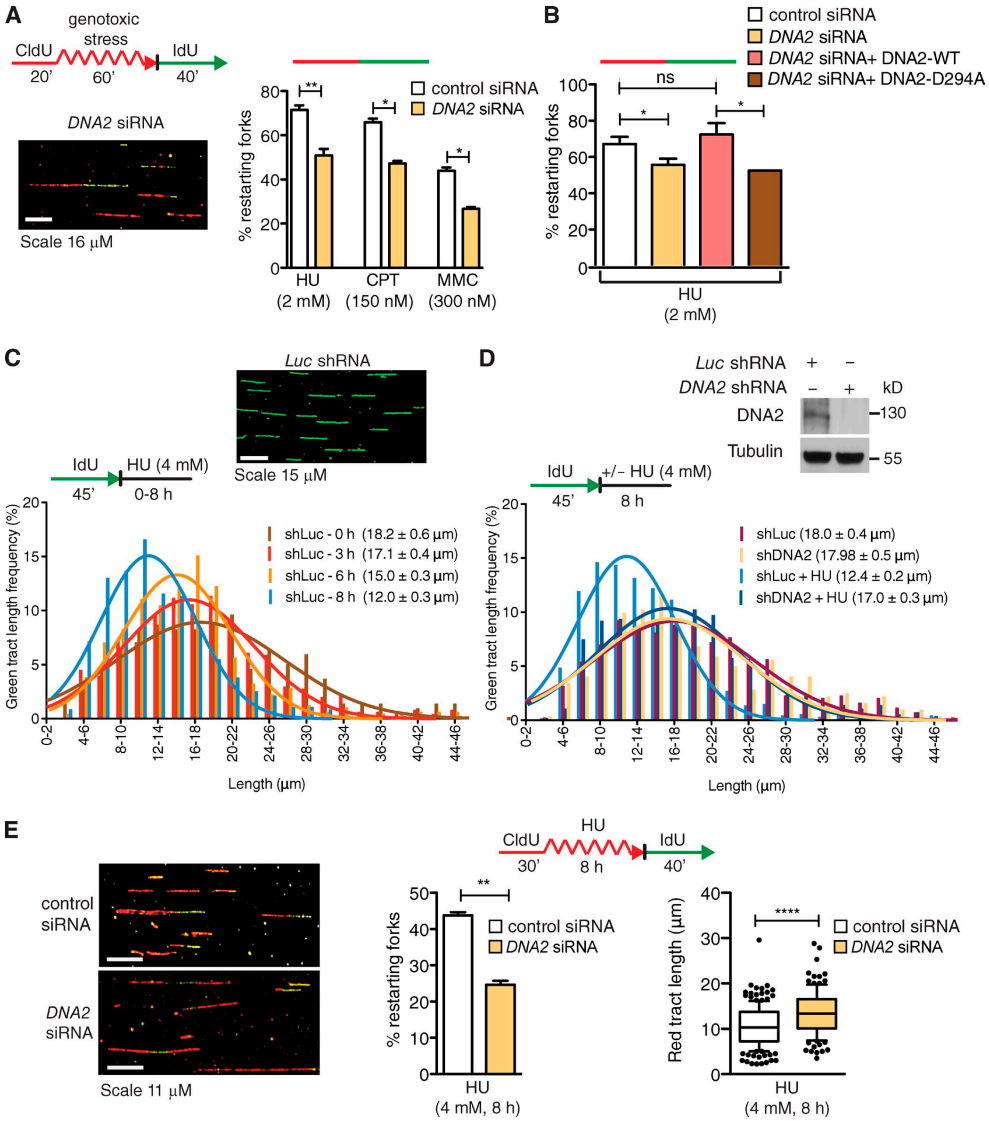

Figure 1. **DNA2 is required for replication fork restart and stalled fork processing upon genotoxic stress.** (A) Schematic of DNA fiber tract analysis. U-2 OS cells were transfected with control siRNA or *DNA2* siRNA before CldU or IdU labeling. Red tracts, CldU; curved red tracts, CldU with genotoxic agents (HU or CPT or MMC); green tracts, IdU. (bottom) Representative DNA fiber image. (right) quantification of red-green contiguous tracts (restarting forks). Mean shown, $n = 3$. Error bars, standard error. ns, not significant; *, $P < 0.05$; **, $P < 0.01$ (paired *t* test). (B) Quantification of restarting forks in DNA2-depleted cells expressing DNA-WT or DNA2-D294A. ns, not significant; *, $P < 0.05$ (paired Student's *t* test). (C, top) Representative DNA fiber image. (bottom) Representative IdU tract length distributions in Luc-depleted cells during different exposure time to HU (out of 3 repeats; $n \geq 300$ tracts scored for each dataset). Mean tract lengths are indicated in parentheses. (D) Top, DNA2 expression after shRNA knockdown. Bottom, representative IdU tracts in DNA2-depleted U-2 OS cells in the presence or absence of HU (out of 2 repeats; $n \geq 700$ scored for each dataset). (E, left) Representative DNA fiber images. (middle) Quantification of red-green contiguous tracts (restarting forks) after 8 h of HU. Mean shown, $n = 3$. Error bars, standard error. **, $P < 0.01$ (paired Student's *t* test). (right) Statistical analysis of CldU tracts detected within contiguous red-green tracts. Whiskers the 10th and 90th percentiles. ****, $P < 0.0001$ (Mann-Whitney test).

Published March 2, 2015

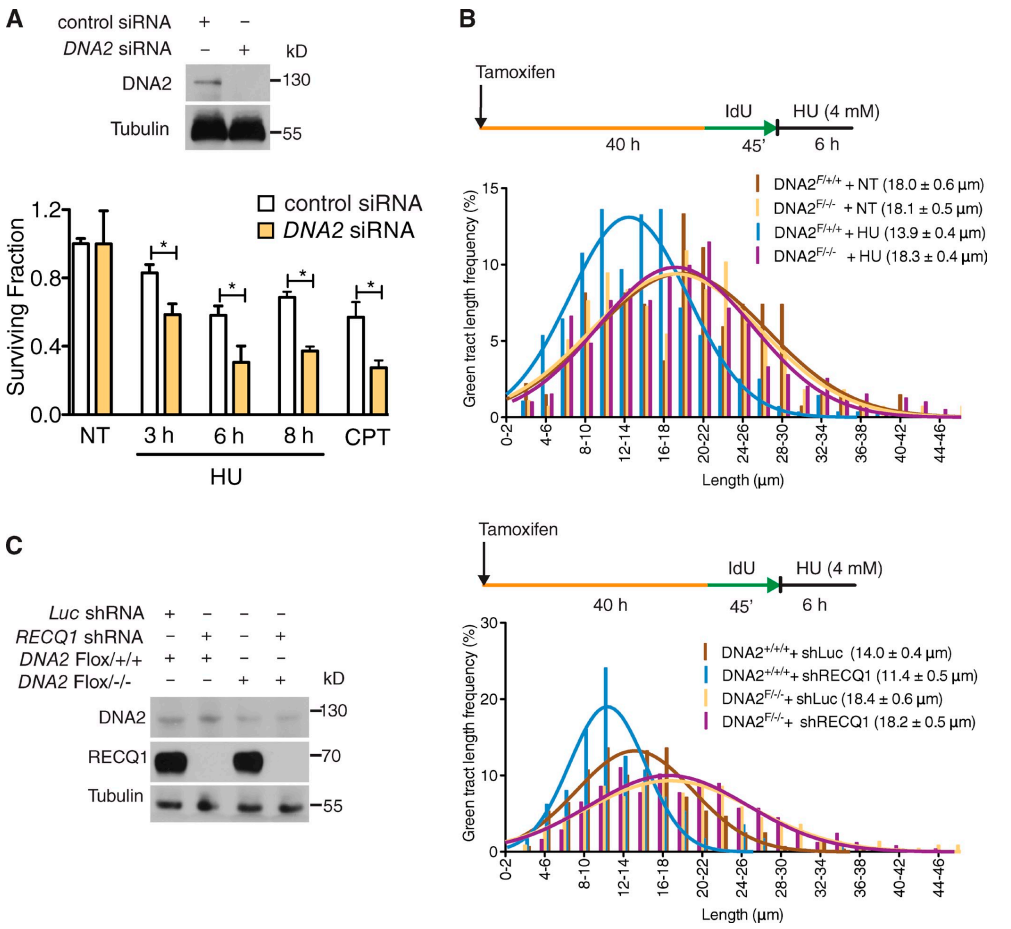

Figure 2. **DNA2 processes stalled replication forks.** (A, top) DNA2 expression after siRNA knockdown. (bottom) Colony-forming assays in control and DNA2-depleted U-2 OS cells treated with 4 mM HU for the indicated time. (B) Representative IdU tracts in DNA2 conditional knockout HCT116 cells (out of two repeats). Tamoxifen was added to generate conditional knockout cells (see Materials and methods). (C, left) Expression of DNA2 and RECQ1 in tamoxifen-treated HCT116 cells. Right, representative IdU tracts in DNA2 conditional knockout HCT116 cells depleted for Luc or RECQ1 (out of three repeats). $n \geq 300$ tracts scored for each dataset shown in B and C.

tracts were substantially shorter in RECQ1-depleted cells compared with control when replication forks were stalled with HU (after 8 h of HU treatment, the mean tract lengths were 7.9 and 12.0 µm, respectively; $P < 0.0001$; Fig. 3, A and B). In agreement with results from luciferase-depleted cells, DNA2 was also responsible for the nascent strand degradation phenotype observed in RECQ1-deficient U-2 OS cells (Fig. 3 C). Analogous results were obtained using the conditional DNA2 knockout HCT116 cell line (Fig. 2 C). In addition, we confirmed that the DNA2-dependent nascent strand degradation observed in the absence of RECQ1 is not limited to a specific replication inhibitor by replacing HU with CPT or MMC (Fig. 3, D and E).

Genetic knockdown–rescue experiments confirmed that complementation in RECQ1-depleted U-2 OS cells with shRNA-resistant WT RECQ1 abrogates the effect of RECQ1 depletion on replication fork processing upon HU treatment (Fig. 3 F). Interestingly, expression of the ATPase-deficient RECQ1 mutant K119R in RECQ1-depleted cells also abrogated the effect of RECQ1 depletion indicating that the ATPase activity of RECQ1 was not required for its role in protecting stalled forks from DNA2-dependent degradation (Fig. 3 F). These results point to an additional role of RECQ1 in protecting replication forks from extensive DNA2-dependent degradation, which is independent of RECQ1 ATPase activity.

Published March 2, 2015

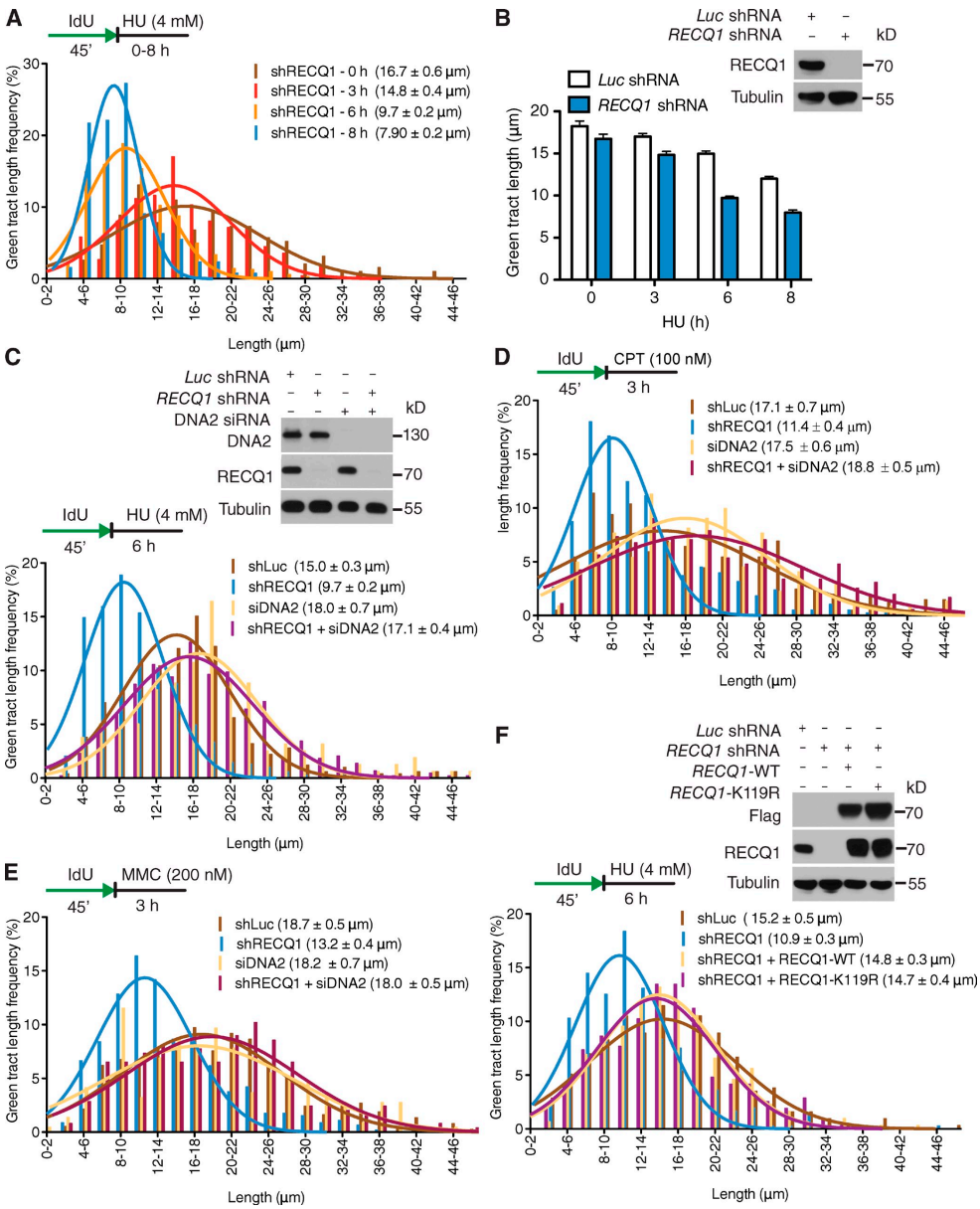

Figure 3. **RECQ1 regulates the DNA2-dependent degradation of stalled forks.** (A) Representative IdU tracts in RECQ1-depleted U-2 OS cells during different exposure time to HU (out of 2 repeats; $n \geq 350$ tracts scored for each dataset). (B) Bar graph represents the mean values of each time point from Figs. 1 C and 2 A. (top) RECQ1 expression after shRNA knockdown. (C, D, and E) Representative IdU tracts in RECQ1-, DNA2-, or RECQ1/DNA2-codepleted U-2 OS cells in the presence of HU (C), CPT (D), and MMC (E; out of 2 repeats; $n \geq 300$ tracts scored for each dataset).(top) RECQ1 and DNA2 expression after shRNA or siRNA knockdown. (F) Representative IdU tracts in RECQ1-depleted U-2 OS cells complemented with shRNA-resistant WT RECQ1 (WT) or ATPase-deficient (K119R) RECQ1 (out of 2 repeats; $n \geq 325$ tracts scored for each dataset). (top) Expression of Flag-tagged RECQ1-WT and RECQ1-K119R in RECQ1-depleted cells.

Published March 2, 2015

DNA2 function in stalled fork processing is distinct from EXO1, Mre11, and CtIP

Next, we tested whether other nucleases share a function similar to DNA2 in stalled fork processing. To address this point, we depleted Mre11, EXO1, and CtIP in U-2 OS cells with siRNA-mediated technologies. We found that none of these nucleases share the same phenotype of DNA2 in RECQ1-proficient cells (Fig. 4 A). Furthermore, depletion of these nucleases had only a marginal effect on the rescue of the prominent nascent strand degradation phenotype observed in the absence of RECQ1, indicating that DNA2 has a unique function in reversed fork processing that is not shared by these human nucleases (Fig. 4, B–D). MUS81 is another structure-specific nuclease that plays a critical role in replication fork rescue by converting stalled replication forks into DNA DSBs that can be processed by Homology Directed Repair (HDR) (Hanada et al., 2007; Franchitto et al., 2008). This raised the possibility that the DNA2-dependent degradation originated from the processing of MUS81-dependent DSBs. However, MUS81 depletion did not prevent nascent strand degradation, indicating that DNA2 is not processing stalled replication intermediates that are cleaved by MUS81 (Fig. 4 E).

DNA2 and WRN act together to process stalled replication forks

DNA2-dependent dsDNA-end resection needs the support of a RecQ helicase to unwind the DNA from the break (Cejka et al., 2010; Niu et al., 2010; Nimonkar et al., 2011). To determine the identity of the helicase that acts in conjunction with DNA2 in stalled fork processing, we measured the extent of nascent strand degradation in BLM-, WRN-, and RECQ4-depleted U-2 OS cells. Our DNA fiber analysis showed that WRN depletion mimicked the effect of DNA2-depletion, completely abrogating the prominent nascent strand degradation phenotype observed in RECQ1-depleted U-2 OS cells (Fig. 5 A). The same results were confirmed using WRN and DNA2 codepleted cells, suggesting that DNA2 and WRN are epistatic in nucleolytic processing of stalled forks (Fig. S1 C). The partial nascent strand degradation observed in RECQ1-proficient U-2 OS cells was also abrogated by WRN depletion (Fig. S1 D). Conversely, BLM depletion had only a marginal effect on the nascent strand degradation phenotype observed in RECQ1-depleted cells, whereas RECQ4 depletion had no effect (Fig. S2, A and B). Thus, the WRN helicase plays a prominent role in assisting DNA2-dependent degradation of stalled replication forks.

We next compared the percentage of restarting replication forks in DNA2-depleted, WRN-depleted, and DNA2/WRN-codepleted cells. WRN depletion leads to a decrease in restarting forks (69 to 50%; P = 0.0068). These results are almost identical to those obtained with the DNA2-depleted or DNA2/WRN-codepleted cells, implying that WRN and DNA2 are epistatic also in the restart process (Fig. 5 B). The notion that DNA2 and WRN functionally interact to process stalled replication intermediates is further supported by our observation that the two proteins form a complex both in the presence and absence of replication stress (Fig. 5 C). Of note, RECQ1 is not part of the WRN:DNA2 complex. Collectively, these results suggest that DNA2 cooperates with WRN to promote nascent strand processing and fork restart after HU treatment.

The nuclease activity of DNA2 and the ATPase activity of WRN are essential to process stalled replication forks

DNA2 is characterized by an N-terminal nuclease domain and by a C-terminal helicase domain, but the function of its helicase activity is still debated (Masuda-Sasa et al., 2006). To assess the roles of these two activities in stalled fork processing, we performed genetic knockdown-rescue experiments where we depleted DNA2 and then attempted to rescue fork processing by expressing a Flag-tagged siRNA resistant WT DNA2 control, nuclease-deficient DNA2-D294A, or ATPase-deficient DNA2-K671E. All the experiments were performed in RECQ1-depleted cells, where the effect of DNA2 is more apparent. DNA fiber analysis showed that complementation with nuclease-deficient DNA2 prevents fork processing, whereas complementation with WT or ATPase-deficient DNA2 leads to the same fork processing phenotype observed in DNA2-proficient cells (Fig. 5 D and Fig. S2 C). Therefore, the nuclease, but not the ATPase activity of DNA2, is necessary for fork processing.

Next, we used a Werner Syndrome (WS) fibroblast cell line (AG11395) expressing missense mutant forms of WRN, which inactivate either the exonuclease (WRN-E84A) or the ATPase (K577M) activity of WRN (Pirzio et al., 2008). The ATPase, but not the nuclease activity of WRN, was important for fork processing (Fig. 5 E and Fig. S2 D). These findings were validated by genetic knockdown-rescue experiments where we complemented WRN-depleted U-2 OS cells either with an shRNA resistant WT WRN control or the ATPase-deficient WRN-K577M mutant and found that complementation with the ATPase-deficient mutant prevented fork processing (Fig. S2, E and F). Collectively, these results show that human DNA2 needs the support of the ATPase activity of WRN to promote degradation of the nascent DNA strands.

DNA2 processes reversed replication forks

To gain insight into the actual replication structures processed by DNA2, we inspected the fine architecture of the replication intermediates using a combination of in vivo psoralen cross-linking and EM (Neelsen et al., 2014). Our analysis showed a substantial fraction of reversed replication forks (~24% of molecules analyzed) in control U-2 OS cells treated with 4 mM HU. RECQ1-depletion, and to an even greater extent DNA2-depletion, resulted in a higher frequency of fork reversal events (~30 and 40%, respectively) compared with HU-treated cells. Co-depletion of RECQ1 and DNA2 further increased the frequency of reversed forks (~50%), suggesting that RECQ1 and DNA2 are involved into two distinct mechanisms of reversed fork processing. Interestingly, RECQ1 and/or DNA2 depletion also led to a significant amount of fork reversal events in unperturbed U-2 OS cells (Fig. 6, A and B). WRN-depletion phenocopied DNA2-depletion in terms of reversed fork accumulation, both the presence and in the absence of HU. Moreover, DNA2/

Published March 2, 2015

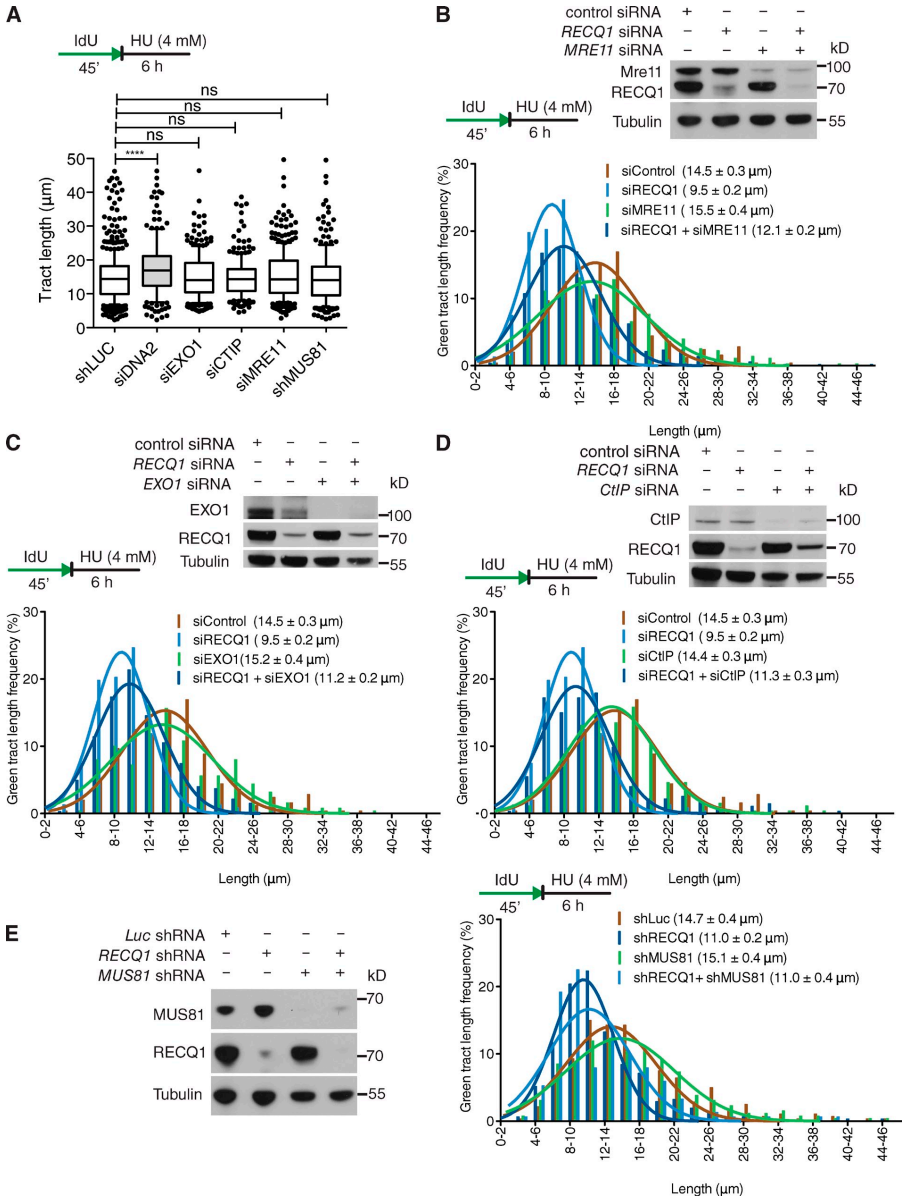

Figure 4. **EXO1, MRE11, CtIP, and MUS81 depletion does not affect stalled fork processing.** (A) Statistical analysis of IdU tracts from U-2 OS cells depleted for the indicated proteins in the presence of 4 mM HU. (B) Representative IdU tracts in control, RECQ1-, MRE11-, or RECQ1/MRE11-codepleted U-2 OS cells (out of 2 repeats). (top) Expression of RECQ1 and MRE11 after siRNA knockdown. (C) Representative IdU tracts in control, RECQ1-, EXO1-, or RECQ1/EXO1-codepleted U-2 OS cells (out of 2 repeats). (top) Expression of RECQ1 and EXO1 after siRNA knockdown. (D) Representative IdU tracts in control, RECQ1-, CtIP-, or RECQ1/CtIP-codepleted U-2 OS cells (out of 2 repeats). (top) Expression of RECQ1 and CtIP after siRNA knockdown. (E) Representative IdU tracts in Luc-, RECQ1-, MUS81-, or RECQ1/MUS81-codepleted U-2 OS cells in the presence of HU (out of 2 repeats). (left) Expression of RECQ1 and MUS81 after shRNA knockdown. $n \geq 300$ tracts scored for each dataset shown in A–E.

Published March 2, 2015

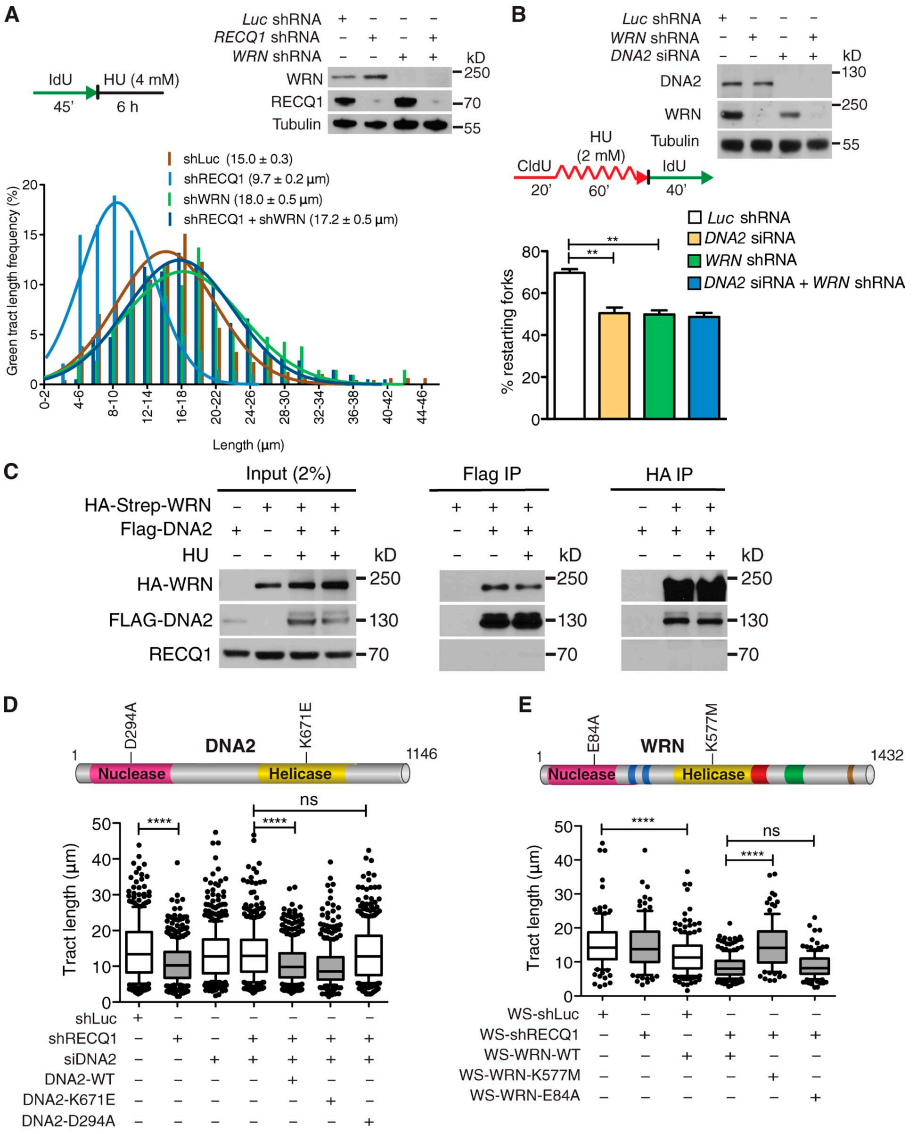

Figure 5. **DNA2 and WRN are epistatic in stalled fork processing and replication restart.** (A) Representative IdU tracts in RECQ1-, WRN-, or RECQ1/WRN-codepleted U-2 OS cells (out of 2 repeats; $n \geq 300$ tracts scored for each dataset). (top) RECQ1 and WRN expression after shRNA knockdown. (B) Quantification of restarting forks in DNA2-, WRN-, or DNA2/WRN-codepleted cells. Mean shown, $n = 3$. Error bars, standard error. *, $P < 0.05$; **, $P < 0.01$ (paired t test). (top) Expression of WRN and DNA2 after shRNA knockdown. (C) Co-IP experiments in HEK293T cells transfected with empty vectors, Flag-DNA2, or Strep-HA-WRN. Cells were treated with 4 mM HU (3 h) where indicated. Whole-cell extracts were analyzed before (input) and after IP. (D) Statistical analysis of IdU tracts from RECQ1/DNA2-codepleted U-2 OS cells complemented with WT, ATPase-deficient (K671E), or nuclease-deficient (D294A) DNA2, when indicated. (E) Statistical analysis of IdU tracts from RECQ1-depleted WS cells complemented with WT, ATPase-deficient (K577M), or nuclease-deficient (E84A) WRN. Whiskers in D and E indicate the 10th and 90th percentiles. ns, not significant; ****, $P < 0.0001$ (Mann-Whitney test). $n \geq 300$ tracts scored for each dataset shown in D and E.

Published March 2, 2015

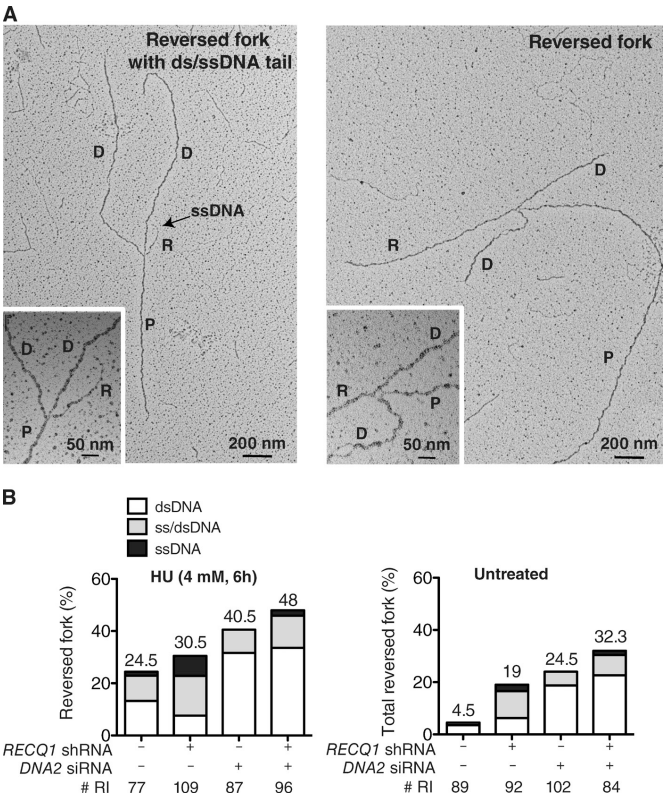

Figure 6. **DNA2 resects reversed replication forks.** (A) Electron micrograph of a partially single-stranded (left) and entirely double-stranded (right) reversed fork observed on genomic DNA upon HU-treatment. The black arrow points to the ssDNA region on the reversed arm. Inset, magnified four-way junction at the reversed replication fork. D, Daughter strand; P, Parental strand; R, Reversed arm. (B) Frequency of fork reversal and ssDNA composition of the reversed arms in RECQ1- or DNA2-depleted U-2 OS cells treated with HU (left) or in unperturbed conditions (right). The percentage values are indicated on the top of the bar. "# RI" indicates the number of analyzed replication intermediates. Data in B are reproduced with very similar results in at least one independent experiment.

WRN-codepletion did not cause a further increase in reversed fork frequency, thus supporting our conclusion that DNA2 and WRN work together in reversed fork processing (Fig. S3 A).

Next, we evaluated the single-strand composition of the regressed arms. To measure ssDNA, we carefully inspected the frequency and length of ssDNA regions on the regressed arms by detecting local difference in filament thickness. DNA2 depletion led to a higher frequency of reversed forks with a dsDNA arm—and a corresponding decrease of partially or entirely single-stranded reversed forks—in both RECQ1-proficient and deficient cells (Fig. 6). Thus, DNA2-mediated resection is directed to completely or partially digest one strand of the reversed arm leading to reversed forks that are either entirely single stranded or have a protruding ssDNA tail. However, prolonged stalling by HU was associated with accumulation of postreplicative ssDNA gaps on replicated duplexes, which was maximal in RECQ1-depleted cells and suppressed by DNA2 depletion (Fig. S3, B and C). Consequently, ssDNA gaps may reflect additional activity of the same nucleolytic apparatus along the postreplicated duplexes or restart of partially resected reversed forks.

As an alternative readout for DNA2-dependent resection, we examined the phosphorylation status of RPA and the checkpoint kinase Chk1 (Zeman and Cimprich, 2014). DNA2 depletion caused a reduction in RPA and Chk1 phosphorylation in both RECQ1-proficient and RECQ1-deficient U-2 OS cells, suggesting that the DNA2-dependent resection of nascent strands might also contribute to checkpoint activation (Fig. S3 D).

RAD51 promotes DNA2-dependent degradation of reversed replication forks

The central recombinase factor RAD51 is directly implicated in reversed fork formation upon genotoxic stress (Zellweger et al., 2015). Thus, we investigated whether RAD51 depletion may affect the reversed fork processing activity of DNA2. We found that RAD51 knockdown largely prevents DNA2 nucleolytic processing both in RECQ1 proficient and RECQ1-deficient cells (Fig. 7 A). Genetic knockdown–rescue experiments confirmed that expression of exogenous RAD51 in RAD51-depleted U-2 OS cells restored the fork processing phenotype (Fig. 7 B). These results indicate that DNA2-dependent nucleolytic

Published March 2, 2015

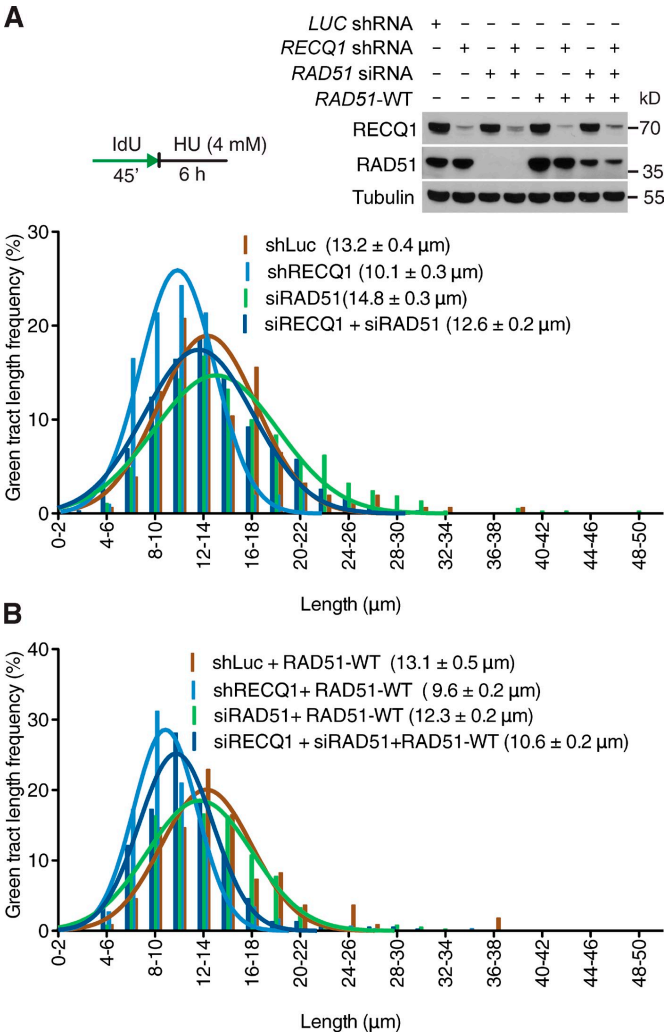

Figure 7. **RAD51 promotes DNA2-depedent degradation of reversed replication forks.** (A) Representative IdU tracts in RECQ1-, RAD51-, or RECQ1/RAD51-codepleted U-2 OS cells (out of 2 repeats). Above, RECQ1 and RAD51 expression after siRNA knockdown RAD51-WT are U-2 OS cells stably expressing siRNA resistant exogenous RAD51. (B) Representative IdU tracts in U-2 OS cells expressing exogenous RAD51 (out of 2 repeats). $n \geq 300$ tracts scored for each dataset shown in A and B.

processing is specifically targeted to reversed fork structures because it is not detected in a genetic background that prevents reversed fork formation—i.e., RAD51 knockdown.

DNA2 preferentially degrades reversed fork structures with a 5′-to-3′ polarity

The notion that DNA2 end resection has a preferential polarity in vivo is consistent with biochemical studies showing that even though DNA2 has the intrinsic capacity to degrade both 5′- and 3′-terminated ssDNA, RPA enforces a primarily 5′-to-3′ end-resection bias (Cejka et al., 2010; Niu et al., 2010; Nimonkar et al., 2011). Thus, we set up new biochemical assays to test whether human DNA2 prefers four-way junction substrates—i.e., reversed replication forks—versus linear DNA duplexes and whether it degrades these substrates with a 5′-to-3′ polarity in the presence of RPA (Fig. 8, A and B). The sequences of the four arms of the four-way junction substrates are mutually heterologous to prevent four-way junction branch migration. DNA2-degraded four-way junction substrates more efficiently than linear dsDNA duplexes, with 20 nM DNA2 required to degrade ∼60% of the four-way junction substrates versus only ∼30% of the linear duplex (Fig. 8 C). Importantly, supplementing the reaction with RPA greatly stimulated the degradation activity of human DNA2 (Fig. 8 D and Fig. S4 A). Additional

Published March 2, 2015

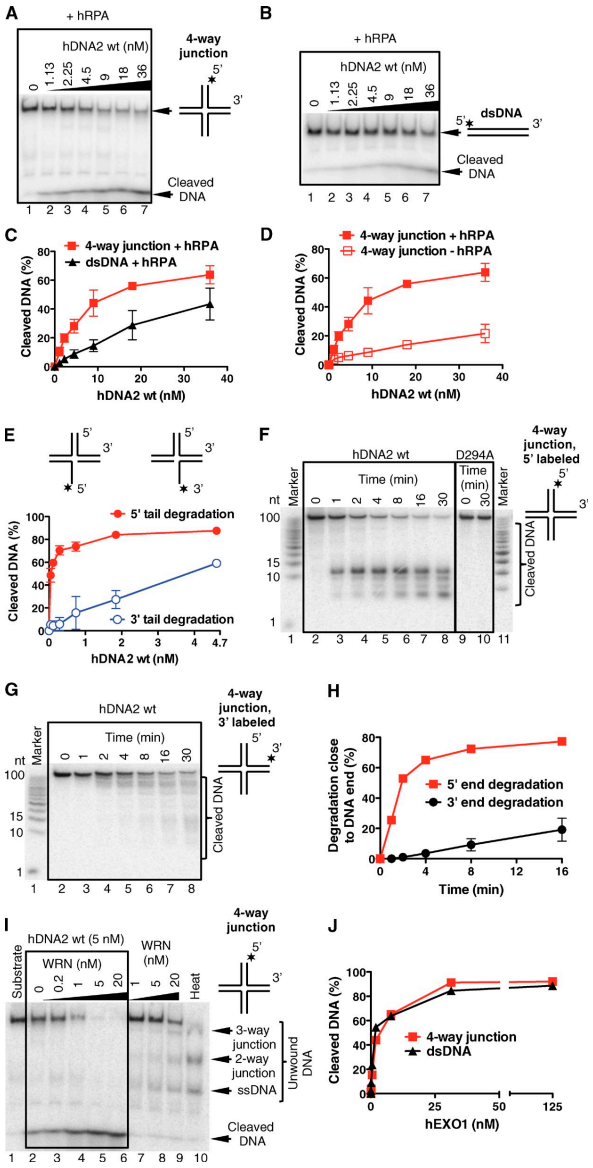

Figure 8. **Human DNA2 preferentially degrades branched DNA in a 5′-3′ direction in reactions stimulated by WRN.** (A) Degradation of a four-way junction by human DNA2 (hDNA2) in the presence of hRPA (native 6% polyacrylamide gel) (B) Experiment as in A, but with dsDNA. (C) Quantitation of data from A and B. Averages shown ± SEM; *n* = 2. (D) DNA degradation is stimulated by hRPA. The data points from +hRPA condition are the same as in C. Averages shown ± SEM; *n* = 2. (E) Quantitation of degradation of a 3′ or 5′ ssDNA-tailed three-way junction by hDNA2. The reactions were performed in 3 mM magnesium acetate and 22.3 nM hRPA. Averages shown ± SEM; *n* = 2. (F) Kinetics of degradation of a four-way junction by hDNA2 (9 nM) in the presence of hRPA (denaturing 20% polyacrylamide gel). The substrate was labeled at the 5′ end (*). D294A, nuclease-dead variant of hDNA2. (G) Experiment as in F, but using a four-way junction labeled at the 3′ end. (H) Quantitation of DNA cleavage near (less than 15 nt) a 5′ or 3′ DNA end from experiments of F and G. Averages shown ± SEM; *n* = 2. (I) WRN and hDNA2 degrade four-way junction DNA in a synergistic manner. Reactions with indicated hDNA2 and/or WRN concentrations and 65 nM hRPA were analyzed on a 6% native polyacrylamide gel. Heat, partially heated DNA substrate indicating the positions of DNA unwinding intermediates. (J) Quantitation of four-way junction and dsDNA degradation by human EXO1 (hEXO1). Averages shown ± SEM; *n* = 2.

experiments using either 5′-end or 3′-end ^{32}P-labeled four-way junctions confirmed that human DNA2 had a strong 5′-to-3′ bias in end resection in the presence of RPA (Fig. 8, E–H; and Fig. S4, B and C). Catalytically dead DNA2 D294A had no capacity to degrade DNA, showing that the nuclease activity is inherent to WT DNA2 (Fig. 8 F). The same results were recapitulated using purified yeast DNA2 (Fig. S5, A–F). Interestingly, addition of the ATPase-deficient RECQ1 mutant (RECQ1-K119R) to the reaction mix significantly inhibited the four-way junction degradation activity of human DNA2 (Fig. S4, D and E). These results suggest that the binding of RECQ1 to stalled replication forks limits the fork processing

Published March 2, 2015

activity of DNA2, as inferred by our cellular studies. However, we cannot rule out the possibility that the inhibitory effect observed in the biochemical assays is simply associated with competition for substrate recognition between the two proteins. In agreement with our in vivo data, we show that WRN promoted the degradative capacity of DNA2 on nicked, gapped, or four-way junction substrates (Fig. 8 I and Fig. S4, F and G); similar behavior was observed when yeast Dna2 was coupled with the Sgs1 helicase (Fig. S5, G and H). DNA was degraded by WRN and DNA2 in a remarkably synergistic manner: 5 nM concentration of either WRN or DNA2 alone led only to a minor DNA unwinding/degradation (Fig. 8 I, lanes 2 and 8). When combined, both enzymes completely degraded the four-way junction DNA (Fig. 8 I, lane 5). In contrast, no such synergy was observed when human DNA2 was combined with the noncognate yeast meiotic Mer3 helicase (Fig. S4 H), suggesting that the species-specific interaction between DNA2 and WRN results in a vigorous DNA degradation. Similarly, WT RECQ1 did not promote DNA degradation by DNA2 (Fig. S4 I).

On the basis of our results that DNA2 does not share the same function of EXO1 in reversed fork processing, we decided to compare the end-resection activities of human DNA2 and human EXO1 using the four-way junction substrates. EXO1—unlike DNA2—degraded both four-way junction substrates and linear duplexes with equal efficiency (Fig. 8 J and Fig. S4, J and K). The use of yeast variants of Dna2 and Exo1 yielded analogous results (Fig. S5, I–K). Collectively, these studies further implicate DNA2, and its nuclease activity, in reversed replication fork degradation—that is specifically stimulated by WRN—and point to an important difference in substrate preference between DNA2 and EXO1. Moreover, the polarity of reversed fork degradation by DNA2 measured in the presence of RPA displays the same bias anticipated from the EM analysis of the replication intermediates.

Discussion

The present work uncovers a new mechanism for reversed fork processing and restart that requires the coordinated activities of the human DNA2 nuclease and WRN helicase (Fig. 9). The DNA2-dependent end resection leads to partially single-stranded reversed forks and is required for efficient replication fork restart under conditions of persistent replication blockage. WRN interacts with DNA2 and its ATPase activity is needed for DNA2-dependent degradation, presumably to transiently open the dsDNA arm of the reversed replication forks.

To date, we have identified two mechanisms of reversed replication fork resolution, one dependent on RECQ1 ATPase and branch migration activity (Berti et al., 2013) and the other on DNA2 nuclease and WRN ATPase activity. Moreover, the DNA2/WRN mechanism is tightly regulated by an ATPase-independent function of RECQ1 that might limit DNA2 activity by binding to reversed forks. Of note, our EM experiments show that reversed replication forks accumulate in RECQ1- and DNA2-depleted cells also in unperturbed conditions suggesting that fork reversal is remarkably frequent when DNA replication faces intrinsic replication fork obstacles, and that RECQ1 and DNA2 have a conserved role in restarting reversed forks in unperturbed S-phase.

DNA2 function during DNA replication is vital for maintenance of genome stability (this study; Duxin et al., 2012; Karanja et al., 2012). These findings indicate that the controlled DNA2-dependent degradation of reversed replication forks is a physiologically relevant mechanism to provide resistance to prolonged genotoxic treatments. This mechanism is distinct from the pathological MRE11-dependent degradation of stalled replication intermediates detected in the absence of crucial Fanconi Anemia (FA)/HR factors (Schlacher et al., 2011, 2012; Hashimoto et al., 2012; Ying et al., 2012).

We find that depletion of the central recombinase factor RAD51 prevents nascent strand degradation. This finding, coupled with the recent observation that RAD51 is directly implicated in reversed fork formation (Zellweger et al., 2015), reinforce our conclusion that the DNA2-dependent pathway starts from the reversed arm of stalled replication forks and acts downstream of the RAD51-mediated replication fork reversal. Given that RAD51 is required for reversed fork formation (Zellweger et al., 2015), we speculate that the MRE11-dependent pathway is only uncovered in the absence of fork reversal—i.e., via a perturbation in RAD51 function—and likely attacks unprotected and nonreversed forks upon prolonged stalling. A crucial challenge for future studies will be to investigate why we do not observe a contribution of the MRE11 pathway in nascent strand degradation upon RAD51 depletion. It is tempting to speculate that RAD51 depletion might interfere with MRE11-dependent fork processing, in addition to preventing fork reversal. Conversely, perturbation of RAD51 function—e.g., via BRCA2 depletion (Schlacher et al., 2011)—might be sufficient to prevent fork reversal—hence DNA2-dependent degradation—but still allow residual RAD51 loading to promote MRE11-dependent degradation.

Our DNA fiber analysis suggests that DNA2 degrades stalled replication intermediates beyond the maximum length of the reversed arms measured by EM (up to several kilobases). A possible interpretation of these results is that after the initial DNA2/WRN-mediated regressed arm degradation is complete, other nucleolytic activities or DNA2 itself may codegrade both sides of the replication fork, thus leading to extensive degradation events detectable by DNA fibers. In this scenario, our EM images likely represent snapshots of the "slow steps" of this reaction—i.e., the DNA2/WRN-mediated degradation of the regressed arms—resulting in the drastic increase in reversed fork frequency observed in the absence of DNA2. Once the regressed arm has been resolved, the nucleolytic degradation might quickly proceed to degrade nascent strands behind the junction—as suggested by the DNA2-dependent increase in ssDNA gaps behind the observed forks—finally leading to reannealing of the parental strands and backtracking of the fork (Fig. S3 E). A new reversal event may occur when this extensive degradation leads to asymmetric ssDNA accumulation at the fork (Zellweger et al., 2015), resetting the backtracked fork to the slow step of the process. However, fork backtracking is only one possible model to explain the extensive degradation detected by DNA fibers and further work would be required to uncover additional nucleolytic activities that might be involved in this process.

Biochemical studies suggested that *Schizosaccharomyces pombe* Dna2 cleaves the leading and lagging reversed strands of

Published March 2, 2015

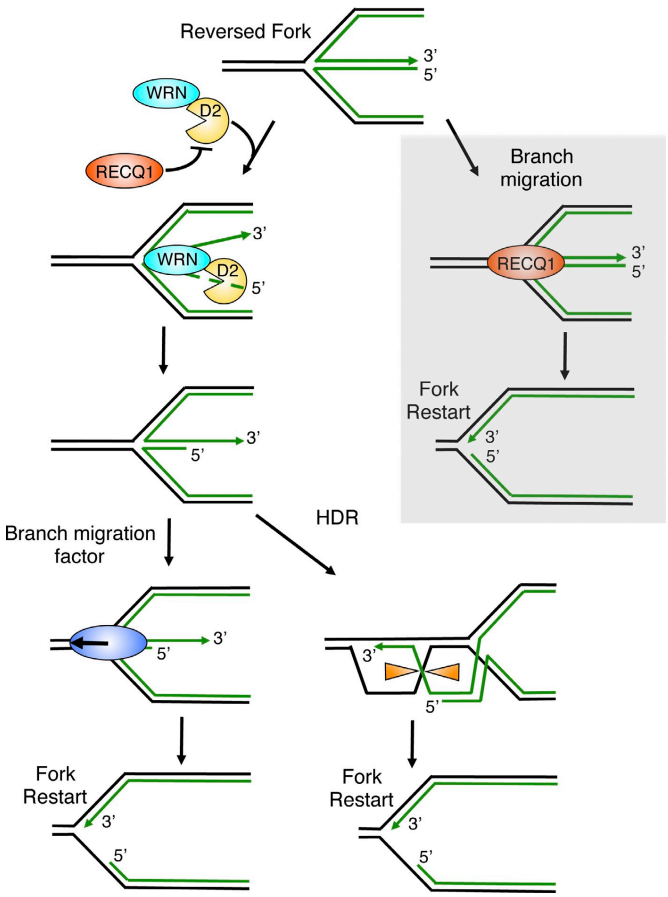

Figure 9. **Schematic model for the combined roles of DNA2 and WRN in reversed fork processing.** DNA2 and WRN functionally interact to process reversed forks. DNA2 degrades reversed forks with a 5′-to-3′ polarity. WRN ATPase activity assists DNA2 degradation possibly by promoting the opening of the reversed arm of the fork. RECQ1 limits DNA2 activity by an ATPase-independent function. Branch migration factors specifically recognize the partially resected reversed forks to promote fork restart. Alternatively, the newly formed 3′ overhang of the reversed fork invades the duplex ahead of the fork, resulting in Holliday junction structures that can be resolved by specific resolvases or dissolvases to promote fork restart. Gray box, RECQ1 can independently restart reversed forks by virtue of its ATPase and branch migration activity.

a model replication fork with similar efficiency in the absence of replication protein A (Hu et al., 2012). However, it is likely that only the 5′-to-3′ directionality is important in vivo, because RPA is known to stimulate the 5′-to-3′ and inhibit the 3′-to-5′ nuclease activity of yeast DNA2 (Cejka et al., 2010; Niu et al., 2010). In agreement with this conclusion, our biochemical data show that DNA2-dependent end resection proceeds with a 5′ to 3′ polarity in the presence of RPA. Moreover, our EM experiments clearly show that DNA2 depletion affects the frequency of reversed forks that are either entirely or partially single-stranded supporting the notion that DNA2-dependent degradation of reversed forks occurs with a preferential polarity in vivo.

The resection activity of human DNA2 was postulated to activate the ATR/Chk1 checkpoint under conditions of replication stress (Karanja et al., 2012). Indeed, we find that DNA2 depletion prevents ATR checkpoint activation after HU treatment. Moreover, the increased origin firing observed upon DNA2 depletion is consistent with observations that the deregulation of checkpoint activity leads to a large increase in the number of newly initiated origins (Couch et al., 2013). However, the extent of ATR activation does not necessarily reflect the amount of ssDNA detected at replication forks, whether at the junction, at ssDNA gaps, or at regressed arms (Zellweger et al., 2015). In light of these findings, we rather suggest that DNA2-dependent ATR activation may reflect DNA2 recruitment to the stalled forks per se, or subtle changes of fork architecture that are associated with its recruitment but possibly escape our EM analysis. This interpretation is supported by the recent discovery that yeast Dna2 has a direct role in Mec1 activation (the ortholog of human ATR), independent from its nuclease or helicase activity (Kumar and Burgers, 2013). Of note, the increased origin firing frequency observed upon DNA2 depletion is not associated to a parallel increase in the frequency of termination events (Fig. S1 A) possibly because the defects in replication fork restart associated

Published March 2, 2015

with DNA2 depletion limit the number of termination events even under conditions of increased origin firing.

WRN plays an important—albeit mechanistically ill-defined—role in the recovery from replication blockage, and mutations in the *WRN* gene are linked to the cancer predisposition disorder Werner Syndrome (Sidorova et al., 2008; Murfuni et al., 2012). Our studies infer that the high genomic instability of WRN-deficient cells may result from aberrant processing of reversed replication intermediates. In particular, given the consolidated role of WRN at difficult-to-replicate regions—e.g., telomeres and fragile sites (Crabbe et al., 2004; Murfuni et al., 2012)—we speculate that WRN, in conjunction with DNA2, is required to process reversed forks arising spontaneously at these genomic loci. Biochemical studies pointed to a putative role of WRN in fork reversal and/or restart by showing that WRN efficiently promotes both the formation and restoration of oligonucleotide-based reversed fork substrates (Machwe et al., 2011). We show that WRN ATPase activity is needed for the DNA2-dependent degradation of reversed replication forks. Our interpretation for the role of WRN ATPase activity is that it facilitates DNA2-dependent degradation of the reversed forks by transiently opening the dsDNA arm of the reversed fork. This mechanism is reminiscent to the DNA2-dependent mechanism of DSB resection where the yeast Sgs1 helicase is required to transiently open the DNA duplex to generate a 5′ ssDNA tail that is in turn degraded by DNA2 (Zhu et al., 2008; Cejka et al., 2010; Niu et al., 2010). We suggest that WRN is the functional homologue of Sgs1 in mammalian cells, at least in the context of DNA2-dependent reversed replication fork processing. However, BLM was also shown to interact and cooperate with DNA2 to resect dsDNA ends in vitro opening the possibility that other human RecQ helicases might substitute for WRN, depending on the nature of the DNA lesion being processed or the particular cellular context (Nimonkar et al., 2011; Sturzenegger et al., 2014). This mechanism seems to be well-conserved throughout evolution because it is highly reminiscent of the stalled fork processing pathway described in *E. coli* where the RecJ nuclease cooperates with bacterial RecQ to process blocked replication intermediates (Courcelle et al., 2003). In addition, the prokaryotic RecBCD helicase-nuclease plays an important role in resecting replication forks after reversal (Seigneur et al., 1998) and DNA2 is of the same family of nucleases as RecB. Whether the DNA2/WRN-mediated resection activity can degrade additional stalled replication intermediates other than reversed forks is worth future investigation.

EXO1, MRE11, and CtIP play central roles in DNA repair and are also implicated in the recovery from replication fork blockage (Cotta-Ramusino et al., 2005; Schlacher et al., 2011; Yeo et al., 2014). None of these nucleases, however, participates in the DNA2-dependent processing of reversed replication forks pointing to a specific role of DNA2 that, unlike its function in DSB resection, is not shared by other nucleases. A possible interpretation of these results is that the reversed forks are characterized by a particular structure of the terminal end that does not require the trimming activity of other nucleases to promote DNA2-dependent resection. However, some of these nucleases might still be able to access stalled forks under specific genetic backgrounds. For example, MRE11 degrades stalled replication intermediates only in a BRCA2-deficent background, as already discussed (Schlacher et al., 2011). Moreover, the cleavage of unresolved replicative intermediates by the structure-specific MUS81 endonuclease is a late response to replicative stress, which becomes activated only when other attempts to overcome stalled replication have been exhausted (Hanada et al., 2007; Franchitto et al., 2008). Thus, MUS81 might still resolve reversed replication forks as a back-up system to unlink sister chromatids and facilitate mitotic segregation in the absence of DNA2 or WRN.

Collectively, these studies highlight a new important mechanism for the recovery from replication blockage. This mechanism relies on the DNA2-dependent processing of reversed forks—leading to ssDNA stretches on the regressed arms—which appear to promote efficient fork restart. A possible explanation for the need of partially single-stranded DNA structures to promote fork restart is that they represent a key intermediate to activate an HDR-like mechanism of reversed fork restart, as recently proposed in *S. pombe* (Carr and Lambert, 2013). In particular, the newly formed 3′ overhang of the reversed fork might invade the duplex ahead of the fork resulting in Holliday junction structures that can be resolved by specific resolvases or dissolved by the combined action of the BLM helicase (Sgs1 in yeast) and the type I topoisomerase TOP3 (Fig. 9). Alternatively, resumption of DNA replication might be obtained by reverse branch migration, where the partially resected reversed fork structures might be specifically recognized by a motor protein—e.g., SMARCAL1 (Béous et al., 2013) or a human RecQ helicase—to promote the branch migration-assisted reestablishment of a functional replication fork.

Materials and methods

Cell lines, culture conditions, and reagents

U-2 OS, HEK 293, and Werner Syndrome fibroblast (AG11395) cells were grown in DMEM supplemented with 10% FBS at 37°C in 5% CO_2. HCT116 cells were grown in McCoy's 5A medium supplemented with 10% FBS. CldU, IdU, BrdU, hydroxyurea, mitomycin C, camptothecin, tamoxifen, puromycin, and hygromycin were obtained from Sigma-Aldrich.

DNA2 conditional knockout HCT116 cells

To examine the response of cells to the complete absence of DNA2, we used a DNA2 conditional knockout cell line where exon 2 of the DNA2 gene is deleted (Karanja et al., 2014). The colorectal carcinoma HCT116 cell line carries 3 copies of DNA2 due to a duplication on chromosome 10. Two chromosomal copies were disrupted using rAAV-mediated gene targeting technology and exon 2 of the third allele was replaced with a conditional exon where the exon was flanked by loxP sites (DNA2flox/−/−). To create a conditional cell line these cells were stably transduced with a tamoxifen (4-OHT)-inducible Cre recombinase. Thus, the cell line is viable and can be propagated. The addition of tamoxifen to the culture media leads to excision of the endogenous DNA2 and the generation of a true DNA2-null cell. Complete loss of DNA2 occurs after 72 h of tamoxifen treatment. However, the DNA fiber experiments were performed after 40 h of tamoxifen treatment to have enough S-phase cells for DNA labeling.

Antibodies

Anti-DNA2 rabbit polyclonal (ab96488; 1:1,000), anti-MUS81 mouse monoclonal (ab14387; 1:1,000), and anti-CldU/BrdU rat monoclonal (ab6326; 1:6) antibodies (all from Abcam); anti-CtIP rabbit polyclonal (A300-488A; 1:1,000), anti-EXO1 rabbit polyclonal (A302-639A; 1:1,000), anti-pRPA32 (S4/S8) rabbit polyclonal (A300-245A; 1:1,000), and anti-pRPA32 (S33) rabbit polyclonal (300-246A; 1:2,000; all from

Published March 2, 2015

Bethyl); anti-WRN rabbit polyclonal (NB100-471; 1:1,000); and anti-MRE11 rabbit polyclonal (NB100-142; 1:2,000; Novus); anti-RAD51 (H-92) rabbit polyclonal (sc-8349; 1:1,000) and anti-RECQ1 rabbit polyclonal (sc-25547; 1:2,000) from Santa Cruz; anti-rat Alexa (594-A11007; 1:1,000); and anti–mouse Alexa Flour (488-A11001; 1:1,000; Invitrogen); anti-rabbit (31460; 1:10,000; Thermo Fisher Scientific); anti-tubulin mouse monoclonal (T5168; 1:5,000; Sigma-Aldrich); anti-IdU/BrdU mouse monoclonal (347580; 1:6) from BD; anti-Chk1 mouse monoclonal (sc-8408; 1:1,000; Santa Cruz Biotechnology, Inc.); anti-p-Chk1 (S345) rabbit monoclonal (2348; 1:1,000; Cell Signaling Technology); anti-RPA32 mouse monoclonal (NA19L; 1:1,000) from EMD Millipore; anti-RECQ1 rabbit polyclonal, raised against residues 634–649 of human RECQ1, is custom made (Mendoza-Maldonado et al., 2011); anti-BLM rabbit polyclonal, raised against residues 1–449 of human BLM (Wu and Hickson, 2003), was a gift from I. Hickson (University of Copenhagen, Copenhagen, Denmark); and anti-RECQ4 rabbit polyclonal, raised against residues 60–111 of human RECQ4 (Yin et al., 2004), was a gift from W. Wang (National Institute on Aging, Baltimore, MD).

Recombinant proteins

Yeast Dna2 was expressed in yeast WDH668 strain from pGAL:DNA2 vector (Budd et al., 2000) and purified as previously described (Levikova et al., 2013). In brief, the cells were lysed and Dna2 was purified by affinity chromatography on Ni-NTA agarose (QIAGEN) and anti-Flag M2 affinity gel (Sigma-Aldrich). Yeast RPA was expressed in yeast BJ5464 strain containing three plasmids coding for Rfa1, Rfa2, and Rfa3 and purified as previously described (Kantake et al., 2003). In brief, the cells were lysed and yeast RPA was purified by affinity on ssDNA cellulose column (USB corporation) and by ion exchange chromatography using HiTrap Q column (GE Healthcare). Human DNA2 was expressed in Sf9 cells from a pFastBac:hDNA2 vector (polyhedrin promoter) provided by J. Campbell (Masuda-Sasa et al., 2006). The soluble extracts were obtained by salt extraction as previously described for Sgs1 (Cejka and Kowalczykowski, 2010). The subsequent purification of hDNA2 was performed as previously described for yeast Dna2 (Levikova et al., 2013) by affinity chromatography using Ni-NTA agarose (QIAGEN) and Anti-Flag M2 affinity gel (Sigma-Aldrich). Human RPA was expressed from p11d-tRPA vector (Henricksen et al., 1994) in BL21 *E. coli* cells and purified as described (Henricksen et al., 1994). In brief, hRPA was first bound to HiTrap Blue column (GE healthcare) and then to HiTrap Q column. The sequence coding for yeast Mer3 helicase was amplified from yeast genomic DNA (SK1 strain) using primers Mer3FO (5′-GCGCGCGGGCCCATGAAAACAAAGTTTGATCGCCTCGGTACAGGAAAAAGAAGTAGACCCTCTCCAAATAATATTGACTTTAACGACCAG-3′) and Mer3RE (5′-CGCGCGCTCGAGTTCAAACTCTATATCGGAAC-3′). The PCR product was digested with ApaI and XhoI restriction endonucleases (both from New England Biolabs) and cloned into corresponding sites in pFB-MBP-Sgs1-his after the polyhedrin promoter, creating pFB-MBP-Mer3-his vector. Mer3 was then expressed in Sf9 cells and purified using affinity chromatography as previously described for Sgs1 (Cejka and Kowalczykowski, 2010). In brief, MBP-tagged Mer3 was first bound to amylose resin (New England Biolabs), eluted and digested with PreScission protease to cleave the MBP tag. Mer3 was further purified by affinity on Ni-NTA agarose (QIAGEN) exploiting the 10x His-tag at its C-terminus. Sequence information is available on request.

Genetic knock-down-rescue experiments

RECQ1, DNA2, and RAD51 genetic knockdown-rescue experiments were performed using the procedure described (Berti et al., 2013; Yata et al., 2012). In brief, RECQ1 is depleted using the pLKO.1-puro-shRECQ1 (5′-GAGCTTATGTTACCAGTTA-3′) construct and rescue experiments are performed using the shRNA resistant pIRES-RECQ1-WT or K119R (ATPase dead) constructs as described (Berti et al., 2013). DNA2 is depleted using an siRNA targeting the 3′UTR of DNA2 (5′-CAGUAUCUCCUCUAGCUAG-3′). At least one isoform of DNA2 is not targeted by this sequence. DNA2 rescue experiments are performed using the pBabe-hygro-3xFLAG-DNA2 WT, D294A (Nuclease dead), or K671E (helicase dead) constructs. RAD51 is depleted using siRNAs targeting the 3′UTR (5′-GACUGCCAGGAUAAAGCUU-3′ and 5′-GUGCUGCAGCCUAAUGAGA-3′) in U-2 OS stable cell lines expressing WT RAD51 as described (Yata et al., 2012). WRN depletions were achieved using pRS-puro-shWRN (5′-AGGCAGGTGTAGGAATTGAAGGAGATCAG-3′; sequence ID: TI333414) and exogenous expression is done with the shRNA resistant Flag-pCMVTag2B-WRN WT or K577M (helicase dead) constructs. Constructs for WRN depletion and overexpression of WT WRN and ATPase-deficient WRN (WRN-K577M) were kind gifts from Dr. Pietro Pichierri (Insituto Superiore di Sanità, Rome, Italy). All transfections were done with Lipofectamine 2000 (Life technologies Catalog no: 11668027). An shRNA targeting luciferase (5′-ACGCTGAGTACTTCGAAATGT-3′) was used for control shRNA experiments. The silencer select negative control (Life technologies, Catalog no. 4390843) or an siRNA targeting luciferase (5′-CGUACGCGGAAUACUUCGA-3′) were used for control siRNA experiments, as indicated. Lentiviral mediated shRNA depletions were achieved using the following sequences cloned into the pLKO.1 lentiviral shRNA expression vector: BLM (5′-CGAAGGAAGTTGTATGCACTA-3′), WRN (5′-GCTGGCAATTACCAGAACAAT-3′), and MUS81 (5′-CACGCGCTTCGTATTTCAGAA-3′). The procedure for lentiviral generation and transduction has been described (Berti et al., 2013). Transduced U-2 OS cells were selected with 6 µg/ml puromycin. siRNA-mediated depletions were achieved using the following siRNAs from Invitrogen: DNA2 (5′-AUAGCCAGUAGUAUUCGAU-3′), CtIP (5′-CGAAUCUUAGAUGCACAAA-3′), EXO1 (Invitrogen-HSS113557), and RAD51 (Invitrogen-1299001). In brief, siRNAs were transfected using Lipofectamine RNAiMAX (Life Technologies) following the manufacturer's protocol. MRE11 (5′-GAAAGGCUCUAUCGAAUGU-3′) and RECQ4 (SMART pool) siRNAs were from Dharmacon and were transfected as previously described (Thangavel et al., 2010).

Microfluidic-assisted DNA fiber stretching

For DNA replication fork restart analysis, asynchronous cells were pulse-labeled with 50 µM CldU for 20–30 min. 2 mM HU, 300 nM MMC, or 150 nM CPT was added to the CldU containing media and incubated for the indicated times. Cells were washed three times with medium and released with 50 µM IdU for 40 min. For nascent strand degradation analysis, asynchronous cells were pulse-labeled with 50 µM IdU for 45 min, washed three times with medium, incubated with 4 mM HU, 100 nM CPT, 200 nM MMC, or medium for times indicated. The pulse-labeled cells were trypsin collected and lysed in agarose plugs to prevent any mechanical breakage of replication tracts. Microfluidic platform for stretching the high-molecular weight DNA, coverslips, immunostaining and image acquisition of replication tracts were performed as described (Sidorova et al., 2009; Berti et al., 2013). In brief, polydimethylsiloxane (PDMS) stamps with microchannels were Oxygen plasma treated and reversibly sealed to the silanized coverslips. High-molecular weight DNA was loaded and stretched by capillary force into the microchannels. PDMS stamps were peeled-off and coverslips were left drying overnight. For immunostaining, DNA-stretched coverslips were denatured (2.5N HCL for 45 min), neutralized (0.1 M sodium borate and 3 washes with PBS), blocked (5% BSA and 0.5% Tween 20 in PBS for 30 min), incubated with primary antibodies (Anti-IdU/BrdU or both anti-IdU/BrdU and anti-CldU/BrdU for 30 min), washed (1% BSA and 0.1% Tween 20 in PBS, 3 times 5 min each) and incubated with secondary antibodies (anti–mouse Alexa Fluor 488-conjugated, or both anti–mouse Alexa Fluor 488–conjugated and anti–rat Alexa Fluor 594–conjugated for 1 h). Washed slides were mounted in prolong gold anti-fade reagent (Life Technologies) and images were sequentially acquired (for double-label) with LAS AF software using TCS SP5 confocal microscope (Leica). A 63×/1.4 oil immersion objective was used. Images were captured at room temperature. $n \geq 300$ fiber tracts scored for each dataset. The DNA tract lengths were measured using ImageJ and the pixel length values were converted into micrometers using the scale bars created by the microscope. Statistical analysis was done using GraphPad Prism.

Clonogenic survival assay

Colony-forming assays were performed as previously described (Franken et al., 2006). In brief, 1,000 cells were plated per well and treated on the next day with 4 mM HU for 3, 6, and 8 h or 100 nM CPT for 6 h. Colonies were fixed, stained, and quantified 10 d after release from genotoxic stress. The plating efficiency and survival fraction were calculated as previously described (Franken et al., 2006). In brief, colonies were counted using an inverted stereomicroscope and the plating efficiency was calculated using the following formula: Plating Efficiency (PE) = (no. of colonies formed/no. of cells seeded) × 100%. From the plating efficiency, the surviving fraction (SF) was calculated as: SF = (no. of colonies formed after treatment/no. of cells seeded) × PE. The experiments were performed in triplicate and the statistical analysis was performed using GraphPad Prism.

Western blotting

Cells were washed with PBS and lysed either in standard RIPA buffer (PBS, 1% NP-40, 0.5% sodium deoxycholate, 0.1% SDS, 10 µg/ml aprotinin, 10 µg/ml PMSF, 1 mM Na_3VO_4, and 1 mM NaF) or MCL buffer (50 mM Tris, pH 8.0, 5 mM EDTA, 0.5% NP-40, 100 mM NaCl, 2 mM DTT, and freshly added protease and phosphatase inhibitors from Roche (1 tablet/10 ml of buffer). Cell lysates were resolved by SDS-PAGE and transferred to

Published March 2, 2015

PVDF membrane (GE Healthcare). Incubation with antibodies was performed overnight at 4°C. Proteins were visualized using ECL (Thermo Fisher Scientific) according to the manufacturer's instructions.

Co-immunoprecipitation experiments

HEK293T cells were transfected with empty vectors, FLAG-DNA2, and Strep-HA-WRN by calcium phosphate. 48 h after transfection, cells were treated with 4 mM HU for 3 h, lysed in benzonase lysis buffer (50 mM Tris-HCl, pH 7.5, 75 mM KCl, 2 mM $MgCl_2$, 20 mM NaF, 10 mM β-glycerophosphate, 0.2 mM Na_3VO_4, and 0.2% Triton X-100) supplemented with protease inhibitors (EDTA-free tablet; Sigma-Aldrich) by passing 10 times through a 26-G syringe needle and incubated 1 h at 4°C with 2 U/µl Benzonase (Sigma-Aldrich) to digest genomic DNA. KCl and EDTA concentrations were adjusted to 120 and 3 mM, respectively, and lysates were centrifuged at 14,000 rpm for 30 min. Immunoprecipitations of clarified lysates were performed with FLAG M2 or HA affinity agarose resin (Sigma-Aldrich) overnight at 4°C. Beads were washed 5 times with wash buffer (50 mM Tris-HCl, pH 7.5, 150 mM KCl, 3 mM EDTA, 2 mM $MgCl_2$, 20 mM NaF, 10 mM β-glycerophosphate, 0.2 mM Na_3VO_4, and 0.2% Triton X-100) and bound proteins were eluted by boiling in SDS-PAGE sample buffer.

EM analysis of genomic DNA in mammalian cells

EM analysis of replication intermediates has been described in detail (Ray Chaudhuri et al., 2012; Neelsen et al., 2014), including a description of the important parameters to consider specifically for the identification and the scoring of reversed forks (Neelsen et al., 2014). In brief, 5–10 × 10^6 U-2 OS cells were harvested and genomic DNA was cross-linked by two rounds of incubation in 10 µg/ml 4,5′,8-trimethylpsoralen (Sigma-Aldrich) and 3 min of irradiation with 366 nm UV light on a precooled metal block. Cells were lysed and genomic DNA was isolated from the nuclei by proteinase K (Roche) digestion and phenol-chloroform extraction. DNA was purified by isopropanol precipitation, digested with PvuII HF in the proper buffer for 3–5 h at 37°C, and replication intermediates were enriched on a benzoylated naphthoylated DEAE–cellulose (Sigma-Aldrich) column. EM samples were prepared by spreading the DNA on carbon-coated grids in the presence of benzyl-dimethyl-alkylammonium chloride and visualized by platinum rotary shadowing. Images were acquired on a transmission electron microscope (JOEL 1200 EX) with side-mounted camera (AMTXR41 supported by AMT software v601) and analyzed with ImageJ (National Institutes of Health).

Preparation of oligonucleotide-based DNA substrates

DNA oligonucleotides were purchased from Microsynth and ^{32}P-labeled either at the 5′ terminus with [γ-^{32}P] ATP and T_4 polynucleotide kinase (New England Biolabs), or at the 3′ end with [α-^{32}P] cordycepin-5′-triphosphate and terminal transferase (New England Biolabs) according to manufacturer's instructions. Unincorporated nucleotides were removed using MicroSpin G25 columns (GE Healthcare). The substrates were prepared by heating the respective oligonucleotides at 95°C and gradually cooling to room temperature. The following oligonucleotides were used for the preparation of the four-way junction (X12-3 TOP L, HJ 1, HJ 2, and HJ 3), three-way junction with 3′ tail (X12-3 TOP L, HJ 1, HJ 2Sb, and HJ 3), three-way junction with 5′ ssDNA tail (X12-3 TOP L, HJ 1S, HJ 2, and HJ 3), nicked four-way junction (X12-3 TOP L, HJ 1, HJ 2Sa, HJ 2Sb, and HJ 3), replication fork (X12-3 TOP L, HJ 1S, HJ 2Sb, and HJ 3), and dsDNA (X12-3 TOP L and Bottom LC), respectively. The sequences of the oligonucleotides were: X12-3 TOP L (93 nt), 5′-GACGTCATAGACGATTACATTGCTAGGACATGCTGTCTAGAGACTATCGCGACTTACGTTCCATCGCTAGGTTATTTTTTTTTTTTTTTTTT-3′ X12-3 HJ 1 (93 nt), 5′-AAAAAAAAAAAAAAAAAAAATAACCTAGCGATGGAACGTAAGTCGCGATGGGCTTAACTAGGATGCTACTGGCCCCGAATCAACCGTACTTGGG-3′ X12-3 HJ 1S (48 nt), 5′-AAAAAAAAAAAAAAAAAAAATAACCTAGCGATGGAACGTAAGTCGCGAT-3′ X12-3 HJ 2 (93 nt), 5′-CCCAAGTACGGTTGATTCGGGGCCAGTAGCATCCTAGTTAAGCCCATTACGATTCGTTACCCATTCACTGTCAGAAGGCACCAGATAGATCTC-3′ X12-3 HJ 2Sa (45 nt), 5′-CCCAAGTACGGTTGATTCGGGGCCAGTAGCATCCTAGTTAAGCCC-3′ X12-3 HJ 2Sb (48 nt), 5′-ATTACGATTCGTTACCCATTCACTGTCAGAAGGCACCAGATAGATCTC-3′ X12-3 HJ 3 (93 nt), 5′-GAGATCTATCTGGTGCCTTCTGACAGTGAATGGGTAACGAATCGTAATAGTCTCTAGACAGCATGTCCTAGCAATGTAATCGTCTATGACGTC-3′ X12-3 BOTTOM LC, 5′-AAAAAAAAAAAAAAAAAAAATAACCTAGCGATGGAACGTAAGTCGCGATAGTCTCTAGACAGCATGTCCTAGCAATGTAATCGTCTATGACGTC-3′.

Nuclease assays

The experiments were performed in a 15-µl volume in 25 mM Tris-acetate (pH 7.5), 2 mM magnesium acetate, 1 mM ATP, 1 mM dithiothreitol, 0.1 mg/ml BSA (New England Biolabs), 1 mM phosphoenolpyruvate, 80 U/ml pyruvate kinase, 1 nM DNA substrate (molecules), and recombinant proteins, as indicated. The reactions were assembled on ice and incubated for 30 min at 30°C for yeast proteins and at 37°C for human proteins. Unless indicated otherwise, RPA was present in the reactions at saturating concentrations corresponding to a threefold excess over DNA, assuming all DNA was single-stranded and a DNA-binding site size of 25 nt for hRPA and of 20 nt for yRPA. The reactions were terminated by adding 5 µl Stop buffer (150 mM EDTA, 2% SDS, 30% glycerol, and 0.01% bromophenol blue), incubated for 30 min at room temperature and separated on polyacrylamide gels in TBE buffer under native conditions. Alternatively, for denaturing conditions, the reaction were terminated by adding 15 µl Formamide stop buffer (95% (vol/vol) formamide, 20 mM EDTA, 0.01% bromophenol blue), denatured by heating at 95°C for 5 min and separated on 20% denaturing polyacrylamide gels in TBE buffer. Gels were fixed, dried, exposed to a storage phosphor screen, and analyzed on Typhoon phosphor imager (GE Healthcare).

Online supplemental material

Fig. S1 shows quantification of stalled forks, new origins, and termination events in DNA2-depleted cells upon genotoxic stress induction, as well as the statistical analysis of IdU tracts from RECQ1-, DNA2-, WRN-, RECQ1/DNA2-, RECQ1/WRN-, WRN/DNA2-, and RECQ1/WRN/DNA2-depleted U-2 OS cells. Fig. S2 shows the IdU tract length distribution in BLM- and RECQ4-depleted cells, respectively, as well as statistical analysis of IdU tracts from RECQ1/WRN-codepleted cells complemented with WT WRN or with ATPase-deficient WRN. Fig. S3 shows additional EM analysis, as well as the Western blot analysis of ATR-checkpoint activation in RECQ1- and/or DNA2-depleted U-2 OS cells. Fig. S4 shows additional biochemical analysis of substrate specificity of human DNA2 and human EXO1. TFig. S5 shows biochemical assays of substrate specificity of yeast Dna2 and yeast Exo1. Online supplemental material is available at http://www.jcb.org/cgi/content/full/jcb.201406100/DC1.

We are grateful to Pietro Pichierri (Istituto Superiore di Sanità, Rome) for providing the WS cells and WRN constructs, Damian Dalcher for his help with the EM analysis, Stephanie Felscher (University of Zurich) for kindly providing human EXO1 protein, Marc Wold (University of Iowa) for human RPA expression construct, Lepakshi Ranjha (University of Zurich) for Mer3 protein, Fumiko Esashi (University of Oxford) for the Rad51 siRNAs and the U-2 OS cells stably expressing exogenous RAD51, and Judith Campbell (California Institute of Technology) for human and yeast DNA2/Dna2 expression constructs. We thank the Research Microscopy Core Facility of Saint Louis University for technical support.

This work was supported by National Institutes of Health grant R01GM108648 to A. Vindigni, by startup funding from the Doisy Department of Biochemistry and Molecular Biology and from the Saint Louis University Cancer Center to A. Vindigni, by grants from the President's Research Fund of Saint Louis University and by the GLIOMA-Interreg (Slovenian-Italian Cooperation 2007-2013) project to A. Vindigni, by the Swiss National Science Foundation grants 31003A_146924 to M. Levikova and PP00P3 133636 to P. Cejka, by National Institutes of Health grant GM0088351 and CA15446 to E.A. Hendrickson, and by a research contract from Horizon Discovery, Ltd to E.A. Hendrickson. M. Berti was supported by an EMBO short-term fellowship to perform EM experiments in M. Levikova laboratory.

The authors declare no competing financial interests.

Submitted: 24 June 2014
Accepted: 14 January 2015

References

Atkinson, J., and P. McGlynn. 2009. Replication fork reversal and the maintenance of genome stability. *Nucleic Acids Res.* 37:3475–3492. http://dx.doi.org/10.1093/nar/gkp244

Ayyagari, R., X.V. Gomes, D.A. Gordenin, and P.M. Burgers. 2003. Okazaki fragment maturation in yeast. I. Distribution of functions between FEN1 AND DNA2. *J. Biol. Chem.* 278:1618–1625. http://dx.doi.org/10.1074/jbc.M209801200

Bae, S.H., K.H. Bae, J.A. Kim, and Y.S. Seo. 2001. RPA governs endonuclease switching during processing of Okazaki fragments in eukaryotes. *Nature.* 412:456–461. http://dx.doi.org/10.1038/35086609

Berti, M., A. Ray Chaudhuri, S. Thangavel, S. Gomathinayagam, S. Kenig, M. Vujanovic, F. Odreman, T. Glatter, S. Graziano, R. Mendoza-Maldonado, et al. 2013. Human RECQ1 promotes restart of replication forks reversed by DNA topoisomerase I inhibition. *Nat. Struct. Mol. Biol.* 20:347–354. http://dx.doi.org/10.1038/nsmb.2501

Published March 2, 2015

Bétous, R., A.C. Mason, R.P. Rambo, C.E. Bansbach, A. Badu-Nkansah, B.M. Sirbu, B.F. Eichman, and D. Cortez. 2012. SMARCAL1 catalyzes fork regression and Holliday junction migration to maintain genome stability during DNA replication. *Genes Dev.* 26:151–162. http://dx.doi.org/10.1101/gad.178459.111

Bétous, R., F.B. Couch, A.C. Mason, B.F. Eichman, M. Manosas, and D. Cortez. 2013. Substrate-selective repair and restart of replication forks by DNA translocases. *Cell Reports*. 3:1958–1969. http://dx.doi.org/10.1016/j.celrep.2013.05.002

Budd, M.E., and J.L. Campbell. 1995. A yeast gene required for DNA replication encodes a protein with homology to DNA helicases. *Proc. Natl. Acad. Sci. USA*. 92:7642–7646. http://dx.doi.org/10.1073/pnas.92.17.7642

Budd, M.E., and J.L. Campbell. 1997. A yeast replicative helicase, Dna2 helicase, interacts with yeast FEN-1 nuclease in carrying out its essential function. *Mol. Cell. Biol.* 17:2136–2142.

Budd, M.E., W. Choe, and J.L. Campbell. 2000. The nuclease activity of the yeast DNA2 protein, which is related to the RecB-like nucleases, is essential in vivo. *J. Biol. Chem.* 275:16518–16529. http://dx.doi.org/10.1074/jbc.M909511199

Carr, A.M., and S. Lambert. 2013. Replication stress-induced genome instability: the dark side of replication maintenance by homologous recombination. *J. Mol. Biol.* 425:4733–4744. http://dx.doi.org/10.1016/j.jmb.2013.04.023

Cejka, P., and S.C. Kowalczykowski. 2010. The full-length *Saccharomyces cerevisiae* Sgs1 protein is a vigorous DNA helicase that preferentially unwinds holliday junctions. *J. Biol. Chem.* 285:8290–8301. http://dx.doi.org/10.1074/jbc.M109.083196

Cejka, P., E. Cannavo, P. Polaczek, T. Masuda-Sasa, S. Pokharel, J.L. Campbell, and S.C. Kowalczykowski. 2010. DNA end resection by Dna2-Sgs1-RPA and its stimulation by Top3-Rmi1 and Mre11-Rad50-Xrs2. *Nature*. 467:112–116. http://dx.doi.org/10.1038/nature09355

Cotta-Ramusino, C., D. Fachinetti, C. Lucca, Y. Doksani, M. Lopes, J. Sogo, and M. Foiani. 2005. Exo1 processes stalled replication forks and counteracts fork reversal in checkpoint-defective cells. *Mol. Cell*. 17:153–159. http://dx.doi.org/10.1016/j.molcel.2004.11.032

Couch, F.B., C.E. Bansbach, R. Driscoll, J.W. Luzwick, G.G. Glick, R. Bétous, C.M. Carroll, S.Y. Jung, J. Qin, K.A. Cimprich, and D. Cortez. 2013. ATR phosphorylates SMARCAL1 to prevent replication fork collapse. *Genes Dev.* 27:1610–1623. http://dx.doi.org/10.1101/gad.214080.113

Courcelle, J., J.R. Donaldson, K.H. Chow, and C.T. Courcelle. 2003. DNA damage-induced replication fork regression and processing in Escherichia coli. *Science*. 299:1064–1067. http://dx.doi.org/10.1126/science.1081328

Crabbe, L., R.E. Verdun, C.I. Haggblom, and J. Karlseder. 2004. Defective telomere lagging strand synthesis in cells lacking WRN helicase activity. *Science*. 306:1951–1953. http://dx.doi.org/10.1126/science.1103619

Duxin, J.P., H.R. Moore, J. Sidorova, K. Karanja, Y. Honaker, B. Dao, H. Piwnica-Worms, J.L. Campbell, R.J. Monnat Jr., and S.A. Stewart. 2012. Okazaki fragment processing-independent role for human Dna2 enzyme during DNA replication. *J. Biol. Chem.* 287:21980–21991. http://dx.doi.org/10.1074/jbc.M112.359018

Franchitto, A., L.M. Pirzio, E. Prosperi, O. Sapora, M. Bignami, and P. Pichierri. 2008. Replication fork stalling in WRN-deficient cells is overcome by prompt activation of a MUS81-dependent pathway. *J. Cell Biol.* 183:241–252. http://dx.doi.org/10.1083/jcb.200803173

Franken, N.A., H.M. Rodermond, J. Stap, J. Haveman, and C. van Bree. 2006. Clonogenic assay of cells in vitro. *Nat. Protoc.* 1:2315–2319. http://dx.doi.org/10.1038/nprot.2006.339

Gari, K., C. Décaillet, M. Delannoy, L. Wu, and A. Constantinou. 2008. Remodeling of DNA replication structures by the branch point translocase FANCM. *Proc. Natl. Acad. Sci. USA*. 105:16107–16112. http://dx.doi.org/10.1073/pnas.0804777105

Gravel, S., J.R. Chapman, C. Magill, and S.P. Jackson. 2008. DNA helicases Sgs1 and BLM promote DNA double-strand break resection. *Genes Dev.* 22:2767–2772. http://dx.doi.org/10.1101/gad.503108

Hanada, K., M. Budzowska, S.L. Davies, E. van Drunen, H. Onizawa, H.B. Beverloo, A. Maas, J. Essers, I.D. Hickson, and R. Kanaar. 2007. The structure-specific endonuclease Mus81 contributes to replication restart by generating double-strand DNA breaks. *Nat. Struct. Mol. Biol.* 14:1096–1104. http://dx.doi.org/10.1038/nsmb1313

Hashimoto, Y., F. Puddu, and V. Costanzo. 2012. RAD51- and MRE11-dependent reassembly of uncoupled CMG helicase complex at collapsed replication forks. *Nat. Struct. Mol. Biol.* 19:17–24. http://dx.doi.org/10.1038/nsmb.2177

Henricksen, L.A., C.B. Umbricht, and M.S. Wold. 1994. Recombinant replication protein A: expression, complex formation, and functional characterization. *J. Biol. Chem.* 269:11121–11132.

Hu, J., L. Sun, F. Shen, Y. Chen, Y. Hua, Y. Liu, M. Zhang, Y. Hu, Q. Wang, W. Xu, et al. 2012. The intra-S phase checkpoint targets Dna2 to prevent stalled replication forks from reversing. *Cell*. 149:1221–1232. http://dx.doi.org/10.1016/j.cell.2012.04.030

Kantake, N., T. Sugiyama, R.D. Kolodner, and S.C. Kowalczykowski. 2003. The recombination-deficient mutant RPA (rfa1-t11) is displaced slowly from single-stranded DNA by Rad51 protein. *J. Biol. Chem.* 278:23410–23417. http://dx.doi.org/10.1074/jbc.M302995200

Karanja, K.K., S.W. Cox, J.P. Duxin, S.A. Stewart, and J.L. Campbell. 2012. DNA2 and EXO1 in replication-coupled, homology-directed repair and in the interplay between HDR and the FA/BRCA network. *Cell Cycle*. 11:3983–3996. http://dx.doi.org/10.4161/cc.22215

Karanja, K.K., E.H. Lee, E.A. Hendrickson, and J.L. Campbell. 2014. Preventing over-resection by DNA2 helicase/nuclease suppresses repair defects in Fanconi anemia cells. *Cell Cycle*. 13:1540–1550. http://dx.doi.org/10.4161/cc.28476

Kumar, S., and P.M. Burgers. 2013. Lagging strand maturation factor Dna2 is a component of the replication checkpoint initiation machinery. *Genes Dev.* 27:313–321. http://dx.doi.org/10.1101/gad.204750.112

Kuo, C., H. Nuang, and J.L. Campbell. 1983. Isolation of yeast DNA replication mutants in permeabilized cells. *Proc. Natl. Acad. Sci. USA*. 80:6465–6469. http://dx.doi.org/10.1073/pnas.80.21.6465

Levikova, M., D. Klaue, R. Seidel, and P. Cejka. 2013. Nuclease activity of *Saccharomyces cerevisiae* Dna2 inhibits its potent DNA helicase activity. *Proc. Natl. Acad. Sci. USA*. 110:E1992–E2001. http://dx.doi.org/10.1073/pnas.1300390110

Liao, S., T. Toczylowski, and H. Yan. 2008. Identification of the Xenopus DNA2 protein as a major nuclease for the 5′->3′ strand-specific processing of DNA ends. *Nucleic Acids Res.* 36:6091–6100. http://dx.doi.org/10.1093/nar/gkn616

Machwe, A., R. Karale, X. Xu, Y. Liu, and D.K. Orren. 2011. The Werner and Bloom syndrome proteins help resolve replication blockage by converting (regressed) holliday junctions to functional replication forks. *Biochemistry*. 50:6774–6788. http://dx.doi.org/10.1021/bi2001054

Masuda-Sasa, T., O. Imamura, and J.L. Campbell. 2006. Biochemical analysis of human Dna2. *Nucleic Acids Res.* 34:1865–1875. http://dx.doi.org/10.1093/nar/gkl070

Mendoza-Maldonado, R., V. Faoro, S. Bajpai, M. Berti, F. Odreman, M. Vindigni, T. Ius, A. Ghasemian, S. Bonin, M. Skrap, et al. 2011. The human RECQ1 helicase is highly expressed in glioblastoma and plays an important role in tumor cell proliferation. *Mol. Cancer*. 10:83. http://dx.doi.org/10.1186/1476-4598-10-83

Mimitou, E.P., and L.S. Symington. 2008. Sae2, Exo1 and Sgs1 collaborate in DNA double-strand break processing. *Nature*. 455:770–774. http://dx.doi.org/10.1038/nature07312

Murfuni, I., A. De Santis, M. Federico, M. Bignami, P. Pichierri, and A. Franchitto. 2012. Perturbed replication induced genome wide or at common fragile sites is differently managed in the absence of WRN. *Carcinogenesis*. 33:1655–1663. http://dx.doi.org/10.1093/carcin/bgs206

Neelsen, K.J., A.R. Chaudhuri, C. Follonier, R. Herrador, and M. Lopes. 2014. Visualization and interpretation of eukaryotic DNA replication intermediates in vivo by electron microscopy. *Methods Mol. Biol.* 1094:177–208. http://dx.doi.org/10.1007/978-1-62703-706-8_15

Nicolette, M.L., K. Lee, Z. Guo, M. Rani, J.M. Chow, S.E. Lee, and T.T. Paull. 2010. Mre11-Rad50-Xrs2 and Sae2 promote 5′ strand resection of DNA double-strand breaks. *Nat. Struct. Mol. Biol.* 17:1478–1485. http://dx.doi.org/10.1038/nsmb.1957

Nimonkar, A.V., J. Genschel, E. Kinoshita, P. Polaczek, J.L. Campbell, C. Wyman, P. Modrich, and S.C. Kowalczykowski. 2011. BLM-DNA2-RPA-MRN and EXO1-BLM-RPA-MRN constitute two DNA end resection machineries for human DNA break repair. *Genes Dev.* 25:350–362. http://dx.doi.org/10.1101/gad.2003811

Niu, H., W.H. Chung, Z. Zhu, Y. Kwon, W. Zhao, P. Chi, R. Prakash, C. Seong, D. Liu, L. Lu, et al. 2010. Mechanism of the ATP-dependent DNA end-resection machinery from *Saccharomyces cerevisiae*. *Nature*. 467:108–111. http://dx.doi.org/10.1038/nature09318

Peng, G., H. Dai, W. Zhang, H.J. Hsieh, M.R. Pan, Y.Y. Park, R.Y. Tsai, I. Bedrosian, J.S. Lee, G. Ira, and S.Y. Lin. 2012. Human nuclease/helicase DNA2 alleviates replication stress by promoting DNA end resection. *Cancer Res.* 72:2802–2813. http://dx.doi.org/10.1158/0008-5472.CAN-11-3152

Pirzio, L.M., P. Pichierri, M. Bignami, and A. Franchitto. 2008. Werner syndrome helicase activity is essential in maintaining fragile site stability. *J. Cell Biol.* 180:305–314. http://dx.doi.org/10.1083/jcb.200705126

Ray Chaudhuri, A., Y. Hashimoto, R. Herrador, K.J. Neelsen, D. Fachinetti, R. Bermejo, A. Cocito, V. Costanzo, and M. Lopes. 2012. Topoisomerase I poisoning results in PARP-mediated replication fork reversal. *Nat. Struct. Mol. Biol.* 19:417–423. http://dx.doi.org/10.1038/nsmb.2258

Schlacher, K., N. Christ, N. Siaud, A. Egashira, H. Wu, and M. Jasin. 2011. Double-strand break repair-independent role for BRCA2 in blocking stalled replication fork degradation by MRE11. *Cell*. 145:529–542. http://dx.doi.org/10.1016/j.cell.2011.03.041

Published March 2, 2015

Schlacher, K., H. Wu, and M. Jasin. 2012. A distinct replication fork protection pathway connects Fanconi anemia tumor suppressors to RAD51-BRCA1/2. *Cancer Cell*. 22:106–116. http://dx.doi.org/10.1016/j.ccr.2012.05.015

Seigneur, M., V. Bidnenko, S.D. Ehrlich, and B. Michel. 1998. RuvAB acts at arrested replication forks. *Cell*. 95:419–430. http://dx.doi.org/10.1016/S0092-8674(00)81772-9

Sidorova, J.M., N. Li, A. Folch, and R.J. Monnat Jr. 2008. The RecQ helicase WRN is required for normal replication fork progression after DNA damage or replication fork arrest. *Cell Cycle*. 7:796–807. http://dx.doi.org/10.4161/cc.7.6.5566

Sidorova, J.M., N. Li, D.C. Schwartz, A. Folch, and R.J. Monnat Jr. 2009. Microfluidic-assisted analysis of replicating DNA molecules. *Nat. Protoc.* 4:849–861. http://dx.doi.org/10.1038/nprot.2009.54

Sturzenegger, A., K. Burdova, R. Kanagaraj, M. Levikova, C. Pinto, P. Cejka, and P. Janscak. 2014. DNA2 cooperates with the WRN and BLM RecQ helicases to mediate long-range DNA end resection in human cells. *J. Biol. Chem.* 289:27314–27326. http://dx.doi.org/10.1074/jbc.M114.578823

Thangavel, S., R. Mendoza-Maldonado, E. Tissino, J.M. Sidorova, J. Yin, W. Wang, R.J. Monnat Jr., A. Falaschi, and A. Vindigni. 2010. Human RECQ1 and RECQ4 helicases play distinct roles in DNA replication initiation. *Mol. Cell. Biol.* 30:1382–1396. http://dx.doi.org/10.1128/MCB.01290-09

Wawrousek, K.E., B.K. Fortini, P. Polaczek, L. Chen, Q. Liu, W.G. Dunphy, and J.L. Campbell. 2010. Xenopus DNA2 is a helicase/nuclease that is found in complexes with replication proteins And-1/Ctf4 and Mcm10 and DSB response proteins Nbs1 and ATM. *Cell Cycle*. 9:1156–1166. http://dx.doi.org/10.4161/cc.9.6.11049

Wu, L., and I.D. Hickson. 2003. The Bloom's syndrome helicase suppresses crossing over during homologous recombination. *Nature*. 426:870–874. http://dx.doi.org/10.1038/nature02253

Yata, K., J. Lloyd, S. Maslen, J.Y. Bleuyard, M. Skehel, S.J. Smerdon, and F. Esashi. 2012. Plk1 and CK2 act in concert to regulate Rad51 during DNA double strand break repair. *Mol. Cell*. 45:371–383. http://dx.doi.org/10.1016/j.molcel.2011.12.028

Yeo, J.E., E.H. Lee, E.A. Hendrickson, and A. Sobeck. 2014. CtIP mediates replication fork recovery in a FANCD2-regulated manner. *Hum. Mol. Genet.* 23:3695–3705. http://dx.doi.org/10.1093/hmg/ddu078

Yin, J., Y.T. Kwon, A. Varshavsky, and W. Wang. 2004. RECQL4, mutated in the Rothmund-Thomson and RAPADILINO syndromes, interacts with ubiquitin ligases UBR1 and UBR2 of the N-end rule pathway. *Hum. Mol. Genet.* 13:2421–2430. http://dx.doi.org/10.1093/hmg/ddh269

Ying, S., F.C. Hamdy, and T. Helleday. 2012. Mre11-dependent degradation of stalled DNA replication forks is prevented by BRCA2 and PARP1. *Cancer Res.* 72:2814–2821. http://dx.doi.org/10.1158/0008-5472.CAN-11-3417

Zellweger, R., D. Dalcher, K. Mutreja, R. Herrador, M. Berti, A. Vindigni, and M. Lopes. 2015. Rad51-mediated replication fork reversal is a global response to genotoxic treatments in human cells. *J. Cell Biol.* 208:563–579.

Zeman, M.K., and K.A. Cimprich. 2014. Causes and consequences of replication stress. *Nat. Cell Biol.* 16:2–9. http://dx.doi.org/10.1038/ncb2897

Zhu, Z., W.H. Chung, E.Y. Shim, S.E. Lee, and G. Ira. 2008. Sgs1 helicase and two nucleases Dna2 and Exo1 resect DNA double-strand break ends. *Cell*. 134:981–994. http://dx.doi.org/10.1016/j.cell.2008.08.037

SUPPLEMENTAL MATERIAL JCB

Thangalev et al., http://www.jcb.org/cgi/content/full/jcb.201406100/DC1

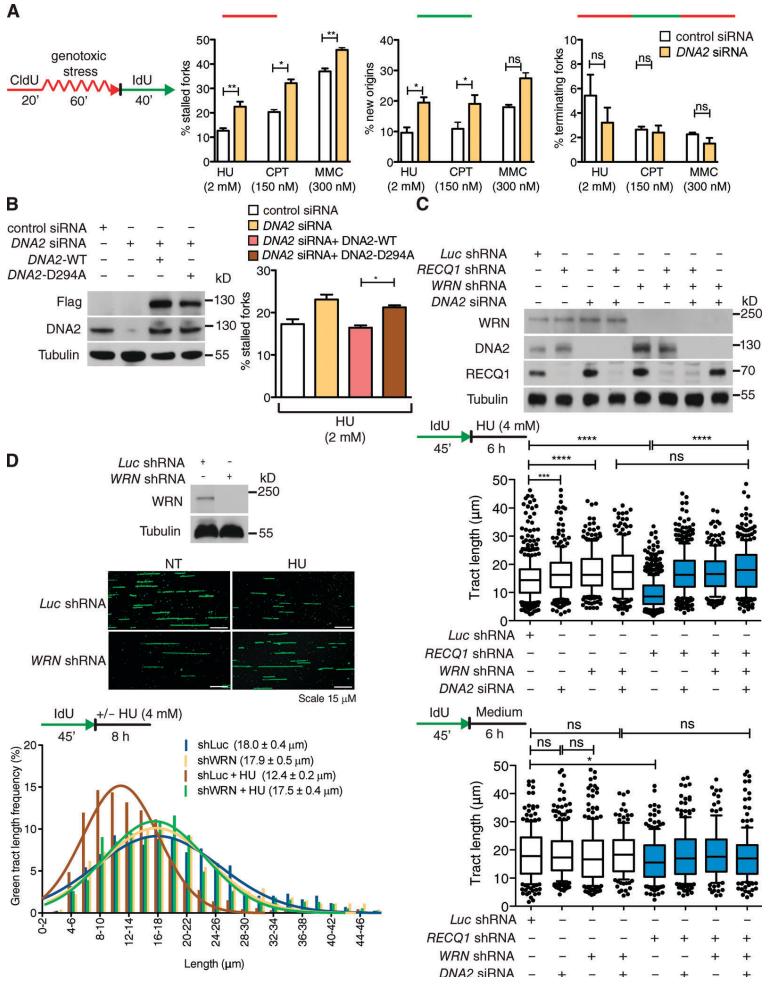

Figure S1. **DNA2 and WRN function in stalled fork processing.** (A, left) Schematic of DNA fiber tract analysis. (right) Quantification of red tracts (stalled forks), green tracts (new origins), and contiguous red–green–red tracts (termination events). Proper quantification of stalled forks is complicated by the fact that termination events might also lead to red tracts if termination occurs before the addition of the second label. Mean shown, $n = 3$. Error bars, standard error. ns, not significant; *, $P < 0.05$; **, $P < 0.01$; ***, $P < 0.001$ (paired Student's t test). (B, left) Expression of Flag-tagged WT (DNA2-WT) or nuclease-dead (DNA2-D294A) DNA2 in DNA2-depleted U-2 OS cells. (right) Quantification of stalled forks in DNA2-depleted cells expressing DNA-WT or DNA2-D294A. Mean shown, $n = 3$. Error bars, standard error. ns, not significant; *, $P < 0.05$ (paired t test). (C, top) Expression of RECQ1, WRN, DNA2, and tubulin in U-2 OS cells transfected with the indicated shRNA or siRNA. (middle) Statistical analysis of IdU tracts from U-2 OS cells depleted for the indicated proteins in the presence of 4 mM HU. (bottom) Statistical analysis of IdU tracts from U-2 OS cells depleted for the indicated proteins in the absence of drug treatment. Whiskers indicate the 10th and 90th percentiles. ns, not significant (Mann-Whitney test). $n \geq 300$ scored for each dataset. (D, top) Expression of WRN after WRN knockdown and representative fiber tract images in Luc- and WRN-depleted U-2 OS cells. Bar, 15 µm. Representative IdU tracts in WRN-depleted U-2 OS cells in the presence or absence of HU (out of 2 repeats; $n \geq 700$ scored for each dataset).

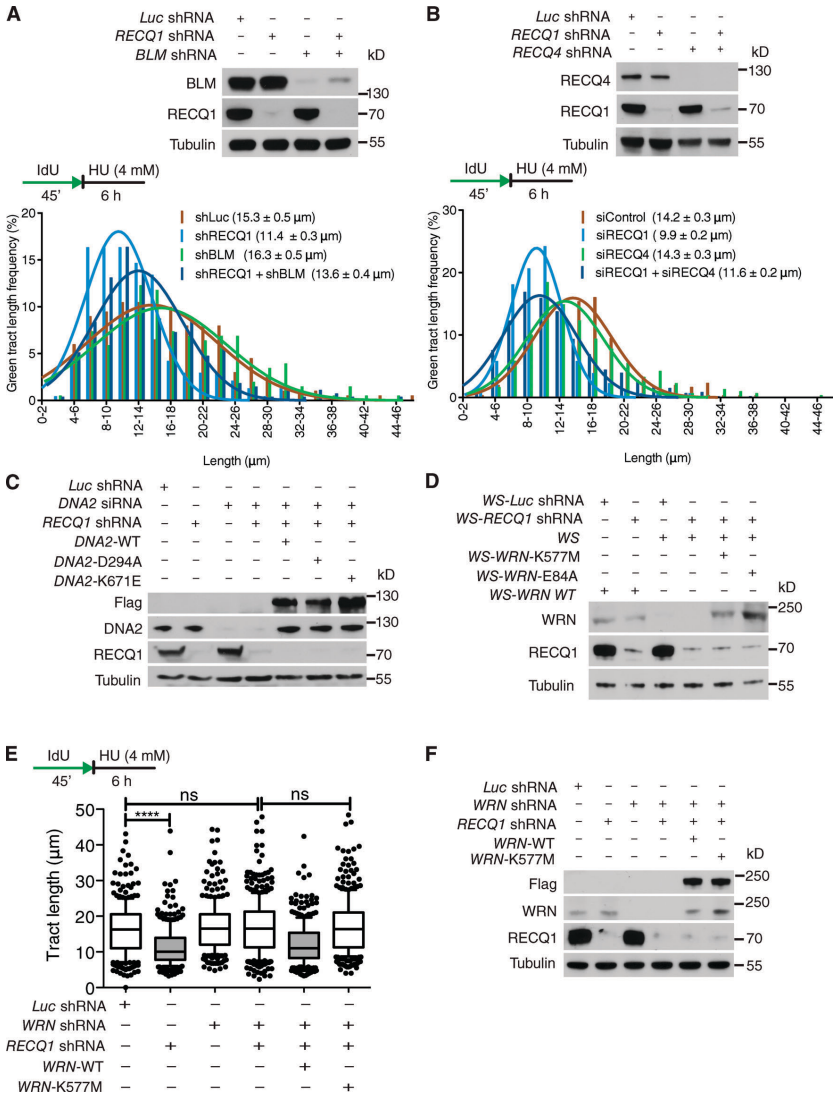

Figure S2. **BLM or RECQ4 depletion does not have a significant effect on stalled fork processing.** (A) Representative IdU tracts in Luc-, RECQ1-, BLM-, or RECQ1/BLM-codepleted U-2 OS cells in the presence of HU (out of 2 repeats; $n \geq 300$ scored for each dataset). (top) Expression of RECQ1, BLM and tubulin in U-2 OS cells transfected with indicated shRNA. (B) Representative IdU tracts in control, RECQ1-, RECQ4-, or RECQ1/RECQ4-codepleted U-2 OS cells in the presence of HU (out of 2 repeats; $n \geq 350$ scored for each dataset). (top) Expression of RECQ1, RECQ4 and tubulin in U-2 OS cells transfected with indicated shRNA. (C) Expression of RECQ1, DNA2-WT, DNA2-K671E, and DNA2-D294A in U-2 OS cells transfected with the indicated shRNA or siRNA. (D) Expression of RECQ1, WRN-WT, WRN-K577M, and WRN-E84A in WS cells. (E) Statistical analysis of IdU tracts from RECQ1-, WRN-, or RECQ1/WRN-codepleted U-2 OS cells. The RECQ1/WRN-codepleted cells were complemented with WT or ATPase-deficient (K577M) WRN, where indicated. Whiskers indicate the 10th and 90th percentiles. ns, not significant; ****, $P < 0.0001$ (Mann-Whitney test). (F) Expression of RECQ1, WRN-WT, and WRN-K577M in U-2 OS cells transfected with the indicated shRNA.

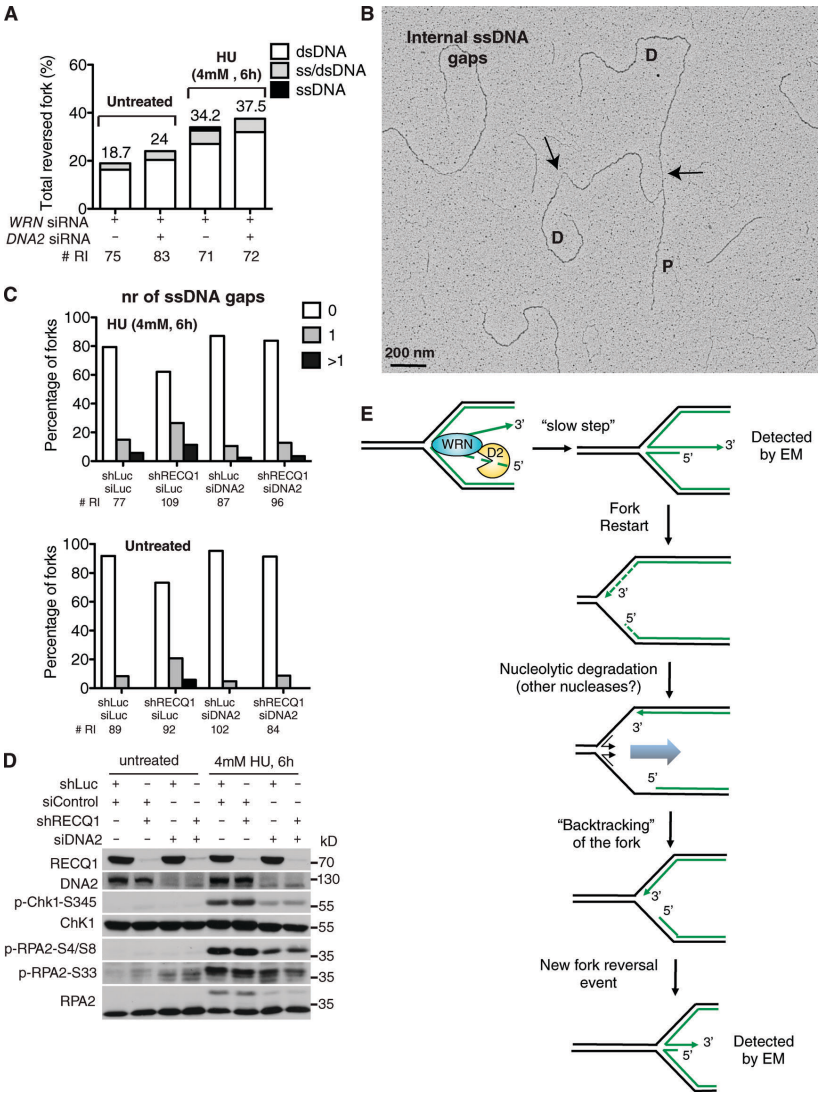

Figure S3. **DNA2 promotes ssDNA gap accumulation on replicated duplexes and the ATR-mediated checkpoint activation.** (A) Frequency of fork reversal and ssDNA composition of the reversed arms in WRN- and/or DNA2-depleted U-2 OS cells in the presence and absence of HU. The percentage values are indicated on the top of the bar. "# RI" indicates the number of analyzed replication intermediates. (B) Representative electron micrographs of replication forks displaying ssDNA gaps on the replicated duplexes or at the replication fork junction observed on genomic DNA in shRECQ1 U-2 OS cells upon HU-treatment. The black arrows point to ssDNA gaps. D, Daughter strand; P, Parental strand. (C) Statistical distribution of ssDNA gaps on newly replicated duplexes in RECQ1- and/or DNA2-depleted U-2 OS cells treated with HU (top) or in unperturbed conditions (bottom). "# RI" is the number of analyzed replication intermediates. (D) Western blot analysis of ATR-checkpoint activation (pChk1 and pRPA) in RECQ1- and/or DNA2-depleted U-2 OS cells with or without HU treatment. Total Chk1 and RPA level are displayed and used as loading control. (E) Schematic of the different structures detected by EM and DNA fibers. EM is a static method, which enriches for snapshots of the "slow steps" of a reaction (i.e., partially resected reversed forks). After fork restart, the nucleolytic degradation quickly proceeds to degrade nascent strands behind the junction. Reannealing of the parental strands leads to "backtracking" of the fork. A new reversal event arises as a consequence of asymmetric degradation, and thus ssDNA accumulation in proximity to the fork. Backtracking is easily detected by DNA fiber, but not by EM because a reversed fork formed after degradation and backtracking is indistinguishable from the original reversed fork present before initial degradation.

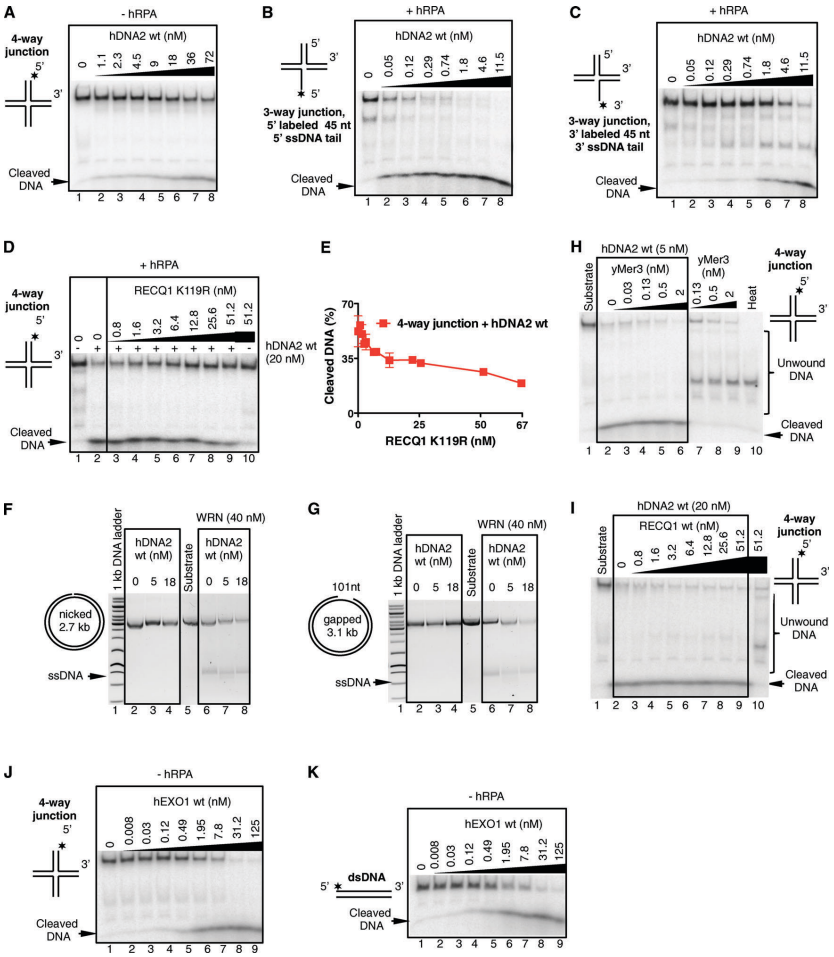

Figure S4. **Human DNA2 but not EXO1 preferentially degrades branched DNA.** (A) Degradation of a four-way junction by hDNA2 without human RPA (hRPA). Reaction products were separated on a native polyacrylamide gel (6%); *, position of the ^{32}P label. (B) Degradation of a three-way junction with a 5′ ssDNA tail by hDNA2 in the presence of hRPA (22.3 nM). Reaction products were separated on a native polyacrylamide gel (6%); *, position of the ^{32}P label. (C) Same experiment as in B, but with a junction containing a 3′ ssDNA tail. (D) RECQ1 K119R (ATPase-dead) inhibits four-way junction degradation by hDNA2. Increasing concentrations of RECQ1 (K119R) were preincubated with the substrate, and then hDNA2 (20 nM) was added to the reaction mixture. All reactions contained hRPA (65 nM). Reaction products were separated on a native polyacrylamide gel (6%); *, position of the ^{32}P label. (E) Quantitation of data from D. Averages shown ± SEM, $n = 2$. (F) Synergistic action of hDNA2 and WRN on a nicked plasmid based DNA substrate. The reactions contained 614 nM hRPA and were incubated at 37°C for 60 min. Products were separated on a 1% agarose gel and stained with GelRed. WRN helicase promotes degradation of nicked DNA by hDNA2. (G) Same experiment as in F, but with a gapped DNA substrate. (H) Degradation of a four-way junction by hDNA2 and *S. cerevisiae* Mer3. hDNA2 only degrades ssDNA unwound by Mer3, no synergy in DNA degradation was observed. All reactions contained hRPA, and were analyzed on a native polyacrylamide gel (6%). (I) Degradation of four-way junction by hDNA2 is not stimulated by WT hRECQ1. All reactions contained hRPA (65 nM). Reaction products were separated on a native polyacrylamide gel (6%). (J) Degradation of a four-way junction by hEXO1. Reaction products were separated on a native polyacrylamide gel (6%); *, position of the ^{32}P label. (K) Same experiment as in J, but with dsDNA.

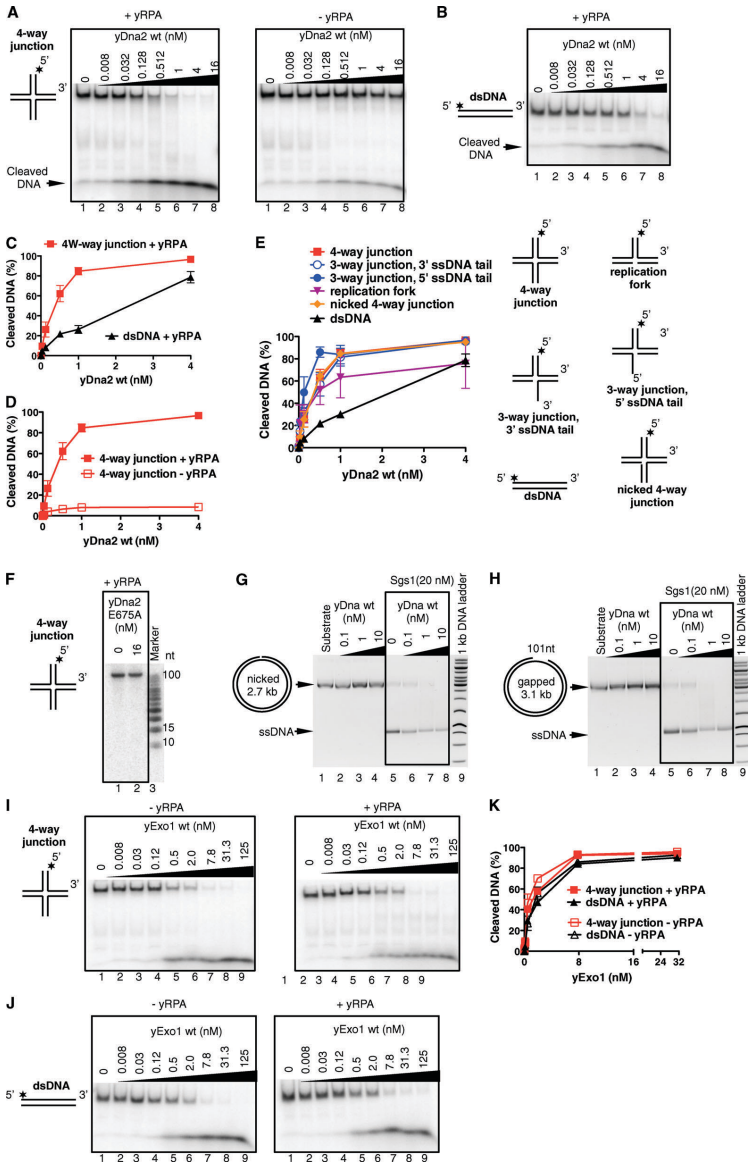

Figure S5. **Yeast Dna2 but not Exo1 preferentially degrades branched DNA.** (A) Degradation of a four-way junction by yDna2 in presence (left) or absence (right) of yeast RPA (yRPA). Reactions were separated on a native polyacrylamide gel (6%), *, position of the ^{32}P label. (B) Experiment as in A, but with dsDNA and yRPA. (C) Yeast Dna2 preferentially degrades four-way junctions in the presence of yRPA. Quantitation of data from A and B. Averages shown ± SEM; *n* = 2. (D) yRPA promotes DNA degradation by yDna2. Quantitation of data from A. The data points representing the degradation of a four-way junction in the presence of yRPA are identical to those from C. Mean shown ± SEM, *n* = 2. (E) Yeast Dna2 preferentially degrades branched structures over dsDNA. Quantitation of degradation of various DNA substrates as indicated (cartoons on the right) by yDna2 WT in presence of yRPA. Averages shown ± SEM; *n* = 2. (F) Denaturing 20% polyacrylamide gel showing that nuclease-dead yDna2 E675A variant does not degrade the four-way junction substrate. (G) Synergistic action of yDna2 and Sgs1 helicase on a nicked dsDNA plasmid based substrates. The reactions contained 770 nM yRPA and were incubated at 30°C for 60 min before being separated on a 1% agarose gel containing GelRed. (H) Experiment as in G, but with gapped DNA substrate. (I) Degradation of a four-way junction by yExo1 in the presence (right) or absence (left) of yRPA. (J) Same experiment as in I, but with dsDNA. (K) Quantitation of data from I and J. Averages shown ± SEM, *n* = 2.

2.3.3 DNA2 cooperates with WRN and BLM RecQ helicases to mediate long-range DNA end resection in human cells

Andreas Sturzenegger, Kamila Burdova, Radhakrishnan Kanagaraj, Maryna Levikova, **Cosimo Pinto**, Petr Cejka and Pavel Janscak

The article was published in the J. Biol. Chem. 2014, 289:27314-27326.

My contribution to this publication was the expression and purification of recombinant human DNA2 together with M. L. and P.C.

THE JOURNAL OF BIOLOGICAL CHEMISTRY VOL. 289, NO. 39, pp. 27314–27326, September 26, 2014

DNA2 Cooperates with the WRN and BLM RecQ Helicases to Mediate Long-range DNA End Resection in Human Cells*

Received for publication, May 3, 2014, and in revised form, August 12, 2014 Published, JBC Papers in Press, August 13, 2014, DOI 10.1074/jbc.M114.578823

Andreas Sturzenegger[‡1], **Kamila Burdova**[§1], **Radhakrishnan Kanagaraj**[‡2], **Maryna Levikova**[‡], **Cosimo Pinto**[‡], **Petr Cejka**[‡], **and Pavel Janscak**[‡§3]

From the [‡]*Institute of Molecular Cancer Research, University of Zurich, 8057 Zurich, Switzerland and the* [§]*Institute of Molecular Genetics, Academy of Sciences of the Czech Republic, 14300 Prague, Czech Republic*

Background: DNA end resection is a critical step in the homology-directed repair of DNA double strand breaks (DSBs).
Results: Human WRN helicase stimulates the DNA2-catalyzed resection of DNA ends and acts in concert with DNA2 to promote DSB repair by single strand annealing.
Conclusion: DNA2 cooperates with WRN or BLM to mediate the resection of DSBs in mammalian cells.
Significance: Defects in DNA end resection might, in part, account for the genomic instability phenotype of Werner syndrome.

The 5′-3′ resection of DNA ends is a prerequisite for the repair of DNA double strand breaks by homologous recombination, microhomology-mediated end joining, and single strand annealing. Recent studies in yeast have shown that, following initial DNA end processing by the Mre11-Rad50-Xrs2 complex and Sae2, the extension of resection tracts is mediated either by exonuclease 1 or by combined activities of the RecQ family DNA helicase Sgs1 and the helicase/endonuclease Dna2. Although human DNA2 has been shown to cooperate with the BLM helicase to catalyze the resection of DNA ends, it remains a matter of debate whether another human RecQ helicase, WRN, can substitute for BLM in DNA2-catalyzed resection. Here we present evidence that WRN and BLM act epistatically with DNA2 to promote the long-range resection of double strand break ends in human cells. Our biochemical experiments show that WRN and DNA2 interact physically and coordinate their enzymatic activities to mediate 5′-3′ DNA end resection in a reaction dependent on RPA. In addition, we present *in vitro* and *in vivo* data suggesting that BLM promotes DNA end resection as part of the BLM-TOPOIIIα-RMI1-RMI2 complex. Our study provides new mechanistic insights into the process of DNA end resection in mammalian cells.

DNA double strand breaks (DSBs)[4] are a very dangerous form of DNA damage because they can cause cell death or chromosomal rearrangements, a hallmark of cancer (1). DSBs can occur accidentally during normal cellular metabolism or upon exposure of cells to exogenous agents such as ionizing radiation and radiomimetic drugs (2). There are also programmed DSBs that drive recombination events essential for physiological processes, such as meiosis and lymphocyte development (3, 4). In eukaryotic cells, DSBs are repaired by one of two major pathways: non-homologous end joining (NHEJ) and homologous recombination (HR). NHEJ involves religation of the broken DNA ends and is frequently associated with a short deletion or insertion of DNA at the break site (5). In contrast, HR restores the DNA integrity accurately because it uses sister chromatids or homologous chromosomes as a template for repair (6, 7). HR is initiated by resection of the broken DNA ends to generate 3′ single-stranded (ss) DNA tails that are utilized by the RAD51 recombinase for a homology search on the donor DNA molecule (6, 7). Genetic and biochemical studies in budding yeast have shown that broken DNA ends are resected in a two-step process (8–10). DNA end resection in yeast is initiated by the Mre11-Rad50-Xrs2 complex in conjunction with Sae2 (8, 9, 11). These proteins may initiate resection of the 5′ strand of the broken DNA to remove a stretch of about 100–200 nucleotides from the DNA end (8, 9, 11). The Mre11-Rad50-Xrs2 complex also recruits the components of the long-range resection pathways Exo1 or Dna2-Sgs1 (8–10, 12, 13). Exo1 is a dsDNA-dependent 5′-3′ exonuclease that preferentially degrades DNA substrates with a 3′ ssDNA tail in a reaction stimulated by the ssDNA-binding protein RPA (13). Dna2 is a ssDNA-specific nuclease and a DNA helicase that functions in conjunction with the RecQ family DNA helicase Sgs1 and RPA to catalyze long-range DNA end resection (10, 14). In this reaction, RPA stimulates DNA unwinding by Sgs1 and promotes degradation of the 5′-terminated strand by Dna2 while protecting the growing 3′ ssDNA tail (10). DNA end resection is also the initial step in two other DSB repair pathways, single strand annealing (SSA) and microhomology-mediated end joining (8, 15).

The molecular machinery of DNA end resection appears to be largely conserved between yeast and man (15–19). However, it remains a matter of debate which DNA helicase mediates DNA2-catalyzed resection in mammalian cells. Mammals pos-

* This work was supported by Swiss National Science Foundation Grants 31003A-129747 and 31003A_146206, by Czech Science Foundation Grant GAP305/10/0281, and by the Stiftung zur Krebsbekämpfung. This work was also supported by Swiss National Science Foundation Grant PP00P3 133636 (to P.C.) and by Forschungskredit of the University of Zurich Grant FK-13-098 (to A. S.).
[1] Both authors contributed equally to this work.
[2] Present address: London Research Institute, Cancer Research UK, Clare Hall Laboratories, South Mimms, Herts, EN6 3LD, UK.
[3] To whom correspondence should be addressed: Institute of Molecular Cancer Research, University of Zurich, Winterthurerstr. 190, 8057 Zurich, Switzerland. Tel.: 41-44-6353470; Fax: 41-44-6353484; E-mail: pjanscak@imcr.uzh.ch.
[4] The abbreviations used are: DSB, double strand break; NHEJ, non-homologous end joining; HR, homologous recombination; ssDNA, single-stranded DNA; SSA, single strand annealing; BTRR, BLM-TOPOIIIα-RMI1-RMI2; nt, nucleotide(s); CPT, camptothecin.

sess five RecQ homologues: RECQ1, BLM, WRN, RECQ4, and RECQ5 (20). Biochemical studies have shown that human DNA2 can act in conjunction with the BLM helicase and RPA to mediate 5′-3′ resection of DNA ends *in vitro* (17). In agreement with these findings, it has been observed that cells depleted of both BLM and EXO1 show a reduction in the formation of RPA foci in response to DSBs and are defective in DSB repair by HR (16, 19). However, studies using *Xenopus* egg extracts and purified proteins have shown that Dna2 mediates DNA end resection together with WRN rather than BLM (21–23). This discrepancy prompted us to investigate the role of WRN in DNA end resection in human cells. Here we demonstrate that WRN helicase is capable of acting in concert with DNA2 and RPA to resect 5′-recessed DNA ends *in vitro* with a catalytic efficiency even higher than that of BLM. Moreover, our results show that human cells may employ either BLM or WRN to assist DNA2 in long-range DNA end resection. Finally, we present data suggesting that BLM acts in DNA end resection as part of the BLM-TOPOIIIα-RMI1-RMI2 (BTRR) complex.

EXPERIMENTAL PROCEDURES

Antibodies and siRNA—Primary antibodies used for immunoblotting were as follows: mouse monoclonal anti-WRN (BD Biosciences, catalog no. 611169), rabbit polyclonal anti-DNA2 (Abcam, catalog no. ab96488), rabbit polyclonal anti-BLM (Abcam, catalog no. ab476), rabbit polyclonal anti-TFIIH (Santa Cruz Biotechnology, catalog no. sc293), mouse monoclonal anti-FLAG (Sigma, catalog no. F1804), and rabbit polyclonal anti-RMI1 (Proteintech, catalog no. 14630-1-AP). Anti-FLAG M2 magnetic beads (Sigma) were used for immunoprecipitation. Primary antibodies used for immunofluorescence staining were as follows: mouse monoclonal anti-RPA2 (Abcam, catalog no. ab2175) and rabbit monoclonal anti-γ-H2AX (Cell Signaling Technology, catalog no. 9718S). Rabbit polyclonal anti-WRN antibody used for immunoprecipitation has been described previously (24).

All siRNA oligoduplexes used in this study were purchased from Microsynth. The sequences of the sense strands of these duplexes were as follows: siLuc, 5′-CGUACGCGGAAUACUUCGAdTdT-3′; siWRN, 5′-UAGAGGGAAACUUGGCAAAdTdT-3′; siBLM, 5′-CCGAAUCUCAAUGUACAUAGAdTdT-3′; siDNA2, 5′-UACCGCUUAAAUCUAAGUCAAdTdT-3′; siEXO1, 5′-CAGCCAUUCUUACUACGCUAAdTdT-3′; siMRE11, 5′-GAGCAUAACUCCAUAAGUAdTdT-3′ (25); siCtIP, 5′-UCCACAACAUAAUCCUAAUdTdT-3′ (26); and siRMI1, 5′-AGCCUUCACGAAUGUUGAUdTdT-3′ (27).

Plasmid Constructions—The human DNA2 (hDNA2) ORF was amplified by PCR without the initiation and stop codons to generate a fragment including ggatcc-hDNA2-ctcgag. After digestion with BamHI and XhoI, the hDNA2 fragment was cloned into pFLAG-CMV2 (Sigma) digested with BglII/SalI (pFLAG-CMV2-hDNA2). The human WRN (hWRN) ORF was inserted into pcDNA3.1/Hygro(−) (Invitrogen) via the NheI and DraI sites (pcDNA3.1-hWRN). The siRNA-resistant form of this construct was generated by changing four nucleotides in the siWRN-targeting region (T270C, A273G, G276C, and A279G) using the QuikChange site-directed mutagenesis kit (Stratagene).

Protein Purifications—Wild-type and mutant forms of WRN, BLM, EXO1, and RPA were produced and purified as described previously (28–31). The TOPOIIIα-RMI1-RMI2 (TRR) complex was a gift from Drs. Kata Sarlos and Ian Hickson (University of Copenhagen, Denmark). DNA2 was produced as a fusion with a His_6 tag (N terminus) and a FLAG tag (C terminus) in Sf9 cells using the Bac-to-Bac baculovirus expression system (Invitrogen). The transfer vector for bacmid preparation was a gift from Dr. Judith L. Campbell (32). The transfer vectors for nuclease-deficient (D227A) and helicase-deficient (K654R) mutants of DNA2 were generated using the QuikChange site-directed mutagenesis kit (Stratagene). Sf9 cells expressing DNA2 fusion proteins were harvested 52 h after infection (typically a 800-ml culture) and washed with PBS. All subsequent steps were carried out at 4 °C. Pelleted cells were resuspended in lysis buffer (25 mM Tris-HCl (pH 7.5), 2 mM β-mercaptoethanol, 1× complete EDTA-free protease inhibitor (Roche), 1 mM phenylmethylsulfonyl fluoride, 30 μg/ml leupeptin, and 15 mM imidazole) and incubated for 20 min under continuous stirring. Subsequently, glycerol and 5 M NaCl were added slowly to final concentrations of 15% (v/v) and 300 mM, respectively, while mixing the sample. The cell suspension was then incubated for an additional 30 min under continuous stirring. The cell lysate was centrifuged at 55,000 × *g* for 30 min to obtain soluble extract, which was then incubated with 5 ml of nickel-nitrilotriacetic acid-agarose beads (Qiagen) for 1 h batchwise. The resin was washed extensively with lysis buffer containing 10% (v/v) glycerol and 1 M NaCl. The protein was eluted with lysis buffer supplemented with 10% (v/v) glycerol, 100 mM NaCl, and 250 mM imidazole. Fractions containing detectable amounts of protein, as measured by Bradford assay, were pooled, diluted 1:1 with TBS buffer (50 mM Tris-HCl (pH 7.5) and 150 mM NaCl) and incubated batchwise with 1 ml of anti-FLAG M2 affinity resin (Sigma) for 30 min. The resin was then transferred to a gravity flow column and washed with TBS-PI buffer (TBS buffer containing 1 mM β-mercaptoethanol and 5 μg/ml leupeptin). Elution of the protein was achieved by adding TBS-PI buffer supplemented with 200 μg/ml 3× FLAG peptide (Sigma). Fractions containing DNA2 were pooled, diluted with 0.5 volumes of water and 1 volume of AQ buffer (25 mM Tris-HCl (pH 7.5), 100 mM NaCl, 10% (v/v) glycerol, and 5 mM β-mercaptoethanol) and loaded onto a 1-ml HiTrap Q column (GE Healthcare) pre-equilibrated with AQ buffer. The column was washed with AQ buffer and DNA2 was eluted by AQ buffer supplemented with 600 mM NaCl. Fractions containing DNA2 were identified by SDS-PAGE, pooled, and stored at −80 °C. The activity of purified recombinant DNA2 proteins was tested using a Y structure oligonucleotide duplex with single-stranded arms (10). In agreement with previous reports, wild-type DNA2 was found to be capable of degrading both ssDNA arms of this structure (data not shown) (10, 17). In the presence of RPA, the cleavage of the 3′ ssDNA arm by DNA2 was inhibited, and DNA2 degraded preferentially the 5′ ssDNA arm (data not shown) (10, 17). The DNA2-D227A mutant did not contain any nuclease activity, which indicated that the nuclease activity of our wild-type DNA2 preparation was inherent to DNA2 (data not shown).

The Role of WRN and BLM in DNA End Resection

Nuclease and Helicase Assays—To test the activity of purified DNA2, we used a 31-bp forked duplex with 19-nt ssDNA arms, as described previously (10). The helicase activity of WRN and BLM was tested using a 29-bp forked duplex generated by annealing of the following oligonucleotides: f-9 (5′-ACTATCATTC AGTCATGTAA CCTAGTCAAT CTGCGAGCTC GAATTCACTG GAGTGACCT-3′) and f-10 (5′-GAGGTCACTC CAGTGAATTC GAGCTCGCAG TCAATGTCGA CATACCTAGT ACTTTACTCC-3′). Both DNA substrates were radiolabeled at the end of the 5′ ssDNA arm.

Nuclease and helicase assays were performed in buffer containing 25 mM Tris acetate (pH 7.5), 2 mM magnesium acetate, 1 mM dithiothreitol, 0.1 mg/ml BSA, 10.7 mM phosphocreatine, and 0.02 mg/ml creatine phosphokinase. Reactions (15 μl) contained 1 nM ^{32}P-labeled forked DNA substrate and the indicated concentrations of DNA2 or WRN/BLM. Where indicated, RPA was present at a concentration of 6 nM. Reactions were assembled on ice and started by addition of ATP to a concentration of 1 mM. Reactions were incubated for 30 min at 37 °C. Termination of the reactions was achieved by adding 1/3 volume of stop solution (150 mM EDTA, 2% (w/v) SDS, 30% (v/v) glycerol, and 0.1% (w/v) bromphenol blue) and 1/15 volume of Proteinase K (10 mg/ml), followed by incubation at 37 °C for 15 min. The reaction products were separated by electrophoresis in a 10% Tris borate-EDTA polyacrylamide gel. Gels were dried on Whatman MM3 paper and analyzed by phosphorimaging using a Typhoon 9400 scanner (GE Healthcare). Images were quantified using ImageQuantTL software.

Construction of DNA Substrates for Resection Assays—The DNA substrates used in resection assays were derived from the plasmid pUC19 (2686 bp). The self-complementary oligonucleotide, 5′-AGCT GCTGAGG GCTGAGG GCTGAGG GCTGAGG AGGCCT CCTCAGC CCTCAGC CCTCAGC CCTCAGC-3′, was annealed to form a duplex that was cloned into the HindIII site of pUC19. This destroyed the HindIII site and inserted a single recognition sequence for StuI (AGGCCT) flanked on each side by four recognition sequences for the nickase Nt.BbvCI (CC*TCAGC; the cleavage position is indicated by the asterisk) that are oriented as an inverted repeat with respect to the StuI site. The resulting pOH-S plasmid allowed us to prepare a linear DNA substrate with 3′ overhangs of 26 nucleotides (nt) in length. A blunt-ended substrate was generated by digestion of pOH-S with StuI (New England Biolabs), followed by DNA purification using a Macherey Nagel NucleoSpin® gel and PCR cleanup kit. The substrate with 26-nt 3′ overhangs was generated as follows. After digestion of pOH-S with StuI and its heat inactivation, Nt.BbvCI (New England Biolabs) was added, and the reaction was incubated further for 2 h at 37 °C. Subsequently, the reaction mixture was diluted six times with water and incubated at 85 °C for 15 min. DNA purification was performed as described above. DNA concentration was determined using a NanoDrop ND-1000 spectrophotometer (Witec AG).

DNA End Resection Assays—DNA end resection reactions were carried out in a buffer containing 25 mM Tris acetate (pH 7.5), 2 mM magnesium acetate, 1 mM dithiothreitol, 0.1 mg/ml BSA, 10.7 mM phosphocreatine, 0.02 mg/ml creatine phosphokinase, and 1 mM ATP. Reactions contained 2 nM DNA substrate (molecules), 8 nM DNA2, 350 nM RPA (100% DNA strand coverage, assuming all DNA was single-stranded), and various concentrations of WRN or BLM as indicated. EXO1 was present at a concentration of 20 nM. The reactions were assembled on ice and initiated by the addition of ATP. Reaction mixtures (15 μl) were incubated at 37 °C for 60 min in the case of protein titration experiments. In time course experiments, 15-μl reaction aliquots were withdrawn at defined time points as indicated. Reactions were terminated as described for the helicase assays. The samples were subjected to electrophoresis in a 1% agarose gel run in 1× TAE buffer. Gels were post-stained with SYBR Gold (Invitrogen) and analyzed using MultiImage Light Cabinet (Alpha Innotech). To monitor resection by hybridization of radiolabeled oligonucleotide probes, terminated reactions (21 μl) were divided equally into two tubes. 5′ end-labeled oligonucleotide probes were then added to a final concentration of 5 nM. This mixture was heated in an oven to 75 °C for 5 min and then slowly cooled down to room temperature over 2.5 h. Reaction products were separated by electrophoresis in a 1% agarose gel. Gels were dried on DE81 anion exchange paper (Whatman) and subjected to phosphorimaging analysis using a Typhoon 9400 scanner (GE Healthcare). Images were quantified using ImageQuantTL software. The relative concentration of the resection products generated in WRN-DNA2 or BLM-DNA2 reactions was calculated as a percentage of the product generated in a reaction containing 20 nM EXO1 at the 2-min time point, which led to 100% resection within the region probed with radiolabeled oligonucleotides. Usually, the EXO1 reaction was loaded on each gel in triplicates. The following oligonucleotides were used for the preparation of the hybridization probes: oligo#224, 5′-GGCCGTCGTTTTACAACGTCGT-3′ (it anneals to the 3′-terminated strand; annealing position, 112–133 nt upstream of the StuI cleavage site; the complementary sequence is underlined); oligo#227, 5′-GGCATAGTTAAGCCAGCCCCGA-3′ (it anneals to the 3′-terminated strand; annealing position, 353–374 nt upstream of the StuI cleavage site); and oligo#237, 5′-GGTCGGGGCTGGCTTAACTATG-3′ (it anneals to the 5′-terminated strand; annealing position, 122–133 nt upstream of the StuI cleavage site). Oligonucleotides were 5′ end-labeled using [γ-^{32}P]ATP and T4 polynucleotide kinase (New England Biolabs). The two noncomplementary dG residues at the 5′ end of the oligonucleotides were added to ensure equal labeling efficiency.

Cell Culture and Transfection—U2OS and HEK293 cells were grown in DMEM (Sigma) supplemented with 10% fetal calf serum (Invitrogen) and streptomycin/penicillin (100 units/ml). Plasmid DNA was transfected using standard linear polyethyleneimine method. Lipofectamine RNAiMAX (Invitrogen) was used for siRNA transfection. To generate HEK293 clones stably expressing FLAG-DNA2, cells were cotransfected with pFLAG-CMV2-hDNA2 and pBABE-puro (Addgene) and subjected to puromycin 1 (μg/ml) selection. Puromycin-resistant clones were tested for expression of FLAG-DNA2 by Western blotting.

Immunoprecipitation—HEK293 cells were transfected with the pcDNA3.1-hWRN and/or pFLAG-CMV2-hDNA2 vectors. Cells were harvested to lysis buffer (50 mM Tris-HCl (pH 8.0), 120 mM NaCl, 20 mM NaF, 15 mM sodium pyrophosphate, and

0.5% (v/v) Nonidet P-40) supplemented before use with protease (Complete EDTA-free, Roche) and phosphatase (PhosSTOP, Roche) inhibitors, 2 mM $MgCl_2$ and benzonase (50 units/ml). Cells were sonicated briefly, and lysates were clarified by centrifugation at 16,000 × *g* for 30 min. Cell extracts (1 mg of protein) were subjected to immunoprecipitation using anti-FLAG M2 magnetic beads (10 μl) or Protein A/G Plus UltraLink Resin (10 μl, Thermo Scientific) coated with rabbit polyclonal anti-WRN antibody (10 μg), which was carried out overnight at 4 °C. Immunoprecipitates were washed four times with lysis buffer. Bound proteins were eluted by Laemmli sample buffer and analyzed by SDS-PAGE and Western blotting. To test the interaction between purified WRN and DNA2 proteins, 500 ng of each protein was mixed in 200 μl of NET-N100 buffer (10 mM Tris-HCl (pH 8.0), 1 mM EDTA, 100 mM NaCl, and 0.5% (v/v) Nonidet P-40) and incubated at 4 °C for 4 h. As a control, DNA2 was incubated in the absence of WRN. The protein mixtures were subsequently subjected to immunoprecipitation using anti-WRN antibody (4 μg), which was carried out at 4 °C for 2 h. Immunoprecipitates were washed four times with NET-N100 buffer. Bound proteins were eluted by Laemmli sample buffer and analyzed by SDS-PAGE and Western blotting.

GST Pulldown Assay—GST-tagged fragments of WRN were produced in the *Escherichia coli* BL21-CodonPlus(DE3)-RIL strain (Stratagene) and bound to GSH Sepharose 4B (GE Healthcare) as described previously (24). As a control, beads were coated with GST protein only. The beads were incubated with 500 ng of purified His_6-DNA2-FLAG protein in 400 μl of NET-N100 buffer at 4 °C for 2 h. After extensive washing with NET-N100 buffer, proteins bound to the beads were analyzed by Western blotting. Blots were first stained in Ponceau S solution (0.1% (w/v) Ponceau S and 5% (v/v) acetic acid) to visualize WRN fragments and subsequently probed with anti-FLAG antibody.

Reverse Transcription and Quantitative Real-time PCR—Total RNA was isolated from cells using the RNeasy mini kit (Qiagen). 200 ng of RNA was used for cDNA synthesis using a high-capacity cDNA reverse transcription kit (Applied Biosystems). The target gene expression level was determined by quantitative real-time PCR that was performed on a ABI Prism 7300 (Applied Biosystems) using SYBR Select Master Mix (Applied Biosystems). The following primer pairs were used to determine EXO1 mRNA levels: 5′-ACCTCTAAGG AACAAGGTTC-3′ (forward) and 5′-AGGAGGAAGC TTTTC-AGAATC-3′ (reverse). The housekeeping gene RPLPO, used as a control, was amplified with the following primers: 5′-CCAG-TCTGGA GAAACTGCTG-3′ (forward) and 5′-CAGCAG-CTGG CACCTTATTGG-3′ (reverse). The Pfaffl equation was used for normalization and calculation of relative EXO1 expression levels in comparison with the control gene (33).

SA-GFP Reporter Assay—SA-GFP reporter assays were performed as described previously (34, 35). HEK293/SA-GFP cells were seeded in poly-L-lysine-coated 6-well plates at a density of 0.5 million cells/well. U2OS/SA-GFP cells were seeded in 6-well plates at a density of 0.25 million cells/well. The next day, cells were transfected with appropriate siRNA (40 nM) using Lipofectamine RNAiMAX (Invitrogen). After 24 h, siRNA-transfected cells were transferred into a 12-well plate, with 200,000 cells/well for HEK293/SA-GFP and 100,000 cells/well for U2OS/SA-GFP. 44 h after siRNA transfection, cells were transfected with 0.6 μg of the I-SceI expression vector pCBASce (36) using linear polyethyleneimine and, 6 h later, with appropriate siRNA (20 nM) using the standard calcium phosphate method. 52 h after I-SceI transfection, cells were harvested and subjected to flow cytometry analysis using LSRII (BD Biosciences) and FlowJo software to determine the percentage of GFP-positive cells. The mean values obtained with control siRNA (siLuc) samples were 0.9% for HEK293/SA-GFP cells and 2.0% for U2OS/SA-GFP cells. To test the effect of ectopic expression of WRN on SSA repair efficiency of WRN-depleted HEK293/SA-GFP cells, the mutant form of the pcDNA3.1-hWRN construct harboring silent mutations in the siWRN-targeting region (0.6 μg) was cotransfected with pCBASce (0.6 μg). The plasmid pcDNA3.1 was used as a control vector in these experiments. Cells were subjected to flow cytometry analysis at 52 h after plasmid transfection.

Immunofluorescence Assays—U2OS cells transfected with the indicated siRNAs were cultured on glass coverslips. 48 h after siRNA transfection, cells were treated with 1 μM camptothecin (CPT) for 1 h. After pre-extraction for 5 min on ice in 25 mM HEPES (pH 7.4) buffer containing 0.5% (v/v) Triton X-100, 50 mM NaCl, 1 mM EDTA, 3 mM $MgCl_2$ and 0.3 M sucrose, cells were fixed with 4% (v/v) formaldehyde for 15 min at room temperature. Subsequently, cells were permeabilized by soaking in 0.2% (v/v) Triton X-100 for 5 min at room temperature. After blocking in PBS containing 10 mg/ml BSA for 30 min at room temperature, fixed cells were incubated for 2 h at room temperature with the indicated primary antibodies. The slides were washed with PBS and incubated for 1 h at room temperature with secondary antibodies diluted in blocking solution (Alexa Fluor 568-conjugated goat anti-rabbit IgG and Alexa Fluor 488-conjugated goat anti-mouse IgG (Invitrogen)). After washing with PBS, coverslips were mounted using Vectashield containing DAPI (Vector Laboratories). Automated image acquisition was performed using an Olympus IX70 microscope equipped with the Scan^R imaging platform. A ×40/1.3 numerical aperture objective was used. 10 z stacks at a spacing of 0.3 μm were taken, and 100 images were acquired for each sample. Analysis was performed using Scan^R analysis software. Nuclei were identified on the basis of the DAPI signal, and RPA foci were identified on the basis of edge-based subobject counts. At least 1000 cells were analyzed for each condition.

RESULTS

DNA2 Can Mediate DNA End Resection in Conjunction with WRN Helicase—To test whether the human WRN helicase can mediate resection of broken DNA ends in concert with DNA2, we purified these proteins to homogeneity and analyzed their activities *in vitro* (Fig. 1*A*). WRN and BLM unwind DNA in the 3′-5′ direction and require a 3′ ssDNA tail for loading onto the DNA substrate (37, 38). Therefore, we generated a derivative of the pUC19 plasmid in which a StuI site was flanked on each side by four recognition sites for the nicking endonuclease Nt. BbvCI. Cleavage of this pUC19 derivative with StuI and Nt.BbvCI resulted in a 2.7-kb-long linear DNA molecule ending with 3′

The Role of WRN and BLM in DNA End Resection

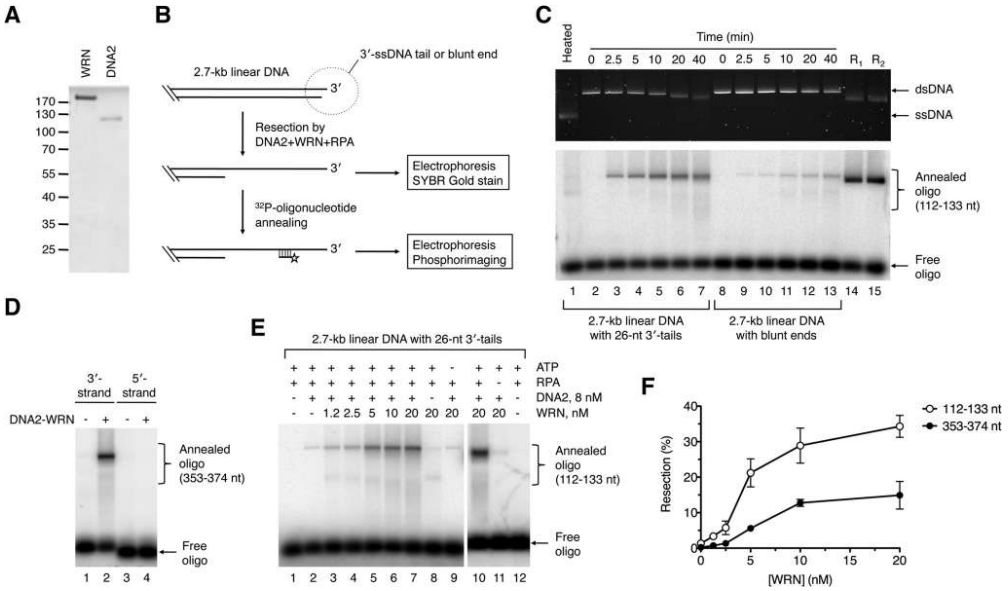

FIGURE 1. **DNA end resection by DNA2 and WRN.** *A*, SDS-PAGE analysis of purified WRN (0.7 μg) and DNA2 (0.4 μg) proteins. Gel was stained with Coomassie Brilliant Blue R-250. The molecular weights of protein standards are indicated on the *left*. *B*, schematic of the DNA end resection assay. The resection products were either left untreated or hybridized with synthetic ^{32}P-labeled oligonucleotides complementary to the 3′-terminated strand. DNA species were separated by electrophoresis in a 1% agarose gel and visualized by SYBR gold staining and phosphorimaging, respectively. Probes complementary to the regions spanning nt positions 112–133 and 353–374 (relative to the 3′ end) were used in this study. Only a part of the DNA substrate is shown. *C*, time course of resection of 3′-tailed (26 nt) and blunt-ended DNA substrates by DNA2 and WRN. Reactions were carried out at 37 °C and contained 2 nM DNA, 350 nM RPA, 10 nM WRN, and 8 nM DNA2. Reaction products at the indicated time points were analyzed as outlined in *B*. The 112- to 133-nt probe was used in this analysis. *Lane 1*, heat-denatured substrate; *lane 14*, 3′-tailed substrate incubated with 20 nM EXO1 and 350 nM RPA for 2 min (R1); *lane 15*, blunt-ended substrate incubated with 20 nM EXO1 and 350 nM RPA for 2 min (R2). *D*, directionality of DNA end resection by WRN-DNA2. Reactions were carried out at 37 °C for 60 min and contained 2 nM 3′-tailed DNA substrate, 350 nM RPA, 8 nM DNA2, and 10 nM WRN. Resection products were annealed with radiolabeled oligonucleotide probes complementary to either 3′-terminated (position 353–374 nt relative to the 3′ end) or 5′-terminated (position 353–374 nt relative to 3′ end) strand and analyzed as in *C*. *E*, 5′ end resection of 3′-tailed DNA substrate by WRN-DNA2 is dependent on WRN concentration and the presence of ATP and RPA. Reactions were carried out at 37 °C for 60 min and contained, as indicated, 2 nM DNA, 350 nM RPA, 1 mM ATP, 8 nM DNA2, and different WRN concentrations. Resection products were detected using the 112–133-nt probe. *F*, dependence of WRN-DNA2-catalyzed resection of 3′-tailed substrate on WRN concentration. Resection at the positions of 112–133 nt and 353–374 nt from the 3′ end of the DNA substrate was monitored. Reactions were carried out as in *E*. Relative concentration of the resection product generated by WRN-DNA2 at each WRN concentration was calculated as a percentage of the product generated by 20 nM EXO1 after 2 min. Data are mean ± S.D. ($n = 3$).

overhangs of 26 nt in length, whereas its cleavage by StuI alone gave rise to a linear DNA molecule with blunt ends. Processing of the DNA substrates was monitored by agarose gel electrophoresis followed by SYBR gold staining (Fig. 1*B*). In addition, ^{32}P-labeled synthetic oligonucleotides complementary to the 3′-terminated strand were used as hybridization probes to detect ssDNA generated by resection at specific positions (Fig. 1*B*) (10). We found that WRN, together with DNA2 and RPA, could catalyze efficient 5′ end resection on the 3′-tailed substrate but not the blunt-ended substrate (Fig. 1*C*). As expected, no reaction products were detected with an oligonucleotide probe complementary to the 5′-terminated strand, indicating that the observed DNA resection activity is limited to the 5′ strand (Fig. 1*D*). Of note, the end product of the resection reaction on the 3′-tailed DNA substrate appeared as a discrete band on SYBR gold-stained gel that was clearly shifted with respect to the unprocessed dsDNA substrate, indicating extensive resection (Fig. 1*C*, *top panel*, compare *lanes 2* and *7*). In contrast, no gradual shift in the electrophoretic mobility of the resection product was apparent after annealing of the radioactive probes. This is most likely due to the fact that DNA2 nuclease generates short oligonucleotides that can reanneal to the resected DNA along with the radioactive probe, leading to a DNA molecule with an electrophoretic mobility similar to that of the DNA substrate. Together, these results clearly demonstrate that DNA2, in conjunction with WRN and RPA, can catalyze extensive 5′ end resection, providing that the DNA substrate contains a 3′ ssDNA overhang.

To further characterize the DNA end resection reaction mediated by WRN-DNA2, reactions with the 3′-tailed substrate were carried out at various WRN concentrations, whereas DNA2 was kept at a concentration of 8 nM. We observed that the amount of resection product increased gradually with WRN concentration, reaching a plateau at about 10 nM (Fig. 1*E*, *lanes 2–7*, and Fig. 1*F*). Quantitative analysis of gel images revealed that about 35% of the DNA substrate was resected to the position of 133 nt from the 3′ end and that about 15% of the DNA substrate was resected to the position of 374 nt

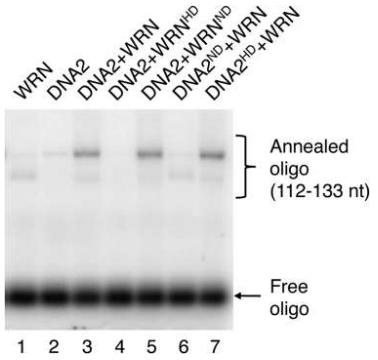

FIGURE 2. **5′ end resection of 3′-tailed DNA substrate by WRN-DNA2 depends on the helicase activity of WRN and the nuclease activity of DNA2.** Reactions were carried out at 37 °C for 60 min and contained 2 nM DNA, 350 nM RPA, 1 mM ATP, 8 nM DNA2, and 10 nM WRN. Resection products were detected using the 112–133 nt probe. *WRN^{HD}*, helicase-deficient mutant of WRN (K567M); *WRNND*, nuclease-deficient mutant of WRN (E84A); *DNA2^{HD}*, helicase-deficient mutant of DNA2 (K654R); *DNA2ND*, nuclease-deficient mutant of DNA2 (D277A).

within 1 h of incubation (Fig. 1*F*). Interestingly, a small amount of resected product (1–2%) could also be detected in the absence of WRN, suggesting that DNA2 itself could slowly resect dsDNA ends, likely following RPA-mediated stabilization of ssDNA ends generated by thermal fraying (Fig. 1*E*, *lane 2*). In the absence of DNA2, WRN was only capable of DNA unwinding, as evident from the appearance of a fast-migrating band (Fig. 1*E*, *lane 8*). The resection process catalyzed by WRN and DNA2 was found to be dependent on the presence of ATP and RPA, as expected for a helicase-driven reaction (Fig. 1*E*, compare *lanes 9–12*).

WRN acts not only as a 3′-5′ DNA helicase, but it also possesses a dsDNA-dependent 3′-5′ exonuclease activity residing in a separate domain located in the N-terminal portion of the protein (39, 40). DNA2 functions as a 5′-3′ helicase and a ssDNA-specific endonuclease (32, 41). To define the functions of the enzymatic activities of WRN and DNA2 in DNA end resection, we carried out a set of resection reactions with the 3′-tailed pUC19 substrate where either WRN or DNA2 were substituted with catalytically inactive mutants. We found that the helicase-deficient mutant of WRN (K567M) failed to stimulate DNA resection by DNA2, whereas the nuclease-deficient mutant of WRN (E84A) behaved similarly as the wild-type WRN in this reaction (Fig. 2, *lanes 2–4*). Substitution of DNA2 with its nuclease-deficient mutant (D277A) completely abolished resection and stimulated unwinding of the plasmid substrate (Fig. 2, *lane 6*). In contrast, the helicase-deficient mutant of DNA2 (K654E) could resect the DNA substrate to the same degree as the wild-type protein (Fig. 2, compare *lanes 3* and *7*). These results indicate that DNA end resection mediated by DNA2, WRN, and RPA is dependent on the helicase activity of WRN and the endonuclease activity of DNA2.

DNA2 and WRN Interact Physically—Yeast Dna2 has been shown to interact physically with Sgs1 (10). Likewise, BLM forms a complex with human DNA2 (17). Therefore, we investigated whether human DNA2 interacts physically with WRN. To this end, HEK293 cells were transfected with plasmids expressing WRN and FLAG-tagged DNA2, respectively, and complex formation between these proteins was tested by immunoprecipitation using beads conjugated with anti-FLAG M2 antibody. We found that WRN coimmunoprecipitated with FLAG-DNA2, indicating that these proteins form a complex *in vivo* (Fig. 3*A*, *lane 3*). This interaction was specific because anti-FLAG beads did not immunoprecipitate WRN from an extract lacking FLAG-DNA2 (Fig. 3*A*, *lane 1*). To further investigate complex formation between WRN and DNA2, we generated a stable HEK293 cell line expressing FLAG-DNA2. By immunoprecipitation using anti-FLAG M2 beads or anti-WRN antibody, we found that FLAG-DNA2 formed a complex with endogenous WRN in these cells (Fig. 3, *B* and *C*). Western blot analysis indicated that the level of FLAG-DNA2 in these cells was only slightly higher than that of endogenous DNA2, suggesting that WRN and DNA2 form a complex under physiological conditions (Fig. 3*B*, *top panel*). Interaction between FLAG-DNA2 and endogenous BLM was also detected as expected (Fig. 3*B*) (17). The cellular concentration of these protein complexes was not altered when cells were subjected to treatment with CPT, which causes breakage of DNA replication forks (Fig. 3*B*, *lanes 2–5*) (42). This suggests that the interaction of DNA2 with WRN and BLM in the cell is not dependent on DNA damage.

To test whether WRN and DNA2 interact directly, purified proteins were mixed and incubated at 4 °C for 4 h. Complex formation between WRN and DNA2 was tested by immunoprecipitation using anti-WRN antibody. We found that DNA2 coimmunoprecipitated with WRN. DNA2 was not present in the immunoprecipitated material whether WRN was omitted, confirming a direct protein-protein interaction (Fig. 3*D*). To map the interaction site of DNA2 on WRN, we tested binding of purified His_6-DNA2-FLAG protein to various WRN fragments covering the entire WRN polypeptide (Fig. 3*E*). The WRN fragments were produced in *E. coli* as fusions with a GST tag and isolated on GSH-Sepharose beads. Using a GST pulldown assay, we found that DNA2 bound specifically to a WRN fragment including the core helicase domain (helicase/Zn^{2+}-binding domains) and the winged helix domain (Fig. 3*F*, compare *lanes 1* and *4*) a binding site of a number of other proteins shown to interact with WRN (43, 44). DNA2 was also bound to a fragment containing only the helicase core or to the C-terminal portion of WRN starting at the beginning of the winged helix domain (Fig. 3*F*, compare *lanes 1*, *3*, *4*, and *5*). In contrast, DNA2 did not bind the N-terminal portion of WRN containing the exonuclease domain (Fig. 3*F*, *lane 2*). Collectively, these results suggest that there are at least two DNA2-interaction sites on WRN: one located in the central helicase domain and the other in the C-terminal region of WRN.

WRN-DNA2 Resects DNA Ends More Efficiently Than BLM-DNA2—Next, we set out to compare WRN and BLM with respect to their abilities to resect DNA ends in concert with DNA2 and RPA *in vitro*. Using a Y structure oligonucleotide duplex (29 bp) with single-stranded arms (30 nt each), we found that our preparations of WRN and BLM exhibited similar levels of specific helicase activity (Fig. 4*A*). For resection reactions, we used the 3′-tailed DNA substrate that was readily processed by

The Role of WRN and BLM in DNA End Resection

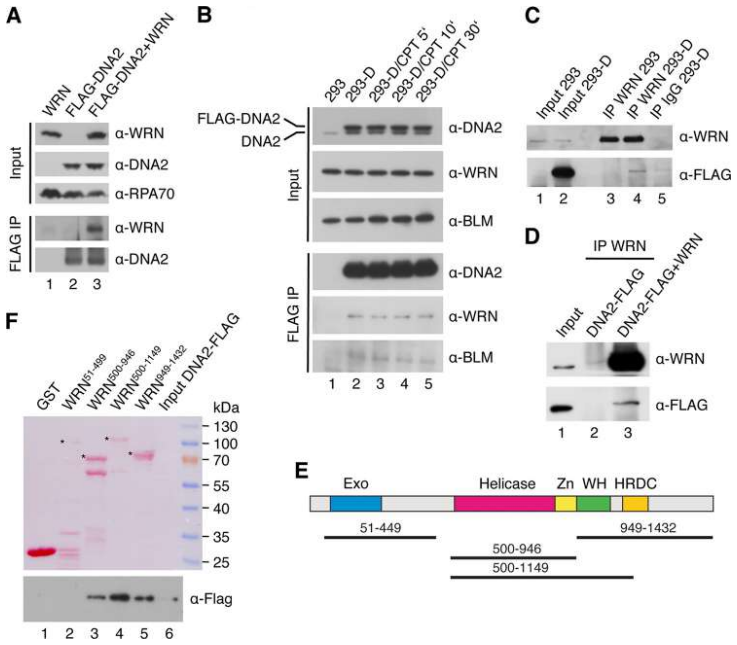

FIGURE 3. **Physical interaction between DNA2 and WRN *in vitro* and *in vivo*.** *A*, coimmunoprecipitation of WRN with DNA2 from human cells. HEK293 cells were transfected with vectors expressing FLAG-DNA2 and WRN as indicated. Cell extracts were immunoprecipitated (*IP*) with anti-FLAG antibody as described under "Experimental Procedures." Blots were probed with the indicated antibodies. 5% of input material was loaded. *B*, effect of DNA damage on the formation of DNA2-WRN and DNA2-BLM complexes in human cells. HEK293 cells stably transfected with the FLAG-DNA2 construct (*HEK293-D*) were treated with 1 μM CPT. At the indicated time points, complex formation between FLAG-DNA2 and endogenous WRN and BLM, respectively, was tested by immunoprecipitation using anti-FLAG antibody. *C*, coimmunoprecipitation of DNA2 with WRN from human cells. Extracts from HEK293-D cells were subjected to immunoprecipitation with anti-WRN antibody or control IgG. The immunoprecipitates were tested for the presence of FLAG-DNA2 and WRN by Western blotting. As a control, a WRN immunoprecipitate from HEK293 cells was also analyzed (*lane 3*). *D*, coimmunoprecipitation of DNA2 with WRN from a mixture of purified proteins. DNA2 (500 ng) was incubated with or without WRN (500 ng) at 4 °C for 4 h. The mixtures were subjected to immunoprecipitation with anti-WRN antibody. *E*, domain organization of WRN. *Exo*, exonuclease domain; *Zn*, zinc-binding domain; *WH*, winged-helix domain; *HRDC*, helicase and RNaseD C-terminal domain. *Black lines* indicate WRN fragments used for mapping the DNA2-interaction site on WRN. *F*, GST pulldown assay. Glutathione beads coated with the indicated GST-tagged fragments of WRN were incubated with purified His_6-DNA2-FLAG protein at 4 °C for 2 h, and bound proteins were analyzed by Western blotting as described under "Experimental Procedures." 1% of input was loaded in *B* and *C*, whereas 10% of input was loaded in *D* and *F*.

WRN-DNA2 in the presence of RPA (Fig. 1*C*). The extent of DNA resection at various reaction time points was monitored by annealing of radiolabeled oligonucleotide probes. These experiments clearly showed that WRN-DNA2 resected the DNA substrate at a much higher rate compared with BLM-DNA2 (Fig. 4, *B* and *C*). Notably, WRN-DNA2-catalyzed resection to the position of 374 nt away from the 3′ end was faster than BLM-DNA2-catalyzed resection to the position of 133 nt (Fig. 4, *B* and *C*). We also compared the activities of WRN-DNA2 and BLM-DNA2 on blunt-ended DNA substrate in the presence of RPA. We found that this DNA substrate was largely refractory not only to processing by WRN-DNA2 but also to processing by BLM-DNA2 (Fig. 4*D*, compare *lanes 4* and *5* to *lanes 10* and *11*). Taken together, we show that WRN-DNA2 resects DNA ends more efficiently than BLM-DNA2 *in vitro*.

Dissection of Pathways Involved in DNA End Resection in Human Cells—To assess whether WRN is involved in DNA end resection *in vivo*, we investigated the effect of its depletion on the efficiency of SSA-mediated repair of endonuclease-induced DSBs in cells that were either proficient or deficient for EXO1 and DNA2, respectively. For this epistasis analysis, we initially used the human embryonic kidney cell line HEK293 stably transfected with the SA-GFP reporter cassette consisting of two truncated *GFP* gene alleles (*5′GFP* and *Sce3′GFP*) that form a direct sequence repeat (280 bp) separated by a region of about 2.4 kb (Fig. 5*A*) (34, 45). SSA-mediated recombination between these homologous sequences triggered by a DSB generated in the distal GFP allele by the I-SceI endonuclease results in the formation of a functional *GFP* gene (Fig. 5*A*). This requires extensive DNA end resection to expose the complementary ssDNA regions for annealing. The proteins of interest were depleted from HEK293/SA-GFP cells by RNA interference. Cells were subsequently transfected with an I-SceI expression vector to create a DSB in the reporter cassette, and the percentage of GFP positive cells arising upon SSA-mediated repair was determined by flow cytometry 2 days after plasmid transfection. We found that cells depleted of either EXO1, WRN, or DNA2 exhibited a marked reduction in the frequency of SSA repair events (55, 65, and 75%, respectively) compared with mock-depleted cells (Fig. 5, *B* and *C*). In contrast, knockdown of

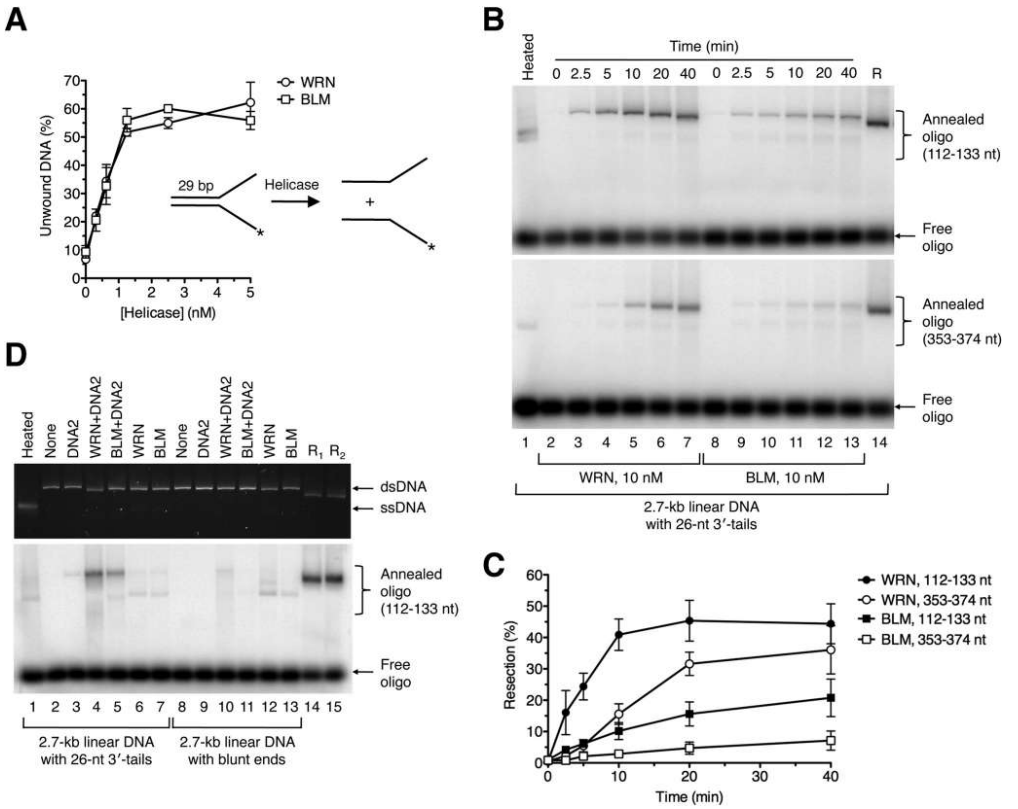

FIGURE 4. **Comparison of DNA end resection activities of WRN-DNA2 and BLM-DNA2.** *A*, comparison of helicase activities of WRN and BLM. Reactions contained 1 nM ^{32}P-labeled forked DNA duplex (*inset*) and different concentrations of WRN or BLM. Reactions were incubated at 37 °C for 30 min, and reaction products were quantified as described under "Experimental Procedures." Data are mean ± S.D. ($n = 3$). *B*, time course of resection of 3′-tailed DNA substrate catalyzed by WRN-DNA2 and BLM-DNA2, respectively. Reactions contained 2 nM DNA, 350 nM RPA, 8 nM DNA2, and 10 nM WRN/BLM. Reaction aliquots withdrawn at the indicated time points were subjected to electrophoresis on a 1% agarose gel after hybridization of radiolabeled probes complementary to 3′-terminated strand at the indicated positions. Radiolabeled DNA species were visualized by phosphorimaging. *C*, quantification of the reactions in *B*. Relative concentration of resection products generated at each time point was calculated as a percentage of the product generated by 20 nM EXO1 after 2 min. Data are mean ± S.D. ($n = 3$). *D*, processing of 3′-tailed (26 nt) and blunt-ended DNA substrates in reactions with indicated composition. Reactions were carried out at 37 °C for 60 min and contained 2 nM DNA, 350 nM RPA, and, where indicated, 8 nM DNA2, 20 nM WRN, and 20 nM BLM. Reaction products were analyzed as in Fig. 1*C*. *Lane 1*, heat-denatured substrate; *lane 14*, 3′-tailed substrate incubated with 20 nM EXO1 for 2 min (R1); *lane 15*, blunt-ended substrate incubated with 20 nM EXO1 for 2 min (R2).

BLM was found to be associated with a significant increase in SSA repair efficiency (140%) compared with control cells (Fig. 5, *B* and *C*). Of note, the SSA repair defect of WRN-depleted cells could be rescued by ectopic expression of the siRNA-resistant form of WRN, excluding an off-target effect of the WRN siRNA used in this study (Fig. 5*D*). Combined depletion of EXO1 and WRN or EXO1 and DNA2 further decreased the repair efficiency compared with the respective single depletions, whereas codepletion of DNA2 and WRN did not (Fig. 5, *B* and *C*). In addition, combined depletion of EXO1 and BLM had nearly the same effect on the SSA repair efficiency as EXO1 depletion (Fig. 5, *B* and *C*). Therefore, these findings suggest that HEK293 cells have at least two pathways for long-range resection of DSB ends: one mediated by EXO1 and the other dependent upon DNA2 and WRN.

To substantiate these findings, we performed a similar set of experiments using U2OS/SA-GFP cells (35). This analysis indicated that combined depletion of EXO1 and DNA2 almost completely abolished (reduced by 91%) SSA-mediated DSB repair in U2OS/SA-GFP cells, as did depletion of MRE11 (by 89%) or CtIP (by 82%), suggesting that long-range DNA end resection in U2OS cells is largely dependent on EXO1 and DNA2 (Fig. 5, *E*–*G*). However, in contrast to the results obtained with HEK293/SA-GFP cells, we observed a significant reduction in SSA repair efficiency not only after depletion of WRN (by 57%) but also after depletion of BLM (by 59%) (Fig. 5, *E* and *F*). Codepletion of BLM and WRN further decreased the repair efficiency to a level comparable with that in DNA2-depleted (by 73%) cells (Fig. 5, *E* and *F*). Moreover, combined depletion of DNA2 with either BLM or WRN had nearly the

The Role of WRN and BLM in DNA End Resection

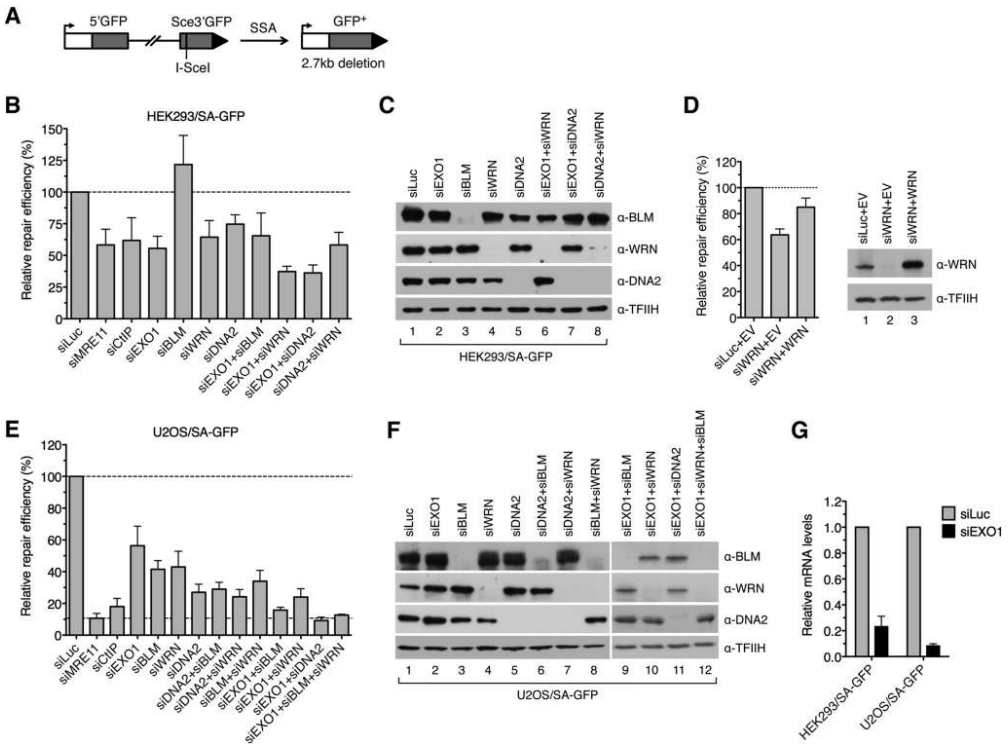

FIGURE 5. **WRN and BLM interact epistatically with DNA2 to promote DSB repair by SSA in human cells.** *A*, schematic of the SA-GFP reporter cassette. SSA-mediated repair of a DSB at the I-SceI-cutting site results in the formation of a functional GFP allele. *B*, efficiency of SSA-mediated repair of I-SceI-induced DSB in HEK293/SA-GFP cells treated with the indicated siRNAs. Cells were transfected with the appropriate siRNAs (40 nM) 2 days prior to transfection of the I-SceI-expressing plasmid. The percentage of GFP-positive cells in each sample was measured by flow cytometry 2 days after I-SceI plasmid transfection and taken as a measure of DSB repair efficiency. The plotted values represent the relative repair efficiency calculated as a percentage of repair efficiency measured in cells transfected with control siRNA (*siLuc*, 100%). Data are mean ± S.D. ($n \geq 3$). *C*, Western blot analysis of extracts from HEK293/SA-GFP cells transfected with indicated siRNAs under the same conditions as for SA-GFP reporter assays. Blots were probed with the indicated antibodies. *D*, rescue of the SSA-repair defect of WRN-depleted HEK293/SA-GFP cells by expression of the siRNA-resistant variant of WRN. An SA-GFP reporter assay was performed as in *B*. The WRN plasmid (*WRN*) or empty vector (*EV*) were cotransfected with the I-SceI plasmid. *E*, efficiency of SSA-mediated repair of I-SceI-induced DSB in U2OS/SA-GFP cells treated with the indicated siRNAs. Experiments were performed as in *B*. *F*, Western blot analysis of extracts from U2OS/SA-GFP cells transfected with the indicated siRNAs. Blots were probed with the indicated antibodies. *G*, quantitative real-time PCR showing that EXO1 mRNA levels are down-regulated by specific siRNA. Data are mean ± S.D. ($n = 3$).

same inhibitory effect on SSA repair as DNA2 depletion (Fig. 5, *E* and *F*). On the contrary, codepletion of EXO1 with either WRN or BLM caused a much higher reduction in repair efficiency than depletion of DNA2 alone, and triple depletion of EXO1, BLM, and WRN brought repair efficiency down to the level measured in cells depleted of EXO1 and DNA2 (Fig. 5, *E* and *F*). Collectively, these data suggest that, in U2OS cells, both WRN and BLM assist DNA2 to mediate long-range resection of broken DNA ends.

To bolster our conclusion that DNA2, WRN, and BLM have an epistatic relationship in DSB end resection, we extended our analysis to measurement of RPA focus formation in U2OS cells treated with CPT. As expected, 1 h after addition of CPT, RPA formed numerous foci in γ-H2AX-positive cells, which were dependent on the presence of CtIP (Fig. 6). Depletion of DNA2 resulted in a marked reduction in the number of RPA foci per cell compared with mock-depleted cells (Fig. 6). Cells depleted of BLM or WRN displayed a mild decrease in RPA focus frequency compared with mock-depleted cells (Fig. 6). In contrast, combined depletion of BLM and WRN caused approximately the same reduction in RPA focus frequency as depletion of DNA2 alone. Moreover, cells depleted of DNA2 and BLM or DNA2 and WRN displayed an RPA foci frequency comparable with that of DNA2-depleted cells (Fig. 6). These data further support the conclusion that DNA2, WRN, and BLM operate in the same DNA end resection pathway.

Role of the BLM-TOPOIIIα-RMI1-RMI2 Complex in DNA End Resection—In human cells, BLM exists in a complex with TOPOIIIα, RMI1, and RMI2, which is known to catalyze double Holliday junction dissolution during HR (46–49). Studies in yeast have shown that Top3α and Rmi1 are also required for DNA-end resection *in vivo* and stimulate DNA end resection by

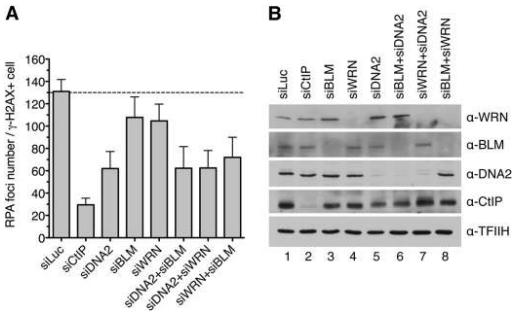

FIGURE 6. **DNA2, WRN, and BLM act in the same pathway of DSB end resection.** *A*, frequency of camptothecin-induced RPA foci in nuclei of U2OS cells depleted of the indicated proteins. Cells were transfected with appropriate siRNAs and, 48 h later, treated with 1 μM camptothecin for 1 h. Cells were then detergent-extracted and fixed with formaldehyde. RPA and γ-H2AX (a marker of DNA damage) were visualized by indirect immunofluorescence. DAPI was used to stain nuclei. The average number of RPA foci per γ-H2AX-positive cell was determined for each sample using an Olympus Scan^R screening station. The data points are mean $\pm$ S.D. ($n = 3$). *B*, Western blot analysis of extracts from U2OS cells transfected with indicated siRNAs. Blots were probed with the antibodies indicated on the *right*.

Sgs1-Dna2 *in vitro* by promoting the helicase activity of Sgs1 (9, 10, 14). Our study revealed that BLM-DNA2 resects DNA ends less efficiently than WRN-DNA2 *in vitro*, whereas *in vivo*, at least in U2OS cells, BLM and WRN appeared to contribute equally to promote DNA end resection (Fig. 5*E*). Therefore, we investigated whether BLM requires TOPOIIIα, RMI1, and RMI2 (TRR) to efficiently support DNA end resection by DNA2. To this end, we first investigated the effect of a purified TRR complex on DNA end resection by BLM-DNA2 *in vitro* (Fig. 7*A*). We found that TRR enhanced resection of the 3′-tailed pUC19 substrate by BLM-DNA2 (Fig. 7, *B* and *C*, *lanes 3–6*). On the contrary, the TRR complex had no effect on DNA end resection by WRN-DNA2 (data not shown). Moreover, it could not enhance DNA end resection by DNA2 in the absence of BLM (Fig. 7, *B* and *C*, compare *lanes 2* and *7*).

Next we tested the effect of depletion of RMI1 on the efficiency of SSA-mediated repair of I-SceI-induced DSBs in U2OS/SA-GFP cells. We found that RMI1 depletion reduced the repair efficiency to the level displayed by BLM- or DNA2-depleted cells (Fig. 7, *D* and *E*). Importantly, codepletion of RMI1 with BLM or DNA2 did not further reduce the repair efficiency compared with single depletions of these proteins, suggesting that RMI1, BLM, and DNA2 act in the same pathway (Fig. 7, *D* and *E*). Collectively, these results suggest that, in human cells, BLM promotes long-range DNA end resection as part of the BTRR complex.

DISCUSSION

Here we present evidence suggesting that human DNA2 acts in conjunction with either WRN or BLM to mediate long-range resection of broken DNA ends *in vivo*. Moreover, we show that WRN helicase can cooperate with DNA2 and RPA to catalyze resection of DNA ends *in vitro*, generating long 3′-terminated ssDNA tails. Our study also reveals that both WRN-DNA2 and BLM-DNA2 require a 3′ ssDNA overhang to efficiently initiate DNA end resection *in vitro*, which is in agreement with the "two-step" resection model in which the initial 5′ end trimming is carried out by the MRE11-RAD50-NBS1/Xrs2 complex in conjunction with CtIP/Sae2 (8, 9, 11, 19). In addition, we present evidence that BLM and DNA2 interact epistatically with RMI1 to mediate DNA end resection *in vivo*. Moreover, we show that the TRR complex stimulates DNA end resection by BLM-DNA2 *in vitro*. These data suggest that, in cells, BLM mediates DNA end resection as part of the BTRR complex.

Our discovery of the involvement of WRN in DNA end resection is consistent with the findings that WRN interacts physically with the MRN complex and accumulates at sites of DSBs in human cells (50, 51). Moreover, it has been demonstrated that WRN depletion leads to a marked reduction in the frequency of RPA and BrdU/ssDNA foci formed in response to ionizing radiation, indicative of a resection defect (52). A similar phenotype has been observed in DNA2-depleted cells (18). Although the previous studies did not address the relationship between WRN and DNA2, they demonstrated that these enzymes act synergistically with EXO1 to promote DNA end resection in human cells (18, 52). A role for WRN as a critical DNA end resection factor is also consistent with the cellular phenotype of Werner syndrome, a severe premature aging disorder caused by inherited mutations in the *WRN* gene (53). Cells derived from Werner syndrome patients are characterized by non-homologous chromosome exchanges, termed variegated translocation mosaicism, and large chromosomal deletions that may result from aberrant DSB repair by NHEJ as a consequence of a defect in DNA end resection (54–56). Indeed, it is becoming clear that NHEJ accounts for most chromosomal translocations in humans (57). Moreover, a role for DNA end resection as the critical determinant of DSB repair pathway choice is well established (58). Accumulating evidence suggests that defects in homology-directed repair pathways, which are dependent on DNA end resection, result in overuse of NHEJ for repair, leading to accumulation of chromosomal rearrangements (57). However, it should be noted that WRN is also known to promote DSB repair by the classical Ku-dependent NHEJ (C-NHEJ) pathway to suppress microhomology-mediated end joining (59, 60). This alternative end joining pathway is capable of producing chromosomal translocations, particularly when Ku-dependent NHEJ is deficient (57). Moreover, WRN has been shown to be involved in the resolution HR intermediates (61, 62). Therefore, it seems that the genomic instability in Werner syndrome is a consequence of multiple defects in DNA repair pathways.

Our finding that the TRR complex stimulates DNA end resection by BLM-DNA2 *in vitro* is consistent with previous reports showing that the association of BLM with TOPOIIIα and RMI1 enhances its DNA unwinding activity, which drives the BLM-DNA2-catalyzed resection reaction (17, 63). Similarly, RMI1 and RMI2 have been shown to enhance the efficiency of the BLM-TOPOIIIα-mediated double Holliday junction dissolution reaction (48, 49, 64). It has also been shown that RMI1 forms a complex with RPA and that this interaction is essential for the stimulatory effect of RPA on double Holliday junction dissolution by the BTRR complex (65). Therefore, it is possible that a physical interaction between RMI1 and RPA

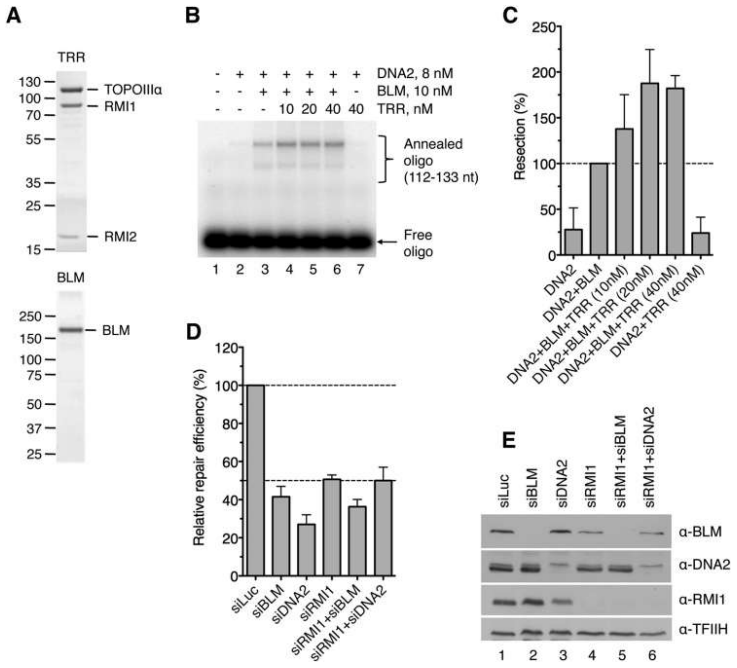

FIGURE 7. **Involvement of TOPOIIIα, RMI1, and RMI2 in DNA end resection.** *A*, SDS-PAGE analysis of purified TRR complex (1.5 μg) and BLM (0.5 μg). The gel was stained with Coomassie Brilliant Blue R-250. The molecular weights of protein standards are indicated on the *left*. *B*, stimulation of BLM-DNA2-catalyzed DNA end resection by the TRR complex. Reactions contained 2 nM 3′-tailed pUC19 substrate, 8 nM DNA2, 10 nM BLM, 350 nM RPA, and varying concentrations of TRR. BLM and TRR were preincubated for 5 min on ice prior to addition to the reaction. Reaction products were analyzed as in Fig. 1*C* using the 112–133-nt probe. *C*, quantification of the product of reactions in *B*. Data are mean ± S.D. (n = 3). The data are normalized to the amount of product in the reaction containing only BLM and DNA2 (100%). *D*, RMI1 acts epistatically with BLM and DNA2 to promote DSB repair by SSA in human cells. Efficiency of SSA-mediated repair of I-SceI-induced DSB in U2OS/SA-GFP cells transfected with indicated siRNAs was measured as in Fig. 5*E*. *E*, Western blot analysis of extracts from U2OS/SA-GFP cells transfected with indicated siRNAs under the same conditions as for SA-GFP reporter assays. Blots were probed with the indicated antibodies.

loaded on the 3′-terminated DNA strand during DNA2-catalyzed resection might enhance the DNA unwinding processivity of the BTRR complex and, hence, increase the efficiency of the resection reaction. However, it should be noted that the stimulatory effect of the TRR complex on DNA end resection by BLM-DNA2 *in vitro* was rather modest under our experimental conditions. On the contrary, RMI1 depletion in U2OS/SA-GFP cells reduced the efficiency of SSA-mediated DSB repair to levels displayed by BLM- or DNA2-deficient cells, suggesting that BLM requires RMI1 to promote DNA end resection *in vivo*. Of note, it has been shown that silencing of RMI1 or RMI2 expression by RNA interference destabilizes both BLM and TOPOIIIα (47, 49). Therefore, it is evident that, in addition to being important for the functional attributes of the BTRR complex, RMI1 and RMI2 are indispensable for the structural integrity of its components *in vivo*.

Although BLM depletion compromised SSA-mediated DSB repair in U2OS/SA-GFP cells, it had an opposite effect on SSA in HEK293/SA-GFP cells. Similarly, the efficiency of SSA-mediated DSB repair in HEK293/SA-GFP cells was elevated significantly upon depletion of RMI1 (data not shown). These findings suggest that, in HEK293 cells, the BTRR complex might act as an SSA suppressor, most likely through unwinding of the annealed intermediate formed following DNA end resection. Strikingly, we found that BLM concentration in HEK293 cells was much higher than in U2OS cells (data not shown). Therefore, it appears that the BTRR complex exerts an inhibitory effect on SSA when its concentration in the cell exceeds certain threshold.

Acknowledgments—We thank Kata Sarlos and Ian D. Hickson for the purified TRR complex, Judith L. Campbell for the transfer vector for preparation of the bacmid expressing His$_6$-hDNA2-FLAG, Jeremy M. Stark for the HEK293/SA-GFP and U2OS/SA-GFP cell lines, Stefano Ferrari and Stephanie Bregenhorn for help with protein purification, and Christiane Koenig for technical assistance.

REFERENCES

1. Jackson, S. P., and Bartek, J. (2009) The DNA-damage response in human biology and disease. *Nature* **461,** 1071–1078
2. Khanna, K. K., and Jackson, S. P. (2001) DNA double-strand breaks: signaling, repair and the cancer connection. *Nat. Genet.* **27,** 247–254
3. Longhese, M. P., Bonetti, D., Guerini, I., Manfrini, N., and Clerici, M. (2009) DNA double-strand breaks in meiosis: checking their formation,

processing and repair. *DNA Repair* **8,** 1127–1138
4. Soulas-Sprauel, P., Rivera-Munoz, P., Malivert, L., Le Guyader, G., Abramowski, V., Revy, P., and de Villartay, J. P. (2007) V(D)J and immunoglobulin class switch recombinations: a paradigm to study the regulation of DNA end-joining. *Oncogene* **26,** 7780–7791
5. Lieber, M. R. (2010) The mechanism of double-strand DNA break repair by the nonhomologous DNA end-joining pathway. *Annu. Rev. Biochem.* **79,** 181–211
6. San Filippo, J., Sung, P., and Klein, H. (2008) Mechanism of eukaryotic homologous recombination. *Annu. Rev. Biochem.* **77,** 229–257
7. Heyer, W. D., Ehmsen, K. T., and Liu, J. (2010) Regulation of homologous recombination in eukaryotes. *Annu. Rev. Genet.* **44,** 113–139
8. Mimitou, E. P., and Symington, L. S. (2008) Sae2, Exo1 and Sgs1 collaborate in DNA double-strand break processing. *Nature* **455,** 770–774
9. Zhu, Z., Chung, W. H., Shim, E. Y., Lee, S. E., and Ira, G. (2008) Sgs1 helicase and two nucleases Dna2 and Exo1 resect DNA double-strand break ends. *Cell* **134,** 981–994
10. Cejka, P., Cannavo, E., Polaczek, P., Masuda-Sasa, T., Pokharel, S., Campbell, J. L., and Kowalczykowski, S. C. (2010) DNA end resection by Dna2-Sgs1-RPA and its stimulation by Top3-Rmi1 and Mre11-Rad50-Xrs2. *Nature* **467,** 112–116
11. Nicolette, M. L., Lee, K., Guo, Z., Rani, M., Chow, J. M., Lee, S. E., and Paull, T. T. (2010) Mre11-Rad50-Xrs2 and Sae2 promote 5′ strand resection of DNA double-strand breaks. *Nat. Struct. Mol. Biol.* **17,** 1478–1485
12. Shim, E. Y., Chung, W. H., Nicolette, M. L., Zhang, Y., Davis, M., Zhu, Z., Paull, T. T., Ira, G., and Lee, S. E. (2010) *Saccharomyces cerevisiae* Mre11/Rad50/Xrs2 and Ku proteins regulate association of Exo1 and Dna2 with DNA breaks. *EMBO J.* **29,** 3370–3380
13. Cannavo, E., Cejka, P., and Kowalczykowski, S. C. (2013) Relationship of DNA degradation by *Saccharomyces cerevisiae* exonuclease 1 and its stimulation by RPA and Mre11-Rad50-Xrs2 to DNA end resection. *Proc. Natl. Acad. Sci. U.S.A.* **110,** E1661–E1668
14. Niu, H., Chung, W. H., Zhu, Z., Kwon, Y., Zhao, W., Chi, P., Prakash, R., Seong, C., Liu, D., Lu, L., Ira, G., and Sung, P. (2010) Mechanism of the ATP-dependent DNA end-resection machinery from *Saccharomyces cerevisiae*. *Nature* **467,** 108–111
15. Truong, L. N., Li, Y., Shi, L. Z., Hwang, P. Y., He, J., Wang, H., Razavian, N., Berns, M. W., and Wu, X. (2013) Microhomology-mediated end joining and homologous recombination share the initial end resection step to repair DNA double-strand breaks in mammalian cells. *Proc. Natl. Acad. Sci. U.S.A.* **110,** 7720–7725
16. Gravel, S., Chapman, J. R., Magill, C., and Jackson, S. P. (2008) DNA helicases Sgs1 and BLM promote DNA double-strand break resection. *Genes Dev.* **22,** 2767–2772
17. Nimonkar, A. V., Genschel, J., Kinoshita, E., Polaczek, P., Campbell, J. L., Wyman, C., Modrich, P., and Kowalczykowski, S. C. (2011) BLM-DNA2-RPA-MRN and EXO1-BLM-RPA-MRN constitute two DNA end resection machineries for human DNA break repair. *Genes Dev.* **25,** 350–362
18. Karanja, K. K., Cox, S. W., Duxin, J. P., Stewart, S. A., and Campbell, J. L. (2012) DNA2 and EXO1 in replication-coupled, homology-directed repair and in the interplay between HDR and the FA/BRCA network. *Cell Cycle* **11,** 3983–3996
19. Shibata, A., Moiani, D., Arvai, A. S., Perry, J., Harding, S. M., Genois, M. M., Maity, R., van Rossum-Fikkert, S., Kertokalio, A., Romoli, F., Ismail, A., Ismalaj, E., Petricci, E., Neale, M. J., Bristow, R. G., Masson, J. Y., Wyman, C., Jeggo, P. A., and Tainer, J. A. (2014) DNA double-strand break repair pathway choice is directed by distinct MRE11 nuclease activities. *Mol. Cell* **53,** 7–18
20. Bernstein, K. A., Gangloff, S., and Rothstein, R. (2010) The RecQ DNA helicases in DNA repair. *Annu. Rev. Genet.* **44,** 393–417
21. Yan, H., McCane, J., Toczylowski, T., and Chen, C. (2005) Analysis of the *Xenopus* Werner syndrome protein in DNA double-strand break repair. *J. Cell Biol.* **171,** 217–227
22. Liao, S., Toczylowski, T., and Yan, H. (2008) Identification of the Xenopus DNA2 protein as a major nuclease for the 5′→3′ strand-specific processing of DNA ends. *Nucleic Acids Res.* **36,** 6091–6100
23. Liao, S., Guay, C., Toczylowski, T., and Yan, H. (2012) Analysis of MRE11's function in the 5′→3′ processing of DNA double-strand breaks. *Nucleic Acids Res.* **40,** 4496–4506
24. Saydam, N., Kanagaraj, R., Dietschy, T., Garcia, P. L., Peña-Diaz, J., Shevelev, I., Stagljar, I., and Janscak, P. (2007) Physical and functional interactions between Werner syndrome helicase and mismatch-repair initiation factors. *Nucleic Acids Res.* **35,** 5706–5716
25. Adams, K. E., Medhurst, A. L., Dart, D. A., and Lakin, N. D. (2006) Recruitment of ATR to sites of ionising radiation-induced DNA damage requires ATM and components of the MRN protein complex. *Oncogene* **25,** 3894–3904
26. Sartori, A. A., Lukas, C., Coates, J., Mistrik, M., Fu, S., Bartek, J., Baer, R., Lukas, J., and Jackson, S. P. (2007) Human CtIP promotes DNA end resection. *Nature* **450,** 509–514
27. Yang, J., O'Donnell, L., Durocher, D., and Brown, G. W. (2012) RMI1 promotes DNA replication fork progression and recovery from replication fork stress. *Mol. Cell Biol.* **32,** 3054–3064
28. Orren, D. K., Brosh, R. M., Jr., Nehlin, J. O., Machwe, A., Gray, M. D., and Bohr, V. A. (1999) Enzymatic and DNA binding properties of purified WRN protein: high affinity binding to single-stranded DNA but not to DNA damage induced by 4NQO. *Nucleic Acids Res.* **27,** 3557–3566
29. Kanagaraj, R., Saydam, N., Garcia, P. L., Zheng, L., and Janscak, P. (2006) Human RECQ5β helicase promotes strand exchange on synthetic DNA structures resembling a stalled replication fork. *Nucleic Acids Res.* **34,** 5217–5231
30. El-Shemerly, M., Janscak, P., Hess, D., Jiricny, J., and Ferrari, S. (2005) Degradation of human exonuclease 1b upon DNA synthesis inhibition. *Cancer Res.* **65,** 3604–3609
31. Henricksen, L. A., Umbricht, C. B., and Wold, M. S. (1994) Recombinant replication protein A: expression, complex formation, and functional characterization. *J. Biol. Chem.* **269,** 11121–11132
32. Masuda-Sasa, T., Imamura, O., and Campbell, J. L. (2006) Biochemical analysis of human Dna2. *Nucleic Acids Res.* **34,** 1865–1875
33. Pfaffl, M. W. (2001) A new mathematical model for relative quantification in real-time RT-PCR. *Nucleic Acids Res.* **29,** e45
34. Bennardo, N., Cheng, A., Huang, N., and Stark, J. M. (2008) Alternative-NHEJ is a mechanistically distinct pathway of mammalian chromosome break repair. *PLoS Genet.* **4,** e1000110
35. Gunn, A., and Stark, J. M. (2012) I-SceI-based assays to examine distinct repair outcomes of mammalian chromosomal double strand breaks. *Methods Mol. Biol.* **920,** 379–391
36. Richardson, C., Moynahan, M. E., and Jasin, M. (1998) Double-strand break repair by interchromosomal recombination: suppression of chromosomal translocations. *Genes Dev.* **12,** 3831–3842
37. Karow, J. K., Chakraverty, R. K., and Hickson, I. D. (1997) The Bloom's syndrome gene product is a 3′-5′ DNA helicase. *J. Biol. Chem.* **272,** 30611–30614
38. Brosh, R. M., Jr., Waheed, J., and Sommers, J. A. (2002) Biochemical characterization of the DNA substrate specificity of Werner syndrome helicase. *J. Biol. Chem.* **277,** 23236–23245
39. Shen, J. C., Gray, M. D., Oshima, J., Kamath-Loeb, A. S., Fry, M., and Loeb, L. A. (1998) Werner syndrome protein: I: DNA helicase and DNA exonuclease reside on the same polypeptide. *J. Biol. Chem.* **273,** 34139–34144
40. Kamath-Loeb, A. S., Shen, J. C., Loeb, L. A., and Fry, M. (1998) Werner syndrome protein: II: characterization of the integral 3′ → 5′ DNA exonuclease. *J. Biol. Chem.* **273,** 34145–34150
41. Kim, J. H., Kim, H. D., Ryu, G. H., Kim, D. H., Hurwitz, J., and Seo, Y. S. (2006) Isolation of human DNA2 endonuclease and characterization of its enzymatic properties. *Nucleic Acids Res.* **34,** 1854–1864
42. Avemann, K., Knippers, R., Koller, T., and Sogo, J. M. (1988) Camptothecin, a specific inhibitor of type I DNA topoisomerase, induces DNA breakage at replication forks. *Mol. Cell Biol.* **8,** 3026–3034
43. Lee, J. W., Harrigan, J., Opresko, P. L., and Bohr, V. A. (2005) Pathways and functions of the Werner syndrome protein. *Mech. Ageing Dev.* **126,** 79–86
44. Kanagaraj, R., Parasuraman, P., Mihaljevic, B., van Loon, B., Burdova, K., König, C., Furrer, A., Bohr, V. A., Hübscher, U., and Janscak, P. (2012) Involvement of Werner syndrome protein in MUTYH-mediated repair of oxidative DNA damage. *Nucleic Acids Res.* **40,** 8449–8459
45. Stark, J. M., Pierce, A. J., Oh, J., Pastink, A., and Jasin, M. (2004) Genetic steps of mammalian homologous repair with distinct mutagenic conse-

quences. *Mol. Cell Biol.* **24,** 9305–9316
46. Wu, L., and Hickson, I. D. (2003) The Bloom's syndrome helicase suppresses crossing over during homologous recombination. *Nature* **426,** 870–874
47. Yin, J., Sobeck, A., Xu, C., Meetei, A. R., Hoatlin, M., Li, L., and Wang, W. (2005) BLAP75, an essential component of Bloom's syndrome protein complexes that maintain genome integrity. *EMBO J.* **24,** 1465–1476
48. Wu, L., Bachrati, C. Z., Ou, J., Xu, C., Yin, J., Chang, M., Wang, W., Li, L., Brown, G. W., and Hickson, I. D. (2006) BLAP75/RMI1 promotes the BLM-dependent dissolution of homologous recombination intermediates. *Proc. Natl. Acad. Sci. U.S.A.* **103,** 4068–4073
49. Xu, D., Guo, R., Sobeck, A., Bachrati, C. Z., Yang, J., Enomoto, T., Brown, G. W., Hoatlin, M. E., Hickson, I. D., and Wang, W. (2008) RMI, a new OB-fold complex essential for Bloom syndrome protein to maintain genome stability. *Genes Dev.* **22,** 2843–2855
50. Cheng, W. H., von Kobbe, C., Opresko, P. L., Arthur, L. M., Komatsu, K., Seidman, M. M., Carney, J. P., and Bohr, V. A. (2004) Linkage between Werner syndrome protein and the Mre11 complex via Nbs1. *J. Biol. Chem.* **279,** 21169–21176
51. Lan, L., Nakajima, S., Komatsu, K., Nussenzweig, A., Shimamoto, A., Oshima, J., and Yasui, A. (2005) Accumulation of Werner protein at DNA double-strand breaks in human cells. *J. Cell Sci.* **118,** 4153–4162
52. Tomimatsu, N., Mukherjee, B., Deland, K., Kurimasa, A., Bolderson, E., Khanna, K. K., and Burma, S. (2012) Exo1 plays a major role in DNA end resection in humans and influences double-strand break repair and damage signaling decisions. *DNA Repair* **11,** 441–448
53. Yu, C. E., Oshima, J., Fu, Y. H., Wijsman, E. M., Hisama, F., Alisch, R., Matthews, S., Nakura, J., Miki, T., Ouais, S., Martin, G. M., Mulligan, J., and Schellenberg, G. D. (1996) Positional cloning of the Werner's syndrome gene. *Science* **272,** 258–262
54. Salk, D., Au, K., Hoehn, H., and Martin, G. M. (1981) Cytogenetics of Werner's syndrome cultured skin fibroblasts: variegated translocation mosaicism. *Cytogenet. Cell Genet.* **30,** 92–107
55. Fukuchi, K., Martin, G. M., and Monnat, R. J., Jr. (1989) Mutator phenotype of Werner syndrome is characterized by extensive deletions. *Proc. Natl. Acad. Sci. U.S.A.* **86,** 5893–5897
56. Melcher, R., von Golitschek, R., Steinlein, C., Schindler, D., Neitzel, H., Kainer, K., Schmid, M., and Hoehn, H. (2000) Spectral karyotyping of Werner syndrome fibroblast cultures. *Cytogenet. Cell Genet.* **91,** 180–185
57. Bunting, S. F., and Nussenzweig, A. (2013) End-joining, translocations and cancer. *Nat. Rev. Cancer* **13,** 443–454
58. Symington, L. S., and Gautier, J. (2011) Double-strand break end resection and repair pathway choice. *Annu. Rev. Genet.* **45,** 247–271
59. Chen, L., Huang, S., Lee, L., Davalos, A., Schiestl, R. H., Campisi, J., and Oshima, J. (2003) WRN, the protein deficient in Werner syndrome, plays a critical structural role in optimizing DNA repair. *Aging Cell* **2,** 191–199
60. Perry, J. J., Yannone, S. M., Holden, L. G., Hitomi, C., Asaithamby, A., Han, S., Cooper, P. K., Chen, D. J., and Tainer, J. A. (2006) WRN exonuclease structure and molecular mechanism imply an editing role in DNA end processing. *Nat. Struct. Mol. Biol.* **13,** 414–422
61. Saintigny, Y., Makienko, K., Swanson, C., Emond, M. J., and Monnat, R. J., Jr. (2002) Homologous recombination resolution defect in Werner syndrome. *Mol. Cell Biol.* **22,** 6971–6978
62. Swanson, C., Saintigny, Y., Emond, M. J., and Monnat, R. J., Jr. (2004) The Werner syndrome protein has separable recombination and survival functions. *DNA Repair* **3,** 475–482
63. Bussen, W., Raynard, S., Busygina, V., Singh, A. K., and Sung, P. (2007) Holliday junction processing activity of the BLM-Topo IIIα-BLAP75 complex. *J. Biol. Chem.* **282,** 31484–31492
64. Raynard, S., Bussen, W., and Sung, P. (2006) A double Holliday junction dissolvasome comprising BLM, topoisomerase IIIα, and BLAP75. *J. Biol. Chem.* **281,** 13861–13864
65. Xue, X., Raynard, S., Busygina, V., Singh, A. K., and Sung, P. (2013) Role of replication protein A in double Holliday junction dissolution mediated by the BLM-Topo IIIα-RMI1-RMI2 protein complex. *J. Biol. Chem.* **288,** 14221–14227

3. DISCUSSION

DNA2 homologues have been found in every eukaryotic organism tested to date including yeast and humans (71, 189, 190). Yeast Dna2 was characterized as a tripartite protein consisting of an N-terminal regulatory domain followed by a RecB-like nuclease domain (66) and a C-terminal superfamily I helicase domain (71). The human homologue hDNA2 only contains the nuclease- and helicase-domain, as the N-terminal domain is only found in lower eukaryotes (69, 139, 191). DNA2 has essential functions in all organisms tested so far, which are dependent on its nuclease activity (77, 139, 191). yDna2 seems to function non-enzymatically via its N-terminal domain only in the S-phase checkpoint in yeast (140). Yeast cells expressing helicase-deficient yDna2 were viable under some growth conditions, but very sensitive to DNA damaging agents (71, 100). The essential function of yDna2 was ascribed to its function in Okazaki fragment processing on its own or in concert with Fen1 (58, 60, 69, 91, 102, 103). However, the role of hDNA2 in the DNA metabolism of human cells is still a matter of discussion. Depletion of hDNA2 in human cells led to genomic instability monitored by the presence of aneuploid cells, interchromatin bridges, micronuclei or the accumulation of cells in late S/G2 phase (75, 133). Such findings indicate that hDNA2 is important for successfully finishing DNA replication. However, neither the kinetics of DNA replication nor the processing of Okazaki fragments were altered upon hDNA2 depletion (75), indicating that hDNA2 helps to finalize DNA replication in an Okazaki fragment processing independent manner. Upon the depletion of endogenous hDNA2 only the ectopic expression of wild type hDNA2 could restore the normal phenotype while the expression of either nuclease- or helicase-deficient hDNA2 led to impaired DNA metabolism indicating that both nuclease and helicase activities of hDNA2 are essential (75).

Furthermore, cells overexpressing nuclease-deficient hDNA2 showed a more severe phenotype then cells overexpressing helicase-deficient or nuclease-helicase-deficient hDNA2 (75). This suggests that the helicase activity of hDNA2 is toxic on its own. However, such findings stand in contrast to biochemical reports showing that recombinant hDNA2 possesses only very limited or no helicase activity (112, 114).

3. 1 Biochemical activities of human DNA2

Since genetic and cell biological studies could not entirely explain hDNA2's essential role in DNA metabolism, we decided to study the enzyme using biochemical approaches. I expressed and purified wild type hDNA2 and its mutant variants using improved purification strategies that already helped to increase the amount and activity of the yeast protein (67, 70, 103). We could recapitulate the nuclease activity of hDNA2 degrading exclusively 5'-terminated ssDNA in the presence of hRPA, which was in agreement with preceding studies (112, 114). In addition, we were able to show that hDNA2 possesses a vigorous and processive DNA unwinding activity dependent on ATP and hRPA. The helicase activity was masked by the enzyme's nuclease activity, meaning it was only detectable when the nuclease was abolished. This is very similar to what was observed for the yeast enzyme (70). DNA unwinding was only observed with oligonucleotide-based DNA substrates that harbor 5' ssDNA and with plasmid-based dsDNA substrates in the presence of hRPA (186). In a collaboration, we could show that hRPA has the potential to melt dsDNA in a concentration-dependent manner (188). Such limited melting at the dsDNA substrates' end could provide hDNA2 with the required 5' ssDNA that is required for the enzyme to load onto a substrate and needed to initiate dsDNA unwinding. The structure of mouse DNA2 shows that the nuclease is positioned ahead of the helicase (118). The ssDNA needs to pass a narrow tunnel containing the nuclease to reach the helicase of hDNA2. However, if the DNA substrate is cleaved before accessing the helicase domain, unwinding could be prevented. This could explain our finding that the strong helicase of hDNA2 is unleashed only upon the inactivation of the nuclease (186). Our conclusion that hDNA2 exhibits a strong DNA helicase activity could explain the severe phenotype generated by the expression of nuclease-deficient hDNA2 in human cells (75). Upon the inactivation of the nuclease, the helicase of hDNA2 could lose its internal regulation mechanism and start unwinding in an uncontrolled way.

Having established that the yeast and human DNA2 polypeptides possess two different enzymatic functions (70, 186), it is of interest if and how the enzyme is regulated.

Unpublished results from our group indicate that yeast Dna2 levels vary in a cell cycle-dependent manner being lowest in the early S phase and highest in late S/G2 phase.

Furthermore, yDna2 gets sumoylated in late S/G2 phase. Treatment of the yeast cells with methyl methanosulfate (MMS) or bleomycin reduced the overall sumoylation *in vivo*. Such post-translational modifications are very likely to regulate proteins' activities. *In vitro* sumoylation of recombinant yDna2 did not affect the helicase activity while the nuclease was reduced (M. Levikova and P. Cejka, manuscript in preparation). However, these sumoylation sites were located to the regulatory N-terminal domain of yDna2 that is lacking in the human polypeptide. This raised the question if a protein interacting with hDNA2 could play a similar role as the N-terminal domain in yeast does? We set out to identify possible interaction partners of hDNA2 via an interaction pull-down and subsequent mass spectrometry analysis. We identified several enzymes potentially modifying hDNA2, but did not yet investigate them in further detail (C. Pinto and P. Cejka, unpublished data).

Another possibility is that the activities of hDNA2 are regulated via the redox state of the iron-sulfur cluster located in the nuclease domain (78, 104, 192). So far, the iron-sulfur cluster is believed to have structural features, but additional functions are unknown and need to be determined.

3.2 The role of human DNA2 in DNA end resection

DNA2 enzymes were shown to interact with cognate RecQ helicases to resect the DNA ends required for the repair of DSBs via homologous recombination (39, 104). The initial short-range resection is mediated by the MRN (MRX in yeast) complex together with CtIP (Sae2 in yeast) in human cells (107, 109). For the subsequent long-range resection two pathways are proposed: either via EXO1/Exo1 or via a RecQ homologue (Sgs1 in yeast, BLM in human) and DNA2 (67, 110, 111, 113, 115, 193). The helicase activity of Sgs1/BLM and the nuclease but not the helicase function of DNA2 were essential for resection (67, 113, 115). Results from a collaboration indicated that in human cells hDNA2 does not only interact with BLM (115) but also with WRN, another RecQ helicase family member found in human cells (116). Having established that hDNA2 possesses a strong and processive helicase activity (186) and knowing that hDNA2 physically and functionally interacts with WRN and BLM helicases (115, 116), we decided to characterize these interplays in more detail. In electrophoresis-based assays, we could show that hDNA2 and WRN/BLM synergize in the degradation of dsDNA

substrates mimicking the ends of DSBs. Such synergies were only observed with hDNA2 and WRN/BLM but not with any other human RecQ homologues or yeast Sgs1, indicating that the interplay is very specific. As expected, such resection reactions were fully dependent on the helicase of WRN/BLM and the nuclease of hDNA2. To our surprise, the helicase-deficient version of hDNA2 was not as efficient in dsDNA degradation as the wild type protein indicating a role for the helicase activity (186). Resection assays are challenging to interpret since DNA unwinding and cleavage can occur at the same time. Using nuclease-deficient hDNA2 and focusing on helicase assays, we could show that WRN/BLM can stimulate the hDNA2 helicase in a non-enzymatic but structural way and vice versa, the WRN or BLM helicase activity is enhanced by the hDNA2 helicase in a structural way (186). Such a stimulation of BLM was already described in the literature (115).

We showed that the active helicase domain of hDNA2 accelerates the degradation of ssDNA especially under physiological conditions where the ssDNA is covered by hRPA (187). We believe that the motor activity of hDNA2 more likely acts as a ssDNA translocase than a dsDNA helicase in eukaryotic cells. Interestingly, the ssDNA degradation capacity of hDNA2 is further increased by the presence of (catalytically inactive) WRN and BLM (187). We supplemented these biochemical data with *in vivo* experiments in yeast showing that the motor function of yDna2 helps to accelerate DNA resection in such a setup as well. Previously, the DNA2's motor seemed dispensable for end resection *in vivo* and *in vitro* (67, 111, 115, 116). However, we believe that in these studies overexpressing DNA2 *in vivo* or using saturating concentrations *in vitro* circumvented the requirement for DNA2's motor activity. Of note, the amount of DNA2 in cells needs to be tightly regulated since the overexpression of yDna2 led to cell cycle arrest (194). This further strengthens the idea that cells require a processive but well balanced resection machinery. Together these results propose a mechanism for DNA end resection where hDNA2 forms a complex with either WRN or BLM. The RecQ homologues WRN and BLM function as leading helicases traveling on one DNA strand in a 3'-5' direction to unwind dsDNA. The presence of hDNA2 and its 5'-3' motor activity helps to speed up the unwinding. Subsequently, hDNA2 nuclease activity degrades the generated 5' terminated ssDNA using its own motor activity to accelerate the process (186, 187).

In prokaryotic organisms the resection machinery can consist of several subunits that interact and enhance their resection capacity synergizing in DNA degradation. For example,

in *E. coli* RecBCD forms a complex using the RecB 3'-5' and RecD 5'-3 helicases to unwind dsDNA and RecB 5'-3' and 3'-5' nuclease to cleave the ssDNA (195-197). In *Bacillus subtilis* the AddAB resection machinery consists of one helicase (AddA) and two nucleases (3'-5' from AddA and 5'-3' from AddB, (198, 199)). Interestingly, the AddB nuclease seems to be similar to DNA2 nuclease since both proteins contain an iron-sulfur cluster (79).

3.3 Human DNA2 and DNA replication

The remodeling of damaged or stalled replication fork into a four-way junction-like structure (or "chicken foot" structure) was proposed to be a mechanism to protect the replication fork from further damage and to be a first step in the repair and restart of perturbed forks (119, 200).

Human DNA2 was proposed to have a function in the completion of DNA replication beyond the Okazaki fragment processing observed in yeast (58, 60, 69, 75, 91, 102) and that DNA2 interacts with the replisome via And-1 (75, 76, 201). In a collaboration, we could show that human DNA2 interacts with WRN but not BLM to degrade reversed replication forks using its 5'-3' nuclease activity and hence help to restart and complete DNA replication (65). This reversed fork processing activity of hDNA2/WRN was tightly regulated by RECQ1 in an ATPase-independent manner, most likely by binding to the reversed forks preventing hDNA2's nuclease access (65). Since the DNA2-dependent pathway in DNA end resection is redundant with the EXO1 pathway (39, 104, 113, 193) and hDNA2 does not or only to a very limited extent contributes to the processing of Okazaki fragments (75), the resolving of such aberrant structures occurring during DNA replication could point towards an essential function of hDNA2.

3.4 Human DNA2 and cancer

hDNA2 was shown to have a multifaceted role in the development of cancer (76, 202). Replication stress in precancerous lesions can lead to high loads of DNA damage, especially DSBs that activate the DNA damage response (DDR). hDNA2 has pivotal roles in DSB repair as well as in DNA replication and is therefore important for maintaining genomic integrity

(65, 75, 76, 116, 186, 202). Estrogens, as the primary female sex hormones, can stimulate cell proliferation and induce DNA damage, thus are tumorigenic. Estrogen-dependent cancers such as breast, uterine and ovarian cancers are among the most dangerous cancers in women (203). Upon the treatment of MCF7 breast cancer cells with estradiol (the primary type of estrogen) the expression of hDNA2 was shown to be elevated (202). Correct function of hDNA2 in the DNA repair pathways can prevent mutations and genomic instability and can counteract cancer development. However, estrogen-dependent cancers were shown to express hDNA2 mutated in its nuclease and helicase domain (202). Therefore, the expression of mutant versions of hDNA2 could lead to genomic instability and cancer development.

Continuous DNA damage response may trigger senescence or apoptosis and hence prevent the formation of malignant lesions (204-207). Coping with increased replication-associated DSBs to maintain the hyperactive DNA replication status is required for precancerous lesion to develop to cancer. Human DNA2 was reported to be overexpressed in a broad range of cancers helping to alleviate replication stress and the overexpression was observed already at an early stage of transformation (76). In breast cancer patients the expression of hDNA2 positively correlated with the probability to develop metastasis and negatively correlated with overall survival (76). Depletion of hDNA2 in breast cancer cell lines decreased the xenograft growth in mice and reduced the formation of lung metastasis indicating a tumor-promoting role for hDNA2 (202). While a complete knockout of DNA2 led to embryonic lethality in mice, heterozygous DNA2+/− mice showed higher cancer susceptibility than wild type mice (77). Together these data indicate that hDNA2 helps to prevent the accumulation of mutations, maintain genomic integrity and prevent cancer development in normal cells. However, in (pre-)cancerous cells higher hDNA2 levels can help to overcome high replication stress and to escape senescence therefore triggering cell survival and cancer development (202).

hDNA2 is linked to many functions in the DNA metabolism and is implicated in cancer development as described above. Such findings implicate that the enzyme could be a putative target in anti-cancer therapy. In fact, targeting the DNA damage response is in focus for novel cancer therapies with PARP1 inhibition in BRCA2 negative cancers as the best example (208). One small molecule inhibitor was described to interfere with hDNA2 nuclease and helicase function inhibiting its DNA end resection, reversed fork restarting and

stalled fork over-resection activities (209). Furthermore, the DNA2 inhibitor sensitized cancer cells to CPT treatment and showed synthetic lethality together with a PARP1 inhibitor (209). We showed that inhibiting the nuclease activity of hDNA2 unleashes its strong helicase activity (186) that could explain the toxic effect of expressing nuclease-deficient hDNA2 in human cells (75). Cells expressing nuclease-deficient hDNA2 die very fast during the course of an experiment while cells expressing the nuclease/helicase-deficient double mutant were maintained at constant levels (75). This raises the possibility that subsequent mutation and inactivation of the helicase activity may lead to resistance of future hDNA2 nuclease inhibitors. The biochemical analysis of hDNA2 in isolation and in interplay with the RECQ helicases WRN and BLM will help to understand the functions of these enzymes in normal and pathological DNA metabolism. In addition, the assays developed in this work will be useful to develop and validate putative cancer treatment agents.

4. PERSPECTIVES

Human DNA2's role in cancer development seems to be ambiguous. In normal cells hDNA2's functions help to avoid genome instability and aberrant activity of hDNA2 can increase the risk of mutations. At later stages, high expression of hDNA2 helps cancer cells to overcome high replication stress and therefore give them a growth advantage. Working with hDNA2 *in vivo* is difficult since the protein is essential and has multifaceted roles in the DNA metabolism. We used a biochemical setup to study hDNA2's functions in a defined reconstituted system.

We characterized the interplay of hDNA2 with RPA and the RECQ helicases BLM and WRN. We could show the synergy of these protein complexes in the degradation of DSB ends and reversed forks. In future studies, it would be interesting to investigate the interaction and interplay of hDNA2 and BLM/WRN in more detail, for example defining specific interaction sites and generate interaction-deficient mutants. These can be analyzed in biochemical and cellular assays. Most likely further proteins such as the MRN complex and TopoIIIα/RMI1/2 support hDNA2-BLM/WRN. Supplementing our reactions with these complexes could give additional information towards the understanding of DNA resection and its regulation.

More detailed mechanistic insights would offer possibilities to impede with hDNA2's functions in cancer cells. This could be achieved by preventing complex formation or by specific inhibition of enzymatic activities and such interferences could lead to a reduction of cancer cells' capability to proliferate. At the moment, we are testing various small molecule compounds that specifically interfere with either DNA2's DNA binding, nuclease or helicase activity. Targeting DNA repair pathways with small-molecule inhibitors blocking the function of proteins involved is a growing field in cancer therapy. hDNA2 and its cognate partners are very interesting candidates to be inhibited and in the future screening for and validation of potential inhibitors will be essential. My work gives a solid base for such drug development strategies.

5. REFERENCES

1. Hanahan D & Weinberg RA (2011) Hallmarks of cancer: the next generation. *Cell* 144(5):646-674.
2. Avery OT, Macleod CM, & McCarty M (1944) Studies on the Chemical Nature of the Substance Inducing Transformation of Pneumococcal Types : Induction of Transformation by a Desoxyribonucleic Acid Fraction Isolated from Pneumococcus Type Iii. *J Exp Med* 79(2):137-158.
3. De Bont R & van Larebeke N (2004) Endogenous DNA damage in humans: a review of quantitative data. *Mutagenesis* 19(3):169-185.
4. Hoeijmakers JH (2001) Genome maintenance mechanisms for preventing cancer. *Nature* 411(6835):366-374.
5. Jacobs AL & Schar P (2012) DNA glycosylases: in DNA repair and beyond. *Chromosoma* 121(1):1-20.
6. Lindahl T (1993) Instability and decay of the primary structure of DNA. *Nature* 362(6422):709-715.
7. Gros L, Ishchenko AA, Ide H, Elder RH, & Saparbaev MK (2004) The major human AP endonuclease (Ape1) is involved in the nucleotide incision repair pathway. *Nucleic Acids Res* 32(1):73-81.
8. Beard WA, Prasad R, & Wilson SH (2006) Activities and mechanism of DNA polymerase beta. *Methods Enzymol* 408:91-107.
9. Sleeth KM, Robson RL, & Dianov GL (2004) Exchangeability of mammalian DNA ligases between base excision repair pathways. *Biochemistry* 43(40):12924-12930.
10. Krokan HE & Bjoras M (2013) Base excision repair. *Cold Spring Harb Perspect Biol* 5(4):a012583.
11. Robertson AB, Klungland A, Rognes T, & Leiros I (2009) DNA repair in mammalian cells: Base excision repair: the long and short of it. *Cell Mol Life Sci* 66(6):981-993.
12. Scharer OD (2013) Nucleotide excision repair in eukaryotes. *Cold Spring Harb Perspect Biol* 5(10):a012609.
13. Hanawalt PC & Spivak G (2008) Transcription-coupled DNA repair: two decades of progress and surprises. *Nat Rev Mol Cell Biol* 9(12):958-970.
14. Gillet LC & Scharer OD (2006) Molecular mechanisms of mammalian global genome nucleotide excision repair. *Chem Rev* 106(2):253-276.
15. Arana ME & Kunkel TA (2010) Mutator phenotypes due to DNA replication infidelity. *Semin Cancer Biol* 20(5):304-311.
16. Palombo F*, et al.* (1996) hMutSbeta, a heterodimer of hMSH2 and hMSH3, binds to insertion/deletion loops in DNA. *Curr Biol* 6(9):1181-1184.
17. Kunkel TA & Erie DA (2005) DNA mismatch repair. *Annu Rev Biochem* 74:681-710.
18. Jiricny J (2013) Postreplicative mismatch repair. *Cold Spring Harb Perspect Biol* 5(4):a012633.
19. Ghodgaonkar MM*, et al.* (2013) Ribonucleotides misincorporated into DNA act as strand-discrimination signals in eukaryotic mismatch repair. *Mol Cell* 50(3):323-332.
20. Jiricny J (2006) The multifaceted mismatch-repair system. *Nat Rev Mol Cell Biol* 7(5):335-346.
21. Li GM (2008) Mechanisms and functions of DNA mismatch repair. *Cell Res* 18(1):85-98.

22. Kunkel TA & Erie DA (2015) Eukaryotic Mismatch Repair in Relation to DNA Replication. *Annu Rev Genet* 49:291-313.
23. Deans AJ & West SC (2011) DNA interstrand crosslink repair and cancer. *Nat Rev Cancer* 11(7):467-480.
24. Kim H & D'Andrea AD (2012) Regulation of DNA cross-link repair by the Fanconi anemia/BRCA pathway. *Genes Dev* 26(13):1393-1408.
25. Prakash S, Johnson RE, & Prakash L (2005) Eukaryotic translesion synthesis DNA polymerases: specificity of structure and function. *Annu Rev Biochem* 74:317-353.
26. Mehta A & Haber JE (2014) Sources of DNA double-strand breaks and models of recombinational DNA repair. *Cold Spring Harb Perspect Biol* 6(9):a016428.
27. Weinfeld M & Soderlind KJ (1991) 32P-postlabeling detection of radiation-induced DNA damage: identification and estimation of thymine glycols and phosphoglycolate termini. *Biochemistry* 30(4):1091-1097.
28. Patel AG*, et al.* (2016) Immunodetection of human topoisomerase I-DNA covalent complexes. *Nucleic Acids Res* 44(6):2816-2826.
29. Lieber MR (2010) NHEJ and its backup pathways in chromosomal translocations. *Nat Struct Mol Biol* 17(4):393-395.
30. Weterings E & Chen DJ (2008) The endless tale of non-homologous end-joining. *Cell Res* 18(1):114-124.
31. Davis AJ & Chen DJ (2013) DNA double strand break repair via non-homologous end-joining. *Transl Cancer Res* 2(3):130-143.
32. Kadyk LC & Hartwell LH (1992) Sister chromatids are preferred over homologs as substrates for recombinational repair in Saccharomyces cerevisiae. *Genetics* 132(2):387-402.
33. Creighton HB & McClintock B (1931) A Correlation of Cytological and Genetical Crossing-Over in Zea Mays. *Proc Natl Acad Sci U S A* 17(8):492-497.
34. Borde V & de Massy B (2013) Programmed induction of DNA double strand breaks during meiosis: setting up communication between DNA and the chromosome structure. *Curr Opin Genet Dev* 23(2):147-155.
35. Heyer WD, Ehmsen KT, & Liu J (2010) Regulation of homologous recombination in eukaryotes. *Annu Rev Genet* 44:113-139.
36. Sfeir A & Symington LS (2015) Microhomology-Mediated End Joining: A Back-up Survival Mechanism or Dedicated Pathway? *Trends Biochem Sci* 40(11):701-714.
37. Ceccaldi R, Rondinelli B, & D'Andrea AD (2016) Repair Pathway Choices and Consequences at the Double-Strand Break. *Trends Cell Biol* 26(1):52-64.
38. Huertas P (2010) DNA resection in eukaryotes: deciding how to fix the break. *Nat Struct Mol Biol* 17(1):11-16.
39. Cejka P (2015) DNA End Resection: Nucleases Team Up with the Right Partners to Initiate Homologous Recombination. *J Biol Chem* 290(38):22931-22938.
40. Henricksen LA, Umbricht CB, & Wold MS (1994) Recombinant replication protein A: expression, complex formation, and functional characterization. *J Biol Chem* 269(15):11121-11132.
41. Krejci L, Altmannova V, Spirek M, & Zhao X (2012) Homologous recombination and its regulation. *Nucleic Acids Res* 40(13):5795-5818.
42. San Filippo J, Sung P, & Klein H (2008) Mechanism of eukaryotic homologous recombination. *Annu Rev Biochem* 77:229-257.

43. Thorslund T & West SC (2007) BRCA2: a universal recombinase regulator. *Oncogene* 26(56):7720-7730.
44. Sung P, Krejci L, Van Komen S, & Sehorn MG (2003) Rad51 recombinase and recombination mediators. *J Biol Chem* 278(44):42729-42732.
45. Renkawitz J, Lademann CA, & Jentsch S (2014) Mechanisms and principles of homology search during recombination. *Nat Rev Mol Cell Biol* 15(6):369-383.
46. Kowalczykowski SC, Dixon DA, Eggleston AK, Lauder SD, & Rehrauer WM (1994) Biochemistry of homologous recombination in Escherichia coli. *Microbiol Rev* 58(3):401-465.
47. Petukhova G, Stratton S, & Sung P (1998) Catalysis of homologous DNA pairing by yeast Rad51 and Rad54 proteins. *Nature* 393(6680):91-94.
48. Nimonkar AV & Kowalczykowski SC (2009) Second-end DNA capture in double-strand break repair: how to catch a DNA by its tail. *Cell Cycle* 8(12):1816-1817.
49. Mazloum N & Holloman WK (2009) Second-end capture in DNA double-strand break repair promoted by Brh2 protein of Ustilago maydis. *Mol Cell* 33(2):160-170.
50. Rijkers T*, et al.* (1998) Targeted inactivation of mouse RAD52 reduces homologous recombination but not resistance to ionizing radiation. *Mol Cell Biol* 18(11):6423-6429.
51. Matos J & West SC (2014) Holliday junction resolution: regulation in space and time. *DNA Repair (Amst)* 19:176-181.
52. Huertas P, Cortes-Ledesma F, Sartori AA, Aguilera A, & Jackson SP (2008) CDK targets Sae2 to control DNA-end resection and homologous recombination. *Nature* 455(7213):689-692.
53. Ira G*, et al.* (2004) DNA end resection, homologous recombination and DNA damage checkpoint activation require CDK1. *Nature* 431(7011):1011-1017.
54. Sartori AA*, et al.* (2007) Human CtIP promotes DNA end resection. *Nature* 450(7169):509-514.
55. Huertas P & Jackson SP (2009) Human CtIP mediates cell cycle control of DNA end resection and double strand break repair. *J Biol Chem* 284(14):9558-9565.
56. Morin I*, et al.* (2008) Checkpoint-dependent phosphorylation of Exo1 modulates the DNA damage response. *EMBO J* 27(18):2400-2410.
57. El-Shemerly M, Hess D, Pyakurel AK, Moselhy S, & Ferrari S (2008) ATR-dependent pathways control hEXO1 stability in response to stalled forks. *Nucleic Acids Res* 36(2):511-519.
58. Bae SH*, et al.* (2001) Tripartite structure of Saccharomyces cerevisiae Dna2 helicase/endonuclease. *Nucleic Acids Res* 29(14):3069-3079.
59. Bae SH & Seo YS (2000) Characterization of the enzymatic properties of the yeast dna2 Helicase/endonuclease suggests a new model for Okazaki fragment processing. *J Biol Chem* 275(48):38022-38031.
60. Kao HI, Veeraraghavan J, Polaczek P, Campbell JL, & Bambara RA (2004) On the roles of Saccharomyces cerevisiae Dna2p and Flap endonuclease 1 in Okazaki fragment processing. *J Biol Chem* 279(15):15014-15024.
61. Choe W, Budd M, Imamura O, Hoopes L, & Campbell JL (2002) Dynamic localization of an Okazaki fragment processing protein suggests a novel role in telomere replication. *Mol Cell Biol* 22(12):4202-4217.
62. Lesur I & Campbell JL (2004) The transcriptome of prematurely aging yeast cells is similar to that of telomerase-deficient cells. *Mol Biol Cell* 15(3):1297-1312.

63. Zheng L*, et al.* (2008) Human DNA2 is a mitochondrial nuclease/helicase for efficient processing of DNA replication and repair intermediates. *Mol Cell* 32(3):325-336.
64. Hu J*, et al.* (2012) The intra-S phase checkpoint targets Dna2 to prevent stalled replication forks from reversing. *Cell* 149(6):1221-1232.
65. Thangavel S*, et al.* (2015) DNA2 drives processing and restart of reversed replication forks in human cells. *J Cell Biol* 208(5):545-562.
66. Budd ME, Choe W, & Campbell JL (2000) The nuclease activity of the yeast DNA2 protein, which is related to the RecB-like nucleases, is essential in vivo. *J Biol Chem* 275(22):16518-16529.
67. Cejka P*, et al.* (2010) DNA end resection by Dna2-Sgs1-RPA and its stimulation by Top3-Rmi1 and Mre11-Rad50-Xrs2. *Nature* 467(7311):112-116.
68. Niu H*, et al.* (2010) Mechanism of the ATP-dependent DNA end-resection machinery from Saccharomyces cerevisiae. *Nature* 467(7311):108-111.
69. Bae SH*, et al.* (1998) Dna2 of Saccharomyces cerevisiae possesses a single-stranded DNA-specific endonuclease activity that is able to act on double-stranded DNA in the presence of ATP. *J Biol Chem* 273(41):26880-26890.
70. Levikova M, Klaue D, Seidel R, & Cejka P (2013) Nuclease activity of Saccharomyces cerevisiae Dna2 inhibits its potent DNA helicase activity. *Proc Natl Acad Sci U S A* 110(22):E1992-2001.
71. Budd ME, Choe WC, & Campbell JL (1995) DNA2 encodes a DNA helicase essential for replication of eukaryotic chromosomes. *J Biol Chem* 270(45):26766-26769.
72. Bae SH*, et al.* (2002) Coupling of DNA helicase and endonuclease activities of yeast Dna2 facilitates Okazaki fragment processing. *J Biol Chem* 277(29):26632-26641.
73. Lee KH*, et al.* (2000) The endonuclease activity of the yeast Dna2 enzyme is essential in vivo. *Nucleic Acids Res* 28(15):2873-2881.
74. Kang YH, Lee CH, & Seo YS (2010) Dna2 on the road to Okazaki fragment processing and genome stability in eukaryotes. *Crit Rev Biochem Mol Biol* 45(2):71-96.
75. Duxin JP*, et al.* (2012) Okazaki fragment processing-independent role for human Dna2 enzyme during DNA replication. *J Biol Chem* 287(26):21980-21991.
76. Peng G*, et al.* (2012) Human nuclease/helicase DNA2 alleviates replication stress by promoting DNA end resection. *Cancer Res* 72(11):2802-2813.
77. Lin W*, et al.* (2013) Mammalian DNA2 helicase/nuclease cleaves G-quadruplex DNA and is required for telomere integrity. *EMBO J* 32(10):1425-1439.
78. Pokharel S & Campbell JL (2012) Cross talk between the nuclease and helicase activities of Dna2: role of an essential iron-sulfur cluster domain. *Nucleic Acids Res* 40(16):7821-7830.
79. Yeeles JT, Cammack R, & Dillingham MS (2009) An iron-sulfur cluster is essential for the binding of broken DNA by AddAB-type helicase-nucleases. *J Biol Chem* 284(12):7746-7755.
80. Burgers PM & Kunkel TA (2017) Eukaryotic DNA Replication Fork. *Annu Rev Biochem*.
81. Stillman B (2008) DNA polymerases at the replication fork in eukaryotes. *Mol Cell* 30(3):259-260.
82. Ogawa T & Okazaki T (1980) Discontinuous DNA replication. *Annu Rev Biochem* 49:421-457.
83. Frick DN & Richardson CC (2001) DNA primases. *Annu Rev Biochem* 70:39-80.
84. Bullock PA, Seo YS, & Hurwitz J (1991) Initiation of simian virus 40 DNA synthesis in vitro. *Mol Cell Biol* 11(5):2350-2361.

85. Hubscher U & Seo YS (2001) Replication of the lagging strand: a concert of at least 23 polypeptides. *Mol Cells* 12(2):149-157.
86. Baker TA & Kornberg A (1992) *DNA replication* (Freeman, New York) Second Ed pp XIV, Taf., 931 S.
87. Abbotts J & Loeb LA (1985) DNA polymerase alpha and models for proofreading. *Nucleic Acids Res* 13(1):261-274.
88. Burgers PM (1998) Eukaryotic DNA polymerases in DNA replication and DNA repair. *Chromosoma* 107(4):218-227.
89. Burgers PM (2009) Polymerase dynamics at the eukaryotic DNA replication fork. *J Biol Chem* 284(7):4041-4045.
90. Podust VN, Podust LM, Muller F, & Hubscher U (1995) DNA polymerase delta holoenzyme: action on single-stranded DNA and on double-stranded DNA in the presence of replicative DNA helicases. *Biochemistry* 34(15):5003-5010.
91. Ayyagari R, Gomes XV, Gordenin DA, & Burgers PM (2003) Okazaki fragment maturation in yeast. I. Distribution of functions between FEN1 AND DNA2. *J Biol Chem* 278(3):1618-1625.
92. Pike JE, Burgers PM, Campbell JL, & Bambara RA (2009) Pif1 helicase lengthens some Okazaki fragment flaps necessitating Dna2 nuclease/helicase action in the two-nuclease processing pathway. *J Biol Chem* 284(37):25170-25180.
93. Rossi ML*, et al.* (2008) Pif1 helicase directs eukaryotic Okazaki fragments toward the two-nuclease cleavage pathway for primer removal. *J Biol Chem* 283(41):27483-27493.
94. Levin DS, Bai W, Yao N, O'Donnell M, & Tomkinson AE (1997) An interaction between DNA ligase I and proliferating cell nuclear antigen: implications for Okazaki fragment synthesis and joining. *Proc Natl Acad Sci U S A* 94(24):12863-12868.
95. Levin DS, McKenna AE, Motycka TA, Matsumoto Y, & Tomkinson AE (2000) Interaction between PCNA and DNA ligase I is critical for joining of Okazaki fragments and long-patch base-excision repair. *Curr Biol* 10(15):919-922.
96. Ishimi Y, Claude A, Bullock P, & Hurwitz J (1988) Complete enzymatic synthesis of DNA containing the SV40 origin of replication. *J Biol Chem* 263(36):19723-19733.
97. Tishkoff DX*, et al.* (1997) Identification and characterization of Saccharomyces cerevisiae EXO1, a gene encoding an exonuclease that interacts with MSH2. *Proc Natl Acad Sci U S A* 94(14):7487-7492.
98. Budd ME*, et al.* (2005) A network of multi-tasking proteins at the DNA replication fork preserves genome stability. *PLoS Genet* 1(6):e61.
99. Nasmyth KA (1977) Temperature-sensitive lethal mutants in the structural gene for DNA ligase in the yeast Schizosaccharomyces pombe. *Cell* 12(4):1109-1120.
100. Formosa T & Nittis T (1999) Dna2 mutants reveal interactions with Dna polymerase alpha and Ctf4, a Pol alpha accessory factor, and show that full Dna2 helicase activity is not essential for growth. *Genetics* 151(4):1459-1470.
101. Budd ME, Reis CC, Smith S, Myung K, & Campbell JL (2006) Evidence suggesting that Pif1 helicase functions in DNA replication with the Dna2 helicase/nuclease and DNA polymerase delta. *Mol Cell Biol* 26(7):2490-2500.
102. Budd ME & Campbell JL (1997) A yeast replicative helicase, Dna2 helicase, interacts with yeast FEN-1 nuclease in carrying out its essential function. *Mol Cell Biol* 17(4):2136-2142.

103. Levikova M & Cejka P (2015) The Saccharomyces cerevisiae Dna2 can function as a sole nuclease in the processing of Okazaki fragments in DNA replication. *Nucleic Acids Res* 43(16):7888-7897.
104. Mimitou EP & Symington LS (2009) DNA end resection: many nucleases make light work. *DNA Repair (Amst)* 8(9):983-995.
105. Trujillo KM, Yuan SS, Lee EY, & Sung P (1998) Nuclease activities in a complex of human recombination and DNA repair factors Rad50, Mre11, and p95. *J Biol Chem* 273(34):21447-21450.
106. Garcia V, Phelps SE, Gray S, & Neale MJ (2011) Bidirectional resection of DNA double-strand breaks by Mre11 and Exo1. *Nature* 479(7372):241-244.
107. Cannavo E & Cejka P (2014) Sae2 promotes dsDNA endonuclease activity within Mre11-Rad50-Xrs2 to resect DNA breaks. *Nature* 514(7520):122-125.
108. Oh J, Al-Zain A, Cannavo E, Cejka P, & Symington LS (2016) Xrs2 Dependent and Independent Functions of the Mre11-Rad50 Complex. *Mol Cell* 64(2):405-415.
109. Anand R, Ranjha L, Cannavo E, & Cejka P (2016) Phosphorylated CtIP Functions as a Co-factor of the MRE11-RAD50-NBS1 Endonuclease in DNA End Resection. *Mol Cell* 64(5):940-950.
110. Mimitou EP & Symington LS (2008) Sae2, Exo1 and Sgs1 collaborate in DNA double-strand break processing. *Nature* 455(7214):770-774.
111. Zhu Z, Chung WH, Shim EY, Lee SE, & Ira G (2008) Sgs1 helicase and two nucleases Dna2 and Exo1 resect DNA double-strand break ends. *Cell* 134(6):981-994.
112. Masuda-Sasa T, Imamura O, & Campbell JL (2006) Biochemical analysis of human Dna2. *Nucleic Acids Res* 34(6):1865-1875.
113. Nimonkar AV*, et al.* (2011) BLM-DNA2-RPA-MRN and EXO1-BLM-RPA-MRN constitute two DNA end resection machineries for human DNA break repair. *Genes Dev* 25(4):350-362.
114. Kim JH*, et al.* (2006) Isolation of human Dna2 endonuclease and characterization of its enzymatic properties. *Nucleic Acids Res* 34(6):1854-1864.
115. Daley JM, Chiba T, Xue X, Niu H, & Sung P (2014) Multifaceted role of the Topo IIIalpha-RMI1-RMI2 complex and DNA2 in the BLM-dependent pathway of DNA break end resection. *Nucleic Acids Res* 42(17):11083-11091.
116. Sturzenegger A*, et al.* (2014) DNA2 cooperates with the WRN and BLM RecQ helicases to mediate long-range DNA end resection in human cells. *J Biol Chem* 289(39):27314-27326.
117. Bizard AH & Hickson ID (2014) The dissolution of double Holliday junctions. *Cold Spring Harb Perspect Biol* 6(7):a016477.
118. Zhou C, Pourmal S, & Pavletich NP (2015) Dna2 nuclease-helicase structure, mechanism and regulation by Rpa. *Elife* 4.
119. Neelsen KJ & Lopes M (2015) Replication fork reversal in eukaryotes: from dead end to dynamic response. *Nat Rev Mol Cell Biol* 16(4):207-220.
120. Ray Chaudhuri A*, et al.* (2012) Topoisomerase I poisoning results in PARP-mediated replication fork reversal. *Nat Struct Mol Biol* 19(4):417-423.
121. Zellweger R*, et al.* (2015) Rad51-mediated replication fork reversal is a global response to genotoxic treatments in human cells. *J Cell Biol* 208(5):563-579.
122. Fugger K*, et al.* (2015) FBH1 Catalyzes Regression of Stalled Replication Forks. *Cell Rep*.

123. Betous R*, et al.* (2012) SMARCAL1 catalyzes fork regression and Holliday junction migration to maintain genome stability during DNA replication. *Genes Dev* 26(2):151-162.
124. Betous R, Glick GG, Zhao R, & Cortez D (2013) Identification and characterization of SMARCAL1 protein complexes. *PLoS One* 8(5):e63149.
125. Ciccia A*, et al.* (2012) Polyubiquitinated PCNA recruits the ZRANB3 translocase to maintain genomic integrity after replication stress. *Mol Cell* 47(3):396-409.
126. Berti M*, et al.* (2013) Human RECQ1 promotes restart of replication forks reversed by DNA topoisomerase I inhibition. *Nat Struct Mol Biol* 20(3):347-354.
127. Gilson E & Geli V (2007) How telomeres are replicated. *Nat Rev Mol Cell Biol* 8(10):825-838.
128. Martinez P & Blasco MA (2015) Replicating through telomeres: a means to an end. *Trends Biochem Sci* 40(9):504-515.
129. Nandakumar J & Cech TR (2013) Finding the end: recruitment of telomerase to telomeres. *Nat Rev Mol Cell Biol* 14(2):69-82.
130. Ghosh AK*, et al.* (2012) RECQL4, the protein mutated in Rothmund-Thomson syndrome, functions in telomere maintenance. *J Biol Chem* 287(1):196-209.
131. Vannier JB, Pavicic-Kaltenbrunner V, Petalcorin MI, Ding H, & Boulton SJ (2012) RTEL1 dismantles T loops and counteracts telomeric G4-DNA to maintain telomere integrity. *Cell* 149(4):795-806.
132. Chai W, Zheng L, & Shen B (2013) DNA2, a new player in telomere maintenance and tumor suppression. *Cell Cycle* 12(13):1985-1986.
133. Duxin JP*, et al.* (2009) Human Dna2 is a nuclear and mitochondrial DNA maintenance protein. *Mol Cell Biol* 29(15):4274-4282.
134. Kaguni LS (2004) DNA polymerase gamma, the mitochondrial replicase. *Annu Rev Biochem* 73:293-320.
135. Copeland WC & Longley MJ (2008) DNA2 resolves expanding flap in mitochondrial base excision repair. *Mol Cell* 32(4):457-458.
136. Shackelford RE, Kaufmann WK, & Paules RS (1999) Cell cycle control, checkpoint mechanisms, and genotoxic stress. *Environ Health Perspect* 107 Suppl 1:5-24.
137. Gobbini E, Cesena D, Galbiati A, Lockhart A, & Longhese MP (2013) Interplays between ATM/Tel1 and ATR/Mec1 in sensing and signaling DNA double-strand breaks. *DNA Repair (Amst)* 12(10):791-799.
138. Bartek J, Lukas C, & Lukas J (2004) Checking on DNA damage in S phase. *Nat Rev Mol Cell Biol* 5(10):792-804.
139. Wanrooij PH & Burgers PM (2015) Yet another job for Dna2: Checkpoint activation. *DNA Repair (Amst)* 32:17-23.
140. Kumar S & Burgers PM (2013) Lagging strand maturation factor Dna2 is a component of the replication checkpoint initiation machinery. *Genes Dev* 27(3):313-321.
141. Bohr VA (2008) Rising from the RecQ-age: the role of human RecQ helicases in genome maintenance. *Trends Biochem Sci* 33(12):609-620.
142. Larsen NB & Hickson ID (2013) RecQ Helicases: Conserved Guardians of Genomic Integrity. *Adv Exp Med Biol* 767:161-184.
143. Croteau DL, Popuri V, Opresko PL, & Bohr VA (2014) Human RecQ helicases in DNA repair, recombination, and replication. *Annu Rev Biochem* 83:519-552.
144. Gray MD*, et al.* (1997) The Werner syndrome protein is a DNA helicase. *Nat Genet* 17(1):100-103.

145. Goto M, Ishikawa Y, Sugimoto M, & Furuichi Y (2013) Werner syndrome: a changing pattern of clinical manifestations in Japan (1917~2008). *Biosci Trends* 7(1):13-22.
146. Lauper JM, Krause A, Vaughan TL, & Monnat RJ, Jr. (2013) Spectrum and risk of neoplasia in Werner syndrome: a systematic review. *PLoS One* 8(4):e59709.
147. Lauper JM & Monnat RJ, Jr. (2014) Diabetes mellitus and cancer in Werner syndrome. *Acta Diabetol* 51(1):159-161.
148. German J (1997) Bloom's syndrome. XX. The first 100 cancers. *Cancer Genet Cytogenet* 93(1):100-106.
149. Sharma S, Doherty KM, & Brosh RM, Jr. (2006) Mechanisms of RecQ helicases in pathways of DNA metabolism and maintenance of genomic stability. *Biochem J* 398(3):319-337.
150. Fairman-Williams ME, Guenther UP, & Jankowsky E (2010) SF1 and SF2 helicases: family matters. *Curr Opin Struct Biol* 20(3):313-324.
151. Gorbalenya AE & Koonin EV (1993) Helicases - Amino-Acid-Sequence Comparisons and Structure-Function-Relationships. *Curr Opin Struc Biol* 3(3):419-429.
152. Liu Z*, et al.* (1999) The three-dimensional structure of the HRDC domain and implications for the Werner and Bloom syndrome proteins. *Structure* 7(12):1557-1566.
153. Bernstein DA & Keck JL (2003) Domain mapping of Escherichia coli RecQ defines the roles of conserved N- and C-terminal regions in the RecQ family. *Nucleic Acids Res* 31(11):2778-2785.
154. Lan L*, et al.* (2005) Accumulation of Werner protein at DNA double-strand breaks in human cells. *J Cell Sci* 118(Pt 18):4153-4162.
155. Karmakar P*, et al.* (2006) BLM is an early responder to DNA double-strand breaks. *Biochem Biophys Res Commun* 348(1):62-69.
156. Samanta S & Karmakar P (2012) Recruitment of HRDC domain of WRN and BLM to the sites of DNA damage induced by mitomycin C and methyl methanesulfonate. *Cell Biol Int* 36(10):873-881.
157. Karow JK, Chakraverty RK, & Hickson ID (1997) The Bloom's syndrome gene product is a 3'-5' DNA helicase. *J Biol Chem* 272(49):30611-30614.
158. Das A*, et al.* (2007) The human Werner syndrome protein stimulates repair of oxidative DNA base damage by the DNA glycosylase NEIL1. *J Biol Chem* 282(36):26591-26602.
159. Ahn B, Harrigan JA, Indig FE, Wilson DM, 3rd, & Bohr VA (2004) Regulation of WRN helicase activity in human base excision repair. *J Biol Chem* 279(51):53465-53474.
160. Harrigan JA*, et al.* (2003) The Werner syndrome protein stimulates DNA polymerase beta strand displacement synthesis via its helicase activity. *J Biol Chem* 278(25):22686-22695.
161. Harrigan JA*, et al.* (2006) The Werner syndrome protein operates in base excision repair and cooperates with DNA polymerase beta. *Nucleic Acids Res* 34(2):745-754.
162. Cooper MP*, et al.* (2000) Ku complex interacts with and stimulates the Werner protein. *Genes Dev* 14(8):907-912.
163. Li B & Comai L (2000) Functional interaction between Ku and the werner syndrome protein in DNA end processing. *J Biol Chem* 275(37):28349-28352.
164. Yannone SM*, et al.* (2001) Werner syndrome protein is regulated and phosphorylated by DNA-dependent protein kinase. *J Biol Chem* 276(41):38242-38248.

165. Wang AT*, et al.* (2015) A Dominant Mutation in Human RAD51 Reveals Its Function in DNA Interstrand Crosslink Repair Independent of Homologous Recombination. *Mol Cell* 59(3):478-490.
166. Wu L, Davies SL, Levitt NC, & Hickson ID (2001) Potential role for the BLM helicase in recombinational repair via a conserved interaction with RAD51. *J Biol Chem* 276(22):19375-19381.
167. Bugreev DV, Yu X, Egelman EH, & Mazin AV (2007) Novel pro- and anti-recombination activities of the Bloom's syndrome helicase. *Genes Dev* 21(23):3085-3094.
168. Hu Y*, et al.* (2007) RECQL5/Recql5 helicase regulates homologous recombination and suppresses tumor formation via disruption of Rad51 presynaptic filaments. *Genes Dev* 21(23):3073-3084.
169. Opresko PL, Sowd G, & Wang H (2009) The Werner syndrome helicase/exonuclease processes mobile D-loops through branch migration and degradation. *PLoS One* 4(3):e4825.
170. Karow JK, Constantinou A, Li JL, West SC, & Hickson ID (2000) The Bloom's syndrome gene product promotes branch migration of holliday junctions. *Proc Natl Acad Sci U S A* 97(12):6504-6508.
171. Bachrati CZ, Borts RH, & Hickson ID (2006) Mobile D-loops are a preferred substrate for the Bloom's syndrome helicase. *Nucleic Acids Res* 34(8):2269-2279.
172. Poot M, Hoehn H, Runger TM, & Martin GM (1992) Impaired S-phase transit of Werner syndrome cells expressed in lymphoblastoid cell lines. *Exp Cell Res* 202(2):267-273.
173. Hand R & German J (1975) A retarded rate of DNA chain growth in Bloom's syndrome. *Proc Natl Acad Sci U S A* 72(2):758-762.
174. Sidorova JM, Kehrli K, Mao F, & Monnat R, Jr. (2013) Distinct functions of human RECQ helicases WRN and BLM in replication fork recovery and progression after hydroxyurea-induced stalling. *DNA Repair (Amst)* 12(2):128-139.
175. Sidorova JM, Li N, Folch A, & Monnat RJ, Jr. (2008) The RecQ helicase WRN is required for normal replication fork progression after DNA damage or replication fork arrest. *Cell Cycle* 7(6):796-807.
176. Constantinou A*, et al.* (2000) Werner's syndrome protein (WRN) migrates Holliday junctions and co-localizes with RPA upon replication arrest. *EMBO Rep* 1(1):80-84.
177. Machwe A, Xiao L, Groden J, & Orren DK (2006) The Werner and Bloom syndrome proteins catalyze regression of a model replication fork. *Biochemistry* 45(47):13939-13946.
178. Machwe A, Xiao L, Lloyd RG, Bolt E, & Orren DK (2007) Replication fork regression in vitro by the Werner syndrome protein (WRN): holliday junction formation, the effect of leading arm structure and a potential role for WRN exonuclease activity. *Nucleic Acids Res* 35(17):5729-5747.
179. Sharma S, Sommers JA, & Brosh RM, Jr. (2004) In vivo function of the conserved non-catalytic domain of Werner syndrome helicase in DNA replication. *Hum Mol Genet* 13(19):2247-2261.
180. Sharma S*, et al.* (2004) WRN helicase and FEN-1 form a complex upon replication arrest and together process branchmigrating DNA structures associated with the replication fork. *Mol Biol Cell* 15(2):734-750.

181. Sharma S*, et al.* (2004) Stimulation of flap endonuclease-1 by the Bloom's syndrome protein. *J Biol Chem* 279(11):9847-9856.
182. Bartos JD, Wang W, Pike JE, & Bambara RA (2006) Mechanisms by which Bloom protein can disrupt recombination intermediates of Okazaki fragment maturation. *J Biol Chem* 281(43):32227-32239.
183. Agrelo R*, et al.* (2006) Epigenetic inactivation of the premature aging Werner syndrome gene in human cancer. *Proc Natl Acad Sci U S A* 103(23):8822-8827.
184. Bird JL*, et al.* (2012) Recapitulation of Werner syndrome sensitivity to camptothecin by limited knockdown of the WRN helicase/exonuclease. *Biogerontology* 13(1):49-62.
185. Futami K, Takagi M, Shimamoto A, Sugimoto M, & Furuichi Y (2007) Increased chemotherapeutic activity of camptothecin in cancer cells by siRNA-induced silencing of WRN helicase. *Biol Pharm Bull* 30(10):1958-1961.
186. Pinto C, Kasaciunaite K, Seidel R, & Cejka P (2016) Human DNA2 possesses a cryptic DNA unwinding activity that functionally integrates with BLM or WRN helicases. *Elife* 5.
187. Levikova M, Pinto C, & Cejka P (2017) The motor activity of DNA2 functions as an ssDNA translocase to promote DNA end resection. *Genes Dev* 31(5):493-502.
188. Kemmerich FE*, et al.* (2016) Force regulated dynamics of RPA on a DNA fork. *Nucleic Acids Res* 44(12):5837-5848.
189. Eki T*, et al.* (1996) Assignment of the closest human homologue (DNA2L:KIAA0083) of the yeast Dna2 helicase gene to chromosome band 10q21.3-q22.1. *Genomics* 37(3):408-410.
190. Gould KL*, et al.* (1998) Fission yeast cdc24(+) encodes a novel replication factor required for chromosome integrity. *Genetics* 149(3):1221-1233.
191. Kang HY*, et al.* (2000) Genetic analyses of Schizosaccharomyces pombe dna2(+) reveal that dna2 plays an essential role in Okazaki fragment metabolism. *Genetics* 155(3):1055-1067.
192. Wu Y & Brosh RM, Jr. (2012) DNA helicase and helicase-nuclease enzymes with a conserved iron-sulfur cluster. *Nucleic Acids Res* 40(10):4247-4260.
193. Gravel S, Chapman JR, Magill C, & Jackson SP (2008) DNA helicases Sgs1 and BLM promote DNA double-strand break resection. *Genes Dev* 22(20):2767-2772.
194. Parenteau J & Wellinger RJ (1999) Accumulation of single-stranded DNA and destabilization of telomeric repeats in yeast mutant strains carrying a deletion of RAD27. *Mol Cell Biol* 19(6):4143-4152.
195. Dillingham MS, Spies M, & Kowalczykowski SC (2003) RecBCD enzyme is a bipolar DNA helicase. *Nature* 423(6942):893-897.
196. Spies M, Amitani I, Baskin RJ, & Kowalczykowski SC (2007) RecBCD enzyme switches lead motor subunits in response to chi recognition. *Cell* 131(4):694-705.
197. Taylor AF & Smith GR (2003) RecBCD enzyme is a DNA helicase with fast and slow motors of opposite polarity. *Nature* 423(6942):889-893.
198. Rocha EP, Cornet E, & Michel B (2005) Comparative and evolutionary analysis of the bacterial homologous recombination systems. *PLoS Genet* 1(2):e15.
199. Yeeles JT & Dillingham MS (2007) A dual-nuclease mechanism for DNA break processing by AddAB-type helicase-nucleases. *J Mol Biol* 371(1):66-78.
200. Atkinson J & McGlynn P (2009) Replication fork reversal and the maintenance of genome stability. *Nucleic Acids Res* 37(11):3475-3492.

201. Wawrousek KE*, et al.* (2010) Xenopus DNA2 is a helicase/nuclease that is found in complexes with replication proteins And-1/Ctf4 and Mcm10 and DSB response proteins Nbs1 and ATM. *Cell Cycle* 9(6):1156-1166.
202. Strauss C*, et al.* (2014) The DNA2 nuclease/helicase is an estrogen-dependent gene mutated in breast and ovarian cancers. *Oncotarget* 5(19):9396-9409.
203. Kramer MM & Wells CL (1996) Does physical activity reduce risk of estrogen-dependent cancer in women? *Med Sci Sports Exerc* 28(3):322-334.
204. Bartkova J*, et al.* (2005) DNA damage response as a candidate anti-cancer barrier in early human tumorigenesis. *Nature* 434(7035):864-870.
205. Gorgoulis VG*, et al.* (2005) Activation of the DNA damage checkpoint and genomic instability in human precancerous lesions. *Nature* 434(7035):907-913.
206. Bartek J & Lukas J (2007) DNA damage checkpoints: from initiation to recovery or adaptation. *Curr Opin Cell Biol* 19(2):238-245.
207. Halazonetis TD, Gorgoulis VG, & Bartek J (2008) An oncogene-induced DNA damage model for cancer development. *Science* 319(5868):1352-1355.
208. Lord CJ & Ashworth A (2017) PARP inhibitors: Synthetic lethality in the clinic. *Science* 355(6330):1152-1158.
209. Liu W*, et al.* (2016) A Selective Small Molecule DNA2 Inhibitor for Sensitization of Human Cancer Cells to Chemotherapy. *EBioMedicine* 6:73-86.

6. ACKNOWLEDGEMENTS

Many thanks to my supervisor Prof. Petr Cejka for giving me the possibility to work in his lab and on this project. His calm and focused nature helps a lot to work in a stress-free and successful manner.

I thank the whole Cejka lab for supporting me with scientific and non-scientific advices during my time in the lab. Special thanks go to Maryna for being a great teacher, mentor, colleague, collaborator and friend!

My PhD committee including Prof. Alex Sartori, Prof. Ralf Seidel and Dr. Pavel Janscak contributed to my PhD with helpful discussions and advices guiding my project in promising directions, thanks for that!

I thank everyone involved in the IMCR for creating a perfect working environment with Prof. Joe Jiricny as face and head of the institute.

Finally, huge thanks to my family and friends for supporting me during my whole life and career.

7. CURRICULUM VITAE

PERSONAL DETAILS

Name:	Cosimo Pinto
Address:	Hubenstrasse 20, 8057 Zurich
Mobile:	+41 76 407 67 65
E-Mail:	cosimopinto@bluewin.ch
Date of birth:	25.06.1989
Nationality:	Swiss
Place of origin:	Hallau, SH
Marital status:	Single

PROFESSIONAL EXPERIENCE

05/2014 - present **PhD Researcher, Institute of Molecular Cancer Research, University of Zurich, Zurich, Switzerland**

- Biochemical analysis of proteins involved in DNA metabolism and in cancer development
- Extensive collaboration with multiple (inter)national groups
- Supervision of students, organization of practical courses
- Laboratory setup and management
- Scientific project management
- Preparation and oral presentation of progress reports
- Writing of publications, reports, grant applications
- Five publications in renowned scientific journals

10/2013 - 04/2014 **Master thesis research, Institute of Molecular Cancer Research, University of Zurich, Zurich, Switzerland**

- Expression and purification of human proteins using several expression systems
- Full time project for the duration of half a year
- Developing hypotheses, planning and execution of project and workflow
- Interpretation of data and suggesting further steps
- Presenting, discussing and defending data in meetings

02/2013 - 04/2013 **Master research project, Institute of Molecular Cancer Research, University of Zurich, Zurich, Switzerland**

- Expression and purification of human proteins using several expression systems

09/2012 - 012/2012 **Master research project, Institute of Biochemistry, ETH Zurich, Zurich, Switzerland**

- Studying mechanism of cell cycle regulation in *Saccharomyces cerevisiae*

EDUCATION

05/2014 - present **PhD in Natural Sciences, Cancer Biology, University of Zurich**
PhD thesis: Institute of Molecular Cancer Research, University of Zurich, Prof. Petr Cejka

09/2012 - 04/2014 **MSc in Biology, Major in Cell Biology (GPA 5.55), ETH Zurich**
Master thesis: Institute of Molecular Cancer Research, University of Zurich, Prof. Petr Cejka

09/2009 - 08/2012 **BSc in Biology (GPA 4.99), ETH Zurich**

08/2004 - 07/2008 **Matura, Kantonsschule Schaffhausen**

TEACHING EXPERIENCES

04/2015, 04/2016 Teaching of block course "BIO 247 Genome Stability and Molecular Cancer Research: biochemical approaches", University of Zurich

PUBLICATIONS

Levikova M[#], **Pinto C[#]**, Cejka P. The motor activity of DNA2 functions as an ssDNA translocase to promote DNA end resection. Genes Dev. 2017. [#]: equal contribution

Pinto C, Kasaciunaite K, Seidel R, Cejka P. Human DNA2 possesses a cryptic DNA unwinding activity that functionally integrates with BLM or WRN helicases. Elife. 2016

Kemmerich FE, Daldrop P, **Pinto C**, Levikova M**,** Cejka P, Seidel R. Force regulated dynamics of RPA on a DNA fork. Nucleic Acids Res. 2016.

Thangavel S, Berti M, Levikova M, **Pinto C**, Gomathinayagham S, Vujanovic M, Zellweger R, Moore H, Lee EH, Hendrickson EA, Cejka P, Stewart S, Lopes M, Vindigni A. DNA2 drives processing and restart of reversed replication forks in human cells. J Cell Biol. 2015.

Sturzenegger A, Burdova K, Kanagaraj R**,** Levikova M, **Pinto C**, Cejka P, Janscak P. DNA2 cooperates with the WRN and BLM RecQ helicases to mediate long-range DNA end resection in human cells. J Biol Chem. 2014.

SCIENTIFIC CONFERENCES

- Fusion Conference “2nd Exploring DNA Repair Pathways as Targets for Cancer Therapy Conference”, Cancun, Mexico, 27 Februar-2 March 2017
  Poster: Human DNA2 possesses a cryptic DNA unwinding activity that functionally integrates with BLM or WRN helicases.
- 13th Charles Rodolphe Brupbacher Symposium "Breakthroughs in Cancer Research and Therapy", Zurich, Switzerland, 1-3 February 2017
  Poster: Human DNA2 possesses a cryptic DNA unwinding activity that functionally integrates with BLM or WRN helicases.
- Swiss Meeting on Genome Stability and Chromatin Dynamics 2016, Emmetten, Switzerland, 8-10 June 2016
  Poster: Human DNA2 possesses slow but processive DNA helicase activity.
- Abcam conference "Mechanisms of Recombination 2016", Alicante, Spain, 16-24 May 2016
  Poster: Human DNA2 possesses a cryptic DNA unwinding activity that functionally integrates with BLM or WRN helicases
- Cancer Biology PhD Student Retreat Davos, Spain, 29-31 March 2016
  Poster: Human DNA2 possesses slow but processive DNA helicase activity
- 6th Cancer Network Zurich Retreat, Emmetten, Switzerland, 12-14 April 2015
  Poster: Biochemical analysis of human DNA2.
- 12th Charles Rodolphe Brupbacher Symposium "Breakthroughs in Cancer Research and Therapy", Zurich, Switzerland, 28-30 January 2015
  Poster: Biochemical analysis of human DNA2.
  of human DNA2.